THESIS
3
2003
54814766

LIBRARY
Michigan State
University

This is to certify that the
thesis entitled

EVALUATING GEOLOGICALLY-CONTRAINED MODELS WITH PUMPING TESTS IN A HETEROGENEOUS ALLUVIAL AQUIFER, HELIPAD SITE AT LAWRENCE LIVERMORE NATIONAL LABORATORY, CALIFORNIA

presented by

Robert Stirling Trahan

has been accepted towards fulfillment
of the requirements for the

M.S. degree in Environmental Science

Gary Weissmann
Major Professor's Signature

8 August 2003
Date

MSU is an Affirmative Action/Equal Opportunity Institution

PLACE IN RETURN BOX to remove this checkout from your record.
TO AVOID FINES return on or before date due.
MAY BE RECALLED with earlier due date if requested.

DATE DUE	DATE DUE	DATE DUE

6/01 c:/CIRC/DateDue.p65-p.15

EVALUATING GEOLOGICALLY-CONTRAINED MODELS WITH PUMPING TESTS IN A HETEROGENEOUS ALLUVIAL AQUIFER, HELIPAD SITE AT LAWRENCE LIVERMORE NATIONAL LABORATORY, CALIFORNIA

By

Robert Stirling Trahan

A THESIS

Submitted to
Michigan State University
in partial fulfillment of the requirements
for the degree of

MASTER OF SCIENCE

Department of Geology

2003

ABSTRACT

EVALUATING GEOLOGICALLY-CONTRAINED MODELS WITH PUMPING TESTS IN A HETEROGENEOUS ALLUVIAL AQUIFER, HELIPAD SITE AT LAWRENCE LIVERMORE NATIONAL LABORATORY, CALIFORNIA

By

Robert Stirling Trahan

Pumping test results and numerical groundwater simulation at the Helipad Site, Lawrence Livermore National Laboratory (LLNL), are used to evaluate four geologically-constrained conceptual models. These include a homogenous-layered model, a homogeneous-layered model, a transition probability geostatistical model, and a stratigraphic transition probability geostatistical model. Each of these models incorporates different aspects of physical heterogeneity observed at this site. At the Helipad Site at LLNL, relatively mature paleosols within the alluvial deposits mark unconformities that separate this alluvial aquifer into a series of stratigraphic zones. This provided the stratigraphic framework in which conceptual models were developed. The results of this study show that multiple realizations for the distributions of hydrofacies within stratigraphic and paleosol units (modeled using transition probability geostatistics) better match pumping test results then conceptual modeling approaches that did not incorporate these finer scale heterogeneities. Based on multiple realizations of hydrofacies distributions, characteristics for the distributions and dimensions of gravel and sand channel were identified that could be later used to filter potential poorly performing realization.

ACKNOWLEDGMENTS

This material is based on work supported by the National Science Foundation under Grant No. EAR-0133666. Additional support was received from Lawrence Livermore National Laboratory under subcontract #B503592. I benefited greatly from discussions with Fred Hoffman, Zafer Demir, Rick Blake, Charles Noyes, Mike Maley, Walt McNab, John Karachewski, and Souheil Ezzedine. Additionally, I appreciate work on this project by Leslie Mikesell, George Bennett, Beth Apple, and Jill Schlanser. Special thanks go toward my adviser, Gary Weissmann, and committee members David Hyndman and M. S. Phanikumar, and especially my loving wife, Kimberly.

TABLE OF CONTENTS

LIST OF TABLES

LIST OF FIGURES

Figure F.1 Ve
m

Figure F.2 Fu
ca
the

Figure F.3 Se
pr
hy
co

Figure F.4 Fu
ap
to

Figure F.5 Fu
ap
to

Figure F.6 Ful
simu
and
LL

Figure F.7 Full
simu
and
LL

Figure F.8 Full
simu
and
LL

Figure H.1 Obse
are d
HSU
(165
wells

Figure H.2 Simu
the la
draw

m
st

Figure H.14a S
th
re

Figure H.14b M
pr
m
str

Figure H.15a Sim
the
res

Figure H.15b Ma
pro
mo
strat

Figure H.16a Sim
the
resu

Figure H.16b Ma
prob
mod
strati

Figure H.17a Simu
the tr
result

Figure H.17b Map
proba
mode
strati

Figure H.18a Simu
the tra
result

Figure H.18b Map
probai

m
st

Figure H.29a S
th
re

Figure H.29b M
pr
m
st

Chapter One

Introduction and Scope of Work

Introduction

In an alluvial aquifer, the structural architecture of sediments is commonly very complex. For example, the architecture of alluvial fans may consist of multiple sequences separated by unconformable surfaces (Weissmann *et al.* 2002a). Within individual sequences, channel sediments, which consist of highly permeable sand and gravel bodies, typically form the main aquifer. These channels while elongate are not necessarily laterally extensive or layered. Intermediate- and fine-grained materials, such as levee, crevasse splay or floodplain deposits, tend to occur laterally and vertically adjacent to the sand and gravel channel deposits. These fine-grained deposits typically consist of sands and silts with lower permeability. Like channel deposits, these materials are not necessarily laterally extensive or layered. Also at time of deposition, these fluvial deposits may be interspersed with debris flow deposits consisting of poorly sorted clay, silt, sand, and gravels. These debris flow deposits typically have lower permeability relative to other deposits due to poor sorting. Pedogenically-altered sediments may also develop, representing a prolonged hiatus in deposition. These pedogenically-altered sediments typically consist of fine-grained sand and clay, may be carbonate rich, and typically have very low permeability. Weissmann *et al.* (2002a) described mature paleosol surfaces as laterally extensive units capping individual stratigraphic units. Though these units are laterally extensive, covering large portions of the fan system, it is

possible that stream or rivers may cut these units creating conduits for fluid flow. Also, these units tend to vary in thickness over the alluvial fan.

At the Lawrence Livermore National Laboratory (LLNL), California (Figure 1.1), the complex structural architecture of channel, floodplain, debris flow, and pedogenically-altered sediments, as well as the stratigraphic arrangement of these sediments, strongly influence the hydraulic response and distribution of contaminants within the alluvial fan aquifer (Blake *et al.*, 1995; Blake *et al.*, 1997; Noyes *et al.*, 1997; Noyes *et al.*, 2000). Remediation efforts at the LLNL site have led to an improved understanding of the subsurface conditions and contaminant distribution in the subsurface. Through a systematic methodology, the aquifer beneath the LLNL property limits and neighboring areas were divided into hydrostratigraphic units or HSUs (Blake *et al.*, 1995; U.S. Department of Energy, 1998; Noyes *et al.*, 2000; Figure 1.2). HSUs were developed by evaluating hydraulic tests, water levels, geophysical well logs, geological core descriptions, and chemical analysis of sediment and groundwater. HSU boundary delineation helped improve placement of extraction wells and implement a more cost effective clean up of site contaminants (U.S. Department of Energy, 1998). Figure 1.2 schematically shows the distribution of hydrostratigraphic units (delineated with black lines) in cross section across the southern portion of the LLNL property. Within HSUs, the locations of volatile organic chemical (VOC) plumes are reasonably resolved. It has also been shown that locally HSU boundaries correlate well to unconformity surfaces which are defined by laterally-extensive, pedogenically-altered sediments that mark possible sequence boundaries (Weissmann, 2001; Bennett and Weissmann, 2001).

Figure 1.1: Law
central Californ
Department of

Figure 1.2: Sch
within hydrostr
1998).

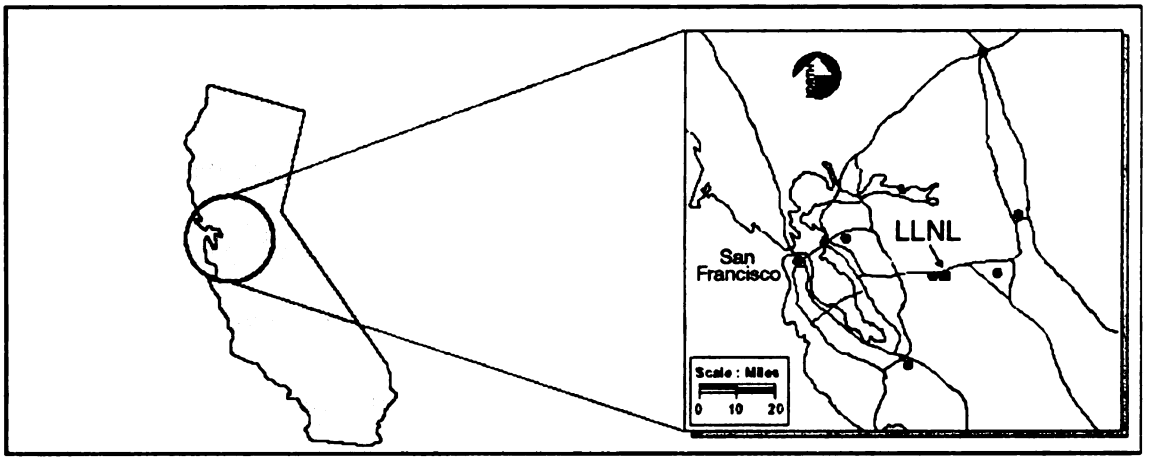

Figure 1.1: Lawrence Livermore National Laboratory (LLNL) is located in west-central California approximately 50km east of San Francisco (modified from US Department of Energy, 1998).

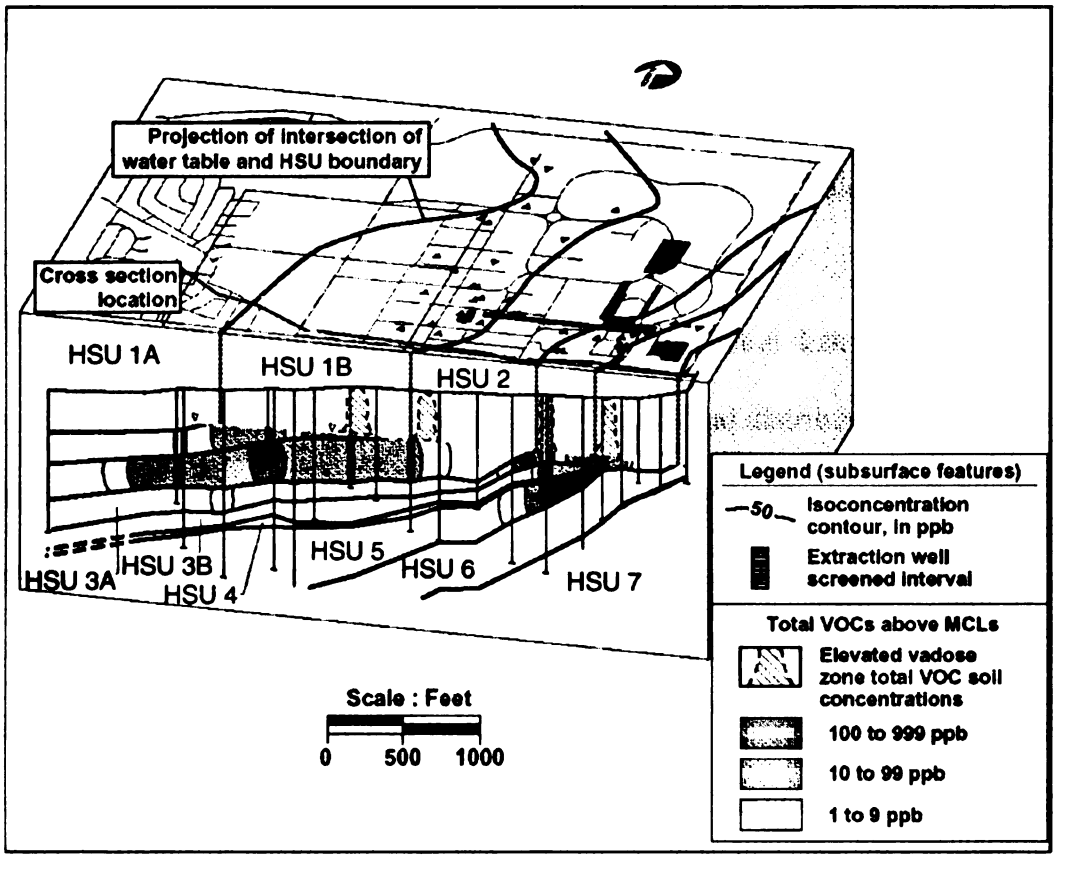

Figure 1.2: Schematic block diagram showing distributions of VOC contaminants within hydrostratigraphic units (HSUs) (Modified from U.S Department of Energy, 1998).

Remediation efforts at the LLNL site have led to a better understanding of the subsurface and contaminant distributions. As a result, HSU boundaries have improved clean up efforts (U.S. Department of Energy, 1998). However, implementation of more detailed heterogeneities will most-likely provide a better description of HSU boundaries and the distribution of hydraulic properties within these boundaries. The need to more accurately simulate fluid flow has led to better heterogeneity characterization approaches through incorporation of more geologic information. Eschard *et al.*, (1998) and Weissmann and Fogg, (1999) have used the geology and stratigraphy as a framework for geostatistical realizations in order to better define regions that are more closely stationary. Generating the spatial distribution of hydrofacies at this site, or heterogeneity within a geologic framework using transition probability geostatistics may provide a better understanding of flow within and across HSU boundaries. Resolving a detailed distribution of hydrofacies within a stratigraphic framework should also aid in remediation efforts at this site.

This thesis explores two approaches to resolve the spatial distribution of the smaller scale heterogeneities, or more specifically, the spatial distribution of hydraulic properties. The first approach is an analytical solution analysis of pumping test results. The second method combines both stochastic realizations and numerical modeling approaches under different conceptual frameworks. Simulated drawdown is then compared to pumping tests for model validation.

Analytical solutions, such as those first derived by Theis (1935) are commonly used for evaluation and interpretation of pumping test results in confined aquifers. By applying these analytical methods, a spatial distribution of hydraulic properties and

anisotropy in the aquifer may be estimated (Gloaguen *et al.*, 2001). However, an approach of this type assumes (among other things) a homogeneous aquifer of constant thickness and infinite extent. There are few (if any) geologic processes that produce an aquifer with these qualities. Hantush and Jacob (1955) derived solutions for a leaky aquifer system, and Neumann and Witherspoon (1972) derived solutions for a multi-layered system. Kruseman and de Ridder (1990) present many equations that have been modified to accommodate confined, unconfined, leaky, anisotropic, and multi-layered aquifers. However, in order to apply each of these equations, assumptions must be made. The overriding assumptions of a homogeneous aquifer of constant thickness and infinite extent are still inaccurate within the context heterogeneous alluvial aquifer. Gravel and sand bodies that generally comprise the main aquifer are not of constant thickness or laterally extensive.

In close proximity to the pumping well, a multi-layered conceptual model may be sufficient for evaluating pumping test with analytical solutions. Over a relatively short distance from the pumping well, it may be assumed that the hydraulic properties within these layers are uniform in which assumptions for analytical solutions may be valid (Appendix E). However, evaluation of pumping test results at observation wells located farther away may be much more difficult. Between pumping and observation wells, there often exists a complex spatial pattern of drawdown which is primarily the result of physical heterogeneities that exist within an alluvial aquifer (Carle, 1996). Klingbeil *et al.* (1999) state that aquifer pumping tests yield hydraulic properties at a scale much larger than the typical length of structures in a heterogeneous aquifer. When characterizing an alluvial aquifer using analytical solutions, smaller scale features are often overlooked.

More rec

heterogeneity us

et al., 2001; Cop

drawdown at dif

statistical metho

structures within

influence on fluid

numerous pumpi

observed segmen

heterogeneous str

necessary to have

generally asses dr

observation wells.

observation points

To better a

stratigraphic zone,

as channel gravels

can be recognized b

processes. Furthern

hydraulic properties

similar hydrogeolog

2001). Within each

sand, gravel, silty sa

More recent methods are being developed to examine the impacts of local-scale heterogeneity using analytical solutions (Schad and Teutsch, 1994; Passinos, 2001; Zhan *et al.*, 2001; Copty and Findikakis 2002). These methods include examining the transient drawdown at different phases (early, middle, and late) through semilog analysis and statistical methods. Interpretations of the transient drawdown are used to infer finer scale structures within the aquifer. These smaller scale features most likely have strong influence on fluid and contaminant migration. Hermann and Teutsch (1994) use numerous pumping tests to investigate different investigational scales. In this study, the observed segmentation of drawdown curves were use to interpret effecting lengths heterogeneous structures. However, they also conclude that numerical models are necessary to have a quantitative interpretation of measured drawdown. These approaches generally asses drawdown from a single pumping well or a pumping well with few observation wells. The work presented here describes an analysis of drawdown at several observation points.

To better account for the smaller scale heterogeneities that are present within each stratigraphic zone, a different approach must be taken. Individual stratigraphic units, such as channel gravels and sands, floodplain deposits, and pedogenically-altered sediments, can be recognized by textures and bedding patterns that originated from the depositional processes. Furthermore, stratigraphic units of the same type tend to posses similar hydraulic properties. The term "hydrofacies" is used to refer to stratigraphic units with similar hydrogeologic properties (Ritzi *et al.*, 1995; Klingbeil *et al.*, 1999; Gaud *et al.*, 2001). Within each individual sediment facies, or in this case, individual hydrofacies (e.g., sand, gravel, silty sand, and paleosol), the hydraulic properties may differ by 2 orders of

magnitude. However, hydraulic properties between each hydrofacies may differ by 5 orders of magnitude or more (Freeze and Cherry, 1979).

Resolving a detailed spatial distribution of hydrofacies requires geologic information. Most geologic information is obtained from boreholes. Core recovered from boreholes can be used to identify geologic structures and sediment facies. Geophysical logs are used to measure resistivity, conductivity, porosity, density, and other parameters. Geophysical logs and borehole descriptions can be used in unison to identify hydrofacies, which may include channel gravels and sands, floodplain sand and silts, and pedogenically-altered sediments within an alluvial fan setting. While borehole data provide excellent coverage in the vertical direction, architectural complexity and borehole spacing is generally too great to yield sufficient insight on sediment facies distributions in the horizontal direction. A stochastic approach (e.g., transition probability) geostatistics can be used to account for the distributions of sediment units in the horizontal direction (Carle and Fogg, 1996; Carle *et al.*, 1998; Weissmann *et al.*, 1999). Weissmann and Fogg (1999) and Weissmann *et al.* (2002b) use transitions probability geostatistics within a geologic framework to create geologically realistic realizations of alluvial aquifer systems that are conditioned to borehole information. Using this approach, they generated three-dimensional realizations of hydrofacies distributions that are geologically reasonable.

Purpose of study

The primary purpose for this work is to study the influence of stratigraphy on aquifer hydraulics. This is accomplished by first modeling the stratigraphy through a

detailed geolog

conceptual of th

simulated draw

solution was use

The Heli

selected for this

preliminary stud

probability geost

well log data were

allowing for cross

measured results

contaminant reme

characterization m

To investig

stratigraphic mode

levels of heterogen

a homogeneous-lay

(HLP), 3) transition

al. 1998) (TPG), ar

framework (STPG)

individual stratigra

(Weissmann and Fo

detailed geologic assessment, analyzing both geophysical and core data. Then, multiple conceptual of this stratigraphy are evaluated using numerical groundwater models were simulated drawdown can be compared to the observed. For completeness, an analytical solution was used to evaluate and interpret observed pumping test results.

The Helipad Site at Lawrence Livermore National Laboratory (LLNL) was selected for this study. Selection of this site was based on the following criteria: 1) preliminary studies were conducted at this site that modeled the system using transition probability geostatistics, 2) a large amount of previously collected core and geophysical well log data were available at the site, 3) a dense spacing of wells at this site exists, allowing for cross-well correlation of facies, 4) a ten day pumping test conducted with measured results was available at this site, and 5) this site is currently undergoing contaminant remediation, thus development of a more detailed hydrologic subsurface characterization may further aid in LLNL remediation efforts.

To investigate the influence of stratigraphy on aquifer hydraulics, four stratigraphic models were developed for the Helipad Site that incorporates different levels of heterogeneity. These models include 1) a homogeneous-layered model (HL), 2) a homogeneous-layered model incorporating relatively low permeable paleosol layers (HLP), 3) transition probability geostatistical simulations (Carle and Fogg 1996; Carle *et al.* 1998) (TPG), and 4) transition probability geostatistical simulation in a stratigraphic framework (STPG). This approach simulates the spatial distribution of hydrofacies for individual stratigraphic zones independently before merging them into a single realization (Weissmann and Fogg, 1999; Weissmann *et al.*, 2002b). Evaluation of these models

were based on a

(Harbaugh *et al*

This document is

- The first s
  of the stu
  LLNL, sp
  remediati
- The secon
  conceptual
  site. This c
  publication
- The third se
  work condu
- Following a
  - App
  - App
  - App
    strati
  - App
    distri

were based on a comparison of simulated pumping test results using Modflow-2000 (Harbaugh *et al.* 2000) to observed field results and utilized numerical modeling software.

Thesis Outline

This document is divided into three main sections with subsequent appendices:

- The first section, covered by Chapter Two, describes the geology and hydrology of the study region. A brief review is given of previous hydrological studies at LLNL, specifically at the Helipad Site, and a brief history of contamination and remediation efforts at this site.
- The second section, covered by Chapter Three, presents a comparison of the four conceptual models for success in modeling a long-term pumping test at the study site. This chapter also forms a draft of a manuscript that will be submitted for publication in Water Resources Research.
- The third section, covered by Chapter Four, revisits conclusions reached for the work conducted for this thesis.
- Following appendices are attached:
    - Appendix A contains well core descriptions used in site characterization.
    - Appendix B includes hydrofacies and geophysical log correlations.
    - Appendix C contains a collection of cross-sections showing well-to-well stratigraphic correlations.
    - Appendix D contains analytical solutions to estimate hydraulic property distributions at the Helipad Site.

- Appendix E contains a series of isopach maps of stream channels for each stratigraphic horizon. Isopach maps are centrally located around the central Helipad study area.
- Appendix F includes a brief description of the transition probability geostatistical approach which utilizes a Markov chain model to resolve a 3-D distribution of hydrofacies. This appendix also outlines the procedures taken in development of the transition probability geostatistical realizations for the study area.
- Appendix G describes generation of numerical groundwater models in which the four conceptual modeling approaches are evaluated.
- Appendix H is a complete record of drawdown results for the Helipad Study Site. This includes both observed and simulated drawdown results.
- Appendix I contains the FORTRAN codes used to transfer geostatistical realizations into a format that could be incorporated into numerical groundwater models.

The Heli

underlain by an

(e.g., silt, sand, g

distribution of th

over relatively sh

influence of the a

assessment of this

characterization w

for evaluation.

To accomp

within the Liverm

investigation throu

geology through a

Livermore region.

at the Helipad Site.

Chapter Two

Geologic Setting and Stratigraphic Assessment

Introduction

The Helipad Site at Lawrence Livermore National Laboratory (LLNL) is underlain by an alluvial aquifer where the complex structural architecture of sediments (e.g., silt, sand, gravel, etc.) strongly influences fluid flow. The heterogeneous distribution of these sediments produces a system where hydraulic properties vary greatly over relatively short distances. Since the main purpose of this thesis is to study the influence of the alluvial stratigraphy on aquifer hydraulics, a detailed geologic assessment of this site was made. This geologic assessment allows for a subsurface characterization where aspects of the geology can be incorporated into conceptual models for evaluation.

To accomplish this, the regional and local geologic setting and the hydrology within the Livermore Basin was investigated. This chapter presents findings from this investigation through two main sections. The first section introduces the background geology through a description of the regional geology and the geologic evolution of the Livermore region. The second section outlines the local geology and hydrology observed at the Helipad Site.

Background Geology

Regional Geologic Setting for the Livermore Valley

The Livermore Valley is located within the California Coast Range Province. This province is composed of late Mesozoic through late Tertiary marine sedimentary rocks deposited on a complex basement of oceanic and continental crust (Figure 2.1). The Coast Range Province consists mainly of sub-parallel mountain ranges that are predominantly aligned with the majority of active faults in this region. While many of the faults are relatively minor, three major fault systems form the majority of tectonic history for western central California (Carpenter *et al.*, 1984) – the San Andreas, the Sur-Nacimiento, and the Coast Range Thrust. The regional alignment of geologic structures is a reflection of the deformation that has occurred.

In this region, most basins have a north-northwest trending pattern. However, the Livermore Basin is an exception to this. It is an east-west trending structural basin that lies within the Diablo Range. The Livermore Valley is approximately 27 kilometers long (east to west) and 12 kilometers wide (north to south) (Figure 2.1). The Lawrence Livermore National Laboratory (LLNL) site is located in the southeastern portion of the Livermore Valley, near the base of the Diablo Mountain Range. The Livermore Basin has a relatively smooth valley floor surface. At the LLNL site, the basin floor gently dips approximately 1 degree to the northwest.

SAN FRA

LIVER

Figure 2.1 R
Valley is ou
in color.

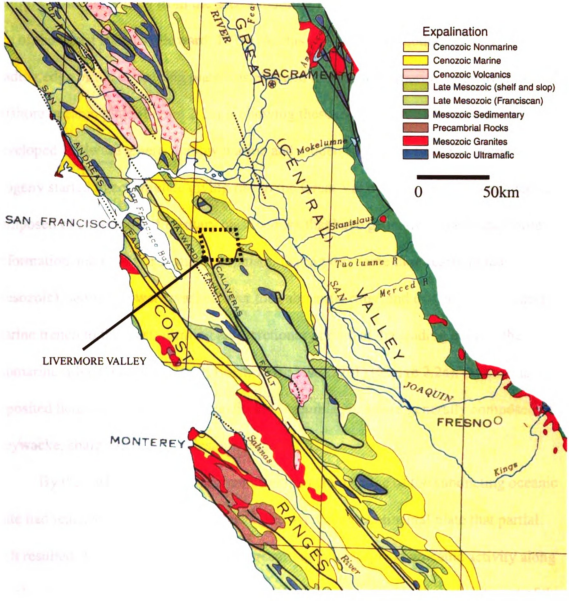

Figure 2.1 Regional geologic map of western-central California. The Livermore Valley is outlined with a dashed line (Modified from USGS, 1966). Image is presented in color.

Geologic Evolution and Stratigraphy of Middle California

After the accretion of the Nevadan Orogeny (early Mesozoic time), subduction in central California shifted from the Sierra foothills 130 kilometers seaward to the present site of the Coast Ranges (Howard, 1979). At this new offshore subduction zone, the leading edge of the overriding plate was elevated to form a submarine ridge over the offshore oceanic plate (Figure 2.2a). Following these events a broad forearc basin developed landward where shallow marine and eroded sediments from the accreted orogeny started to accumulate giving rise to the Great Valley Sequence. This sequence is composed of stratified sedimentary clastic rocks that have generally experienced little deformation and mild burial metamorphism. During this same time (early to late Mesozoic), sediments were washed over the submarine ridge and deposited into a deep marine trench to the west, forming an accretionary prism at the leading edge of the submarine ridge (Hamilton, 1969; Ernst, 1970; Hsu, 1971) (Figure 2.2a). Sediments deposited here are known as the Franciscan Assemblage and are generally composed of greywacke, shale, chert, and limestone (Figure 2.3).

By the early Cretaceous, sediments at the leading edge of the subducting oceanic plate had reached sufficient depth beneath the overriding continental plate that partial melt resulted. Magma rose to the surface resulting in widespread volcanic activity along the elevated ridge (Figure 2.2b). Volcanic rocks were deposited both east and west of this newly formed volcanic arc.

By the late Cretaceous, continued subduction from the offshore oceanic plate resulted in crumpling and metamorphism of Franciscan sediments giving metagraywacke, argillite, blueschist, and greenstone rocks. Through continued deposition and subduction,

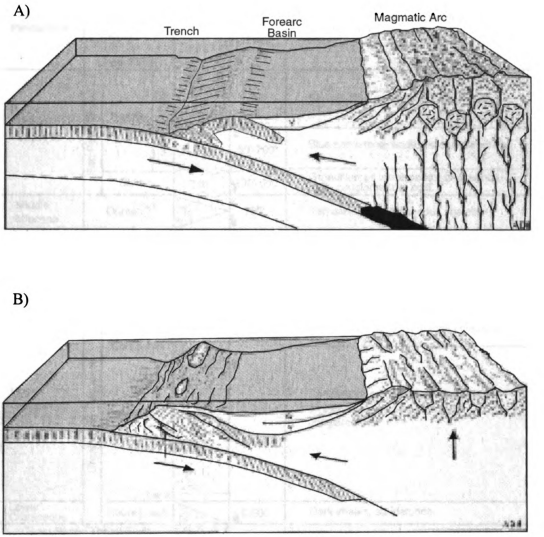

Figure 2.2: A) Generalized depiction of Late Jurassic to early Cretaceous landscape of western central California (modified from Howard, 1979). B) Generalized depiction of Late Cretaceous landscape of western central California (modified from Howard, 1979).

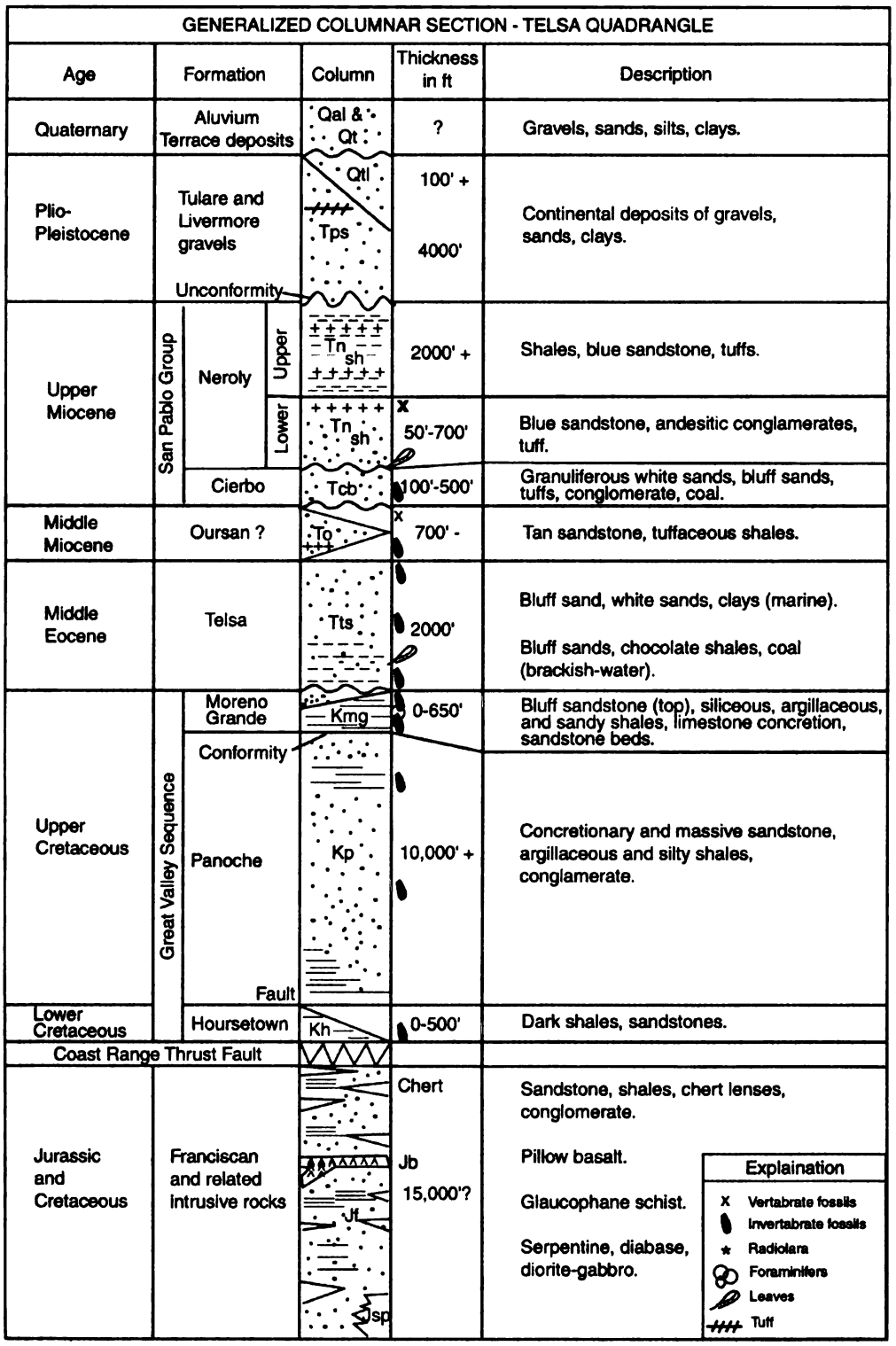

Figure 2.3 Stratigraphic column for the Livermore Valley (modified from Huey, 1948).

younger sediments were wedged under the leading edge of the overriding continental plate resulting in further elevation of this submarine ridge (Figure 2.2b). Also during this time, portions of the Franciscan Assemblage were forced beneath sediments of the Great Valley Sequence, the boundary between these units being a low angle thrust fault composed of mafic and ultramafic rocks (Howard 1979; Carpenter *et al.*, 1984; Figure 2.3). However, the complex geology of this region makes it difficult to distinguish a depositional contact between the Franciscan Assemblage and the Great Valley Sequence deposits (Dickerson, 1965). Generally, the differentiation of these two formations is based on the juxtaposition of rock with different layering attitudes and degrees of metamorphism.

During the late Cretaceous to early Miocene, the Kula Plate ceased subduction in this region and the leading edge of the continent was torn off by the northern movement of the Pacific seafloor (Howard, 1979). This event formed the proto-San Andreas Fault System. The northern movement of the Pacific seafloor eventually carried the actively subducting Farallon Plate into this region. At this time, faulting along the San Andreas ceased. Is was not until subduction of the Farallon Plate ceased that the present day San Andreas Fault System became active (early to late Miocene).

At the close of the Cretaceous, there was a prolonged period of erosion of the folded western Great Valley Sequence over which tertiary sediments would be later deposited (Huey, 1948; Dibblee and Darrow, 1981). In the Great Valley, shallow marine sediments accumulated under conditions of fluctuating sea levels and differential subsidence of the basin floor. Today these sediments outcrop to the east in the Almont Hills (Figure 2.4) and to the west in along the East Bay Hills. Sediments deposited during

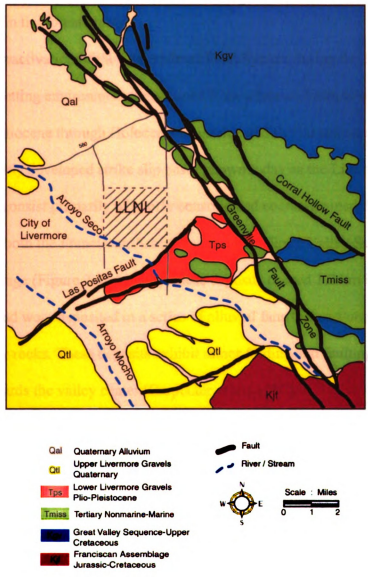

Figure 2.4 Generalized geologic map of the Lawrence Livermore National Laboratories and vicinity (Modified from Dibblee, 1980). Image is presented in color.

this time cons
conglomerate.
1981). Early T
that accumulat

With th
the depositiona
basin. From the
deposited in a n
These sediments
2.3) eroded from
nearby Diablo R
(CDWR, 19~4) a
deformed Tertiar
downwarped tow

In the eas
logs indicate tha
(CDWR, 1966).
over 60 meters a
heterogeneity of
distances.

this time consist primarily of sandstone and shale, with lesser amounts of tuff and conglomerate, and all show signs of significant deformation (Sweeny and Springer, 1981). Early Tertiary deposits also contained abundant amounts of volcanic sediments that accumulated in the forearc basin.

With the reactivation of the San Andreas Fault System during the Pliocene time, the depositional setting environment transitioned from a forearc basin to a strike slip basin. From the Miocene through Holocene, lacustrine and fluvial sediments were deposited in a newly developed strike slip basin known today as the Livermore Basin. These sediments consist primarily of poorly consolidated coarse-grained debris (Figure 2.3) eroded from both the Franciscan Assemblage and the Great Valley Sequence of the nearby Diablo Range (Figure 2.4). Locally, these deposits exceed 1.2 km in thickness (CDWR, 1974) and were deposited in a series of alluvial fans that rest unconformably on deformed Tertiary rocks. These deposits exhibit minor folding and faulting, and are downwarped towards the valley center (Carpenter *et al.*, 1980).

In the eastern portion of the Livermore Valley (location of the LLNL site), well logs indicate that the alluvium is composed of interfingering gravel, sand, silt, and clay (CDWR, 1966). The upper Livermore formation ranges in thickness from a few meters to over 60 meters and it generally increases in thickness toward the west. From the complex heterogeneity of this system, sediment correlation from well logs is difficult over large distances.

Helipad Site Geology

Core and Facies Descriptions

For identification of the sediment architecture at the Helipad Site, several sources of geologic data were available. Subsurface data included geophysical logs from 32 wells with depths up to 61 meters and approximately 1220 meters of core recovered from 28 of these wells. Characterization of the Helipad Site involved a visual description of textural and sedimentologic characteristics in core. This included a visual estimation of grain size, shape, sorting and color, as well as description of sedimentary and pedogenic structures. In addition, geophysical logs were obtained from each well and were used for correlation of hydrofacies across boreholes.

Four hydrofacies dominate the Helipad Site stratigraphic section (Appendix A). These include *gravel* and *sand* hydrofacies of channel deposits, *sandy silt* hydrofacies of overbank deposits, and *paleosol* hydrofacies facies.

The *gravel* hydrofacies is typically dominated by clast-supported gravels consisting of pebbles and cobbles. Deposits tend to be massive at a core scale. Clasts are commonly weathered and supported within a reddish, clay-rich matrix. Clay coats are common on clasts. Manganese oxides are also common on the clay coatings which may be an indication of a wetting and drying of sediments. This is also consistent with pedogenic alteration related to present and probable past climates. *Gravel* hydrofacies display the highest hydraulic conductivity. However, with the presence of thick clay coatings, hydraulic conductivities may be significantly reduced in relation to more typical gravel deposits.

The *sand* hydrofacies typically consists of well to moderately well sorted, fine to medium sand with interspersed layers of coarse to very coarse sand. Grains are typically subrounded to subangular. Sand deposits are generally massive and show possible signs of cross-stratification. Within some sections, clay coatings are present indicating a degree of pedogenic alteration.

The *silty sand* hydrofacies typically consists of silt that contains amounts of fine to medium sand. This hydrofacies commonly displays some evidence of pedogenic alteration. This includes the presence of root traces that are commonly clay-filled and surrounded by reduction halos. The *silty sand* hydrofacies typically have thin clay coats, dispersed manganese oxides, and a brown coloration. These sediments are most likely floodplain deposits.

Pedogenically-altered deposits or *paleosol* hydrofacies typically consists of clay-rich silty sand deposits. They show evidence of significant pedogenic alteration that includes very thick clay coats, continuous manganese oxide coats, slightly prismatic to prismatic or blocky structure, occasional root traces, and reddish coloration. Due to the processes involved in the pedogenic alteration, most root races are destroyed. Additionally, some of these deposits contain significant calcium carbonate.

Comparison of Core to Geophysical Well Logs

As previously stated, well core from 28 out of the 32 wells in the Helipad study were recovered. Recovered core from these wells were generally incomplete. Sections of core as a result of drilling difficulty, handling, and sampling were missing or had been shifted such that elevations were no longer aligned. Also, core recovered from these wells

were used for various site investigations resulting in removal for sampling purposes. To account for sections of missing core and to correct for elevations, geophysical logs were used. Multiple geophysical logs including gamma, conductivity, caliper, resistivity logs were recorded for each well within the study area. *Gravel, sand, silty sand*, and *paleosol* hydrofacies were correlated to geophysical logs (Appendix B).

Weissmann (2001) observed that *gravel, sand, and sitly sand* hydrofacies character was easily distinguished in geophysical logs. The *gravel* hydrofacies is distinguished by relatively high resistivity and relatively low gamma ray signature. The *sand* hydrofacies is distinguished by relatively high resistivity and relatively low gamma ray signatures, where the resistivity signatures for the *sand* hydrofacies are typically less than those observed with the *gravel* hydrofacies. The *silty sand* or *sandy silt* hydrofacies are distinguished by relatively low resistivity and relatively high gamma ray signature. On geophysical logs, the *paleosol* hydrofacies character is difficult to distinguish from the *silty sand* hydrofacies since it shows a relatively low resistivity and relatively high gamma ray signature. However, the gamma ray signature for *paleosol* hydrofacies often displays a slightly higher signature than the *silty sand* hydrofacies.

Correlations and Cross Sections

The correlation of well core to the geophysical logs allowed for sections of core to be adjusted back to their correct elevation. Also, damaged or otherwise missing sections of core were interpreted to one of the four defined hydrofacies. These adjustments and interpretation together gave more complete facies descriptions in wells that could then be

used for stratigraphic correlation of hydrofacies between wells. Across the Helipad study site, fourteen cross sections were generated (Appendix C).

Channel sand and gravel bodies are correlated with confidence across short distances. However, these bodies do not correlate across larger distances (Figure 2.5). The only unit that could be correlated between most wells with a degree of confidence was the *paleosol* hydrofacies. Since the paleosol hydrofacies are laterally extensive. In places where the paleosols are missing, *gravel* and *sand* hydrofacies exist. It is interpreted that stream channels eroded the paleosol surface at these location. There are however, a few instances where paleosol units are missing and the *silty sand* hydrofacies exist where paleosol is expected. This is interpreted to be a location where conditions were not adequate for development of a paleosol or where fine-grained sediment filled the channel.

Paleosols identified in cross section appear to be laterally extensive across the entire model area in a manner similar to that described by Weissmann *et al.* (2002a). Using this reasoning, paleosols could be correlated throughout the Helipad study site. Using paleosol correlations from cross sections, the tops and bottoms of paleosol surfaces were generated with Rockworks 2002 (Rockware Inc., 2002) using an inverse distance linear algorithm (Figure 3.2). Paleosol units are informally named Ab trough F and paleosol-bounded stratigraphic units are informally named Ab through F following Weissmann (2001). Surfaces generated with this type of algorithm were deemed reasonable for the purpose of this study. These surfaces separate stratigraphic units used in evaluating the influence of heterogeneity on aquifer hydraulics (described in more detail in Chapter 3). Only those sections that lie below the water table were analyzed in

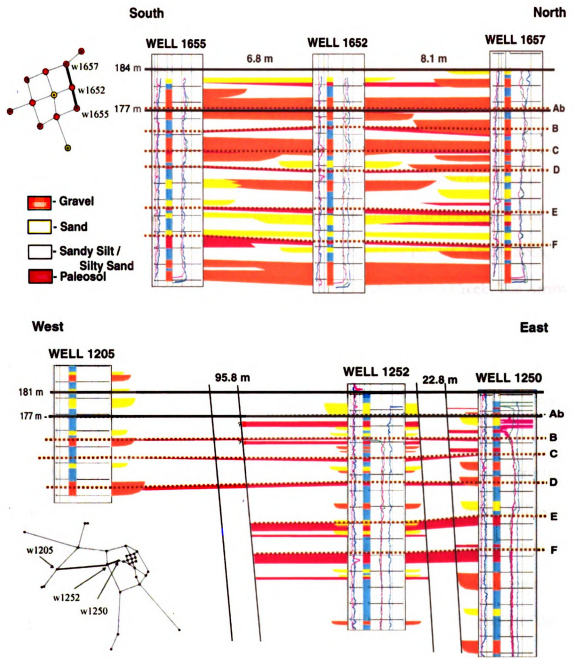

Figure 2.5: Stratigraphic cross sections at the Helipad Site. Top paleosol surfaces are shown (dashed line). Paleosols are informally named following Weissmann (2001). Image presented in color.

detail for this study. Weissmann (2001) indicated that there is a striking similarity between paleosols and hydrostratigraphic units and suggested that HSU boundaries should be updated accordingly.

Hydrology in the Livermore Basin

The Livermore Valley Groundwater Basin lies within the Diablo Range, and encompasses approximately 17,000 hectares. Prominent streams for this basin (all of which are ephemeral) include the Arroyo del Valle, Arroyo Las Positas, Arroyo Seco, Arroyo Mocho, Alamo Creek, South San Ramon Creel, and Tassajara Creek. The Arroyo del Valle and Arroyo Mocho are the largest of these streams and drain the largest area. All of these streams flow north and westward toward the valley floor until converging with the Arroyo de la Laguna, which flows southward out of the Livermore Valley into the Sunol Valley Groundwater Basin (Figure 2.6).

At the LLNL site, natural drainages have been altered by continuing construction activities. As a result, the current location of the Arroyo Seco and the Arroyo Las Positas streams are not representative of historical paths. These stream channels merge about 1.6 kilometers to the west of the LLNL property before continuing toward the Livermore Basin and merging with the Arroyo Macho. Historical (1940) aerial photographs of the Livermore property show locations of old stream channels for the Arroyo Seco and Arroyo Las Positas (Figure 2.7). Currently, Arroyo Seco is located in the southwest corner of the property. The Arroyo Las Positas was redirected north then west along the property line. Flood control and prevention of water infiltration were the main goals of the stream channel redirection.

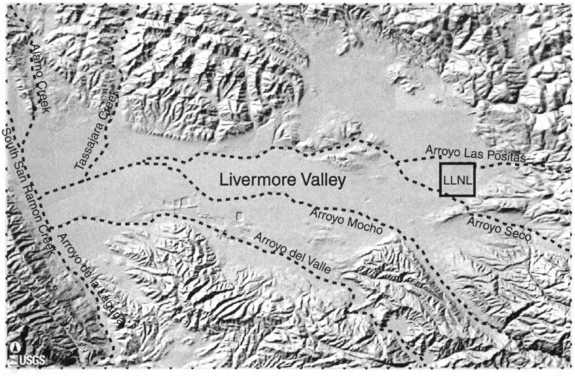

Figure 2.6: Illustrated in this Figure are major streams within the Livermore Valley. Streams are marked by dashed lines; the position of the LLNL property is outlined with a box and labeled.

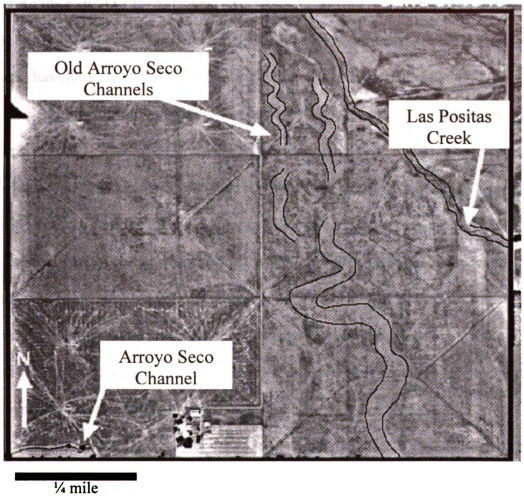

Figure 2.7: Aerial photograph (from 6/8/1940) of the LLNL property area. Indicated are northwest trending river channels of the Las Positas and the Arroyo Seco. Also indicated is the more recent location of the Arroyo Seco stream channel.

The L

as a sequenc

system from

toward the ce

the Sunol Va

Basin has elir

The gr

Upper and Lo

has an average

1995). Storage

alluvium (Upp

thickness. How

less. The Uppe

permeable (Sa

groundwater so

The dep

LLNL (Carpen

this site, groun

groundwater g

pump and treat

across the Live

northeast corne

gradient of 0.00

The Livermore Valley ground water system is described by Harrach *et al.* (1995) as a sequence of semi-confined aquifers. Groundwater moves down gradient through the system from the valley perimeter (Franciscan and Great Valley Sequence Formations) toward the central valley and then flows westward toward the southwest of the basin into the Sunol Valley Basin. However, since 1945, heavy water usage from the Livermore Basin has eliminated subsurface flow out of the Livermore Basin.

The groundwater system in this basin is composed of two main aquifers – the Upper and Lower Members of the Livermore Formation (Figure 2.3). The lower member has an average thickness of 1,000 meters over an area of 250 kilometers (Harrach *et al.*, 1995). Storage capacity for this aquifer is significantly greater then the overlying alluvium (Upper Livermore Formation), which is on average only 100 meters in thickness. However, hydraulic conductivity for the Lower Livermore Formation is much less. The Upper Livermore Formation is less consolidated and therefore is more permeable (San Francisco RWQCB, 1982). Consequently, this alluvium is the principal groundwater source within the Livermore Valley.

The depth to groundwater varies from about 10 meters to about 45 meters beneath LLNL (Carpenter *et al.*, 1984; Thorp *et al*, 1990). Prior to major remediation project at this site, groundwater flow was generally from southeast to northwest, however, current groundwater gradients have been significantly altered partially as a result of remedial pump and treat practices at the LLNL site. Figure 2.8 shows the groundwater gradient across the Livermore property in 1997. At this location, gradients are greatest in the northeast corner at about 0.15 meter/meter and decreases toward the southwest at a gradient of 0.002 meter/meter (Harrach *et al.*, 1995).

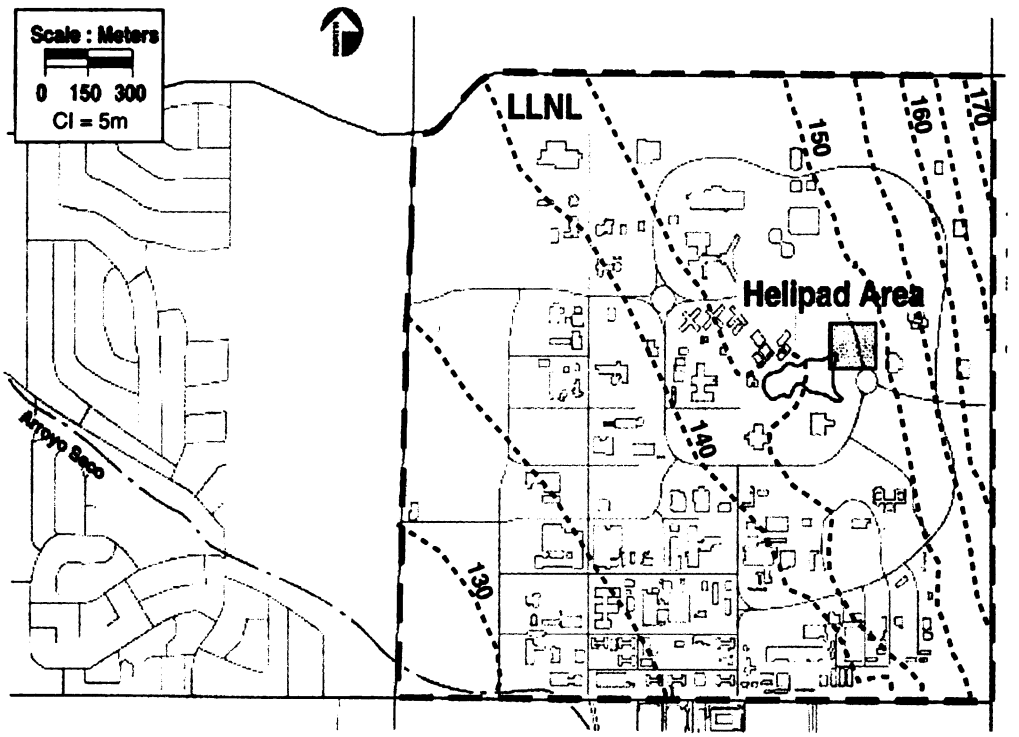

Figure 2.8: Water table elevations beneath the LLNL property, recorded in 1997 (Modified from Harrach, 1998).

Chapter Three

Pumping Test Evaluation in a Heterogeneous Alluvial Aquifer

(Note: This chapter forms a manuscript that will be submitted to Water Resources Research and was authored by Trahan, R.S., Phanikumar M.S.,, Hyndman, D.W., and Weissmann, G.S., Dept. of Geological Sciences, Michigan State University, East Lansing, MI, 48824)

Abstract: Pumping test results at the Helipad Site, Lawrence Livermore National Laboratory (LLNL), are used to evaluate four conceptual models. Each of these models incorporates different aspects of the physical heterogeneity observed. At this site, relatively mature paleosols within the alluvial deposits are observed. These paleosols mark unconformities that separate stratigraphic zones within this aquifer. Top and bottom surfaces for each paleosol unit are identified in geophysical well logs and core. This provides the stratigraphic framework in which conceptual models are developed. By resolving heterogeneity at the hydrofacies level within each stratigraphic zone and paleosol unit (simulated using transition probability geostatistics, conditioned to geophysical well log and core data), a better match pumping to test results was possible relative to conceptual modeling approaches that do not resolve the heterogeneity at the hydrofacies level. This study also shows that analytical solutions for heterogeneous systems do not accurately capture the observed geology for this site.

Introduction

In an alluvial aquifer, the structural architecture of sediments is generally very

complex. In these types of systems, the distribution of hydrofacies (e.g., silt, sand, gravel, etc.) will strongly affect fluid flow through an aquifer. The heterogeneous distribution of these hydrofacies produces a system where hydraulic conductivity and storage coefficient values can vary by orders of magnitude over only a few meters. Several examples show how the spatial distribution of these hydraulic properties greatly influences the subsurface migration of fluids (Freyberg, 1986; Sudicky, 1986; Ritzi *et al.*, 1994; Carle, 1996; Dominic and Ritzi, 1996; Fogg *et al.*, 1998; Zhang *et al.*, 2000; Weissmann *et al.*, 2002b Biteman *et al.*, in press; Weissmann *et al.*, in press). These study sites show that subsurface heterogeneities strongly influence fluid migration. Therefore, accurate prediction of fluid flow and solute transport requires reliable and realistic subsurface characterization (Webb and Davis, 1998; Boutt *et al.*, 2001).

There are many approaches to characterize subsurface. Commonly, analytical or geostatistical methods are employed. In evaluating pumping test results, analytical methods may be used to solve for average hydraulic conductivity (K) and storage coefficient (Ss) values between well pairs. This is accomplished through Theis curve matching (or some variation on this analytical solution) of drawdown histories. However, interpretation of these solutions with respect to the distributions of hydrofacies within a system is difficult. Using analytical solutions to interpret transient drawdown histories, Schad and Teutsch (1994) and Copty and Findikakis (2002) examined the impacts of local-scale heterogeneity in a larger scale system. These studies attempt to use transient drawdown histories to infer finer scale structures within the aquifer than conventional analytical solutions which only provide effective parameters for a homogeneous aquifer. Geostatistical methods are also commonly used to develop a spatial distribution of

hydraulic conductivity (K) and storage coefficient (Ss) values. These simulations of the heterogeneity may be incorporated into numerical groundwater models for evaluation. Teles *et al.*, (2002) use a combination of semi-empirical and statistical approaches to roughly reproduce a heterogeneous aquifer. Froukh (2002) and Yang *et al.*, (2002) develop conceptual models based on large-scale geologic features (i.e., formation contacts) where reasonable hydraulic parameters based on composition are assigned. These large-scale models of the system heterogeneity are then calibrated to better match observed data (i.e., head distributions, geochemistry, etc.).

However, common approaches for defining the structural architecture of an aquifer system often tend to overlook smaller scale geologic features. These smaller scale features may have a significant influence on fluid migration. Also, methods for generating reasonable geologic structures such as process-imitating methods cannot be conditioned to geologic data (Koltermann and Gorelick, 1996). Klingbeil *et al.* (1999) state that aquifer pumping tests yield hydraulic properties at a scale much larger than the typical length of structures. Likewise, analytical solutions for pumping tests estimate effective system parameters in which smaller scale structures are not well resolved.

In this paper, we explore the influence of heterogeneity on aquifer hydraulics. We present a comparison of four different conceptual models of the geology from a simple homogeneous-layered model to a more complex model of the stratigraphy and facies. Also, we evaluate analytical solutions for measured drawdown histories. Numerical groundwater models are used to evaluate each conceptual model through a comparison of pumping test results. To generate more complex models of the spatial distributions of hydraulic parameters, a transition probability geostatistical approach within a

stratigraphic framework (Carl and Fogg, 1996; Carle *et al.*, 1998; Weissmann and Fogg, 1999; Weissmann *et al.*, 2002b). Conceptual models of the geology include a homogeneous-layered model (HL), a homogeneous-layered model incorporating relatively low permeable paleosol layers (HLP), a full block volume transition probability geostatistical simulation (TPG) following methods of Carle *et al.* (1998), and a stratigraphic transition probability geostatistical simulation (STPG) following methods of Weissmann and Fogg (1999).

Study Area

The Helipad Study Site at Lawrence Livermore National Laboratory (LLNL) (Figure 3.1) was selected for this study because of the large amount of previously collected core and geophysical well log data that was available. There was also a dense spacing of wells that allowed for correlation of faces across boreholes. A long term pumping test conducted with measured results was available. Also, since this site is currently undergoing contaminant remediation, development of a more detailed hydrologic subsurface characterization may further aid in these efforts.

The Helipad Site is regionally located along the southeastern margin of the Livermore Valley Basin within the Coast Range Province of California, approximately 55 kilometers east of San Francisco. As a result of weathering, eroded debris from the Diablo Mountain Range has produced a thick succession (over 1,000 meters) of unconsolidated Quaternary alluvial-fan deposits. Our study focuses on the upper 70 meters of a multi-layered alluvial fan deposit. The Helipad Study Site has an average

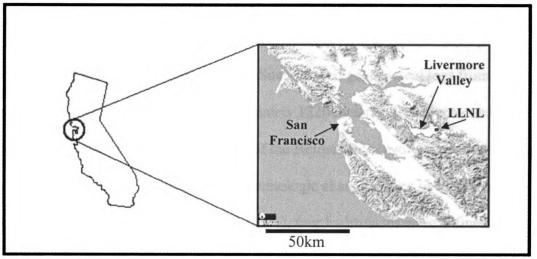

Figure 3.1: Lawrence Livermore National Laboratory (LLNL) is located east of San Francisco, within the coast range province of California (modified from US Department of Energy, 1998).

surface elevation of 190 meters (MSL) that gently slopes to the northwest. Locally the water table is approximately 29 meters below the ground surface and grades toward the southeast.

Several plumes are recognized at the LLNL site, generally bounded within hydrostratigraphic units (HSUs) (Blake *et al.*, 1995, Noyes *et al.*, 2000). HSUs were defined on the basis of an interconnected network of relatively highly permeable deposits (i.e., sands and gravels) with lower permeable sediments (i.e., silts and clays) set around those deposits. Boundaries separating HSUs were defined as laterally correlating low permeable zones that significantly reduced vertical flow. For remediation of local plumes, the Helipad Site was developed for an electro-osmosis remediation project. This project goal was to locally remediate VOC contaminants within HSUs 3A and 3B. At this site nine closely spaced wells were used to facilitate this remediation plan (1550 and 1650 series wells).

Site Geology and Stratigraphy

For development of the conceptual models, several sources of geologic data were available. Subsurface data at the Helipad Site included geophysical logs from 32 wells with depths up to 61 meters and approximately 1220 meters of core recovered from 28 of these wells. Subsurface characterization of the Helipad Site involved a visual description and evaluation of both textural and sedimentologic characteristics in core. Based on these descriptions (Appendix A; Weissmann, 2001), four hydrofacies were defined for this study area. The *gravel* hydrofacies has a relatively high permeability and is generally composed of coarse-grained, clast-supported gravel with thick reddish clay coats on clasts. The *sand* hydrofacies has a relatively moderate permeability and is composed of a moderately sorted, fine to medium-grained sand. The *silty sand* hydrofacies has a relatively low permeability and is predominately composed of silt containing minor fine to medium-grained sand. The *paleosol* hydrofacies has a relatively very low permeability and is composed of pedogenically-altered soils that are clay rich and generally contain significant calcium carbonate.

It was observed that the *gravel, sand, and sitly sand* hydrofacies character was easily distinguished in geophysical logs (Weissmann, 2001; Appendix B). With the correlation of hydrofacies from well core to geophysical logs, sections of core were adjusted to the depth reported on the geophysical logs. Damaged or otherwise missing sections of core were interpreted over short intervals based on the geophysical logs. These adjustments and interpretations together provided a more continuous hydrofacies log that could then be used for stratigraphic correlation of hydrofacies between wells across the Helipad Study Site.

Fourteen cross sections were created for the Helipad Site correlating *gravel, sand,* and *paleosol* hydrofacies across boreholes (Appendix C). However, the *paleosol* hydrofacies was the only unit that could be correlated between wells with any degree of confidence. This was because paleosol units were observed to be laterally extensive representing periods of fan exposure (Weissmann *et al.*, 2002a). These paleosol units separated the alluvial fan into a series of stratigraphic units which provided the geologic framework used for development of conceptual models. In cross section, paleosol units also closely correlate to hydrostratigraphic units defined by LLNL. However, paleosol units may not represent the only boundaries between HSUs.

Based on these observations, a three-dimensional model of the stratigraphy was developed (Figure 3.2). Top and bottom surfaces of paleosol units were interpolated using an inverse distance algorithm. Both paleosol and stratigraphic units are informally named Ab trough F (Weissmann, 2001). Only those units that lie below the water table (C through F) were used for conceptual model development.

Pumping Test Data

For implementation of the electro-osmosis remediation project at the Helipad Site, eight wells (1650, 1651, 1652, 1653, 1654, 1655, 1656, and 1657) were arranged in a square array and spaced approximately 8 meters apart (Figure 3.3). All eight wells were screened across HSUs 3A and 3B approximately 30 to 39 meters below the ground surface. Continuous pumping from wells 1551 and 1552 (Figure 3.3) was conducted over a ten day interval during which groundwater elevations from surrounding wells were recorded. Observations from well 1651 were rejected due to a suspected poor well

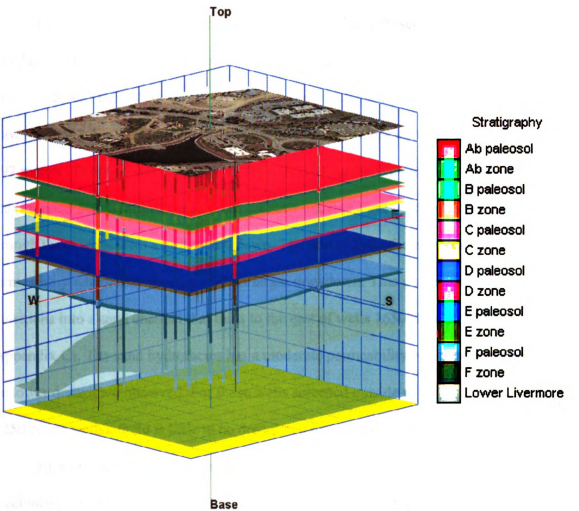

Figure 3.2: Shown above is an illustrated conceptual model of the Helipad Study Site. Six paleosol surfaces (colored) have been identified which are used to separate depositional sequences (transparent) (Appendix C). Also indicated is the saturated zone (translucent blue shading). Image presented in color.

construction or poor annular seal. Monthly groundwater elevations for this well reflect monthly groundwater elevations for HSU 4 which is approximately 3 meter less than measured in HSU 3A and 3B.

Drawdown histories from observation wells in the 1650 series wells are grouped into three different clusters (Figure 3.4). After one day, the hydraulic response from wells 1650, 1656, and 1653 show an average drawdown of 1.9 meters, well 1652 shows a drawdown of 1.4 meters, and wells 1651, 1655, and 1657 shows an average drawdown of 0.97 meters. These drawdown histories strongly correlate to the facies distributions at the site (Figure 3.5a). Central helipad cross sections indicate a gravel channel passing through those wells with a larger drawdown. The gravel hydrofacies has a relatively high permeability which may account for this larger drawdown. This gravel channel transitions into a sand channel that thins to the east of wells 1650, 1656, and 1653 (Appendix C). The sand hydrofacies has a moderate permeability which may account for the lower drawdown observed. For those wells screened outside of HSUs 3A and 3B (1250 series wells), there is little to no drawdown recorded (Figure 3.4).

An analytical solution based on observed drawdown in 1650 series wells was developed (Appendix D). For solutions of hydraulic conductivity, transmissivity, and storage coefficients, individual drawdown histories for 1650 series wells were matched to leaky aquifer type curves (Hantush and Jacob, 1955; Appendix D). For these solutions, it was assumed that pumping was only from the 1551 well. This assumption was made because pumping from well 1551 was six times greater than from well 1552. Here the effects of pumping from well 1552 were assumed to be negligible. Likewise, a type curve matching approach is unable to perform a simultaneous analysis for drawdown.

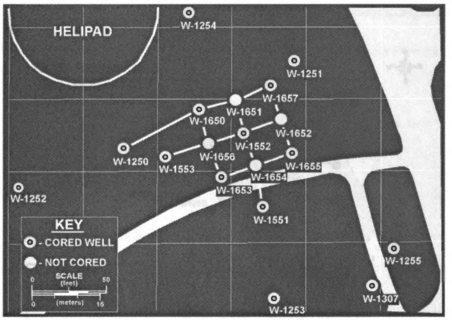

Figure 3.3: Well and cross section locations within the Helipad Site study area.

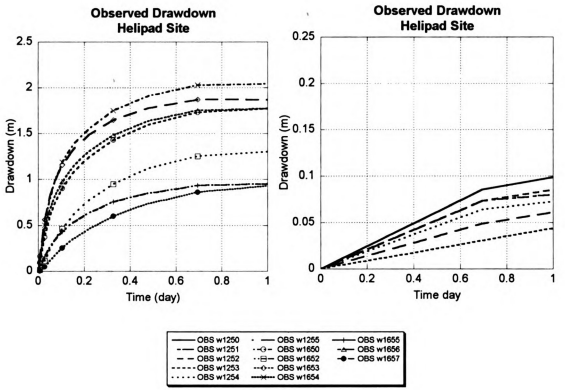

Figure 3.4: Observed drawdown history for 1650 (left) and 1250 (right) series wells. Three different clusters of drawdown are observed due to the physical heterogeneity of the alluvial system.

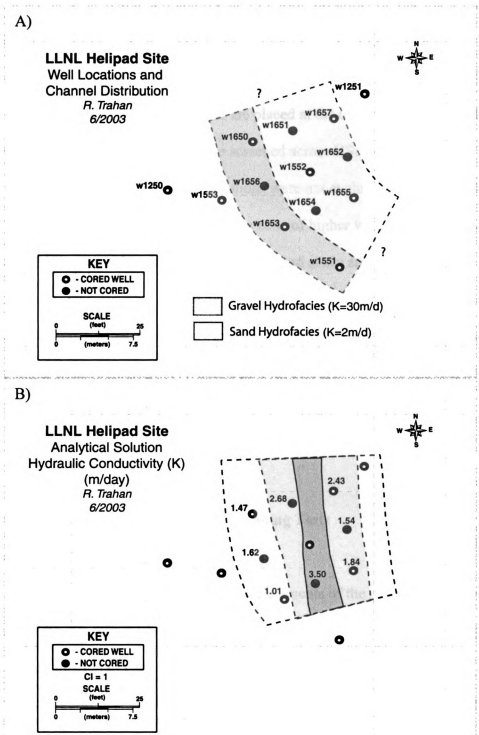

Figure 3.5: A) Well locations and interpreted distribution for gravel and sand hydrofacies within the E3 channel. Pumping wells are indicated with black circles. B) Analytical solution to observed drawdown histories at the Helipad Site showing a contour map of hydraulic conductivity, values are measured in m/s.

Superposition may be used to account for the effects of multiple pumping wells. However, even with this solution, there are many assumptions about the aquifer that must be made. In a heterogeneous system, many of these assumptions are invalid.

Results for the analytical solutions are placed at the observation wells and contoured. Since the 1250 series wells are screened across HSU 4 and out of the stratigraphic unit of interest, analytical solutions were not evaluated for these wells. The solution for hydraulic conductivity indicated a zone of higher values passing through wells 1655, 1552, and 1651 within the central Helipad study area (Figures 3.5b). Transmissivity and storage coefficient values are indicated in Appendix D. Distribution of hydraulic conductivities are contrary to the observed geology (Figure 3.5a) which shows a higher permeability gravel channel passing through wells 1650, 1656, and 1653. At this location, the geology correlates well to observed drawdown, however the analytical solution for this site does not.

Modeling Pumping Tests

The Conceptual Models:

Four conceptual models that incorporate elements of the physical heterogeneity that exists within the alluvial fan system were developed for the Helipad Site (Figure 3.6a-d). For evaluation of each conceptual model, drawdown histories were simulated using Modflow-2000 (Harbaugh *et al.*, 2000; Hill *et al.*, 2000). These simulated results should reflect the observed differential hydraulic responses. The first conceptual model is a homogeneous-layered model (HL) (Figure 3.6a). Stratigraphic sections are separated according to top paleosol surfaces, with a geologic model that resembles the HSU model

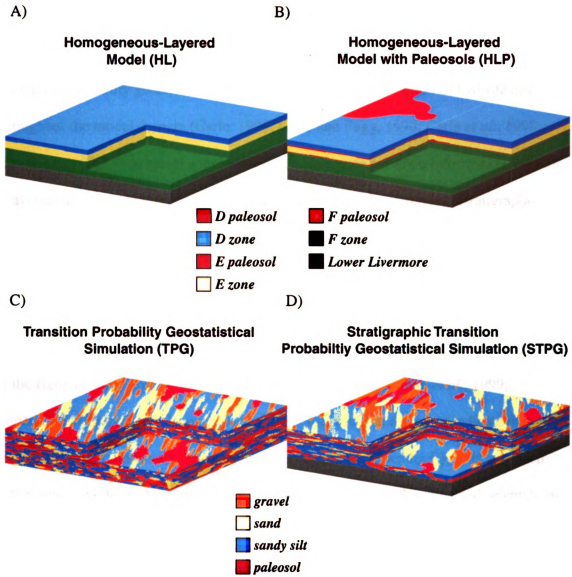

Figure 3.6: A) Homogeneous-layered model. B) Homogeneous-layered model incorporating paleosol layers. C) Transition probability geostatistical simulation. D) Stratigraphic transition probability geostatistical simulation (stratigraphic zones are simulated separately and later merged). Image presented in color.

used by LLNL. The second conceptual model is a modified version of the HSU model in which solid, low hydraulically conductive paleosol units (C through F) are incorporated between homogeneous stratigraphic units (Figure 3.6b). The third conceptual model uses transition probability geostatistics to generate the spatial distribution of hydrofacies throughout the model domain (Carle, 1996; Carle and Fogg, 1996; Carle *et al.*, 1998; Figure 3.6c). This conceptual approach incorporates more geologic information in terms of average channel orientation and widths, where each of the individual stratigraphic units was simulated simultaneously (Appendix E and F). The fourth conceptual model incorporates the most geologic information and uses transition probability geostatistics using a Markov chain model like the third. However, individual stratigraphic units and paleosol units are simulated individually and later merged to produce one final realization of the Helipad study area (Weissmann and Fogg, 1999; Weissmann *et al.*, 1999; Appendix F; Figure 3.6d). Isopach maps for channel sands and gravels indicate that widths and orientations vary between stratigraphic units (Appendix E). This approach better preserved these characteristics by assigning mean channel widths and orientations to individual simulations from their corresponding stratigraphic unit. Merging each of these simulations results in a realization where the alignment of sand and gravel hydrofacies is different across stratigraphic zones. This approach is time consuming and requires significant geologic data. However realizations generated are more geologically realistic and accurate then approaches that do not incorporate this level of detail.

Building Conceptual Models:

The layered stratigraphic conceptual model was developed following the HSU model developed by LLNL. Since HSUs were well correlated with paleosol units, these paleosol units were used as the basis to separate stratigraphic units. These surfaces were modeled across the study area with an inverse distance linear algorithm conditioned to the top of correlated paleosol units. Individual stratigraphic units were assigned values of hydraulic conductivity (K), specific storage (Ss), and vertical and horizontal anisotropy based from analytical solutions (Table 3.1, Appendix G). Vertical anisotropy values were assigned to contain drawdown within unit E (pumping layer), while horizontal anisotropy values were assigned to induce an elliptical drawdown cone to better match observed results. Values of K and Ss were calibrated for the E zone to better match the observed drawdown data.

The second conceptual model is similar to the first. However, paleosol units with relatively low K were incorporated between stratigraphic units. Bottom paleosol surfaces were also generated using an inverse distance linear algorithm conditioned to the observed bottom of paleosol units at each well. Paleosol units were assigned to have a minimum thickness of 0.5m (vertical model resolution). Individual stratigraphic units were assigned the same initial values of K and Ss as in the first model. In this conceptual model, paleosol layers which had a relatively low permeability assigned to them, limiting fluid flow across stratigraphic units (Table 3.1). Therefore, vertical anisotropy values were assigned to one. Horizontal anisotropy values were assigned to induce an elliptical drawdown cone which provides a better match to observed results. Values of K and Ss

were calibrated for the E unit to better match observed drawdown (Table 3.1, Appendix G).

Following the methods of Carle (1996), Carle and Fogg (1996), and Carle *et al.*, (1998), the third conceptual model was generated with transition probability geostatistics, or T-PROGS (Carle, 1999). Imbedded transition probabilities for the horizontal dimensions incorporated mean channel lengths, widths and orientations from the E unit (Appendix E). This simulation was generated using a 2m x 2m x0.5m grid which was later refined around pumping wells to match the Modflow grid. In this type of conceptual model, the spatial distribution of hydrofacies accounts for any anisotropy in the system. Individual cells are assumed to be isotropic. One realization using this approach was generated.

The fourth conceptual model was developed in the same manor as the third, however, geologic information in the form of mean channel lengths, widths, and channel orientations based off channel isopach maps corresponding to each individual stratigraphic unit were used (Appendix E). Also, this approach incorporated paleosol units. Hydraulic parameters were then assigned to each hydrofacies (Table 3.1, Appendix G). Multiple realizations for the distribution of hydrofacies were produced for this model type (Appendix F). Hydraulic properties from one random realization was then calibrated, these calibrated values of hydraulic parameters were used to simulate drawdown for each realization generated with transition probability geostatistics. Twenty-five realizations using this approach were generated.

Homogeneous-Layered Model:		
Layers	Hydraulic conductivity (m/d)	Storage Coefficient (1/m)
C zone	1	0.00018
D zone	1	0.00021
E zone	0.25	0.00075
F zone	1	0.0002
Lower Livermore	1	0.0003

Homogeneous-Layered Model with Paleosols:		
Layers	Hydraulic conductivity (m/d)	Storage Coefficient (1/m)
Paleosol layers	0.000046	0.0007
C zone	1	0.00018
D zone	1	0.00021
E zone	0.5	0.00005
F zone	1	0.0002
Lower Livermore	1	0.0003

Transition Probability Geostatistical Simulation:		
Hydrofacies	Hydraulic conductivity (m/d)	Storage Coefficient (1/m)
Gravel	30	0.00005
Sand	2	0.0002
Silty Sand	0.0009	0.0003
Paleosol	0.000046	0.0007
Lower Livermore	0.01728	0.0003

Table 3.1: Listed above are hydraulic parameters assigned to either layers or hydrofacies used in each of the modeling approaches. Listed values have been calibrated to best match observed drawdown histories.

Groundwater Modeling:

Groundwater modeling software used for this study to calculate head distributions for both steady and transient states was MODFLOW-2000 (Harbaugh *et al.*, 2000; Hill *et al.*, 2000). The groundwater model consisted a 360m by 310m by 39m grid (easting, northing, and vertical respectively). Grid cells have a maximum horizontal dimension of 2m by 2m and are refined around the pumping wells (1551 and 1552) to a minimum cell size of 0.15m by 0.15m. Eastern and western boundaries were set as constant head based on a measured water table; northern and southern boundaries are perpendicular to flow and were assigned as no flow boundaries. Drawdown was observed from the 1650 series wells and pumping was from wells 1551 and 1552 at rates of 16.34m^3/d and 2.72m^3/d respectfully. Pumping wells are screened across HSU 3 which correlates to the E stratigraphic unit (~28m to 38m depth below the ground surface). Results from simulations are illustrated in Figures 3.7 and 3.8.

Results and Discussion

The simulated groundwater drawdown results for the Helipad Study Site shows that the conceptual models that incorporate the most geologic information (i.e., stratigraphic transition probability geostatistical simulations) best matched the observed drawdown histories for most wells (1650, 1653, 1654, 1655, and 1656) (Figure 3.7). However not all twenty five STPG realizations accurately reflected the observed drawdown histories, (Appendix H). The sum of squared residuals for the first STPG simulation was 3.48 (calibrated results), compared to the HL, HLP, and TPG models which had squared residual sums of 8.45, 7.95, and 43.64 respectively. The TPG

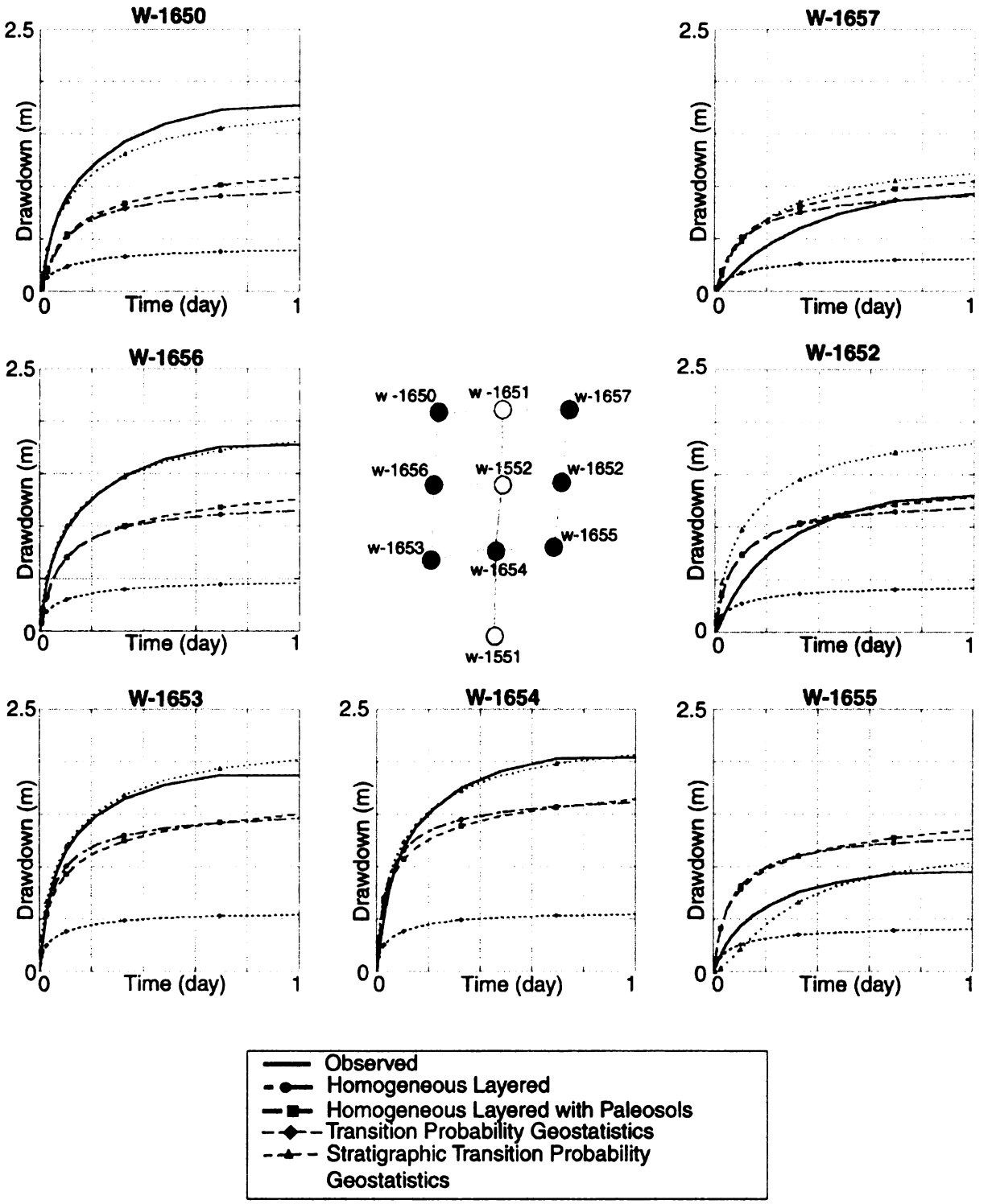

Figure 3.7: Drawdown results for modeling approaches are plotted for each observation well. Positions of plots are similar to there locations at the Helipad Site (a representation of well locations are illustrated in the center of this figure). For each graph, drawdown is in meters (y-axis) and time is in days (x-axis). Pumping wells are 1551 and 1552. Observed drawdown for well 1651 is not included due to poor well construction.

simulation used calibrated parameters from the calibrated STPG realization. Both the HL and HLP models were calibrated individually. The HL, HLP, TPG conceptual modeling approaches do not adequately capture the heterogeneous alluvial fan aquifer response (Figure 3.7 and 3.8). The hydraulic response of the aquifer produced three clusters of drawdown, wells 1650, 1656, and 1653 had a high drawdown, well 1652 had a moderate drawdown, and wells 1651, 1655, and 1657 had little drawdown (Figure 3.4 and 3.7). The calibrated STPG realization model shows two main clusters of drawdown where individual well drawdown is similar to the observed values. This characteristic is also observed in other STPG simulations. Simulated drawdown from well 1652 is high. North and south of this observation well, there are low conductive paleosol hydrofacies in the STPG realization. The close proximity of these paleosols around well 1652 creates a local zone of increased drawdown. This may account for the higher simulated drawdown. It is also possible that hydrofacies parameters need to be further calibrated to better match the observed drawdown.

Simulated drawdown from conceptual models is presented in cross section and in map view in Figure 3.8. In cross section, each conceptual model is adequate for containing drawdown within the main pumping stratigraphic layer (unit E). With the first conceptual model type, vertical anisotropy was responsible for containing drawdown. In the other conceptual model types, the low hydraulic conductivity of paleosol units was responsible for containing drawdown. However, in map view, only those conceptual models which resolved heterogeneity at the hydrofacies level showed a drawdown cone that was similar to observed data (Figure 3.8c-d and 3.9). In these simulations the

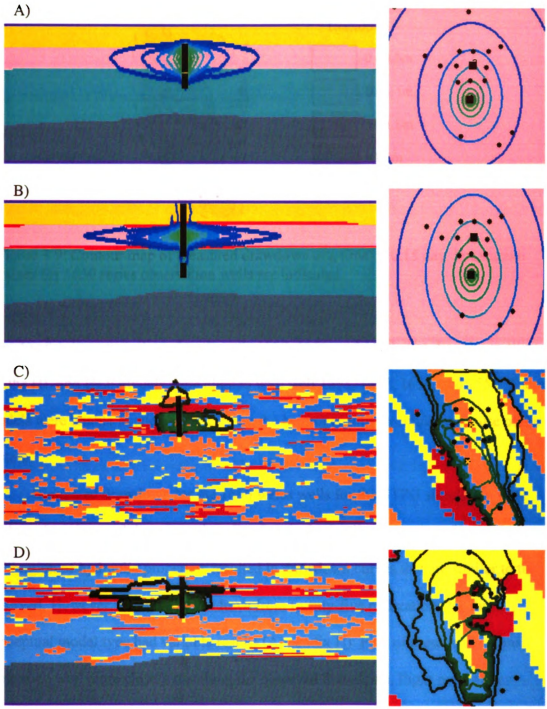

Figure 3.8: Cross section and map views of drawdown propagation at time of 0.15 day A) Simulated drawdown for the homogeneous-layered conceptual model. B) Simulated drawdown for the homogeneous-layered model incorporating paleosol layers. C) Simulated drawdown for the transition probability geostatistics conceptual model. D) Simulated drawdown for the stratigraphic transition probability geostatistics conceptual model. Image presented in color.

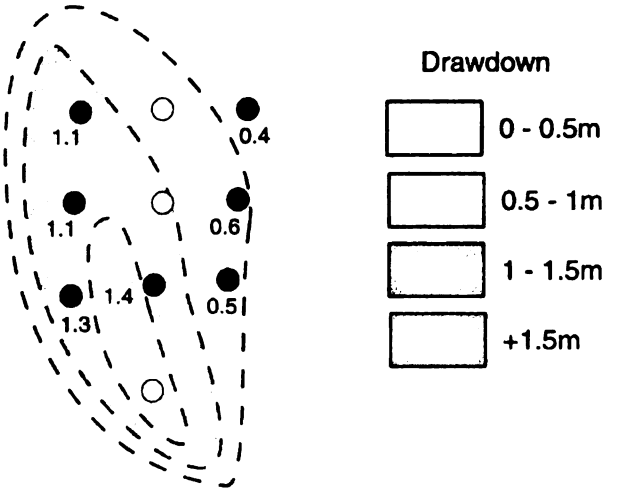

Figure 3.9: Contour map of measured drawdown at a time of 0.15 day. Drawdown values for 1650 series observation wells are indicated.

drawdown eclipse was aligned with wells 1650, 1656, and 1653. The drawdown ellipses for the HL and HLP models were aligned with well 1651, 1552, 1654, and 1551. These models were unable to adequately capture the heterogeneous hydraulic response of the system.

Simulated drawdown for the 1650 series wells for the STPG simulation were calibrated to observed drawdown by adjusting the hydraulic properties of hydrofacies. Calibration of hydraulic properties resulted in drawdown curves that are similar to the observed. However, simulated drawdown from twenty-five realizations for this conceptual model type had variable results (Appendix H). Five of these realizations preformed well more closely matching the observed drawdown. Eight realizations preformed moderately, and twelve realizations preformed poorly. Calibration of individual simulations may produce better simulated drawdown that more closely match the observed drawdown. Common characteristics of hydrofacies distribution of those realizations that preformed poorly include over-elongated sand and gravel channel bodies

that extend across the model area. These channels generally have widths greater then 20 meters. Also realizations that have narrow channel widths, generally less then 8 meters, and short channel lengths, generally less then 20 meters, performed poorly. Only those realizations that show discrete gravel intervals (8m by 30m) within moderately elongated sand bodies (10-15m by 40-60m) had the best results.

Given these general characteristics of channel bodies, it would be advisable to generate many realizations for the distribution of hydrofacies. Then filter through these realizations excluding those realizations that have over elongate or discrete channel characteristics. From the remaining realizations, only use those realizations that seem to accurately reflect the observed pumping test for modeling contaminant remediation.

Conclusions

Heterogeneity of sediments within an alluvial fan aquifer has a significant influence on the hydraulic response of the aquifer system. A long term pumping test at the Helipad Study Site shows that drawdown is along a preferential flow path. Results of this pumping test were used to evaluate four conceptual models. These included a homogeneous-layered model (HL), a homogeneous-layered model incorporating relatively low conductivity paleosol layers (HLP), a transition probability geostatistics simulation (TPG) for the model area following methods of Carle (1996), and a stratigraphic transition probability geostatistics simulation (STPG) following methods of Weissmann and Fogg (1999). Only those models that resolved heterogeneity at the hydrofacies level using transition probability geostatistics produced drawdown results that were consistent within the context of the heterogeneous alluvial fan system.

Simulated drawdown from the HL and HLP were able to confine drawdown within the main pumping layer, however the propagation of the drawdown cone was inconsistent with the observed results.

In development of conceptual models for subsurface characterization, large scale geologic features, such as unconformities separating stratigraphic units or regional contacts, are commonly incorporated. However, in many cases, heterogeneities at scales smaller then regional contacts are simply not incorporated. Local evaluation of an aquifer using analytical solutions to pumping tests may not be valid as was observed in this study. For the development of conceptual models used for site investigations, it is important to include detailed geologic information. Since the hydraulic response of an aquifer is directly related to the physical heterogeneity of the system, incorporating aspects of the geology is necessary for reasonable and realistic pumping test modeling. Our results show that incorporating heterogeneities at the hydrofacies level reasonably matched the hydraulic response of a heterogeneous alluvial fan aquifer.

Chapter Four

Conclusions

Alluvial Fan Heterogeneity

The general architecture of alluvial fans consists of sequences separated by unconformable surfaces. Within individual sequences, channel gravel and sand, which consist of highly permeable sand and gravel, form the main aquifer. Floodplain deposits which are generally composed of lower permeable sands and silts are deposited adjacent to these channel deposits. Pedogenically-altered sediments or paleosols which consist of fine-grained sand and clay may develop capping individual stratigraphic units. These units tend carbonate rich and typically have very low permeability and represent a prolonged hiatus in deposition. In alluvial fan development, rivers and streams may erode through these deposits. This provides conduits for fluid flow between sequences. At the Lawrence Livermore National Laboratory (LLNL), California, a similar structural architecture of channel, floodplain, debris, and paleosols exists.

Conceptual Model Development

Four conceptual models incorporating elements of the physical heterogeneity were developed. The first conceptual model is a homogeneous-layered model where stratigraphic sections were separated according to interpolated top paleosol surfaces. This type of model was developed to resemble the HSU model used by LLNL. The second conceptual model was a modified version of the first in that paleosol units were incorporated between stratigraphic units. The third conceptual model used transition

probability geostatistics with a Markov chain to generate the spatial distribution of hydrofacies where each of the individual stratigraphic units was simulated simultaneously (Appendix F). This approach incorporated geologic information in terms of an average channel length, width and orientation. The fourth conceptual model used transition probability geostatistics with a Markov chain model to generate simulations over the entire block volume for each stratigraphic and paleosol unit (Appendix F). Corresponding stratigraphic intervals bounded by paleosol surfaces were pulled out of these full block volumes and merged to produce a final realization for the distribution of hydrofacies. This approach incorporated the most geologic information in comparison to other models developed. In total twenty-five of these realizations were generated.

Evaluation of Conceptual Models

For evaluation of each conceptual model, drawdown histories were simulated using Modflow-2000 (Harbaugh *et al.*, 2000; Hill *et al.*, 2000). These simulated results should reflect the differential hydraulic response observed. The Grid used within the groundwater model was 360m by 310m by 39m (x, y, and z respectively). Grid cells were refined around pumping wells and consisted of approximately 5 millions cells. Eastern and western boundaries were assigned as constant head boundaries, northern and southern boundaries were assigned as no flow. These boundary conditions were assigned to generate a groundwater gradient that was representative of the true system (Appendix G). From numerical groundwater models, drawdown was observed from 1650 series wells. Evaluation of conceptual models showed that the heterogeneity within the alluvial aquifer had a significant influence on the hydraulic response of the system.

A long term pumping test at the Helipad Study Site shows that drawdown is along a preferential flow path. Only those models that incorporated finer scales of heterogeneity using transition probability geostatistics produced drawdown results that were consistent within the context of the heterogeneous alluvial fan system. Simulated drawdown from both homogeneous models were able to confine drawdown within the main pumping layer, however the propagation of the drawdown cone was inconsistent with the observed results.

Calibration of hydraulic properties for hydrofacies within the stratigraphic transition probability geostatistical simulation was able to produce drawdown curves that were similar to the observed. Simulated drawdown from the other twenty-four realizations of this model type produced variable results (Appendix H). It was observed that there were common characteristics to those realizations that preformed well. Those realizations that showed discrete gravel intervals (8m by 30m) within moderately elongated sand bodies (10-15m by 40-60m) produces the best results.

Analytical Solution Evaluation

An analytical solution based on observed drawdown in 1650 series wells was developed (Appendix D). Results from this solution produced fields of transmissivity, storage coefficient, and hydraulic conductivity values within the central Helipad study. Results of this analytical solution were contrary to the observed geology. The geology indicated a gravel channel passing through wells located to the west of the Helipad Site and a sand channel passing through the other wells. Since gravels generally have a higher permeability then sands, it would be expected that the results of the solution would also

indicate this. However, the results indicate a zone of high conductance passing through the central wells at the Helipad Site. These results indicate analytical solutions are inaccurate within the context of this system.

Future Considerations

Given the general characteristics of transition probability geostatistical simulations that preformed well, future simulations generated with transition probability geostatistics should be analyzed to filter out realizations that have poorly performing characteristics. From the remaining realizations, only use those realizations that seem to reasonably reflect the observed pumping test when using this type of model for remediation efforts.

Due to time limitations, other issues were not able to be analyzed in great detail within this study. These include the effects of defining hydrofacies based on sediment descriptions. Within individual hydrofacies, hydraulic properties are variable. In core, a gravel may be identified and is given a gravel hydrofacies classification. This classification has the highest hydraulic conductivity. However, a range of clay content was observed in described gravels. This ranged form little clay to very thick clay coats. So by defining gravel, which contains thick clay coats, as a gravel hydrofacies may be inaccurate. Assigning a hydrofacies classification that has lower associated hydraulic conductivities may be more reasonable. In future, realizations, it might be advisable to incorporate hydraulic variability within individual hydrofacies. Within this study, hydrofacies were assigned based on identified sediment type.

There were also concerns with the simulation quenching routine. Simulation quenching of large models did not reach the objective function assigned within the TPSIM parameter file. This may be due to the relatively high angle (30^{o}+) between the grid orientation and the Markov chain model orientation (Weissmann, personal comment). This may account for some of the poor drawdown result for the transition probability geostatistical simulations.

Future work may allow groundwater models be optimized with parameter estimation routines that can account for updating well files in highly heterogeneous systems as well as optimize to drawdown instead of head values. Finally, both tracer tests and pumping tests were conducted for the Helipad Site. However, time limitations prevented using tracer data for evaluating conceptual models. Running particle transport models is recommended to further evaluate conceptual models developed within this study.

Appendix A

Core Descriptions

Core description for wells located in the model area followed the previous work conducted by Weissmann (2001) with addition of wells 220, 653, 906, 1205, 1206, 1207, 1208, 1223, 1303, 1306, 1401, and 1416. Core descriptions for wells 1307, 1250, 1251, 1252, 1253, 1254, 1255, 1550, 1551, 1552, 1553, 1650, 1653, 1655, and 1657 previously described by Weissmann (2001) were also used for evaluation of this site.

Four hydrofacies are denoted. These include the *gravel* hydrofacies (Figure A.1), *sand* hydrofacies (Figure A.2), *silty sand* hydrofacies (Figure A.3), and *paleosol* hydrofacies (Figure A.4). Gravel and sand hydrofacies are interpreted to be channel deposits, silty sand hydrofacies are interpreted to be overbank deposits, and paleosol hydrofacies are interpreted to represent a depositional hiatus where alluvial fan surfaces are exposed allowing soil development. Core descriptions are presented in Figures A.5 through A.16.

Gravel Facies

Figure A.1: Gravel Facies

- Clast supported.
- Massive.
- Typically contains thick, reddish, clay coats on grains.

Sand Facies

Figure A.2: Sand Facies

- Typically fine to medium sand, with some coarse to very coarse sand and/or gravel, commonly silty.
- Grains are typically subrounded.
- Well to moderately sorted with some clay coats on grains.

Silty Sand Facies

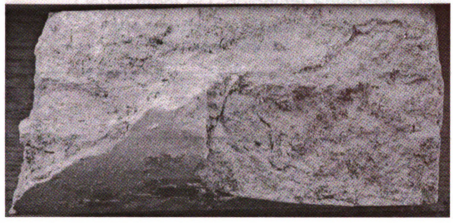

Figure A.3: Silty Sand Facies

- Massive.
- Common root traces.
- Typically brown (10YR) with mottling around root traces.
- Light pedogenic alteration (thin to no clay coats, minor MnO, no visible pedogenic structures).

Paleosol Facies

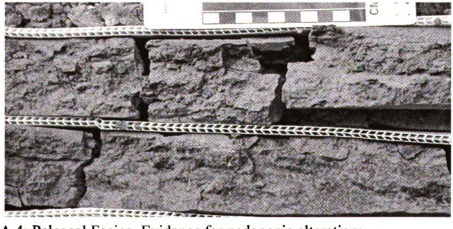

Figure A.4: Paleosol Facies -Evidence for pedogenic alteration:

- Thick clay coats on ped faces.
- Preservation of soil structures (blocky to prismatic).
- Reddish color (5 to 7.5 YR typical).
- Common Mn- and Fe-oxides.
- Common carbonate in upper paleosols (above 50 ft) and Lower Livermore. Formation; Carbonate is present in lower paleosols (below 50 ft), however are less common.
- Occasional root traces.

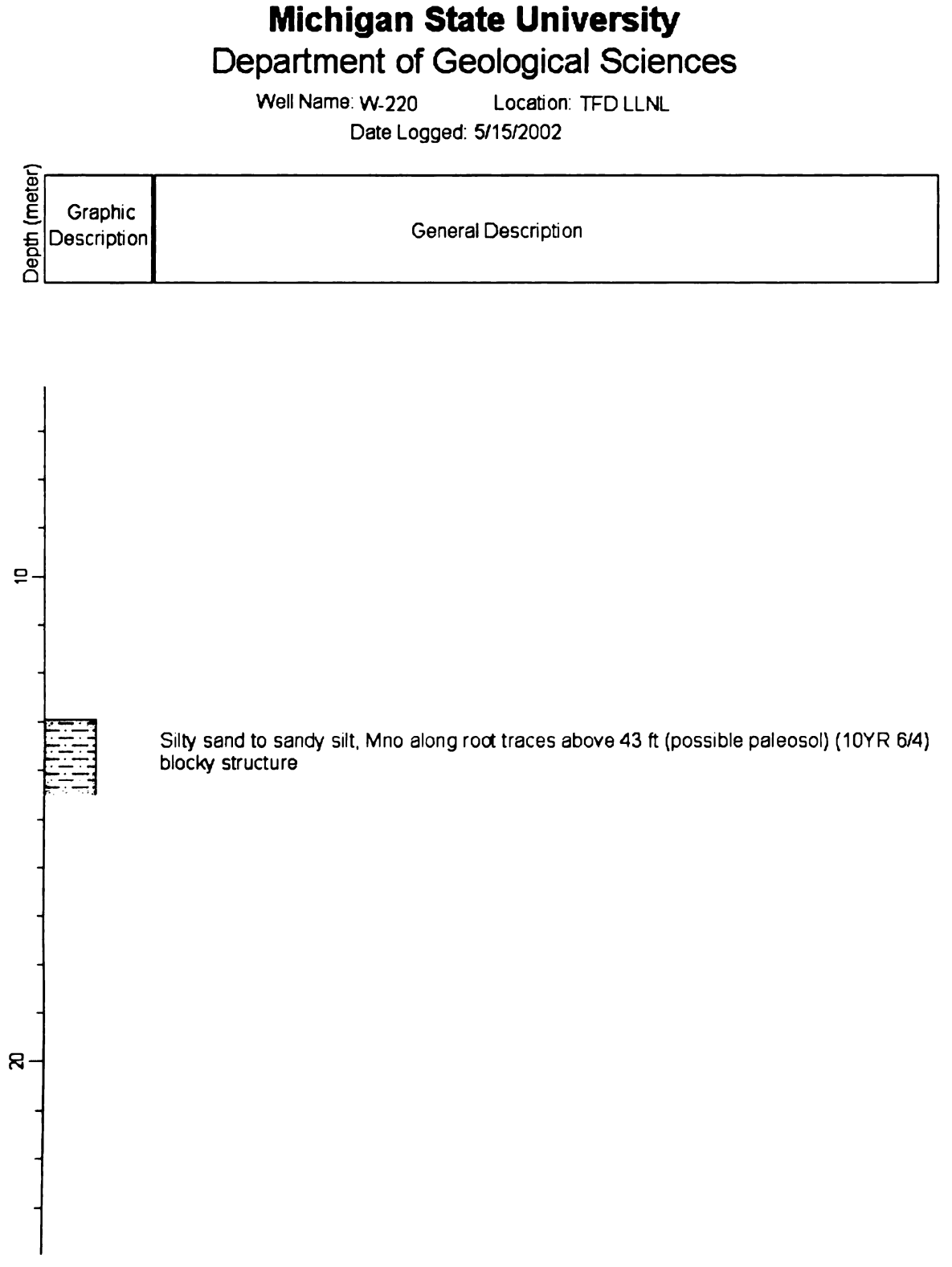

Figure A.5a: Core description of facies identified in well 220.

Michigan State University

Department of Geological Sciences

Well Name: W-220 Location: TFD LLNL

Date Logged: 5/15/2002

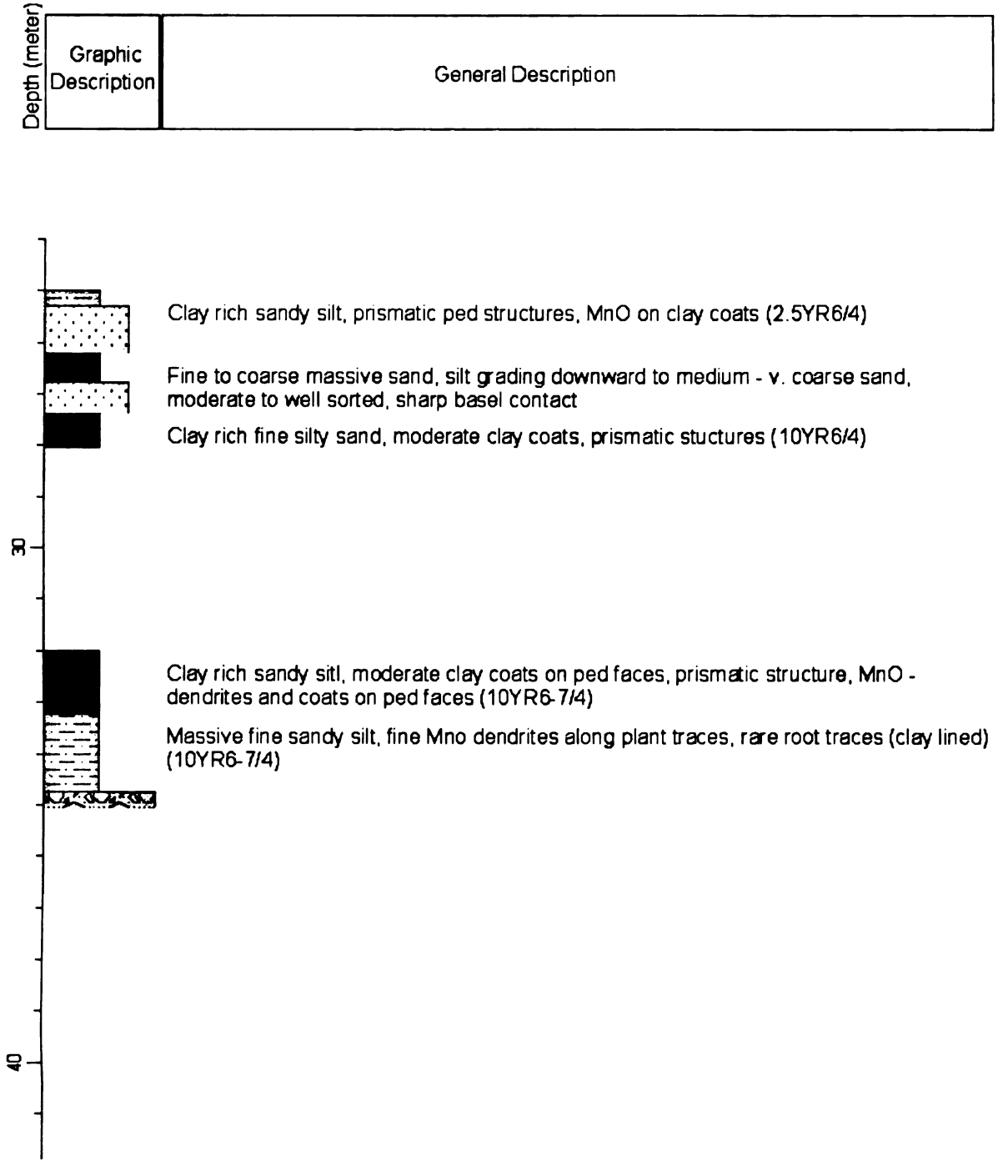

Figure A.5b: Core description of facies identified in well 220 continued.

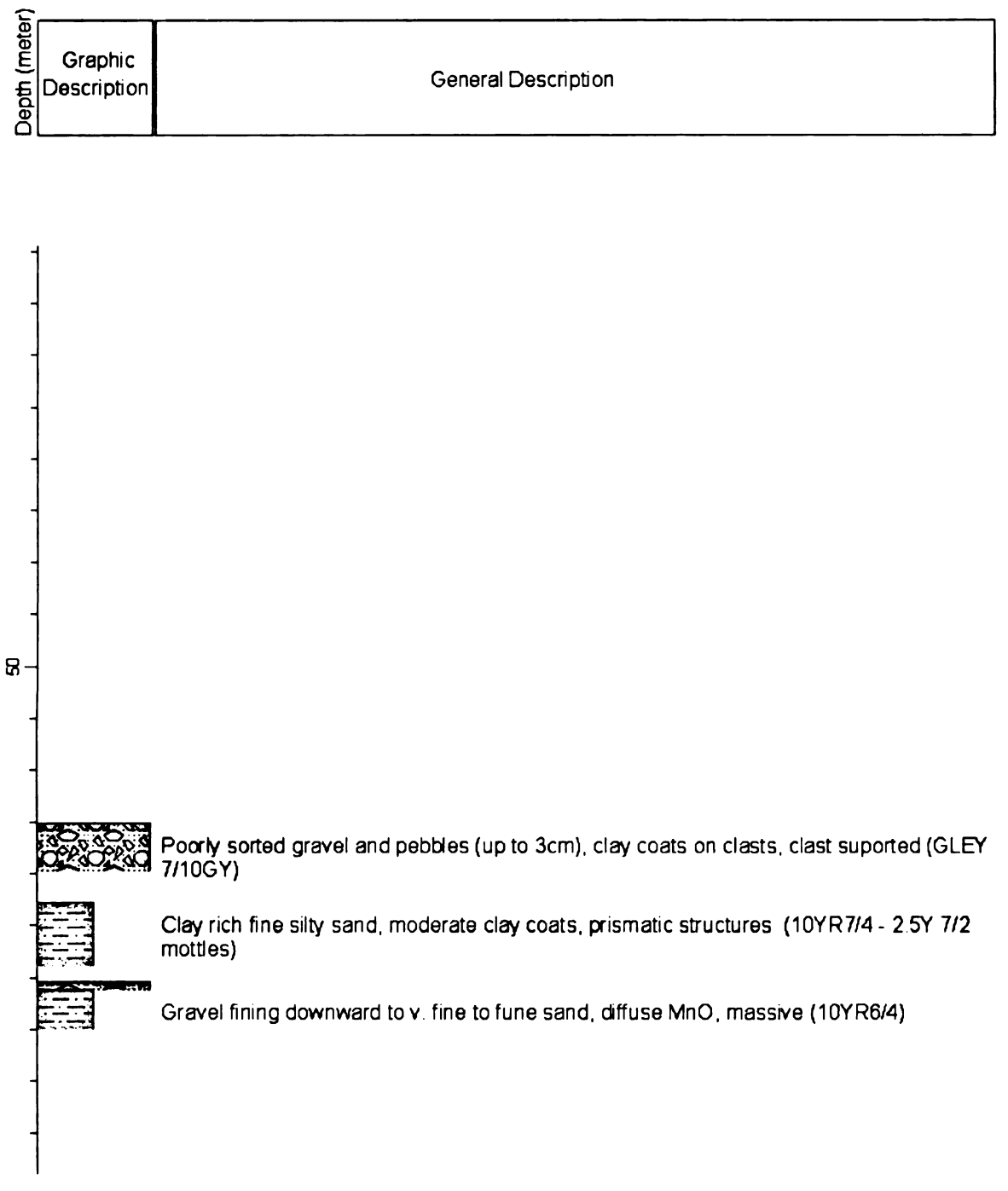

Figure A.5c: Core description of facies identified in well 220 continued.

Michigan State University

Department of Geological Sciences

Well Name: W-653 Location: TFD LLNL

Date Logged: 6/5/2002

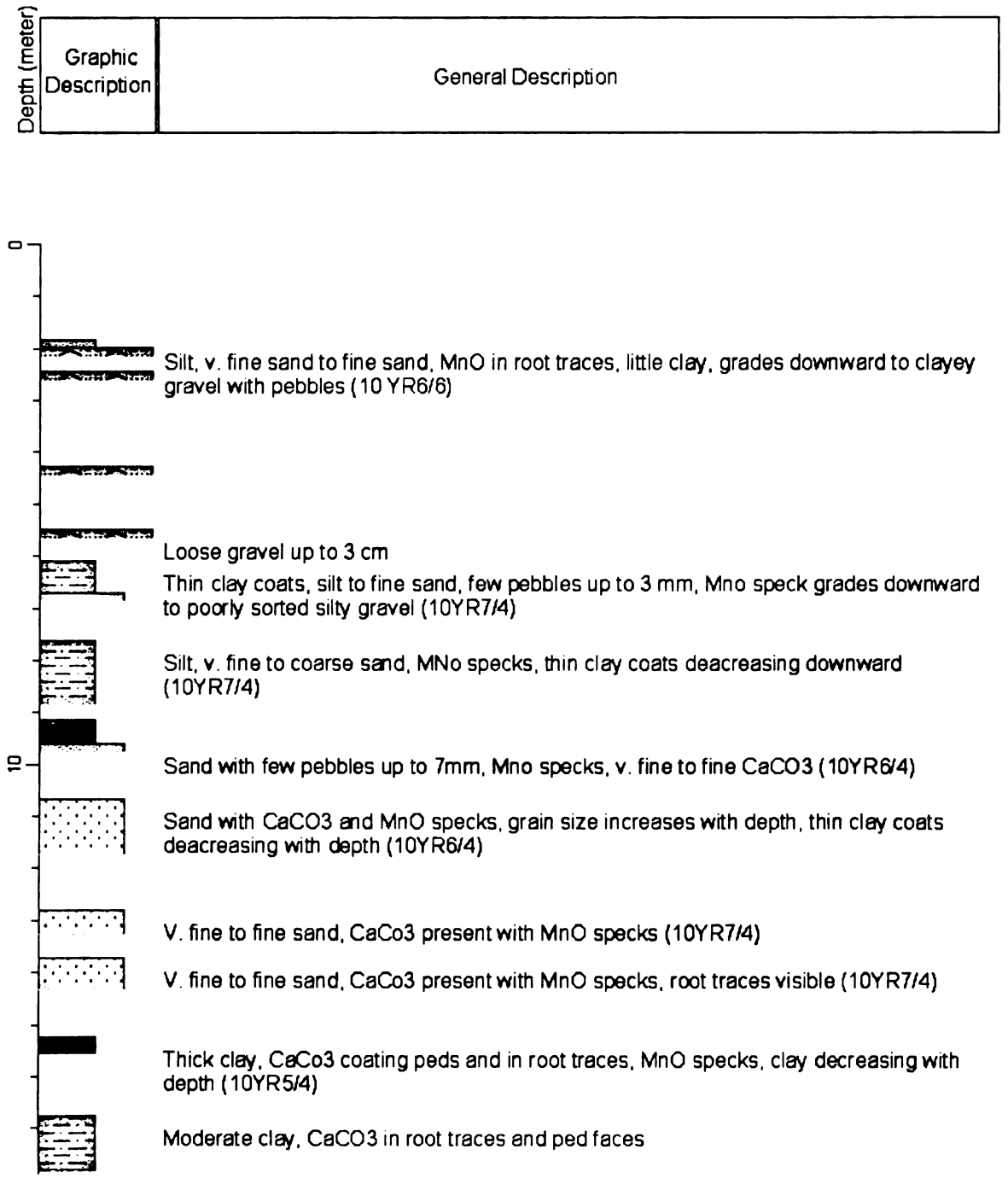

Figure A.6a: Core description of facies identified in well 653.

Michigan State University

Department of Geological Sciences

Well Name: W-653 Location: TFD LLNL

Date Logged: 6/5/2002

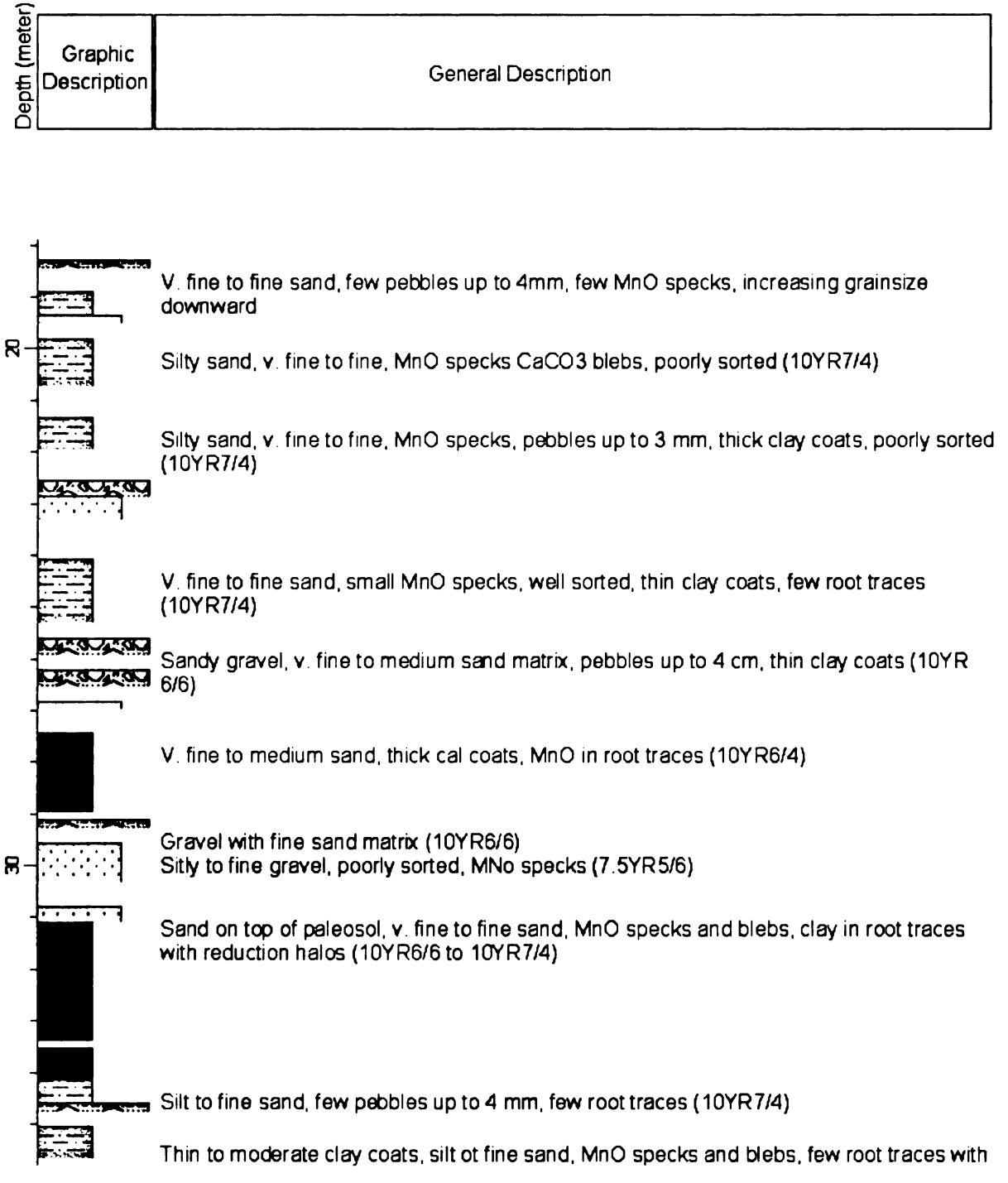

Figure A.6b: Core description of facies identified in well 653 continued.

Michigan State University

Department of Geological Sciences

Well Name: W-653 Location: TFD LLNL

Date Logged: 6/5/2002

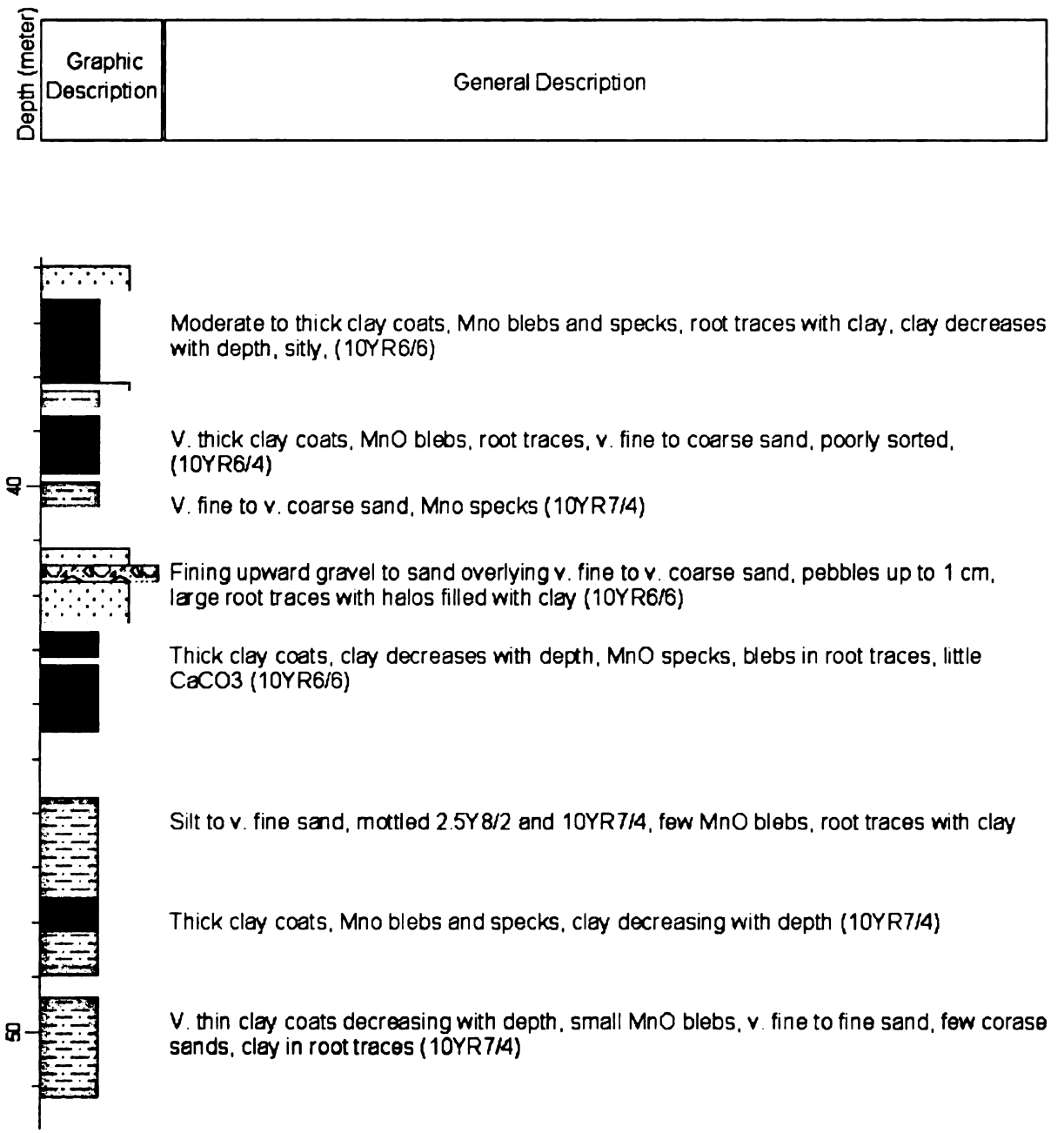

Figure A.6c: Core description of facies identified in well 653 continued.

Michigan State University

Department of Geological Sciences

Well Name: W-906 Location: TFD LLNL

Date Logged: 6/4/2002

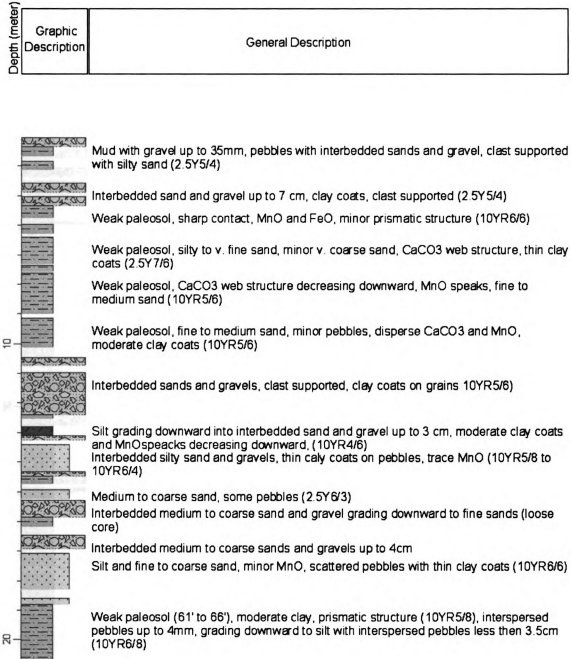

Figure A.7a: Core description of facies identified in well 653 continued.

Michigan State University

Department of Geological Sciences

Well Name: W-906 Location: TFD LLNL

Date Logged: 6/4/2002

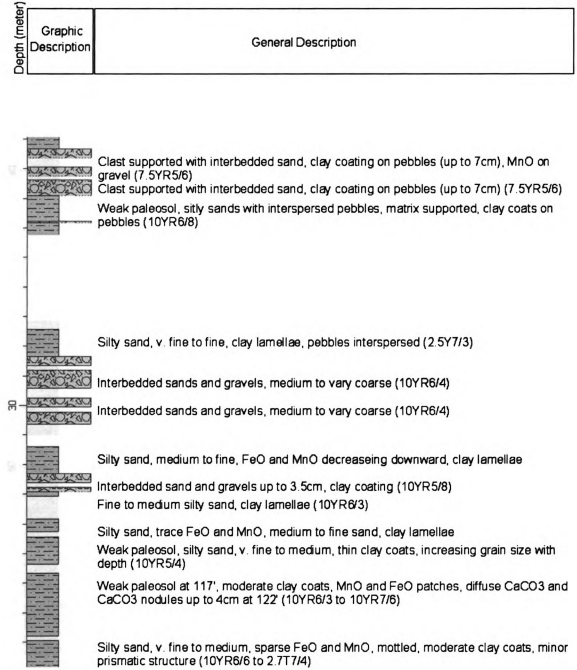

Figure A.7b: Core description of facies identified in well 906 continued.

Michigan State University

Department of Geological Sciences

Well Name: W-906 Location: TFD LLNL

Date Logged: 6/4/2002

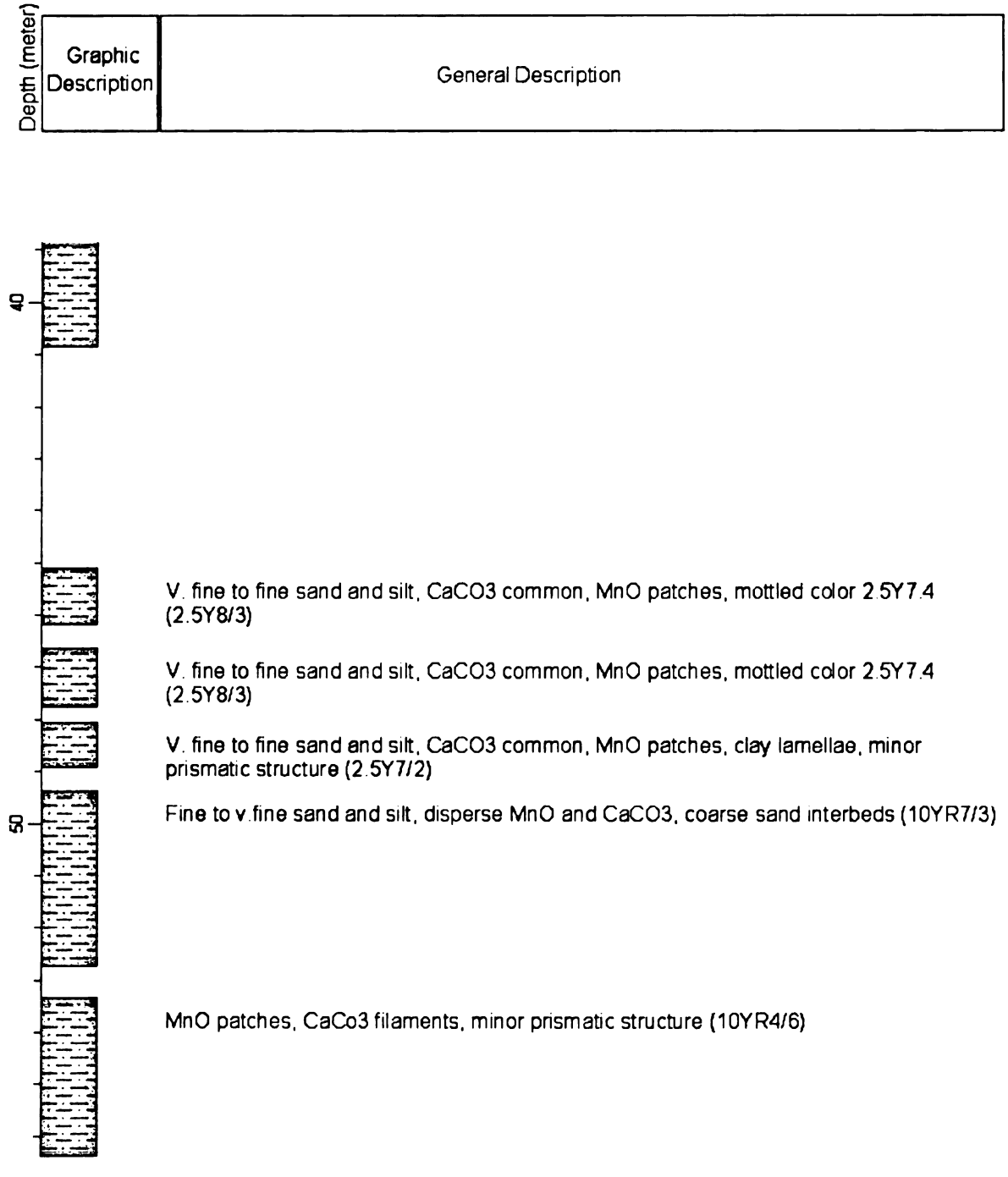

Figure A.7c: Core description of facies identified in well 906 continued.

Michigan State University

Department of Geological Sciences

Well Name: W-1205 Location: TFD LLNL

Date Logged: 6/5/2002

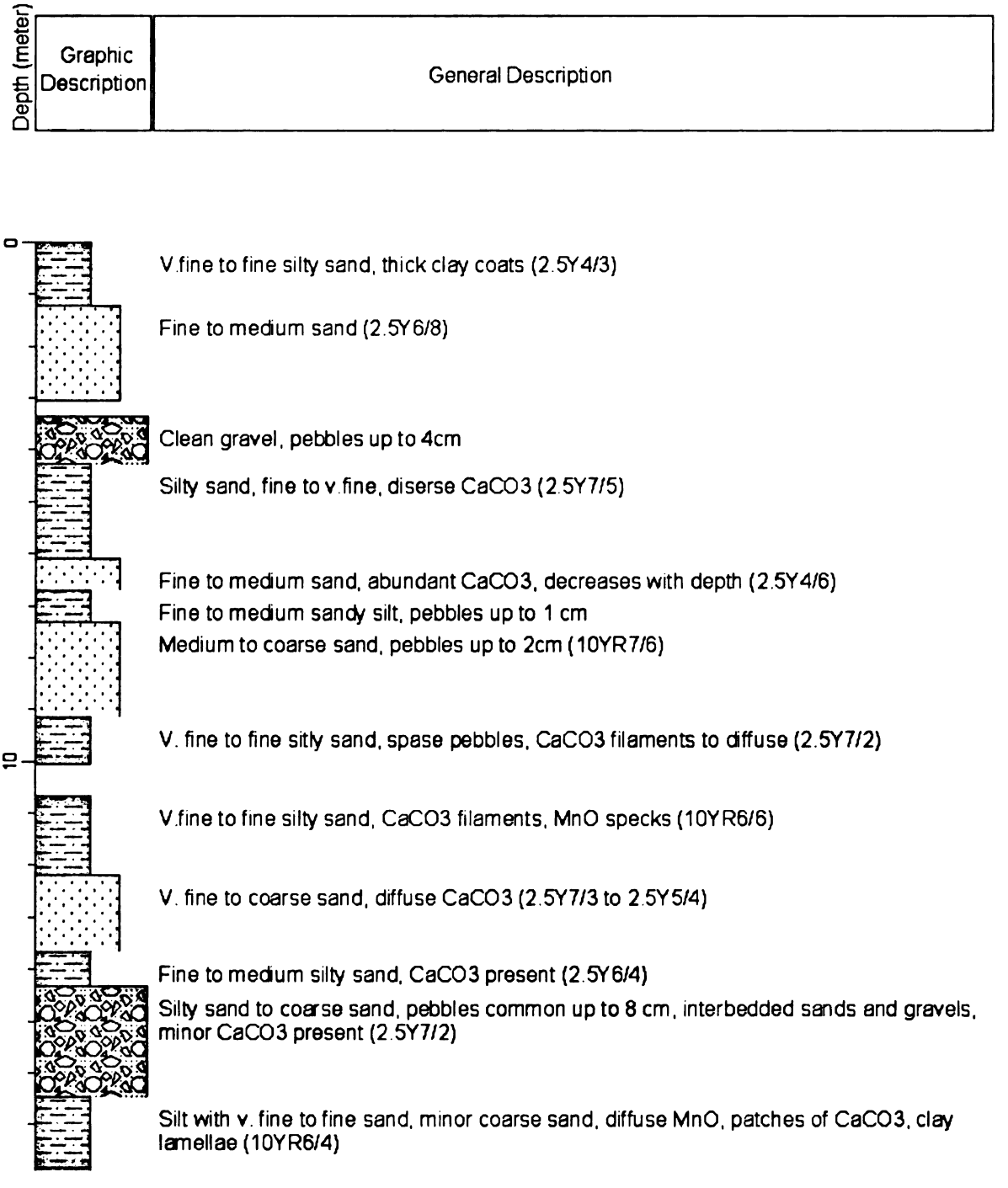

Figure A.8a: Core description of facies identified in well 1205.

Michigan State University

Department of Geological Sciences

Well Name: W-1205 Location: TFD LLNL

Date Logged: 6/5/2002

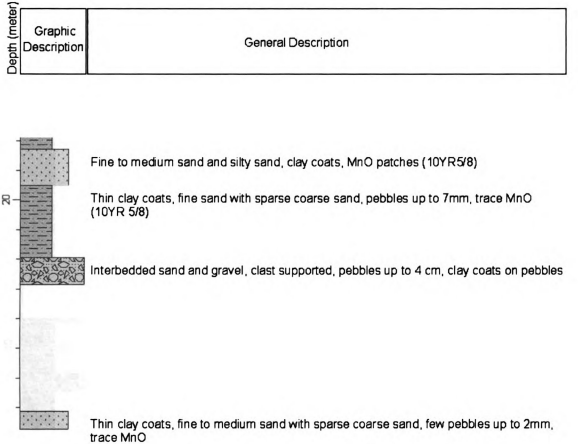

Figure A.8b: Core description of facies identified in well 1205 continued.

Michigan State University
Department of Geological Sciences

Well Name: W-1206 Location: TFD LLNL
Date Logged: 6/6/2002

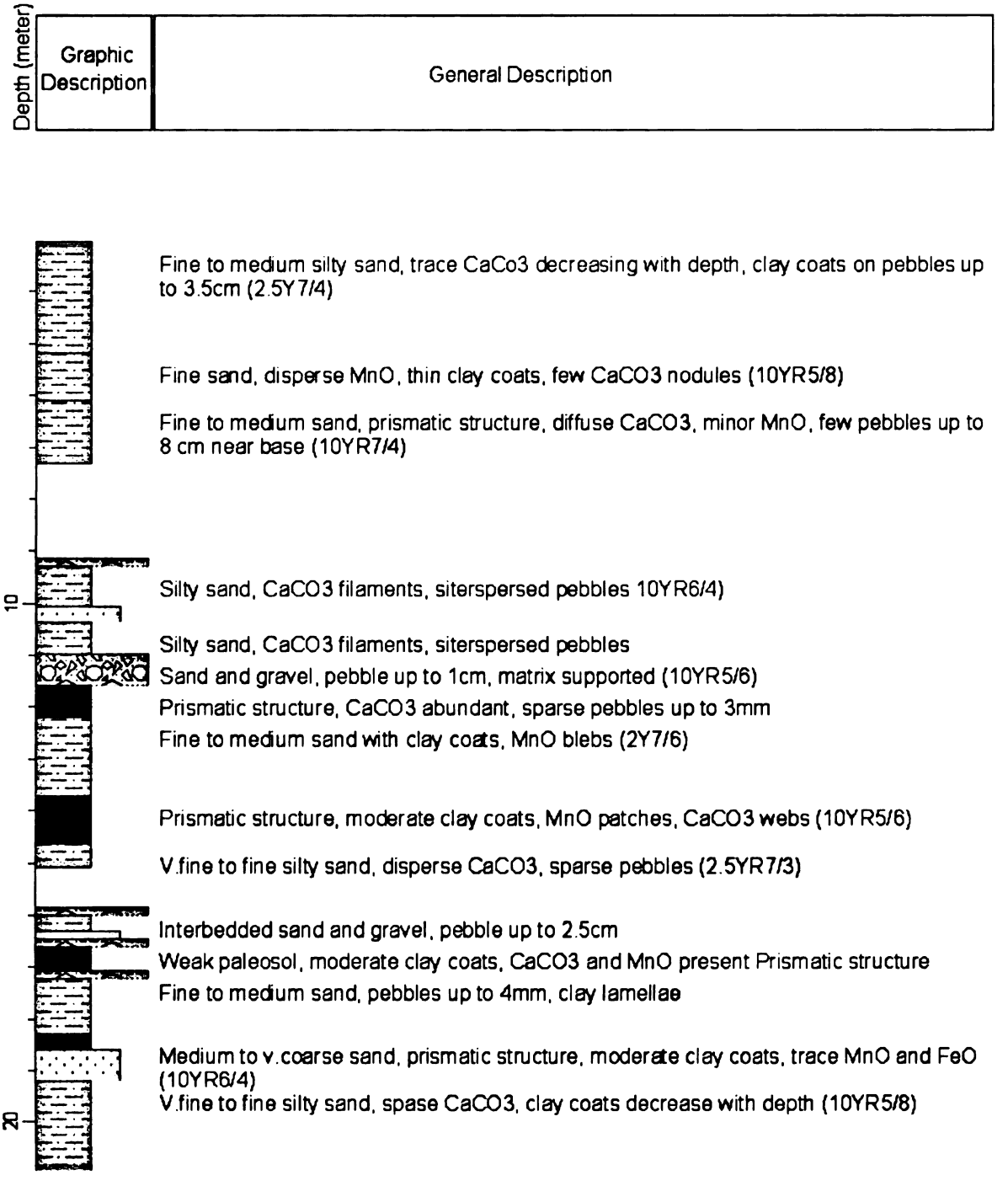

Figure A.9a: Core description of facies identified in well 1206.

Michigan State University
Department of Geological Sciences

Well Name: W-1206 Location: TFD LLNL
Date Logged: 6/6/2002

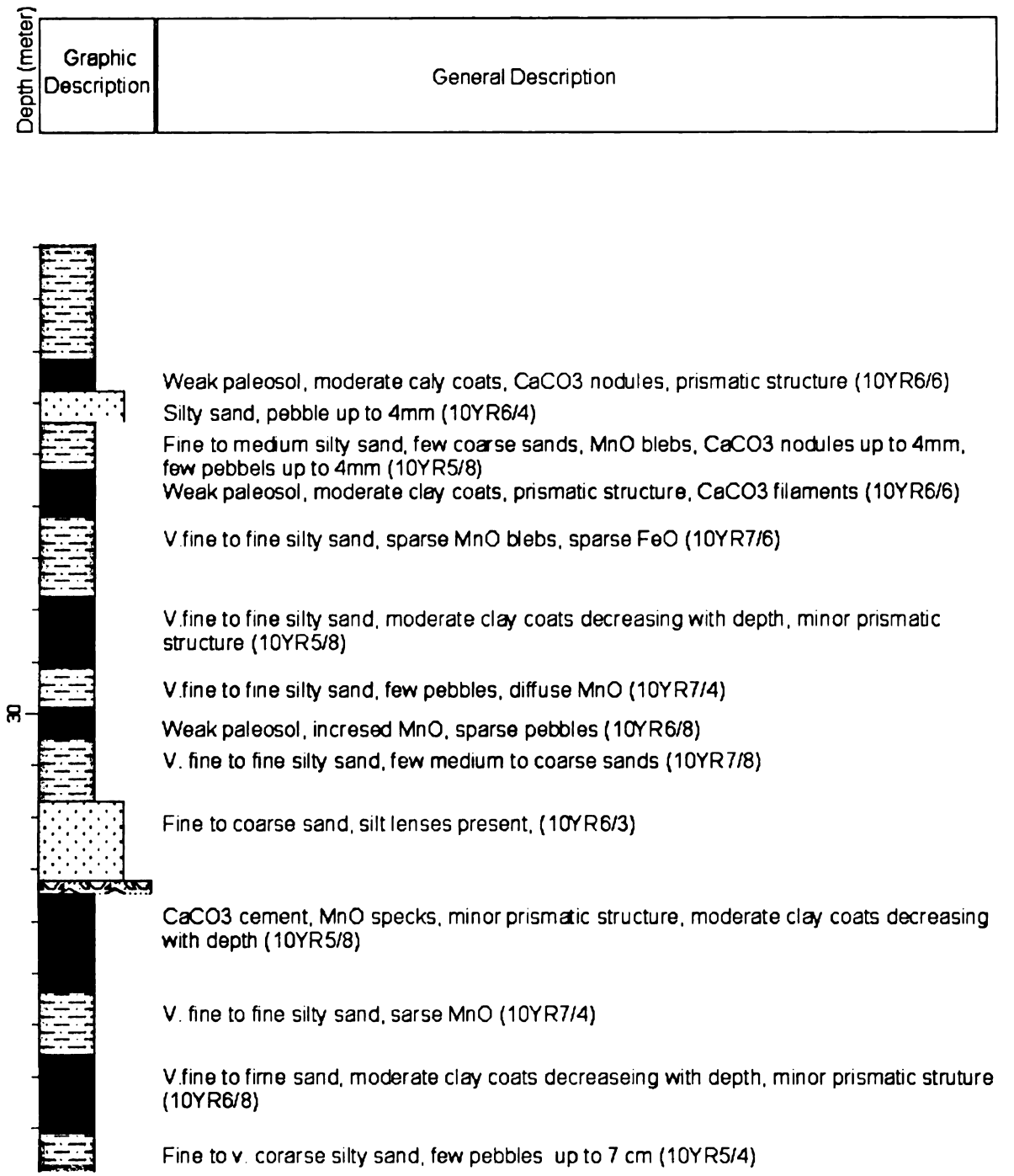

Figure A.9b: Core description of facies identified in well 1206 continued.

Michigan State University

Department of Geological Sciences

Well Name: W-1206 Location: TFD LLNL

Date Logged: 6/6/2002

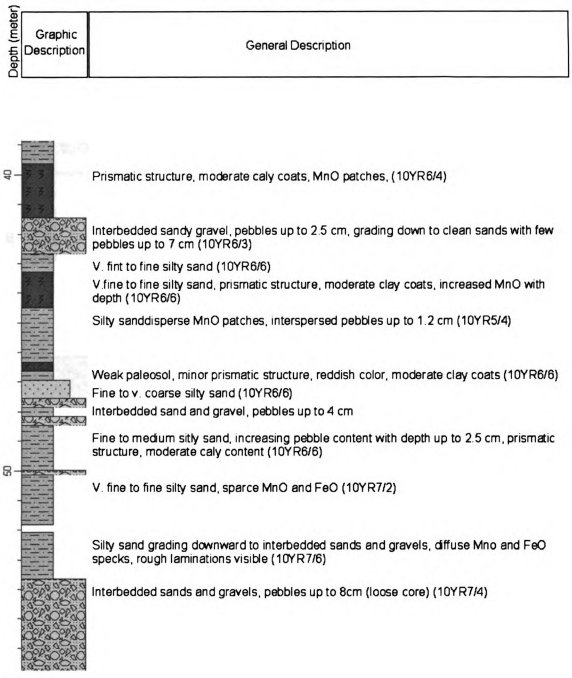

Figure A.9c: Core description of facies identified in well 1206 continued.

Michigan State University

Department of Geological Sciences

Well Name: W-1206 Location: TFD LLNL

Date Logged: 6/6/2002

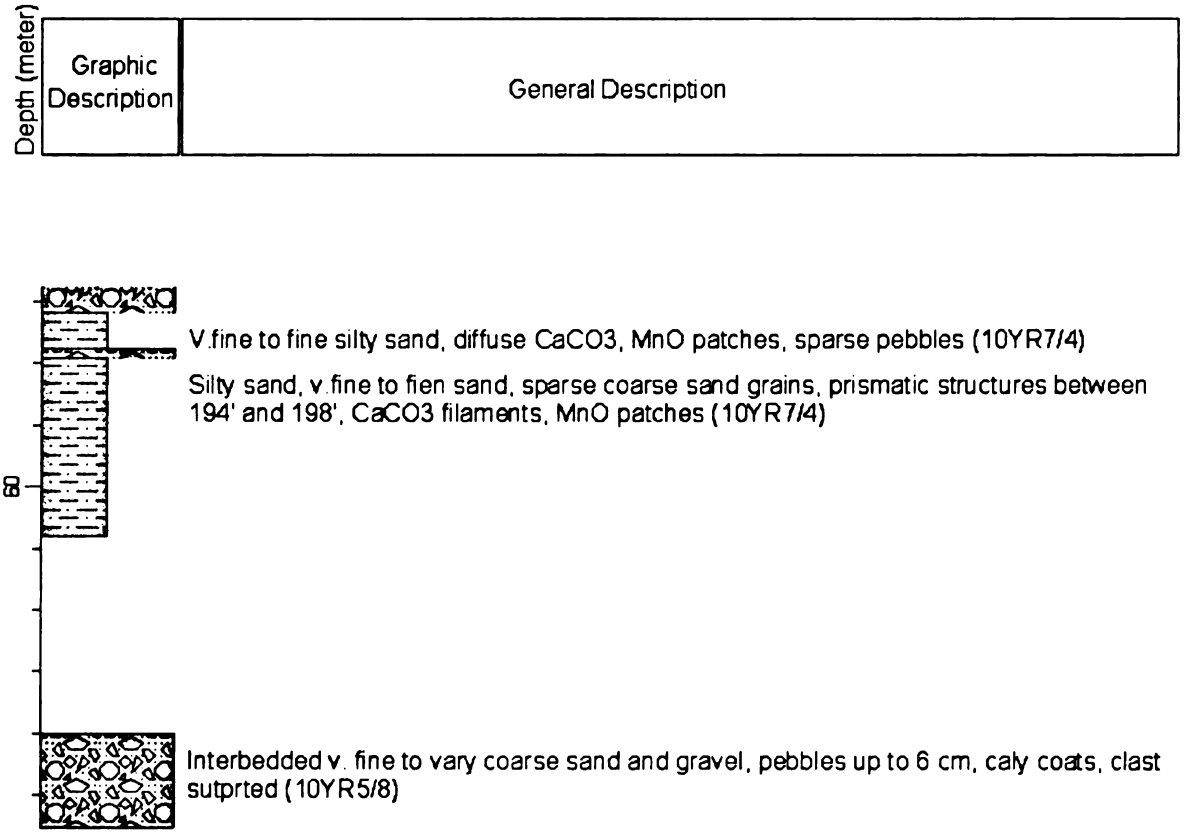

Figure A.9d: Core description of facies identified in well 1206 continued.

Michigan State University

Department of Geological Sciences

Well Name: W-1207 Location: TFD LLNL

Date Logged: 6/4/2002

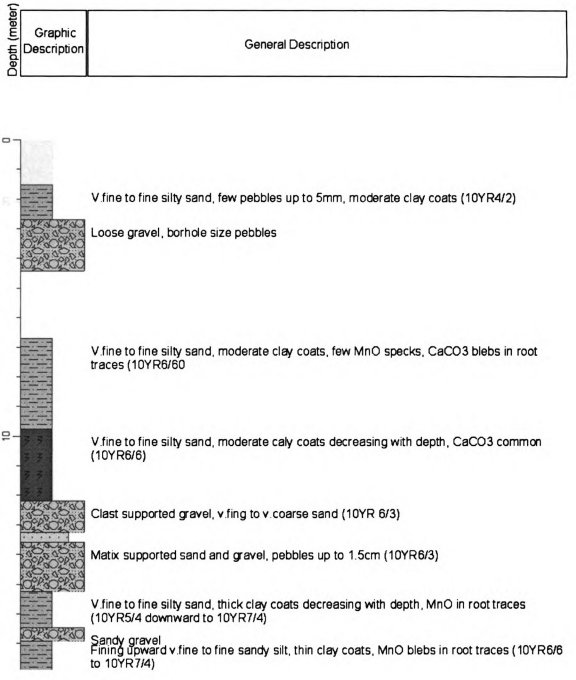

Figure A.10a: Core description of facies identified in well 1207.

Michigan State University

Department of Geological Sciences

Well Name: W-1207 Location: TFD LLNL

Date Logged: 6/4/2002

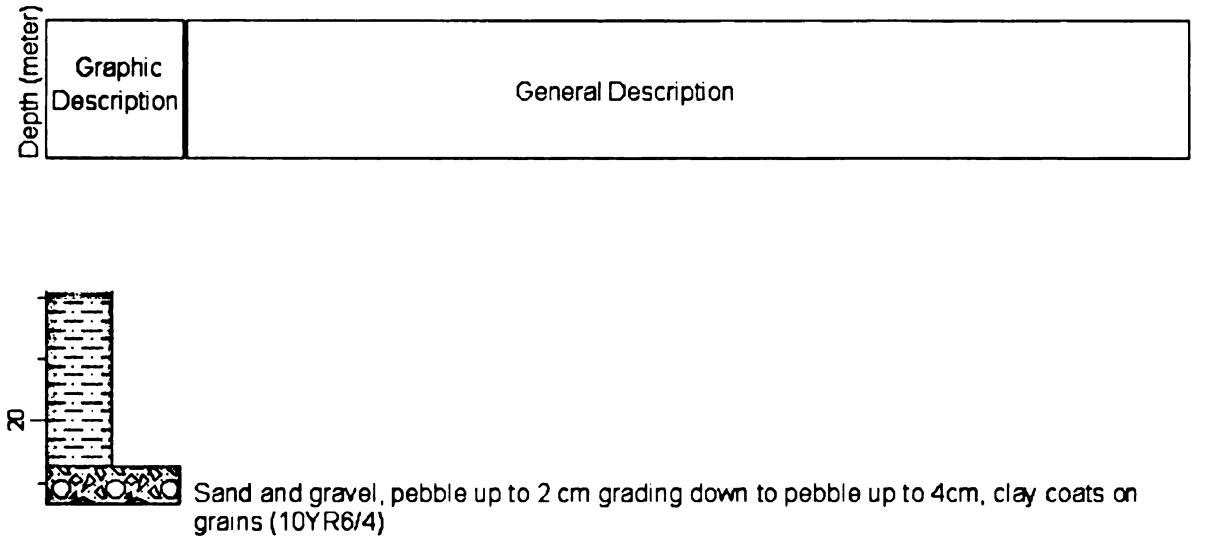

Figure A.10b: Core description of facies identified in well 1207 continued.

Michigan State University

Department of Geological Sciences

Well Name: W-1208 Location: TFD LLNL

Date Logged: 6/6/2002

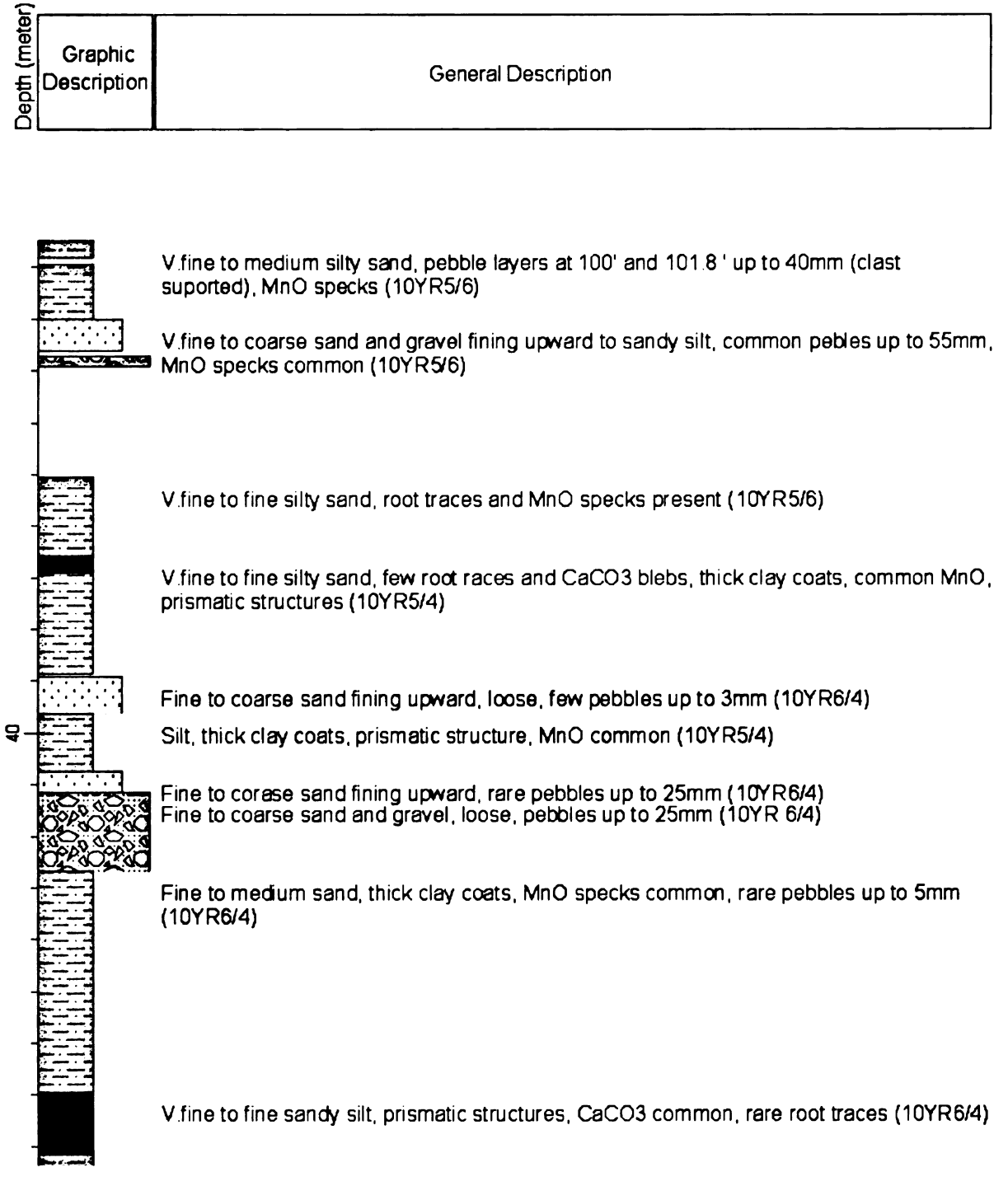

Figure A.11a: Core description of facies identified in well 1208.

Michigan State University

Department of Geological Sciences

Well Name: W-1208 Location: TFD LLNL

Date Logged: 6/6/2002

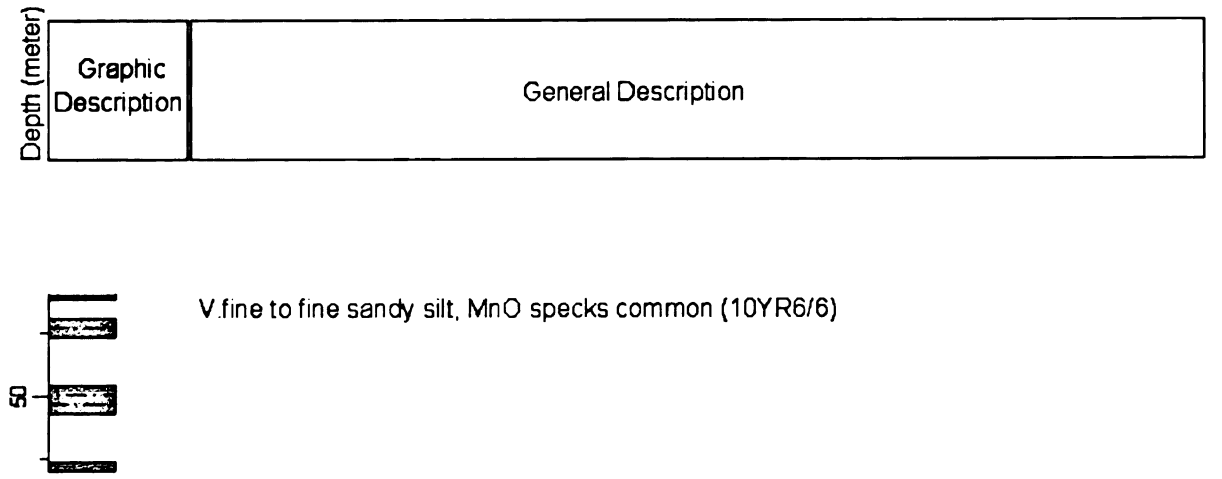

Figure A.11b: Core description of facies identified in well 1208 continued.

Michigan State University

Department of Geological Sciences

Well Name: W-1223 Location: TFD LLNL

Date Logged: 5/14/2002

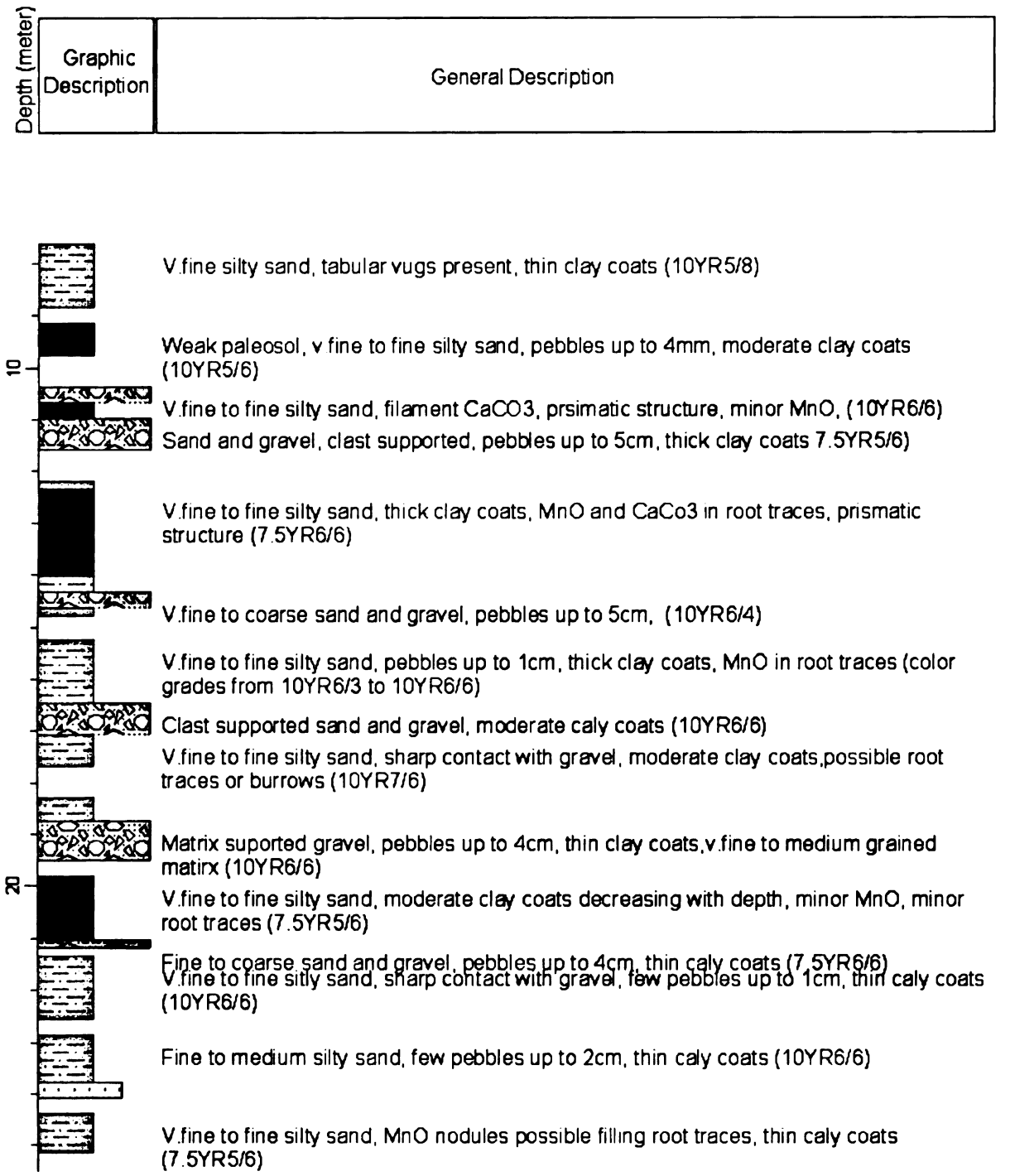

Figure A.12a: Core description of facies identified in well 1223.

Michigan State University

Department of Geological Sciences

Well Name: W-1223 Location: TFD LLNL

Date Logged: 5/14/2002

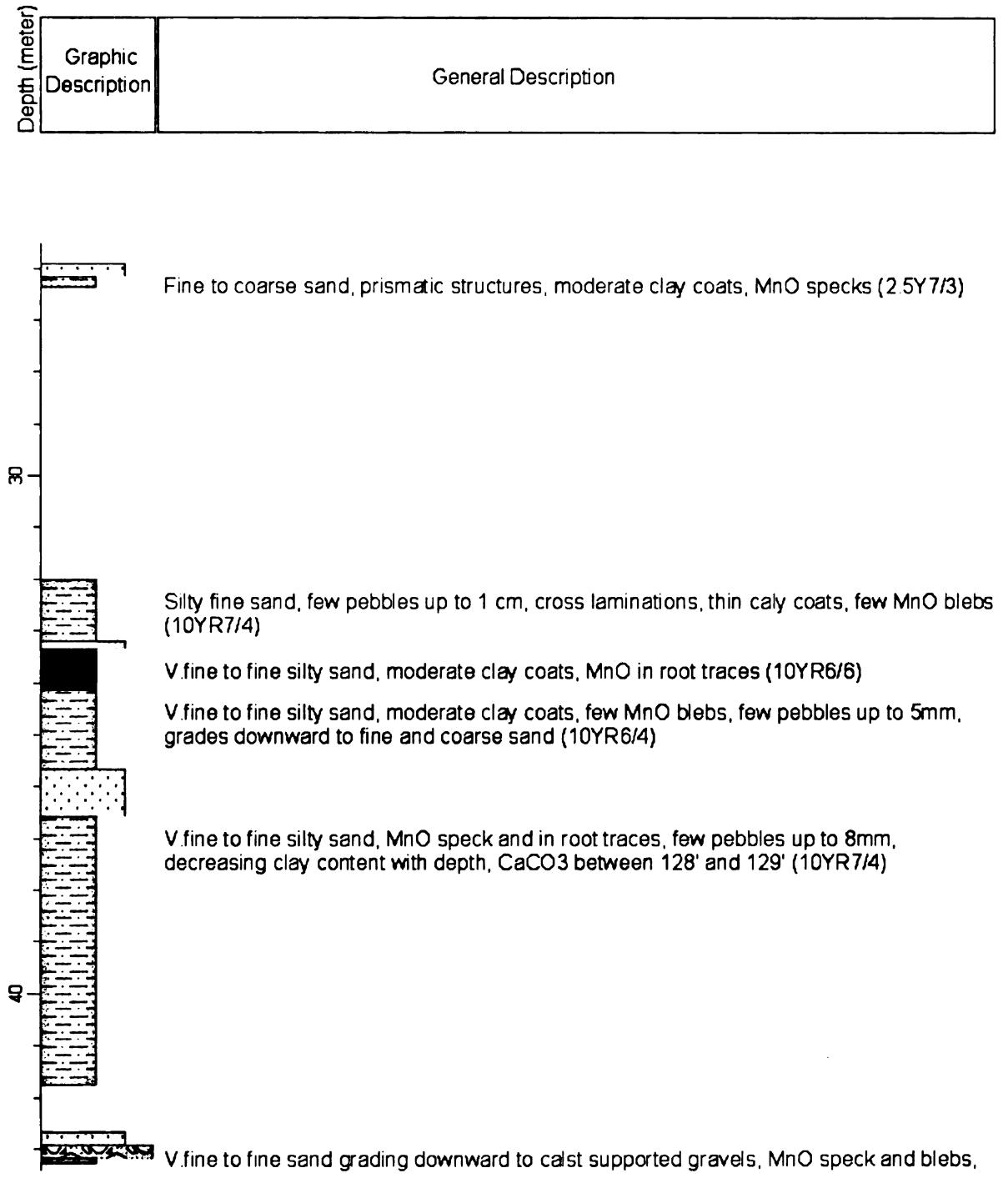

Figure A.12b: Core description of facies identified in well 1223 continued.

Michigan State University

Department of Geological Sciences

Well Name: W-1223 Location: TFD LLNL

Date Logged: 5/14/2002

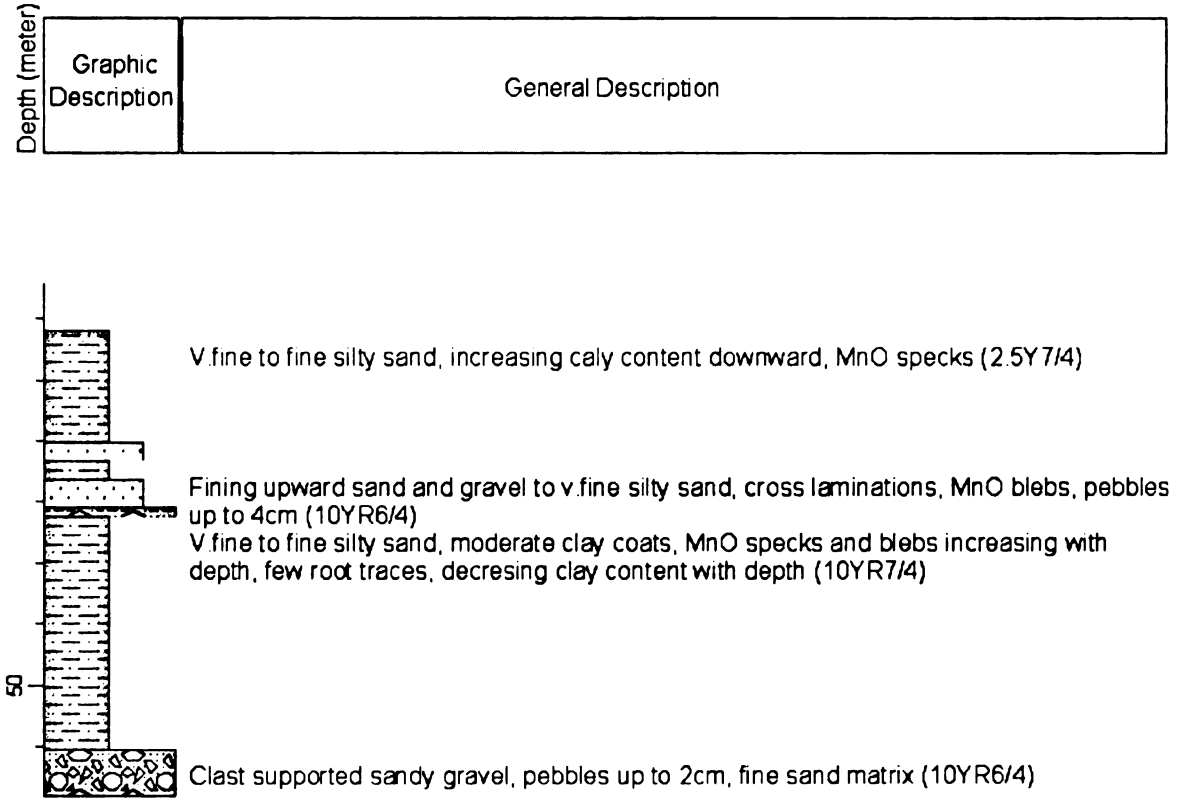

Figure A.12c: Core description of facies identified in well 1223 continued.

Michigan State University

Department of Geological Sciences

Well Name: W-1303 Location: TFD LLNL

Date Logged: 5/17/2002

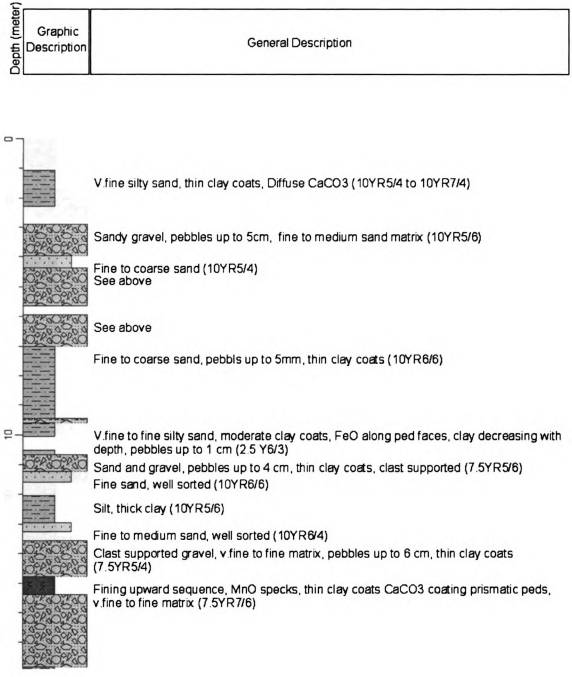

Figure A.13a: Core description of facies identified in well 1303.

Michigan State University

Department of Geological Sciences

Well Name: W-1303 Location: TFD LLNL

Date Logged: 5/17/2002

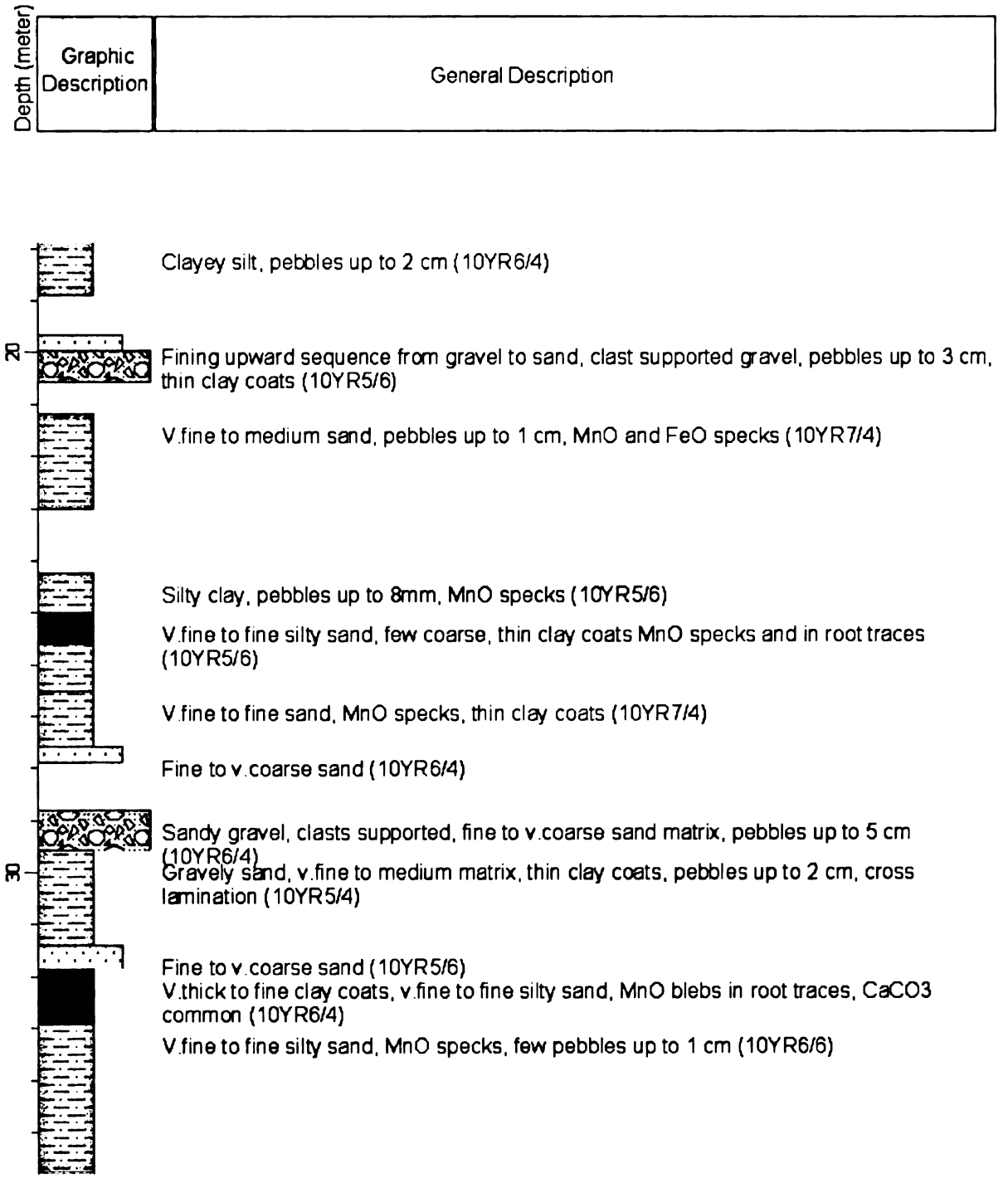

Figure A.13b: Core description of facies identified in well 1303 continued.

Michigan State University

Department of Geological Sciences

Well Name: W-1303 Location: TFD LLNL

Date Logged: 5/17/2002

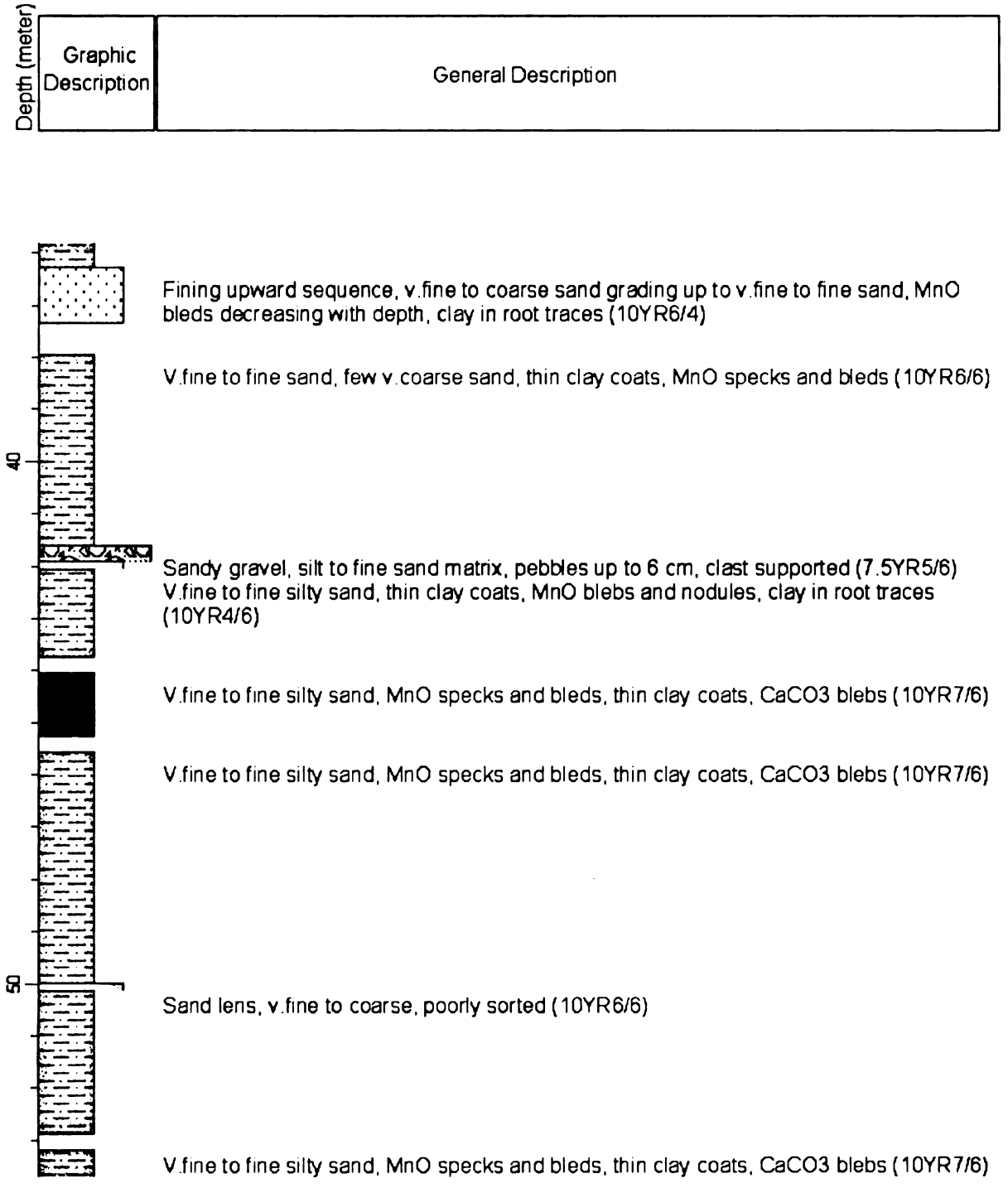

Figure A.13c: Core description of facies identified in well 1303 continued.

Michigan State University

Department of Geological Sciences

Well Name: W-1303 Location: TFD LLNL

Date Logged: 5/17/2002

Depth (meter)	Graphic Description	General Description
	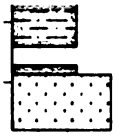	Fining upward sequence, v.fine to fine sand grading down to fine to coarse sand, pebbles up to 3 cm (5Y8/1)

Figure A.13d: Core description of facies identified in well 1303 continued.

Michigan State University

Department of Geological Sciences

Well Name: W-1306 Location: TFD LLNL

Date Logged: 5/14/2002

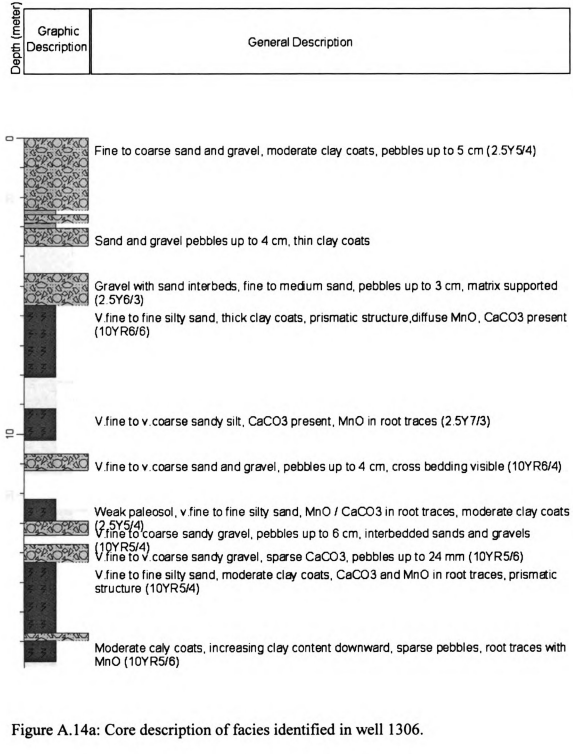

Figure A.14a: Core description of facies identified in well 1306.

Michigan State University

Department of Geological Sciences

Well Name: W-1306 Location: TFD LLNL

Date Logged: 5/14/2002

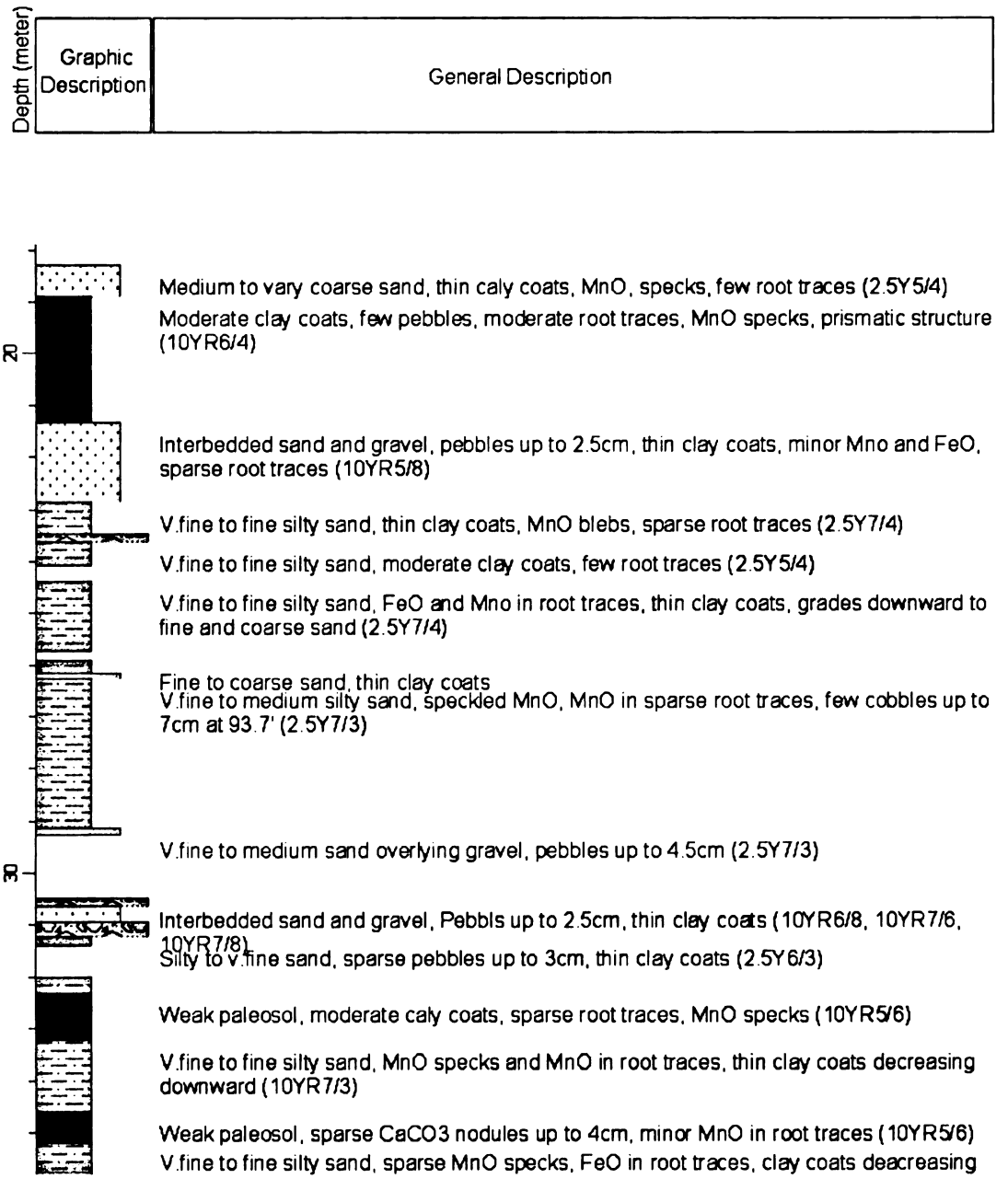

Figure A.14b: Core description of facies identified in well 1306 continued.

Michigan State University
Department of Geological Sciences

Well Name: W-1306 Location: TFD LLNL
Date Logged: 5/14/2002

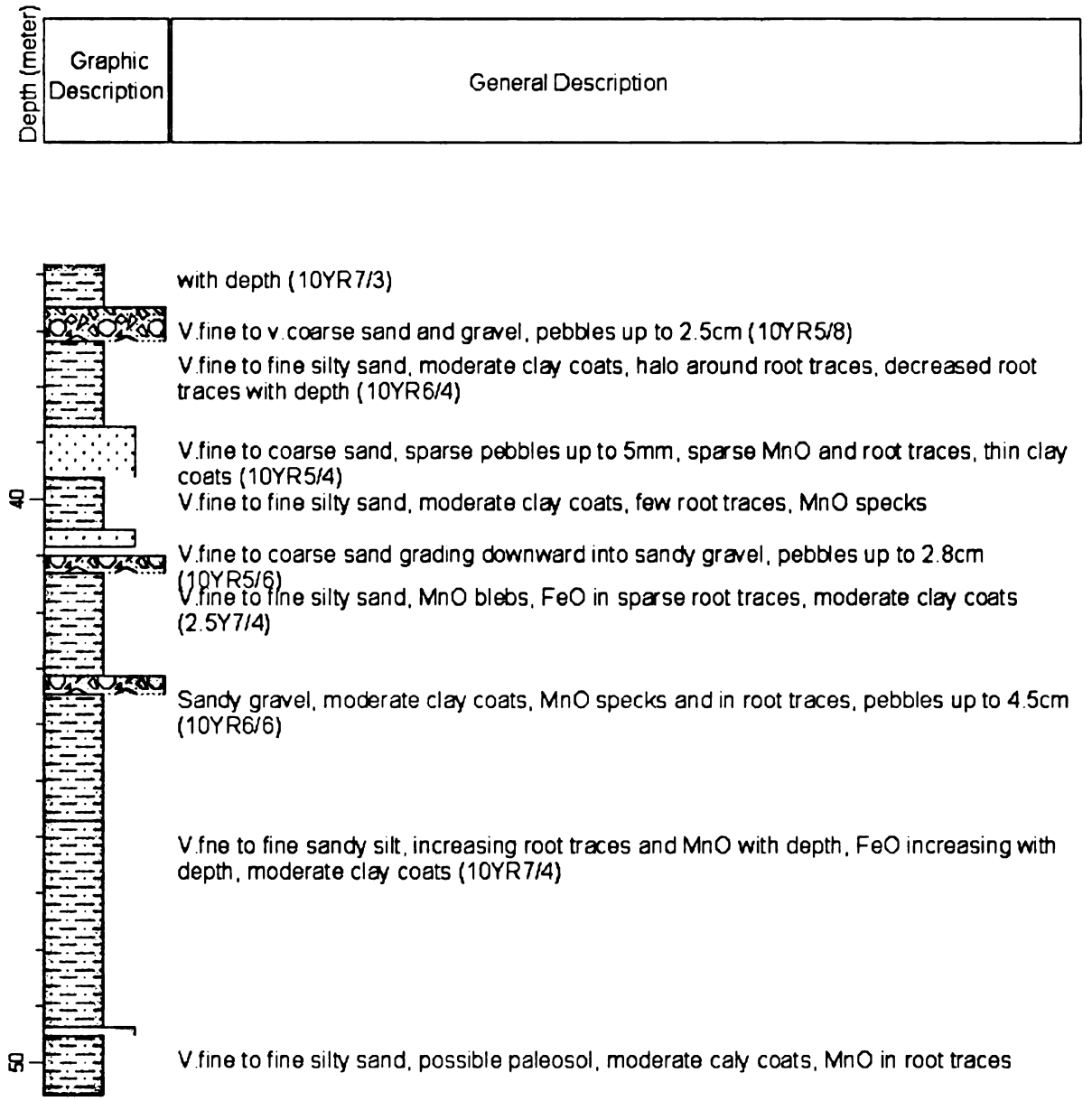

Figure A.14c: Core description of facies identified in well 1306 continued.

Michigan State University

Department of Geological Sciences

Well Name: W-1401 Location: TFD LLNL

Date Logged: 6/10/2002

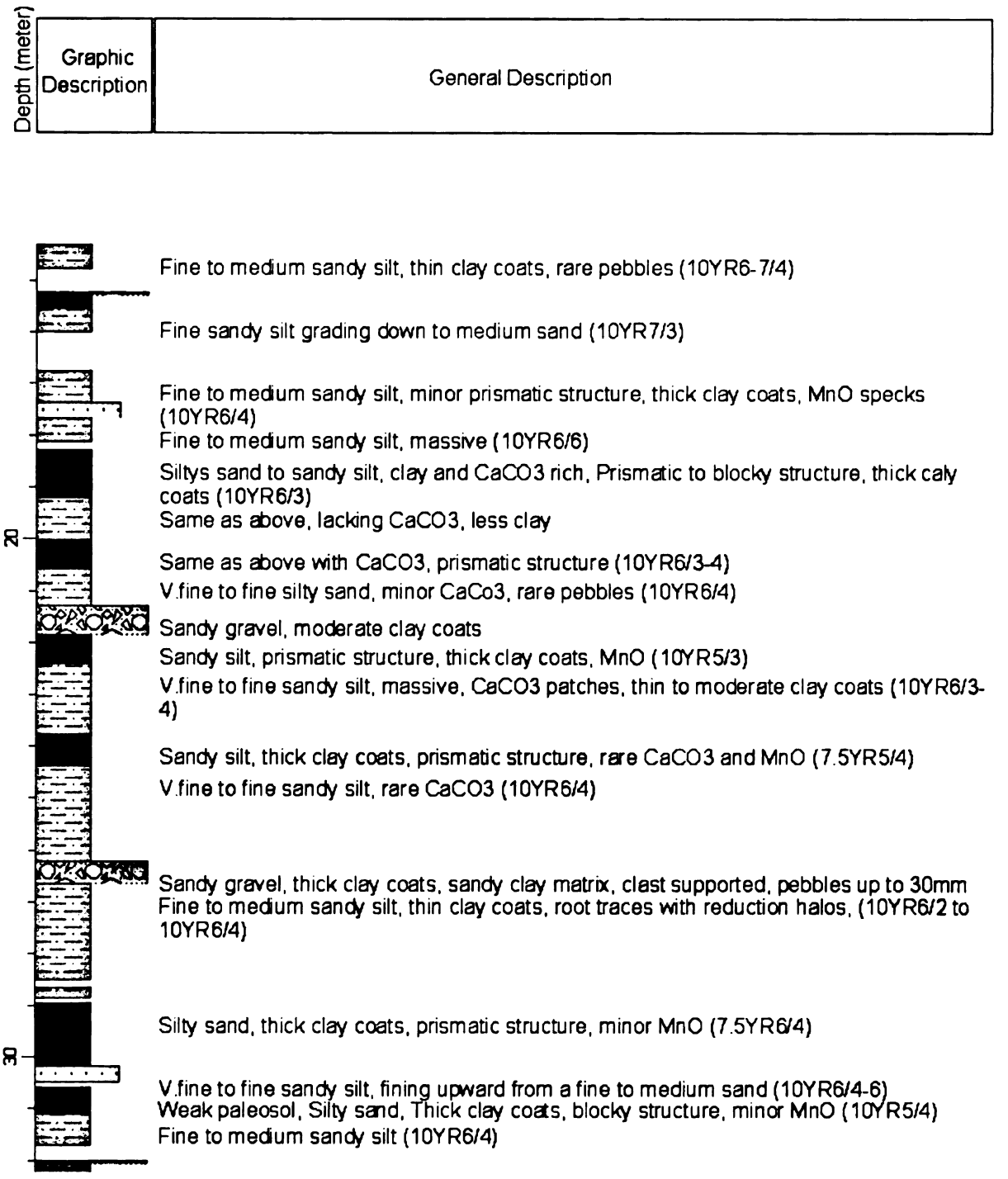

Figure A.15a: Core description of facies identified in well 1401.

Michigan State University
Department of Geological Sciences

Well Name: W-1401 Location: TFD LLNL
Date Logged: 6/10/2002

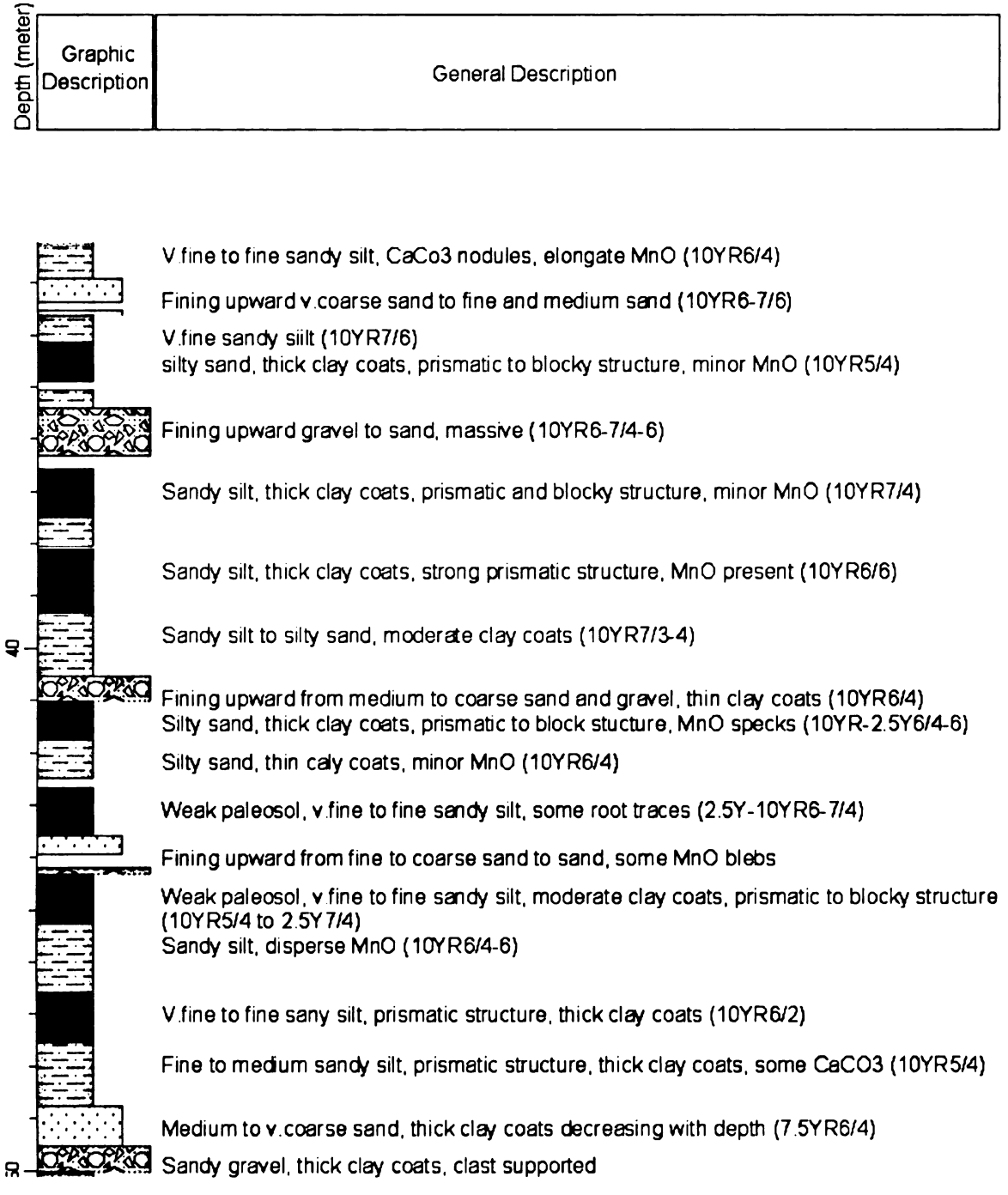

Figure A.15b: Core description of facies identified in well 1401 continued.

Michigan State University

Department of Geological Sciences

Well Name: W-1401 Location: TFD LLNL

Date Logged: 6/10/2002

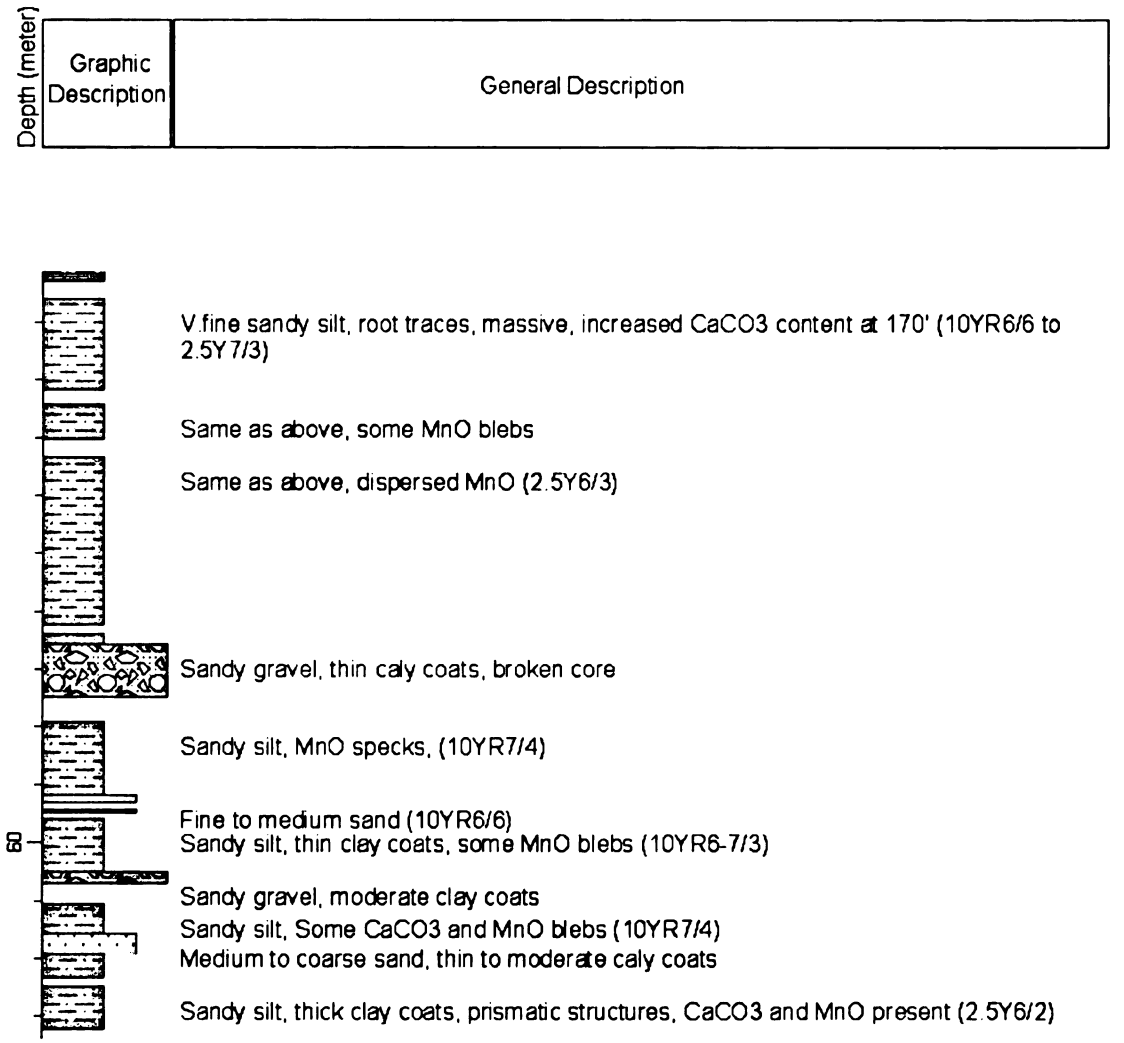

Figure A.15c: Core description of facies identified in well 1401 continued.

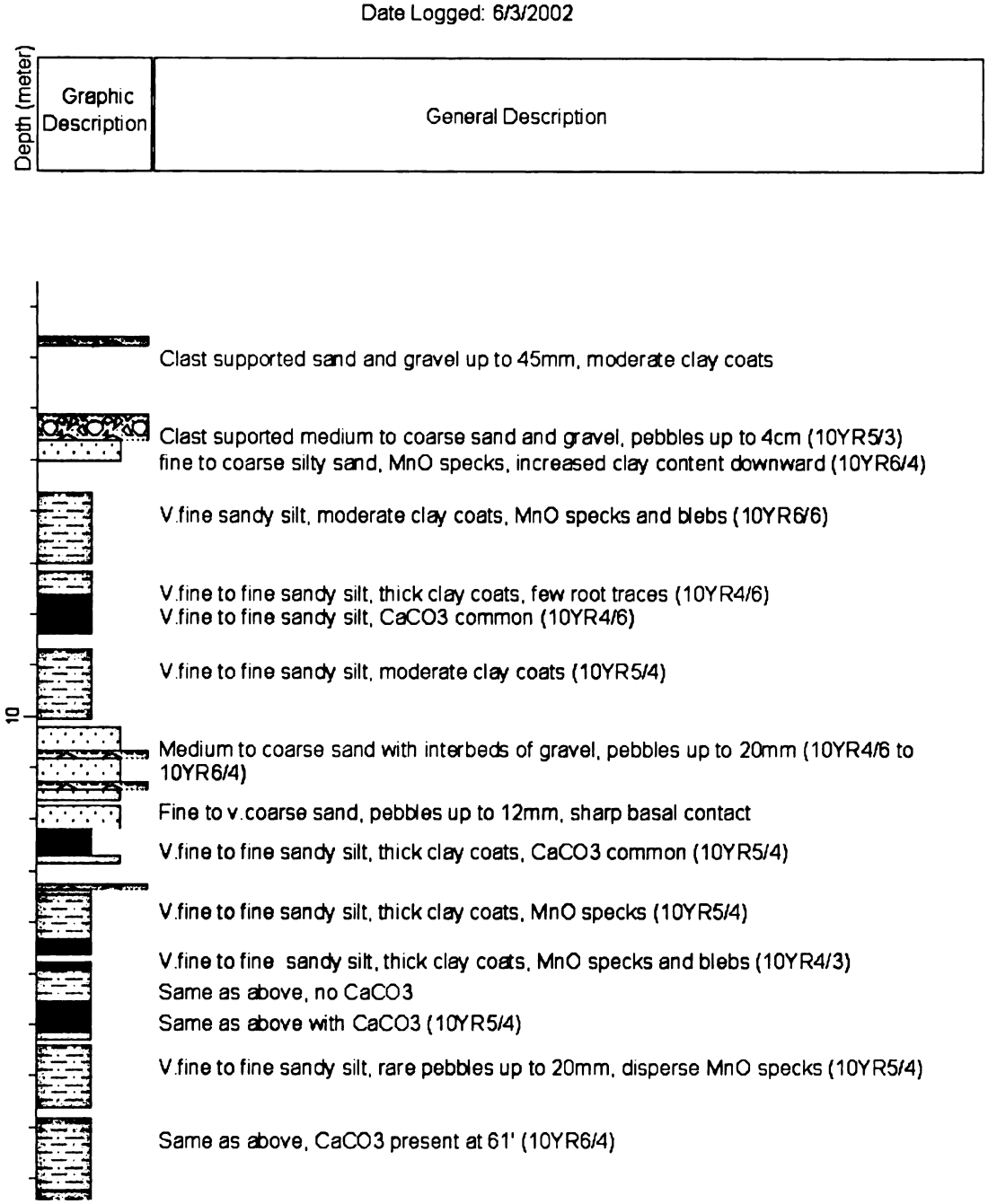

Figure A.16a: Core description of facies identified in well 1416.

Michigan State University

Department of Geological Sciences

Well Name: W-1416 Location: TFD LLNL

Date Logged: 6/3/2002

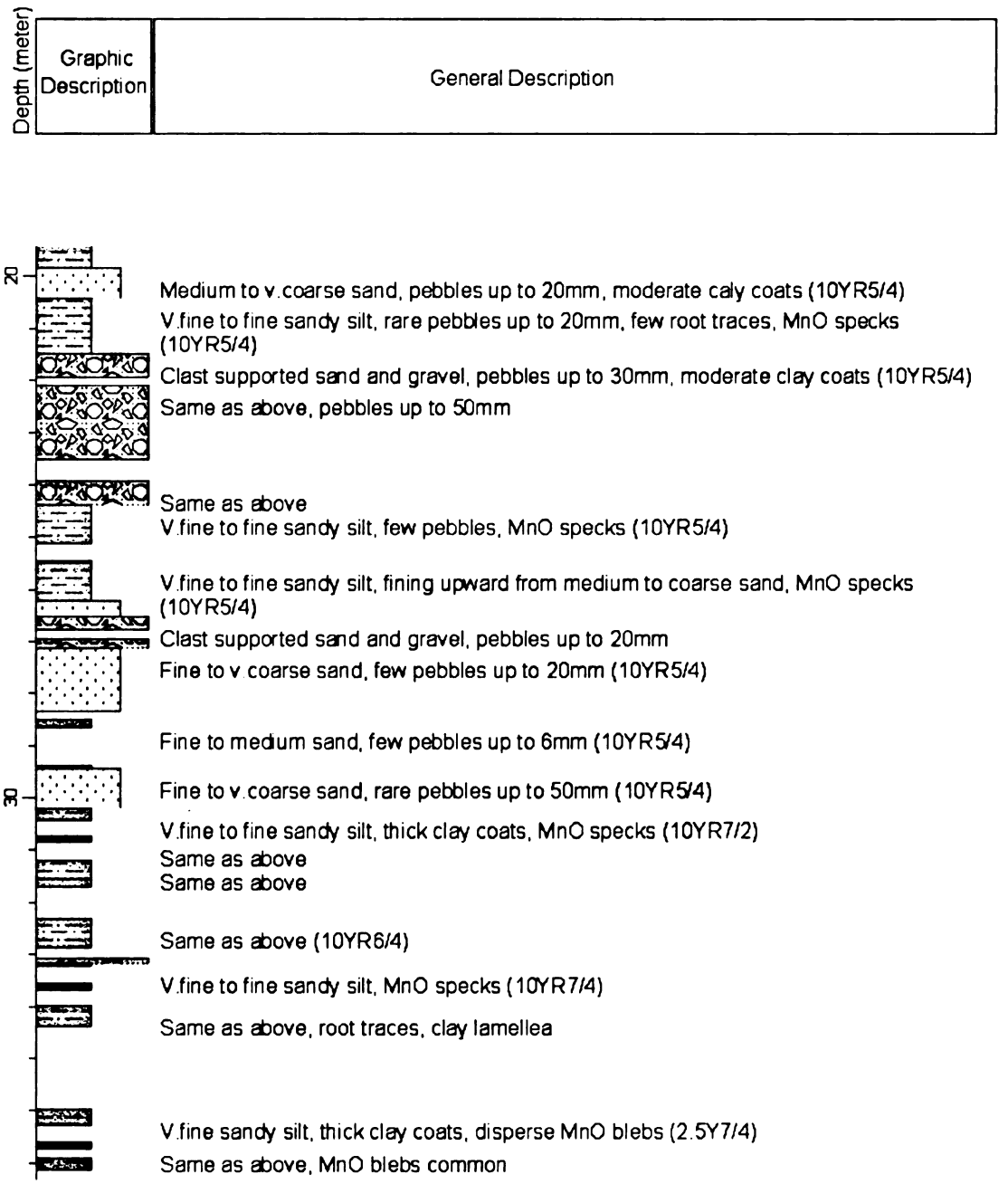

Figure A.16b: Core description of facies identified in well 1416 continued.

Michigan State University

Department of Geological Sciences

Well Name: W-1416 Location: TFD LLNL

Date Logged: 6/3/2002

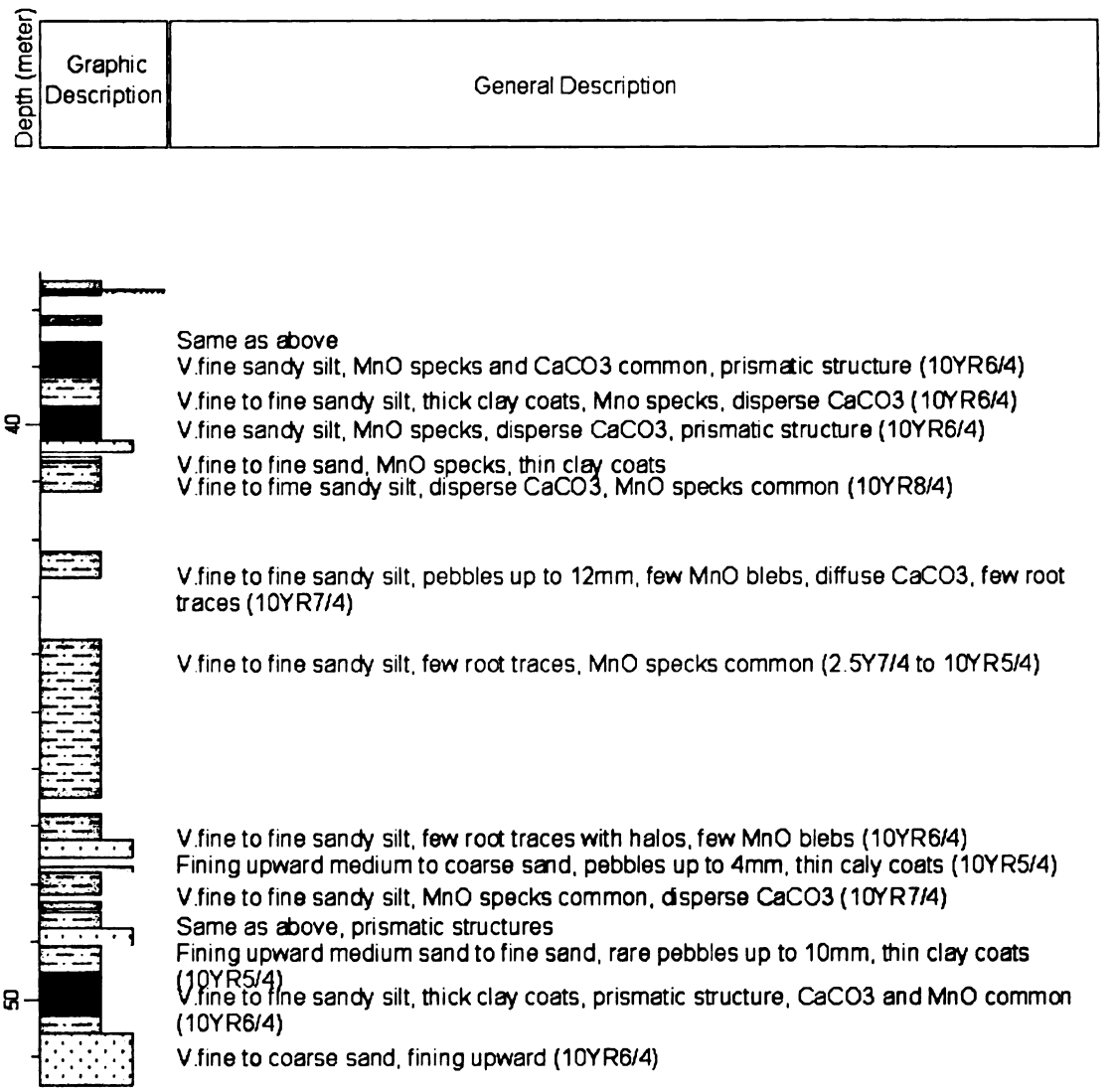

Figure A.16c: Core description of facies identified in well 1416 continued.

Appendix B

Geophysical to Well Core Correlations

This appendix contains 32 Geophysical logs for wells located in the Helipad Site study area, LLNL California. Four major hydrofacies were described from core recovered within the study area – *gravel, sand, silty sand* and *paleosol* (Weissmann, 2001). These hydrofacies show relatively unique geophysical character, high resistivity spikes relative to SPR are an indication of gravel or sand Hydrofacies (Weissmann, 2001). Low resistivity spicks relative to SPR are an indication of silty sand and paleosol hydrofacies (Weissmann, 2001). Based on these observations, hydrofacies elevations in core were adjusted to match geophysical logs. Gravel and sand hydrofacies are interpreted as channel deposits; silty sand hydrofacies are interpreted as floodplain deposits. Paleosol hydrofacies may overprint any of these facies (through weathering and by addition of clay and carbonate).

Indicated in these figures (B.1 through B.32), are correlation of gravel, sand, silty sand, and paleosol hydrofacies to a combination of single point resistance (SPR), resistance (RES, LRES, RI), conductivity (Cond), 16–inch short normal resistivity (16IN), 64–inch long normal resistivity (64IN), natural gamma ray (Gamma), and caliper. The stratigraphy shown in these logs (B.1 through B.31) was used to develop cross well correlations (Appendix C).

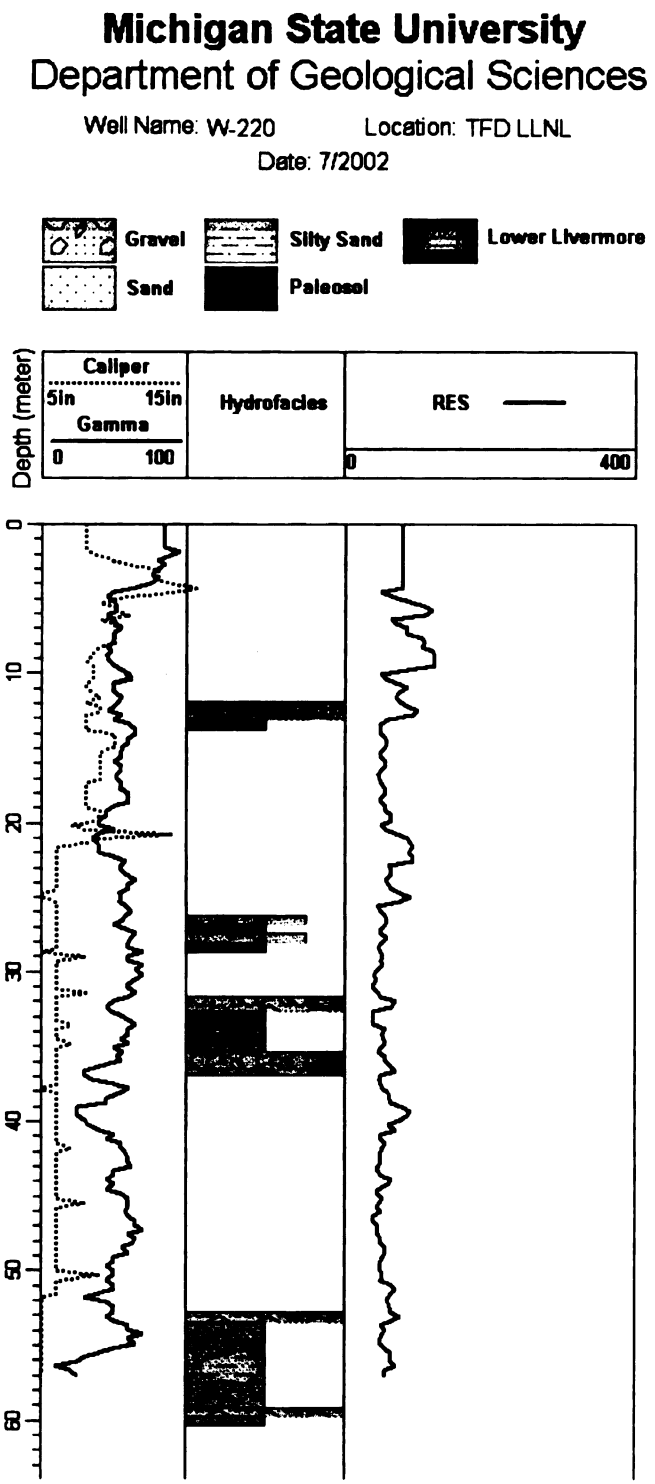

Figure B.1: Geophysical well logs and core descriptions for well 220.

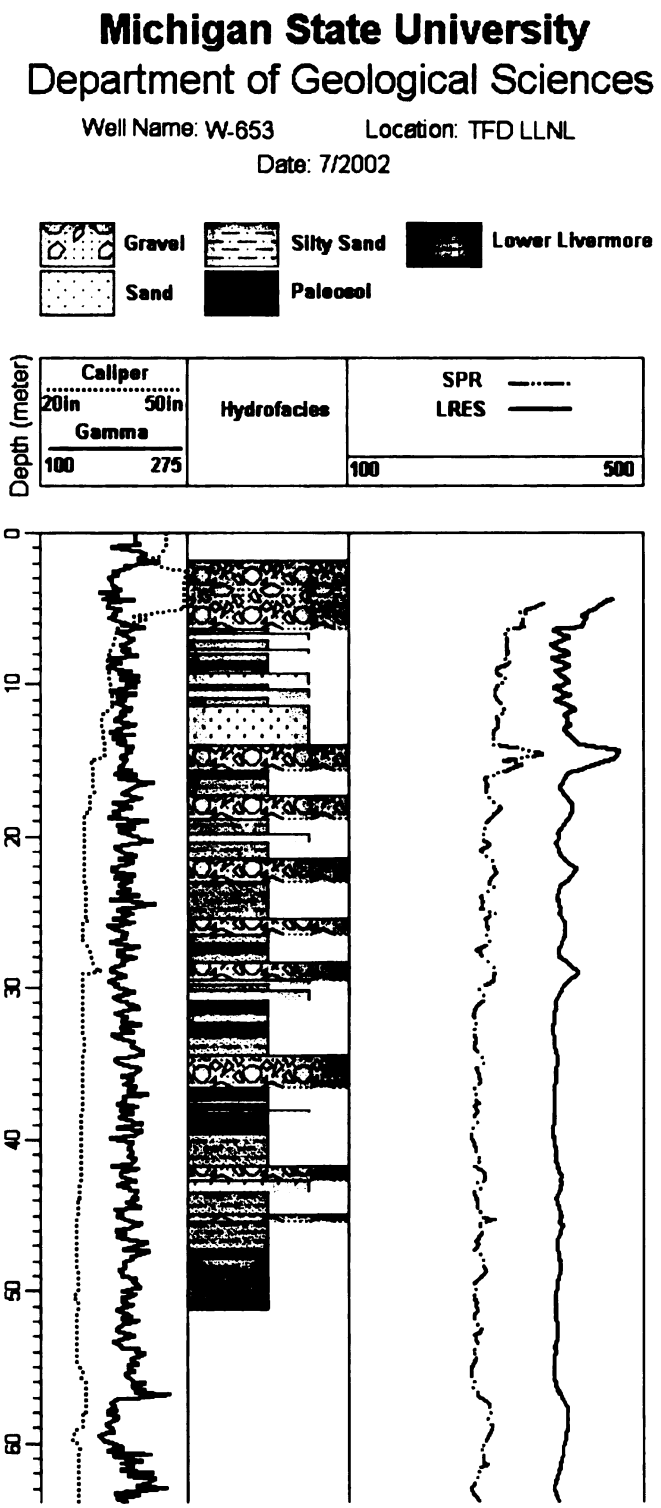

Figure B.2: Geophysical well logs and core descriptions for well 653.

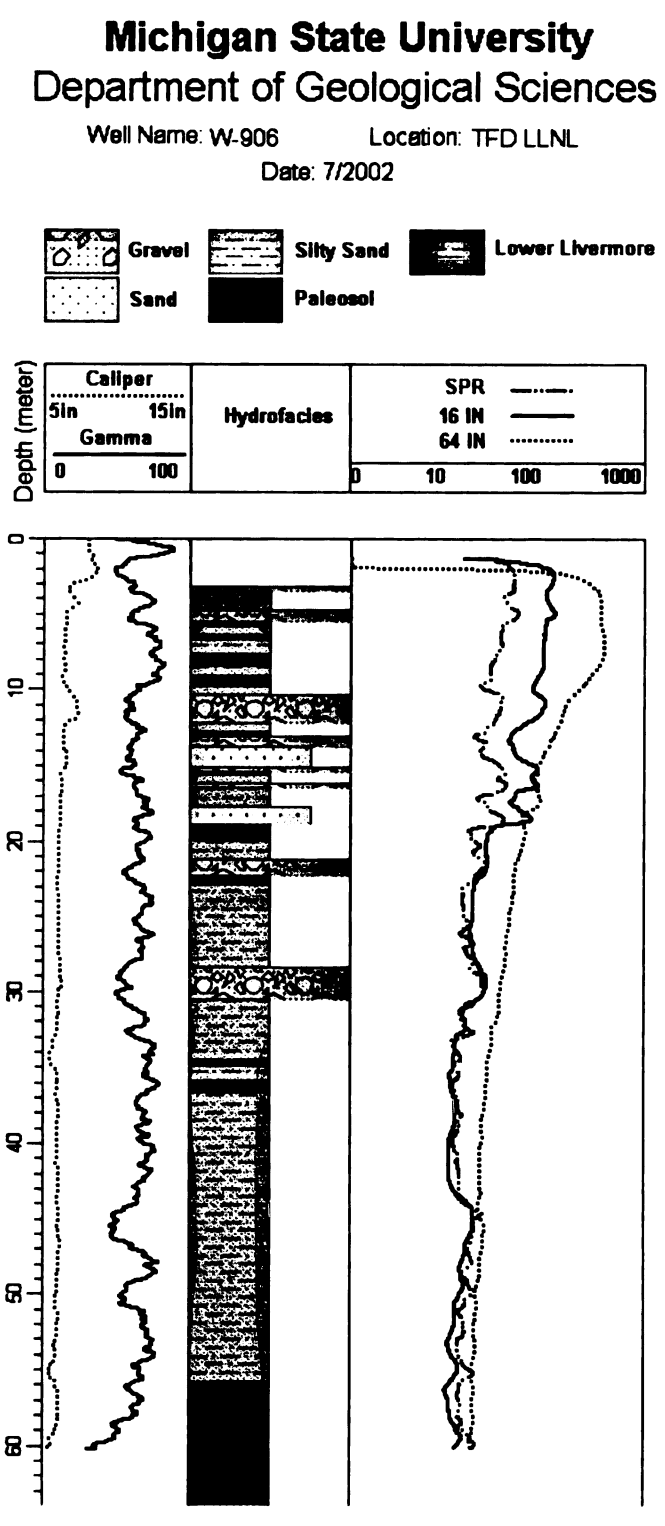

Figure B.3: Geophysical well logs and core descriptions for well 906.

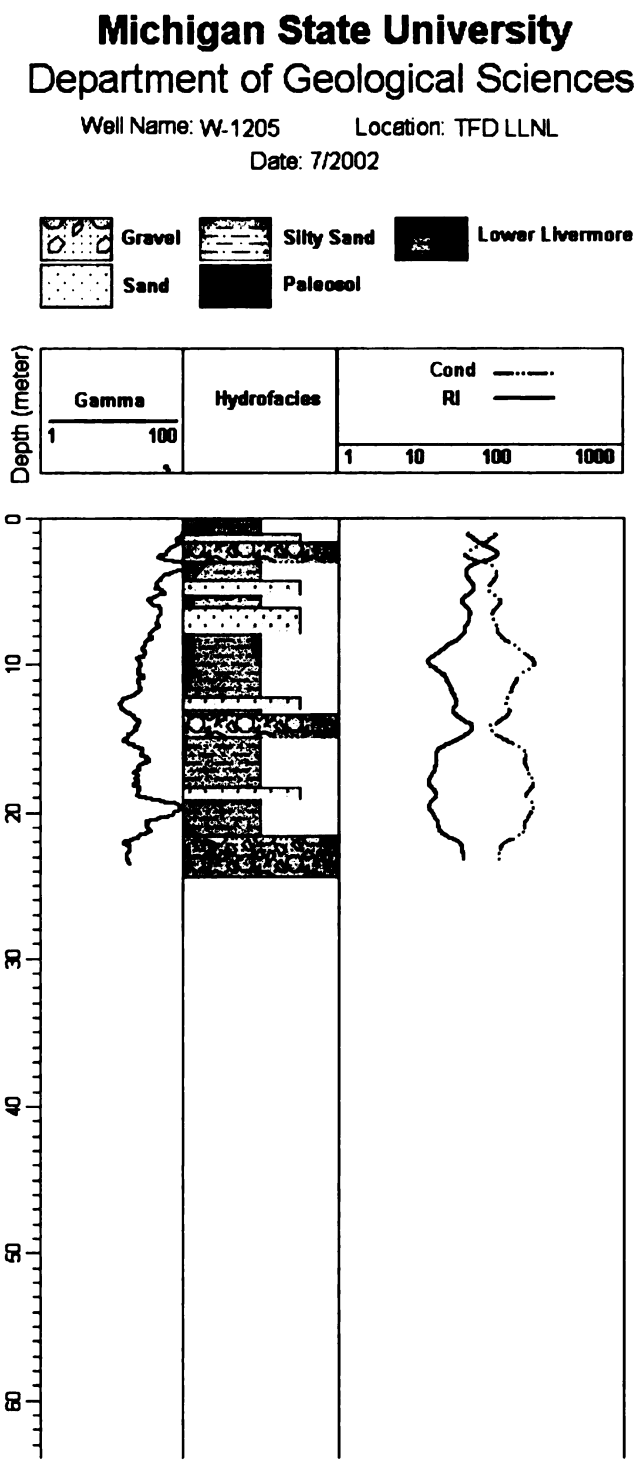

Figure B.4: Geophysical well logs and core descriptions for well 1205.

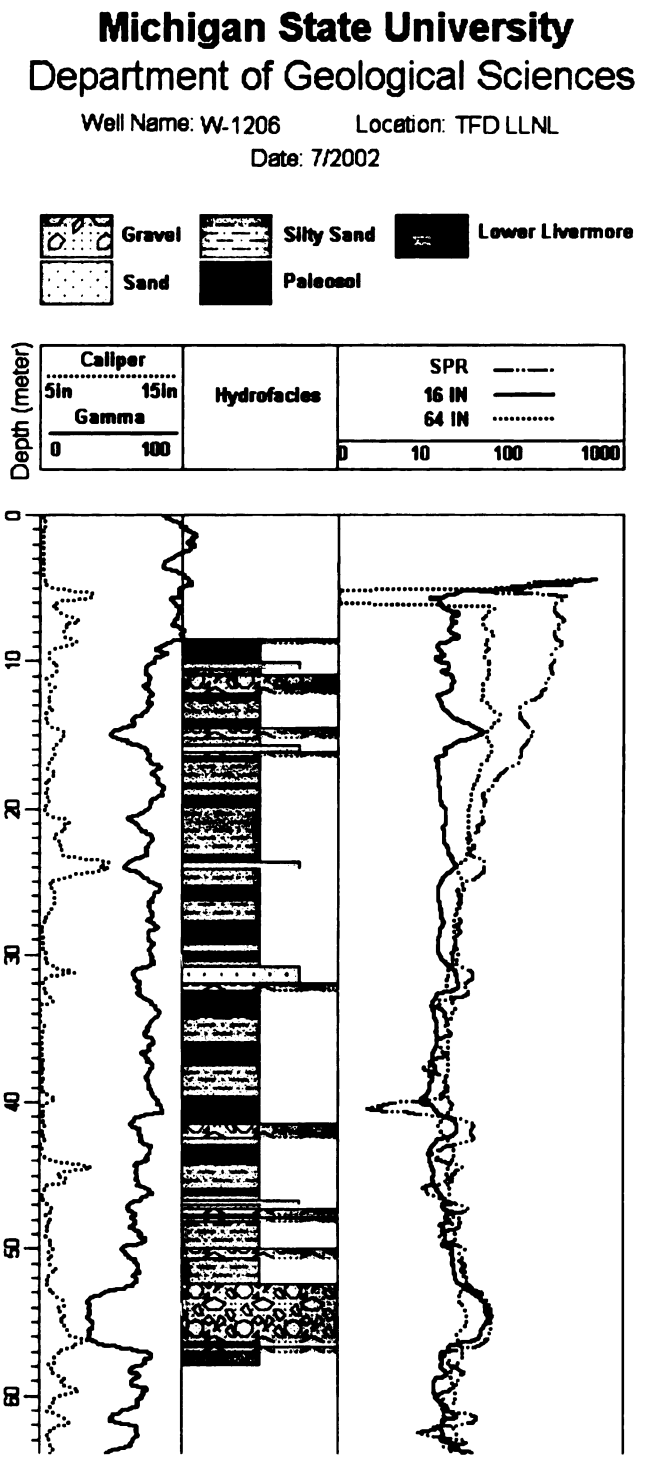

Figure B.5: Geophysical well logs and core descriptions for well 1206.

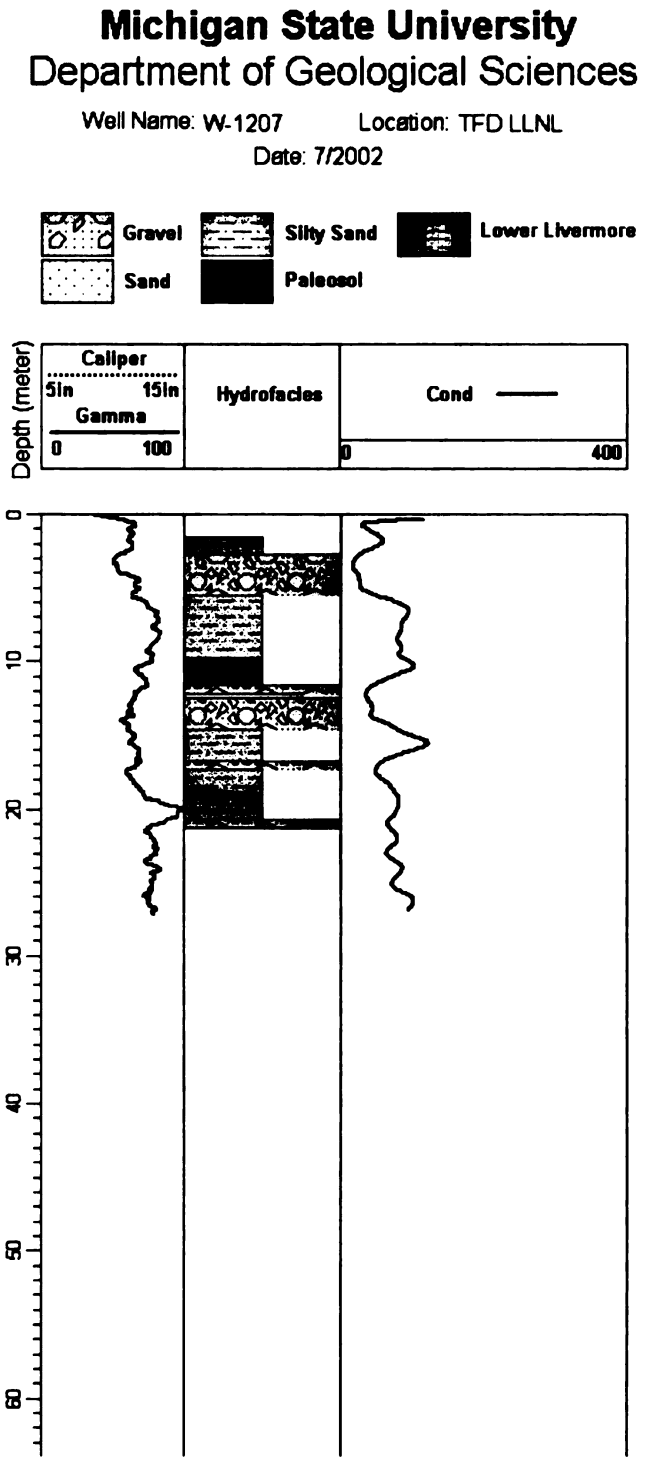

Figure B.6: Geophysical well logs and core descriptions for well 1207.

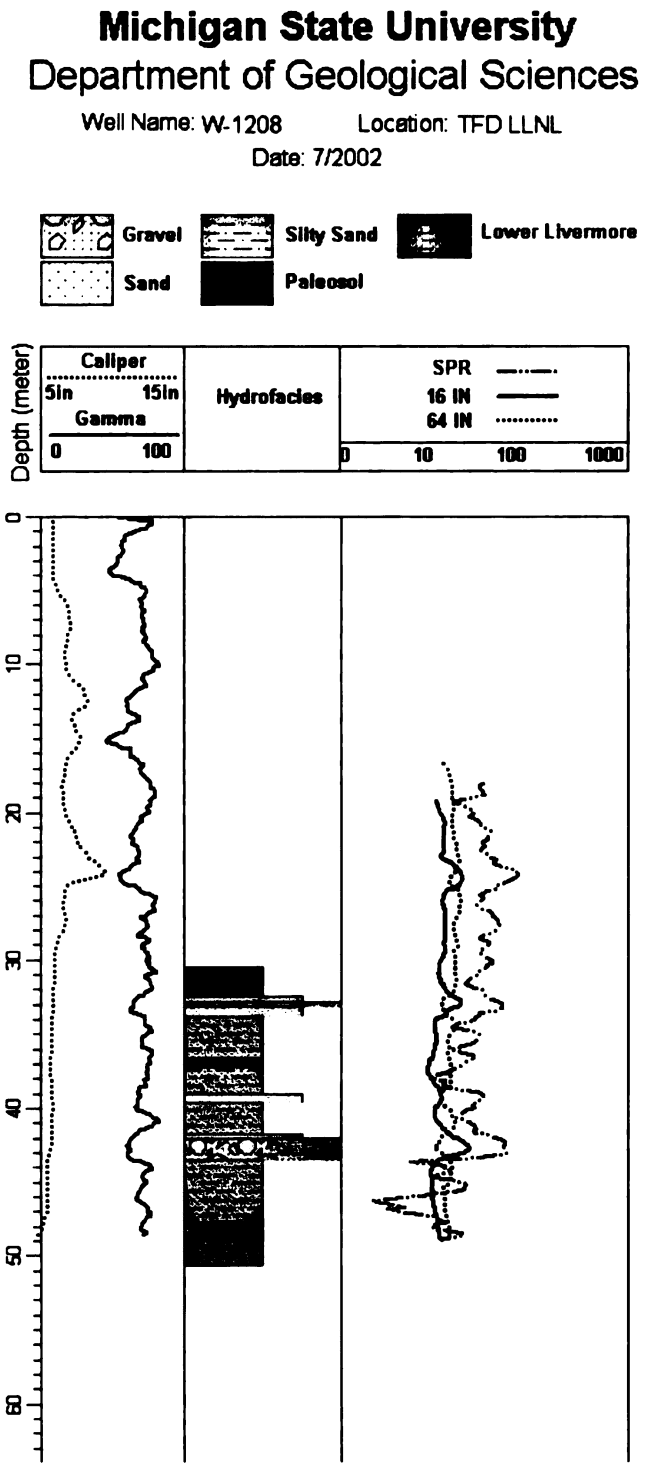

Figure B.7: Geophysical well logs and core descriptions for well 1208.

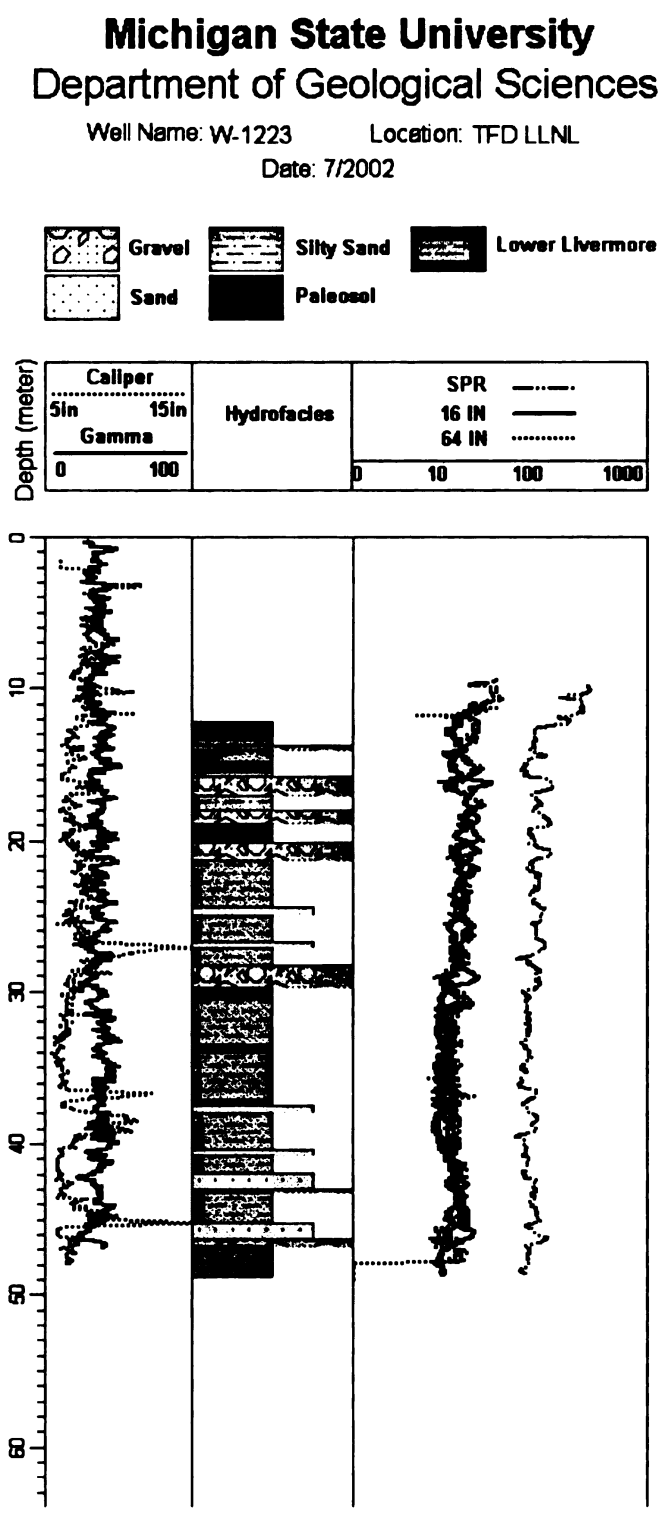

Figure B.8: Geophysical well logs and core descriptions for well 1223.

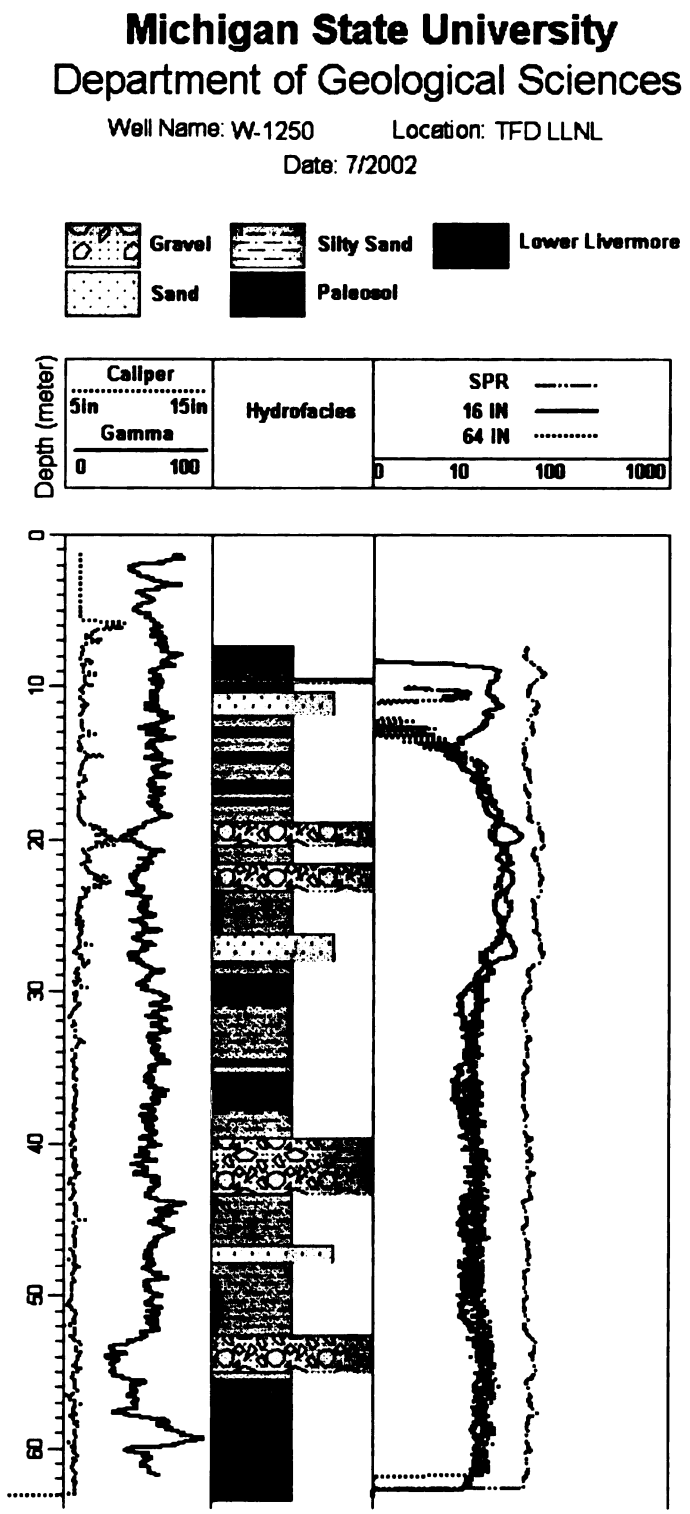

Figure B.9: Geophysical well logs and core descriptions for well 1250.

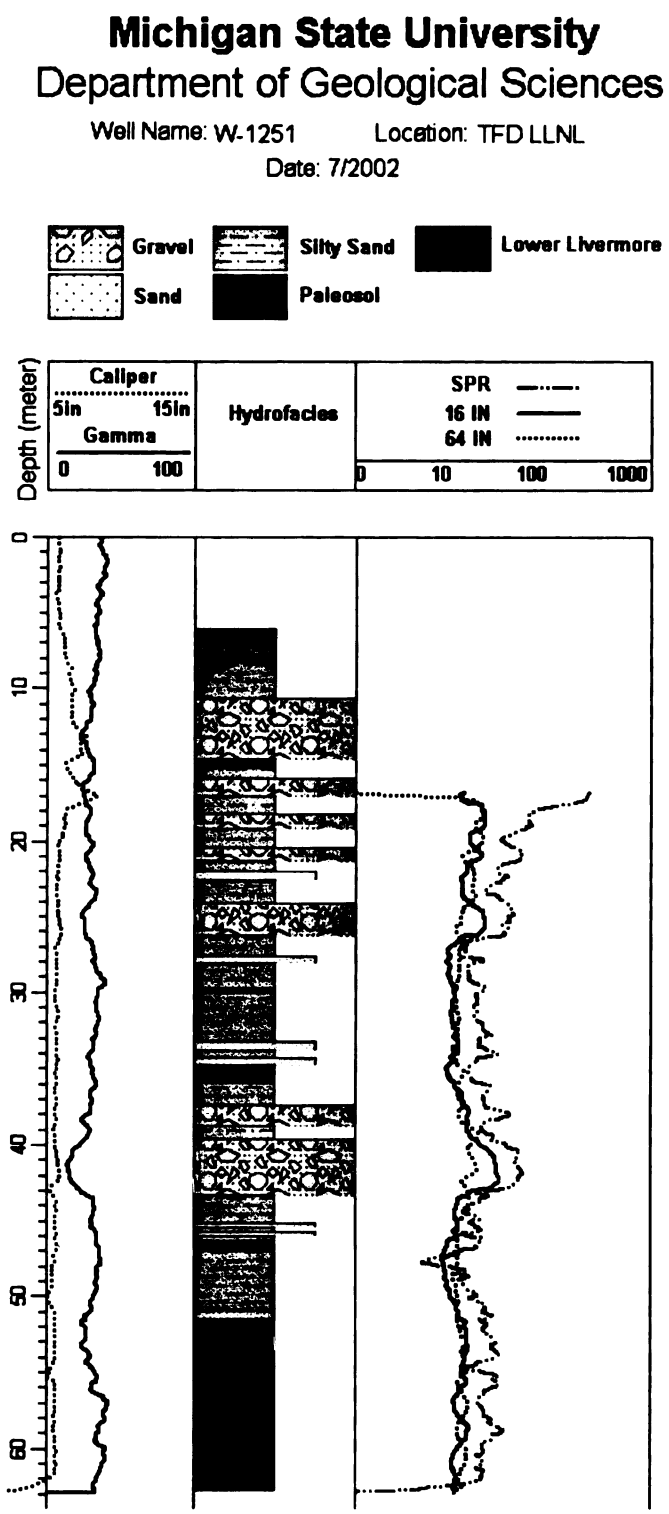

Figure B.10: Geophysical well logs and core descriptions for well 1251.

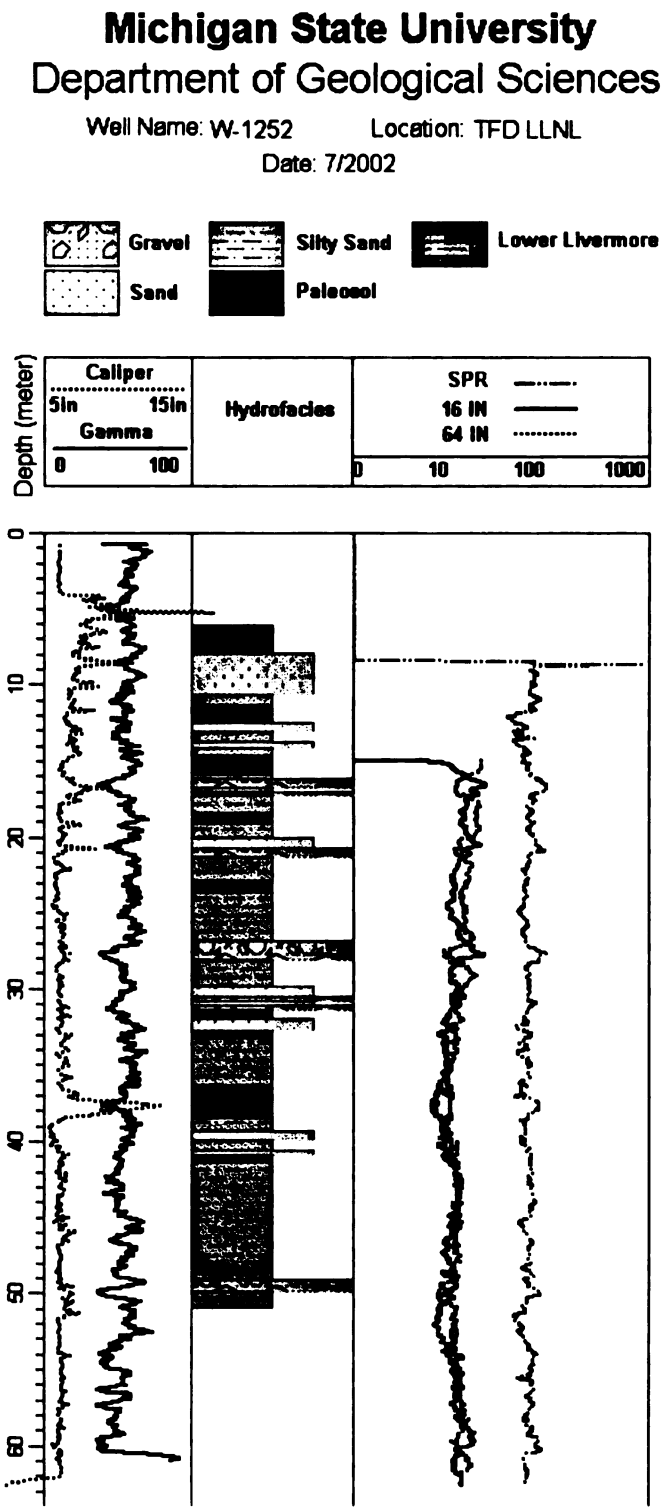

Figure B.11: Geophysical well logs and core descriptions for well 1252.

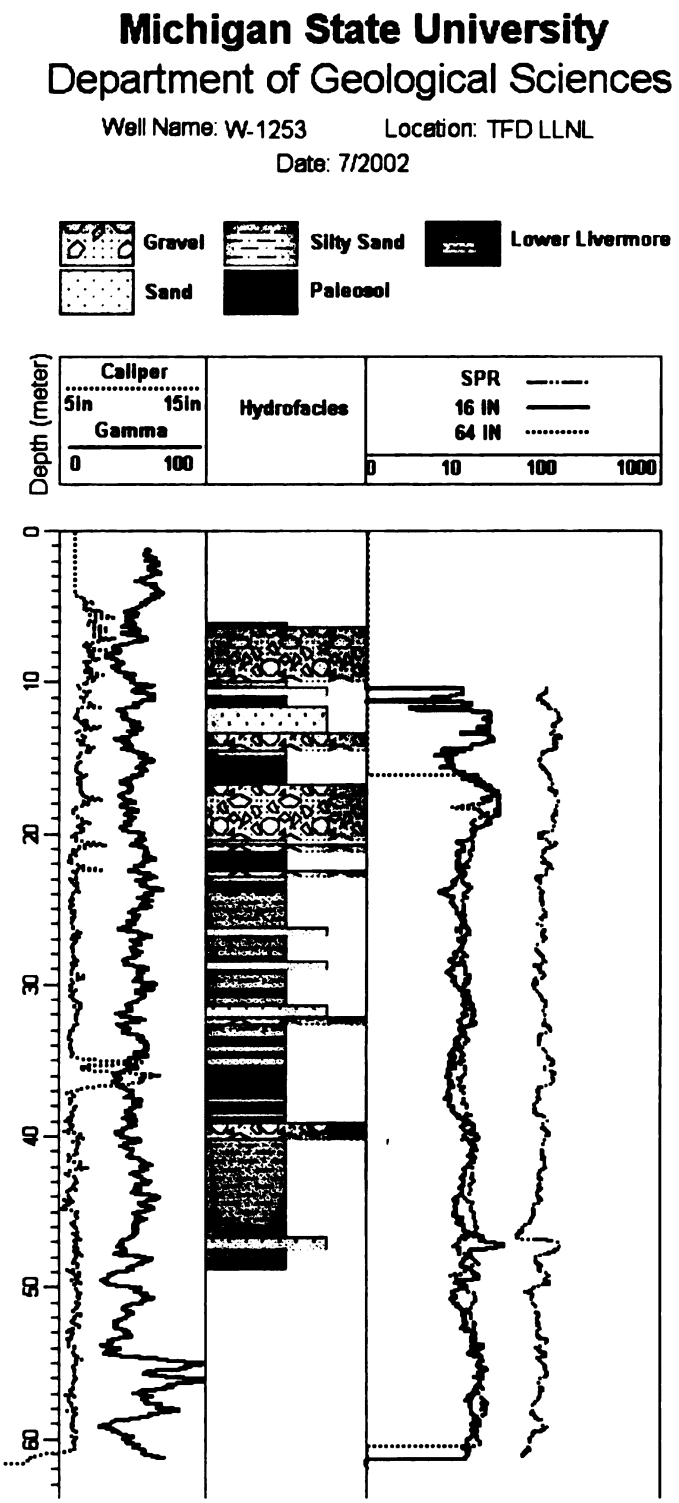

Figure B.12: Geophysical well logs and core descriptions for well 1253.

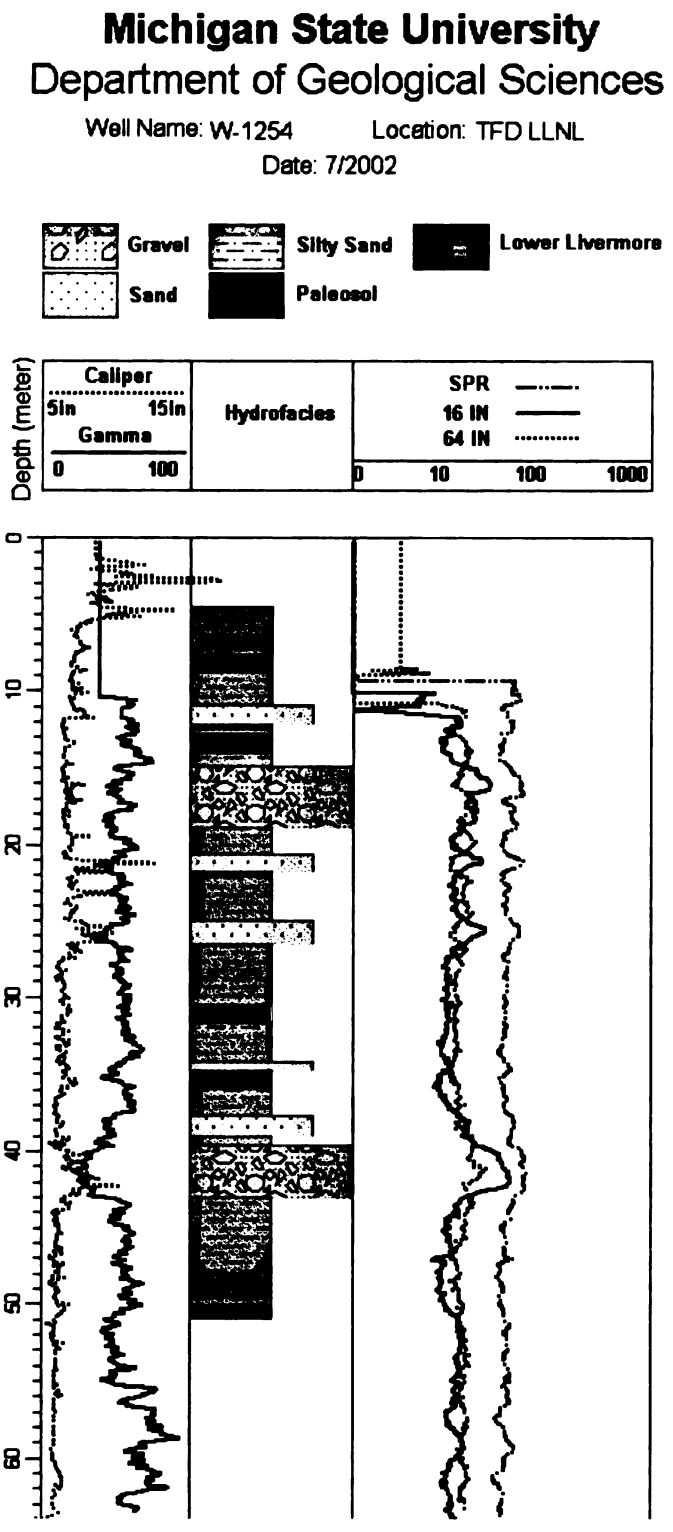

Figure B.13: Geophysical well logs and core descriptions for well 1254.

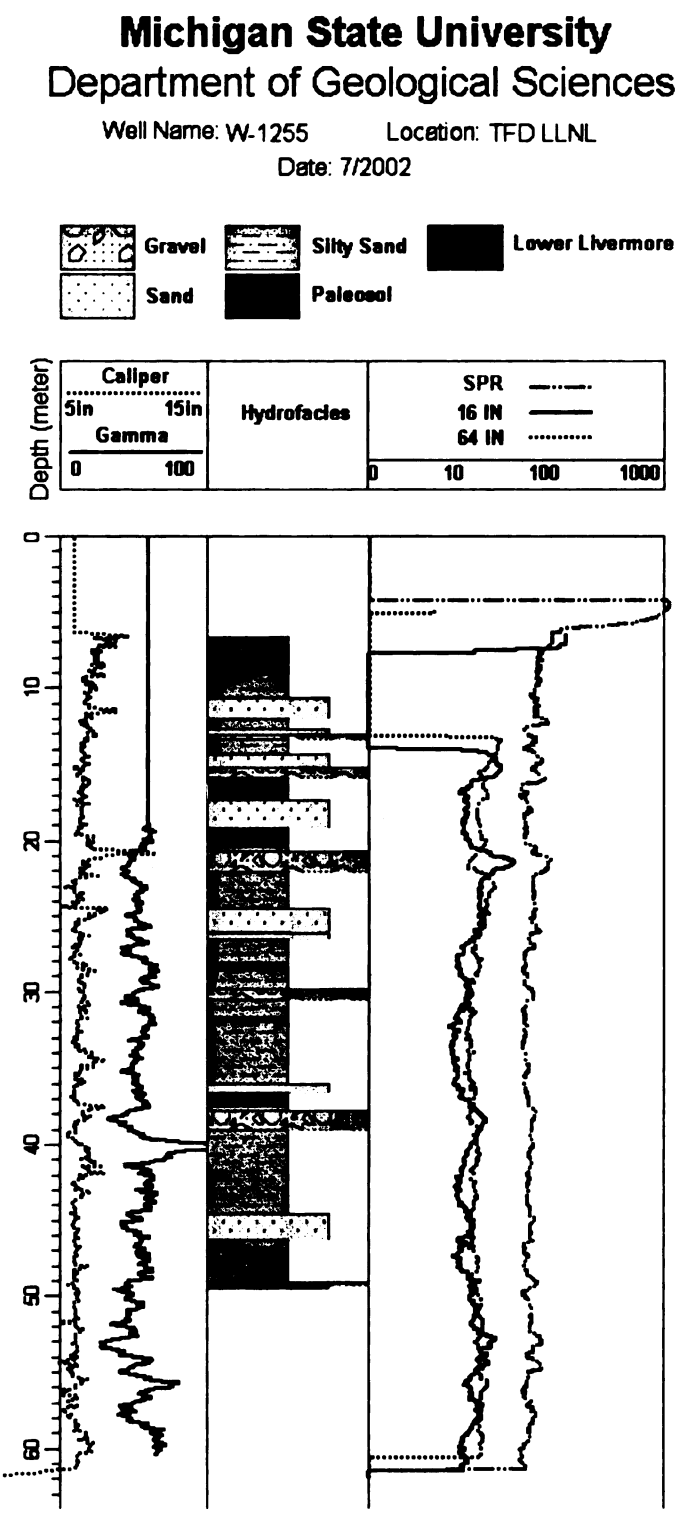

Figure B.14: Geophysical well logs and core descriptions for well 1255.

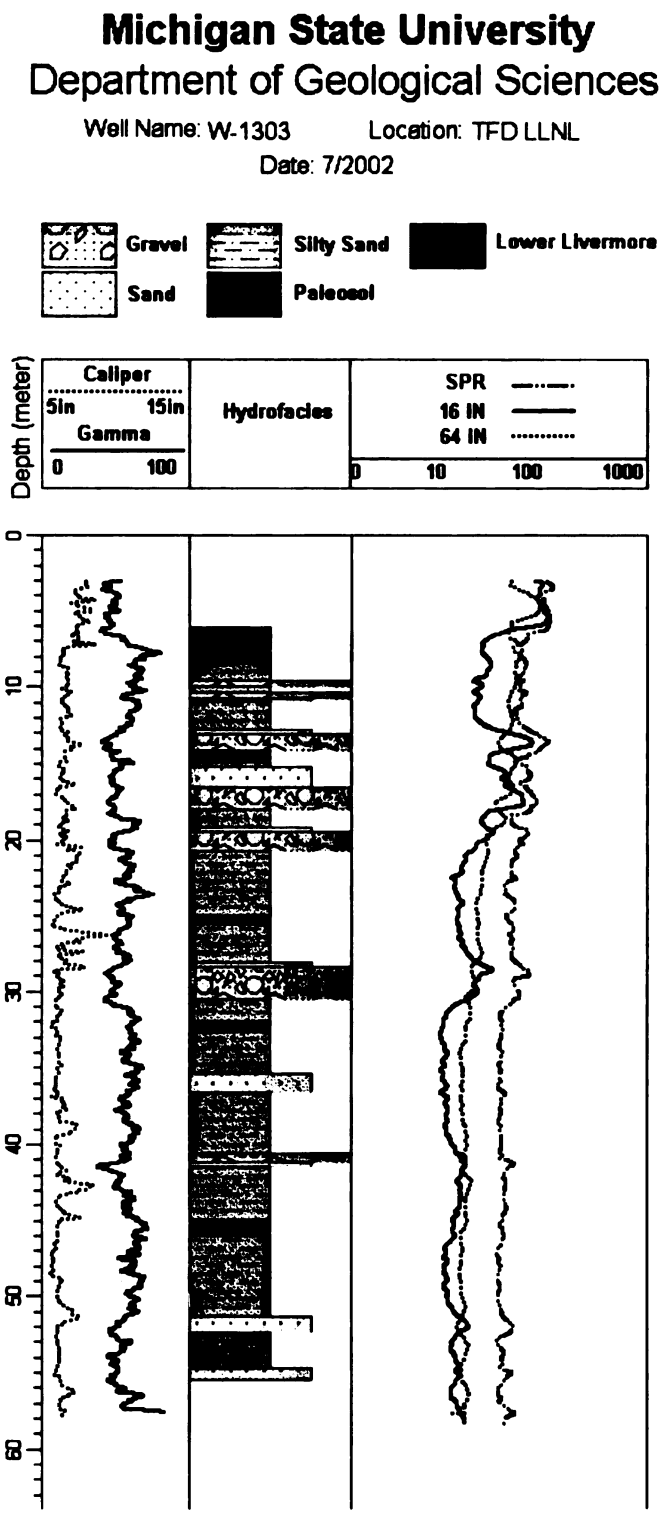

Figure B.15: Geophysical well logs and core descriptions for well 1303.

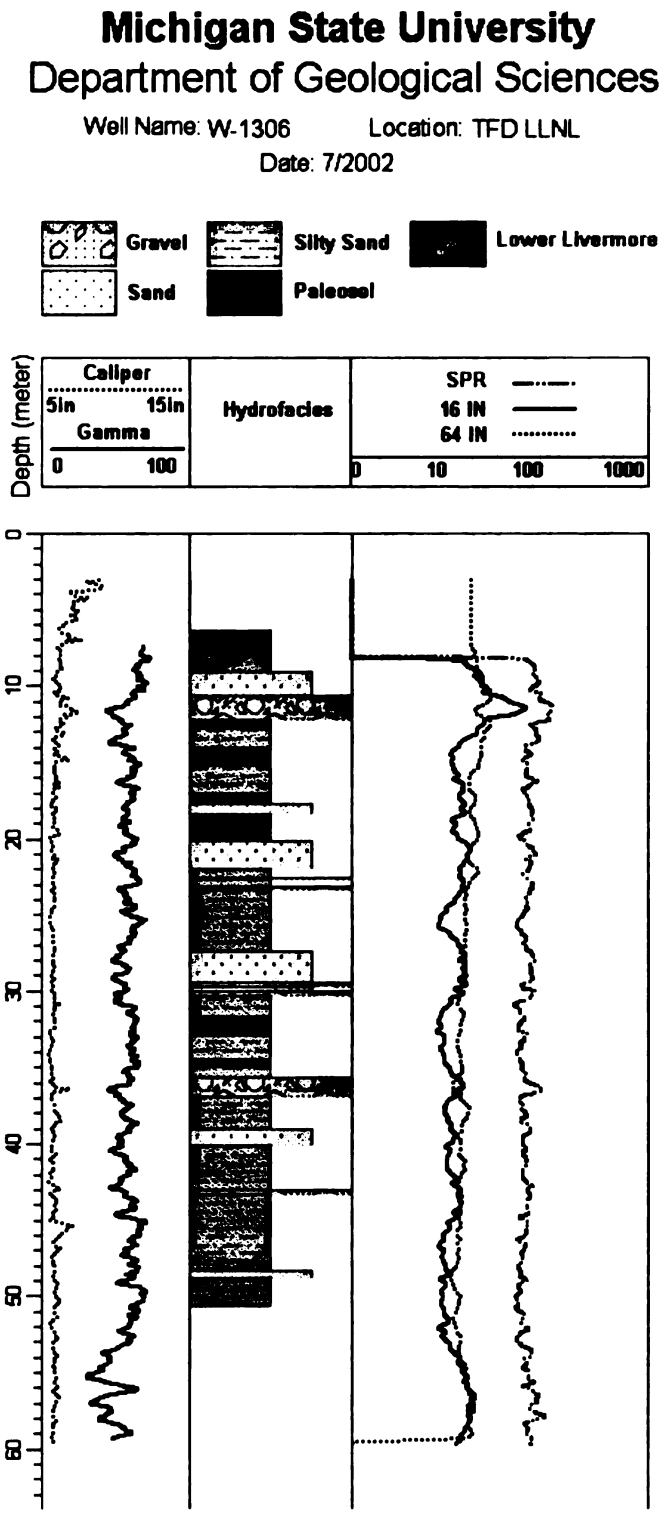

Figure B.16: Geophysical well logs and core descriptions for well 1306.

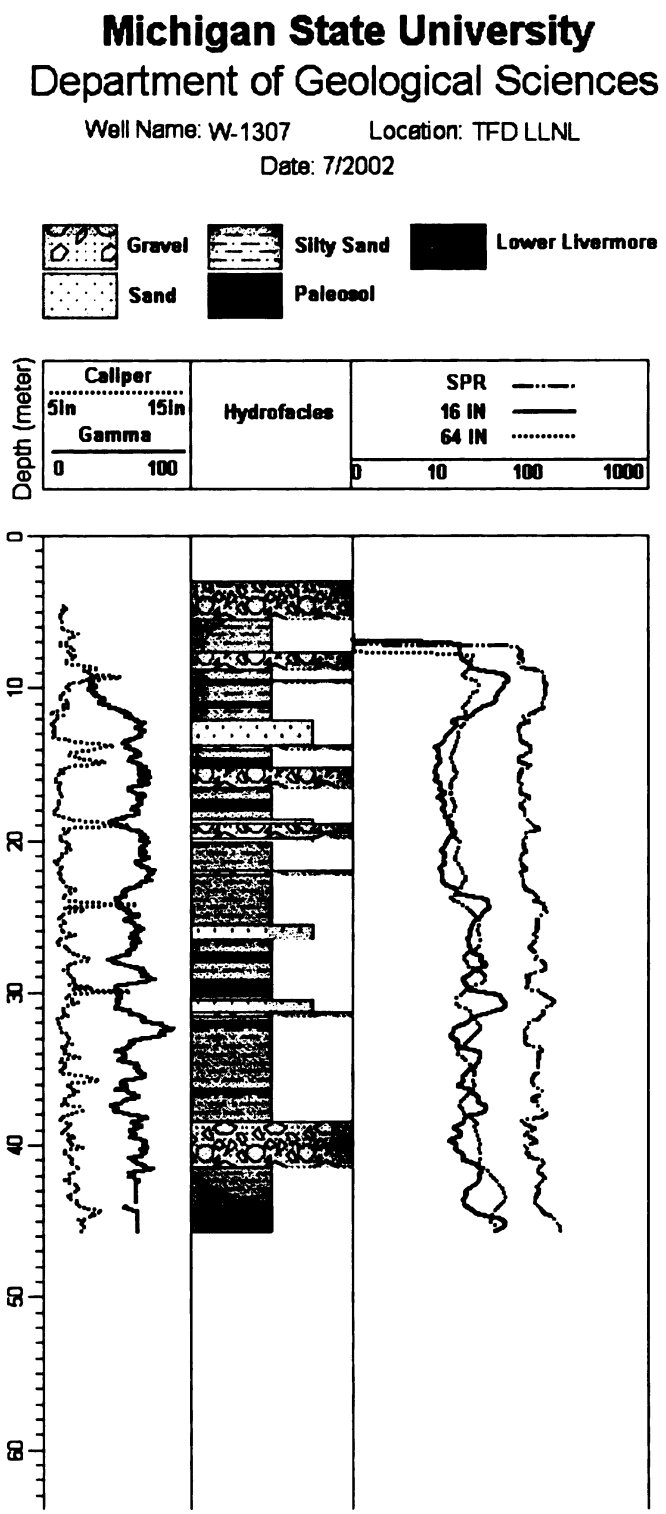

Figure B.17: Geophysical well logs and core descriptions for well 1307.

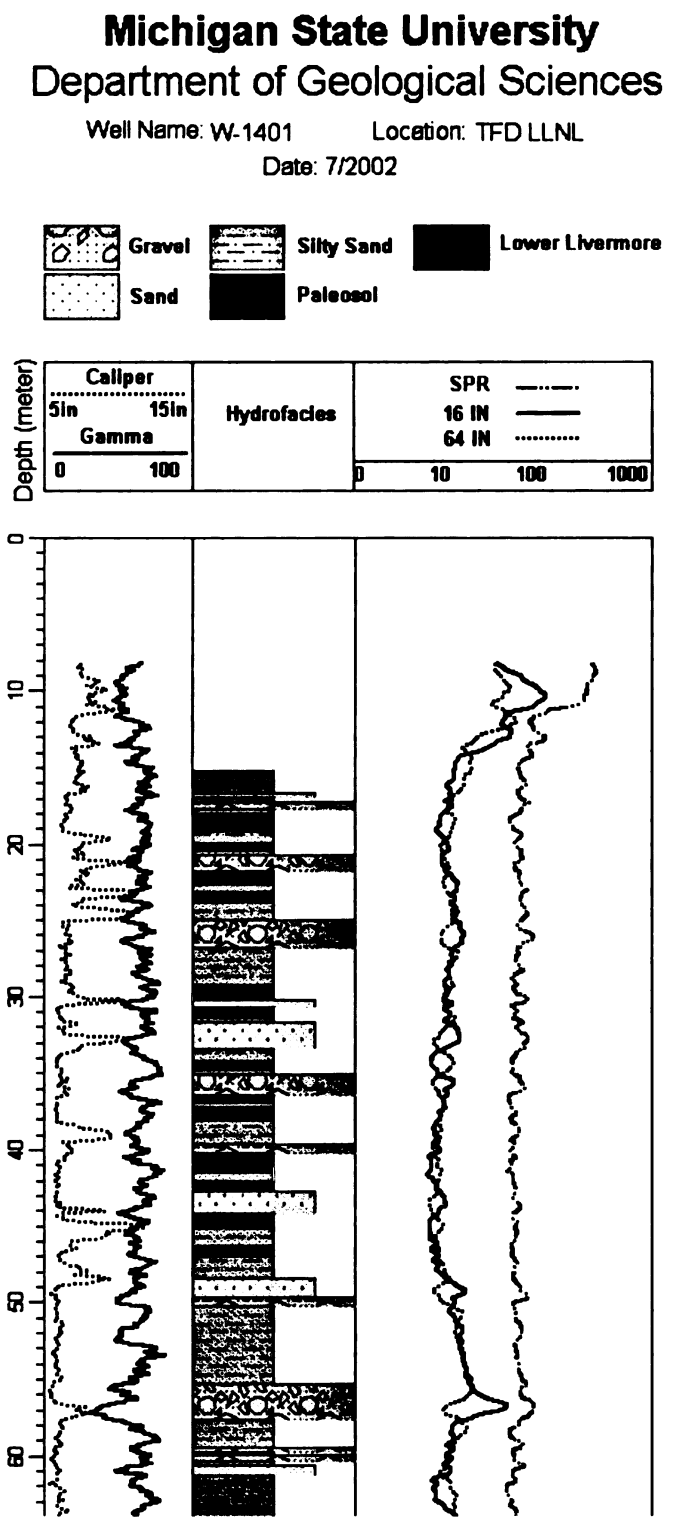

Figure B.18: Geophysical well logs and core descriptions for well 1401.

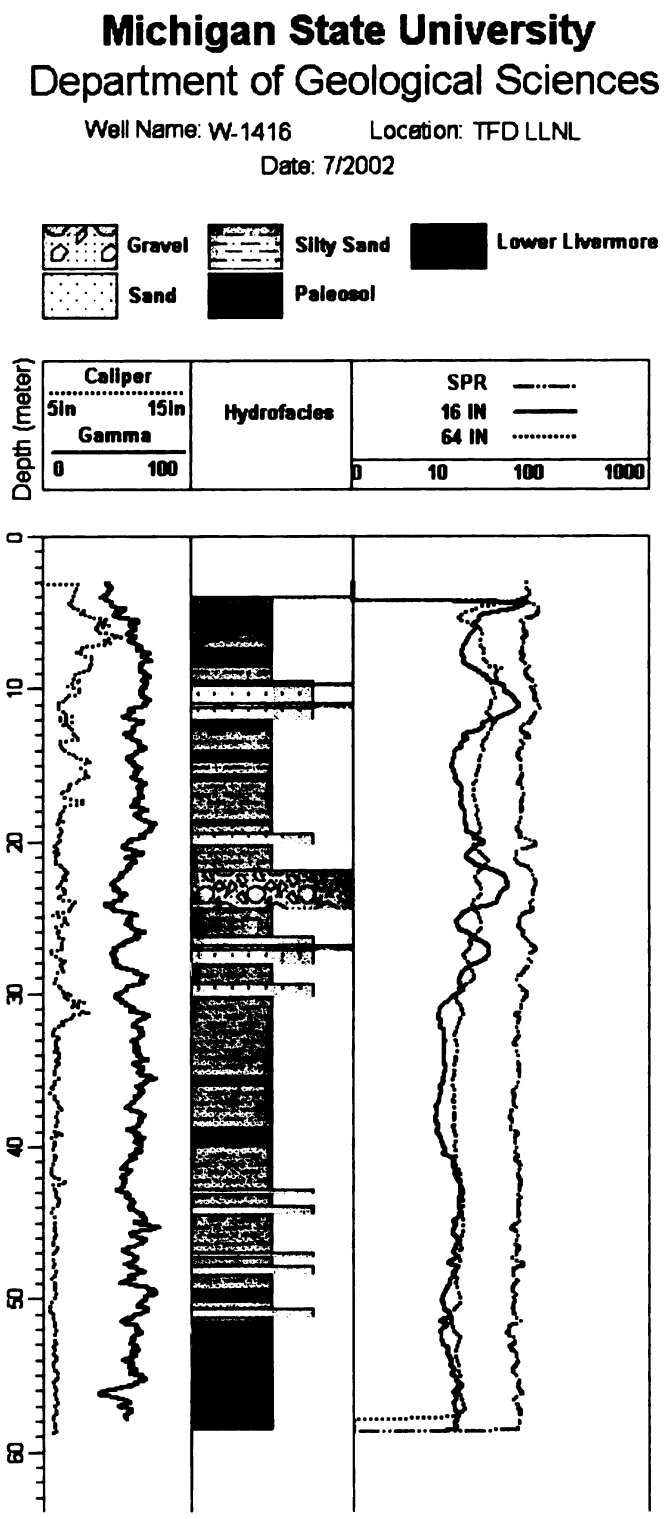

Figure B.19: Geophysical well logs and core descriptions for well 1416.

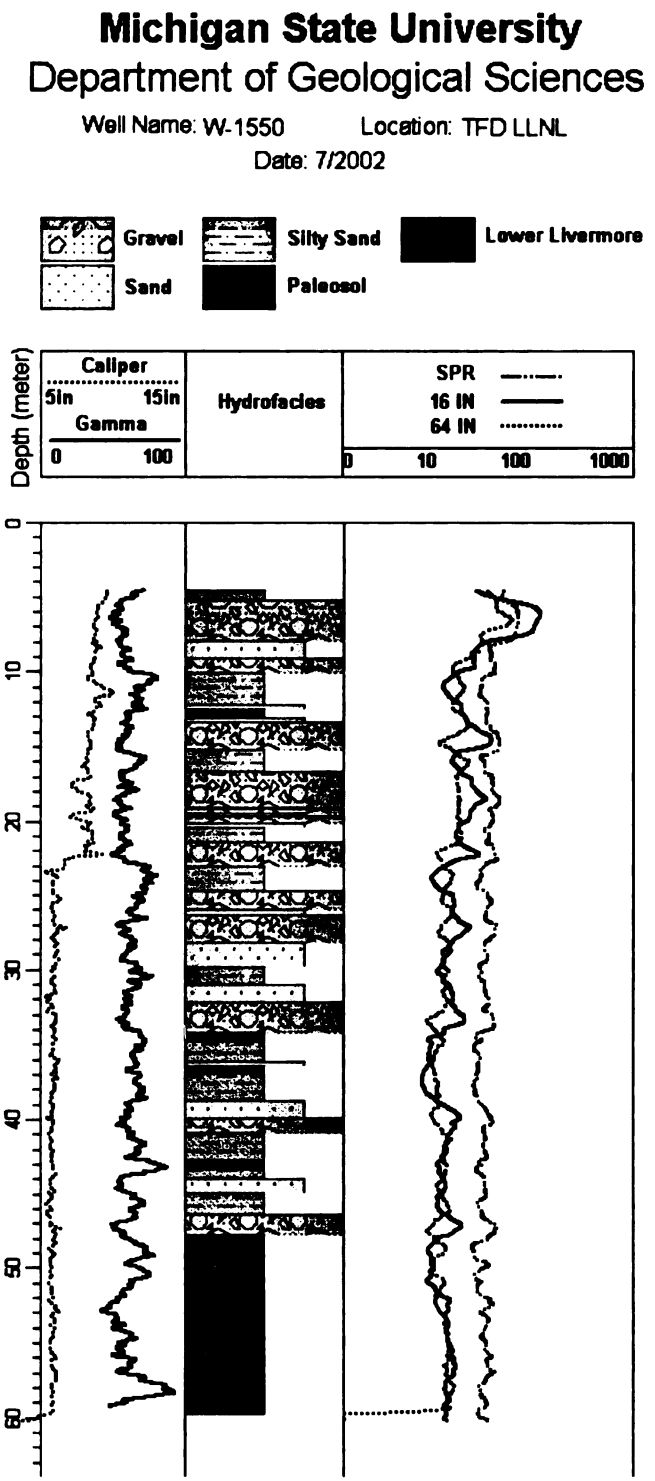

Figure B.20: Geophysical well logs and core descriptions for well 1550.

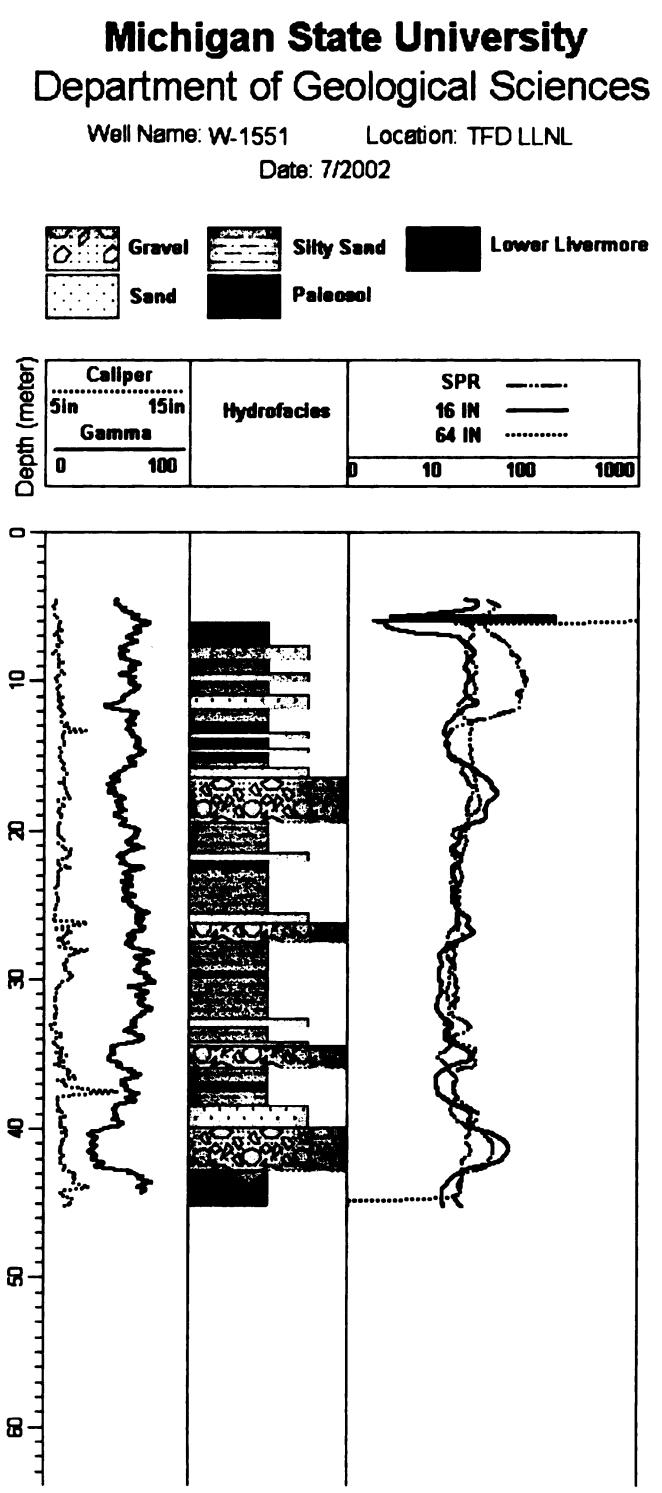

Figure B.21: Geophysical well logs and core descriptions for well 1551.

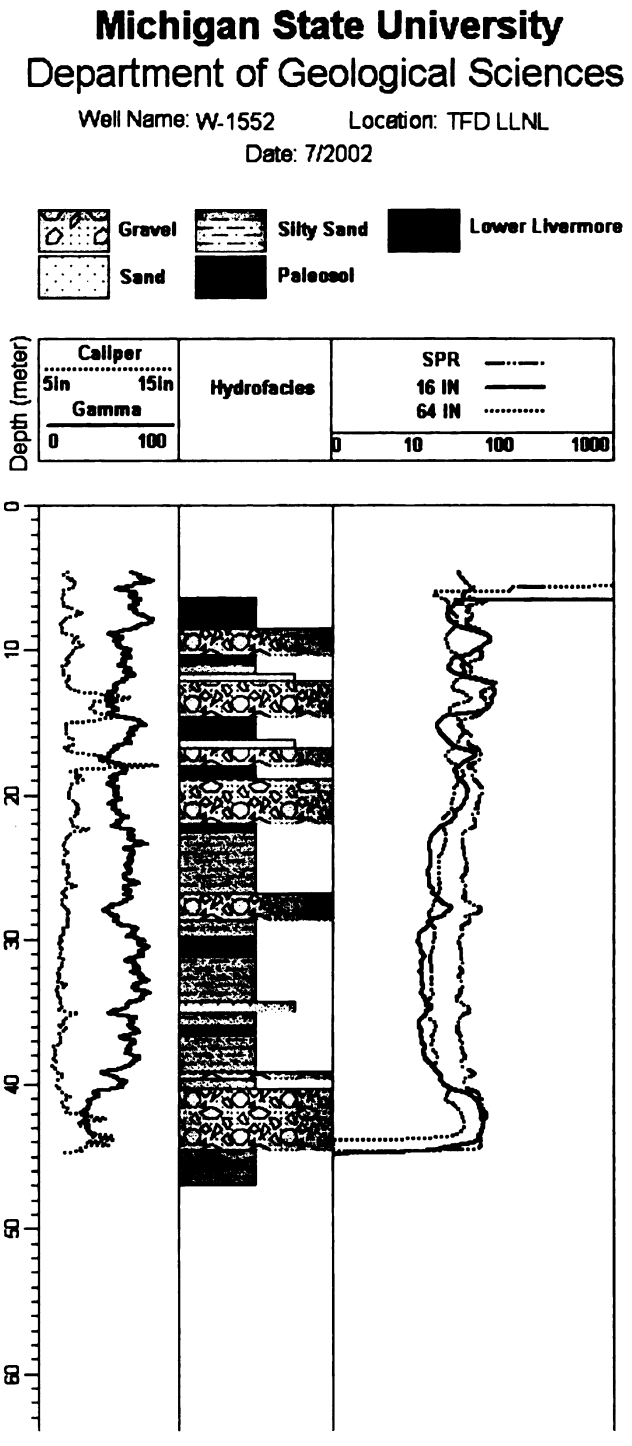

Figure B.22: Geophysical well logs and core descriptions for well 1552.

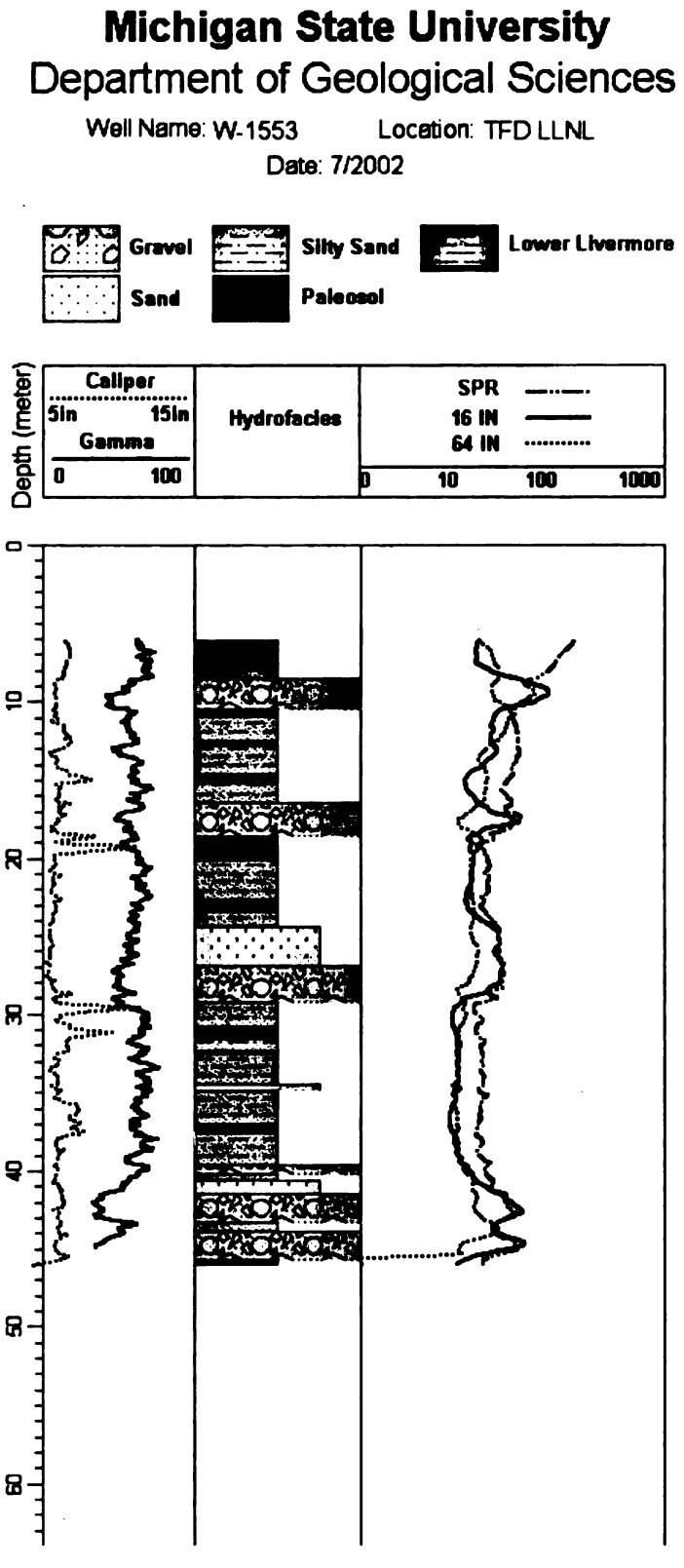

Figure B.23: Geophysical well logs and core descriptions for well 1553.

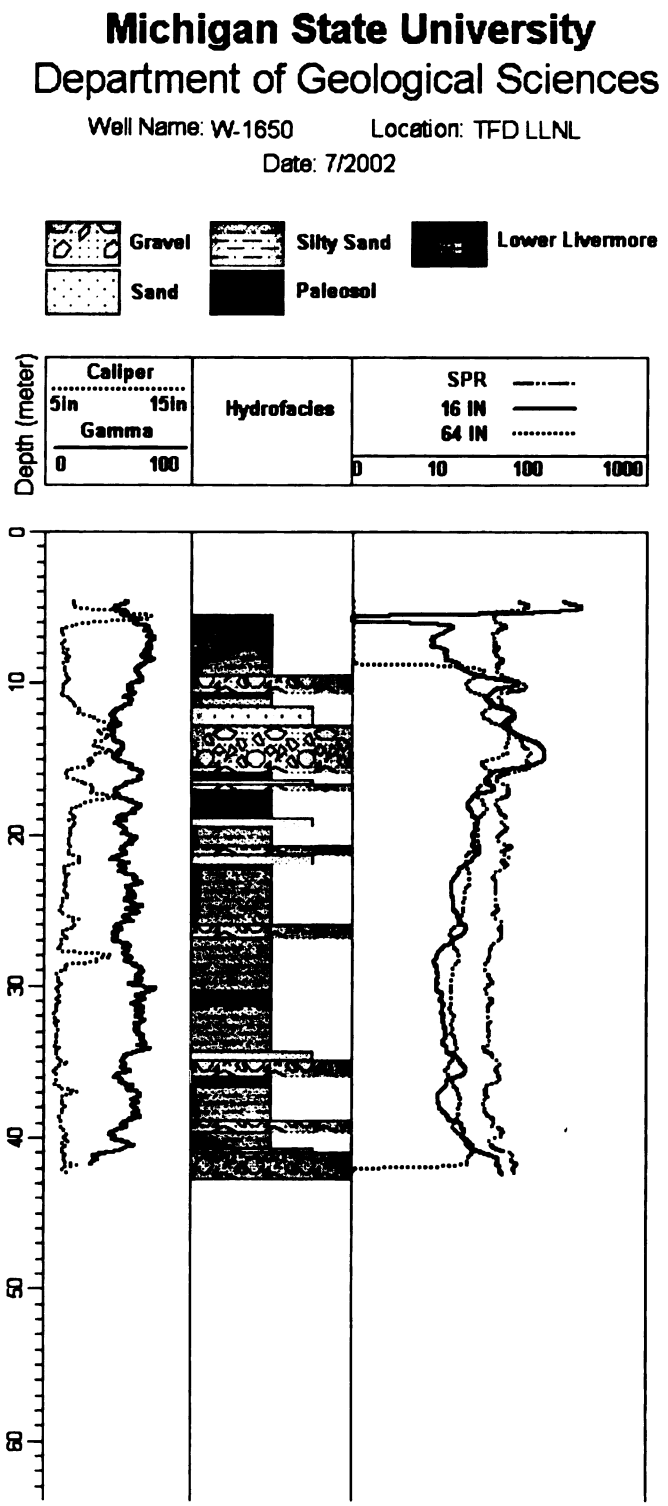

Figure B.24: Geophysical well logs and core descriptions for well 1650.

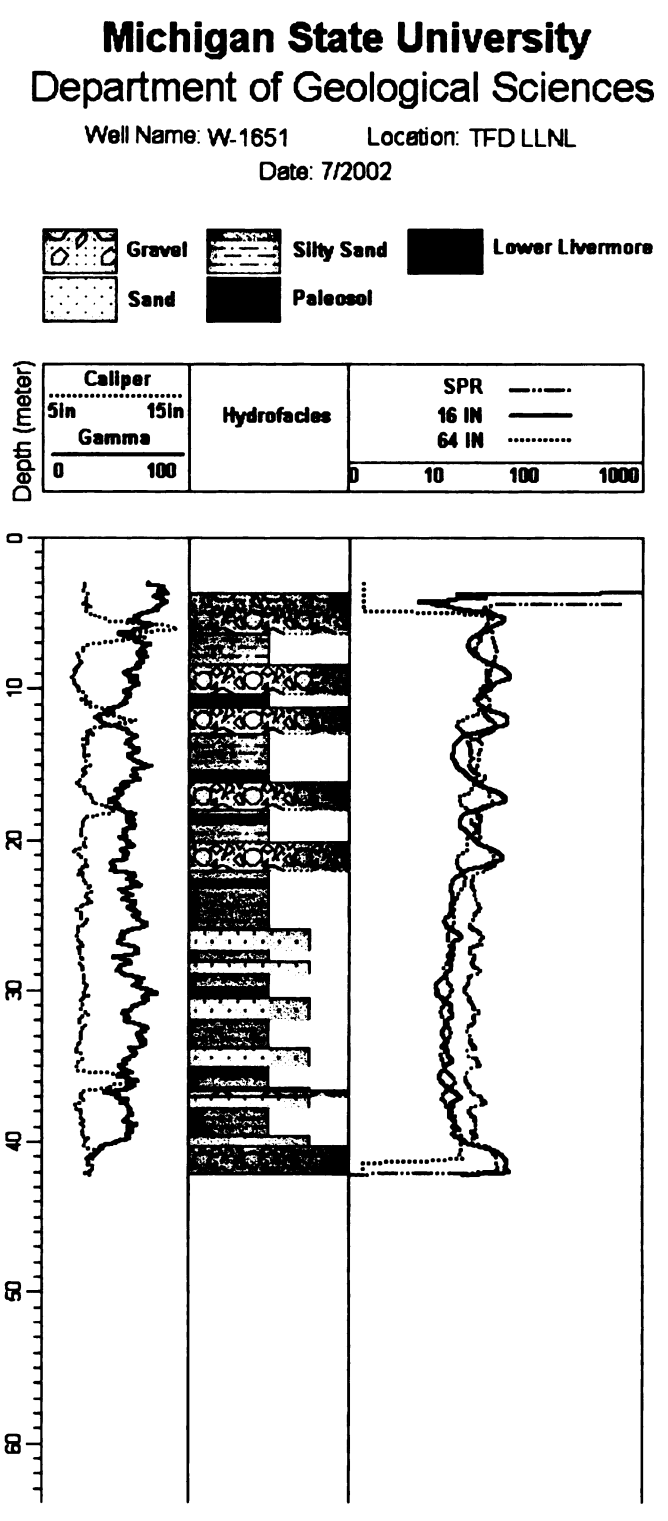

Figure B.25: Geophysical well logs and core descriptions for well 1651.

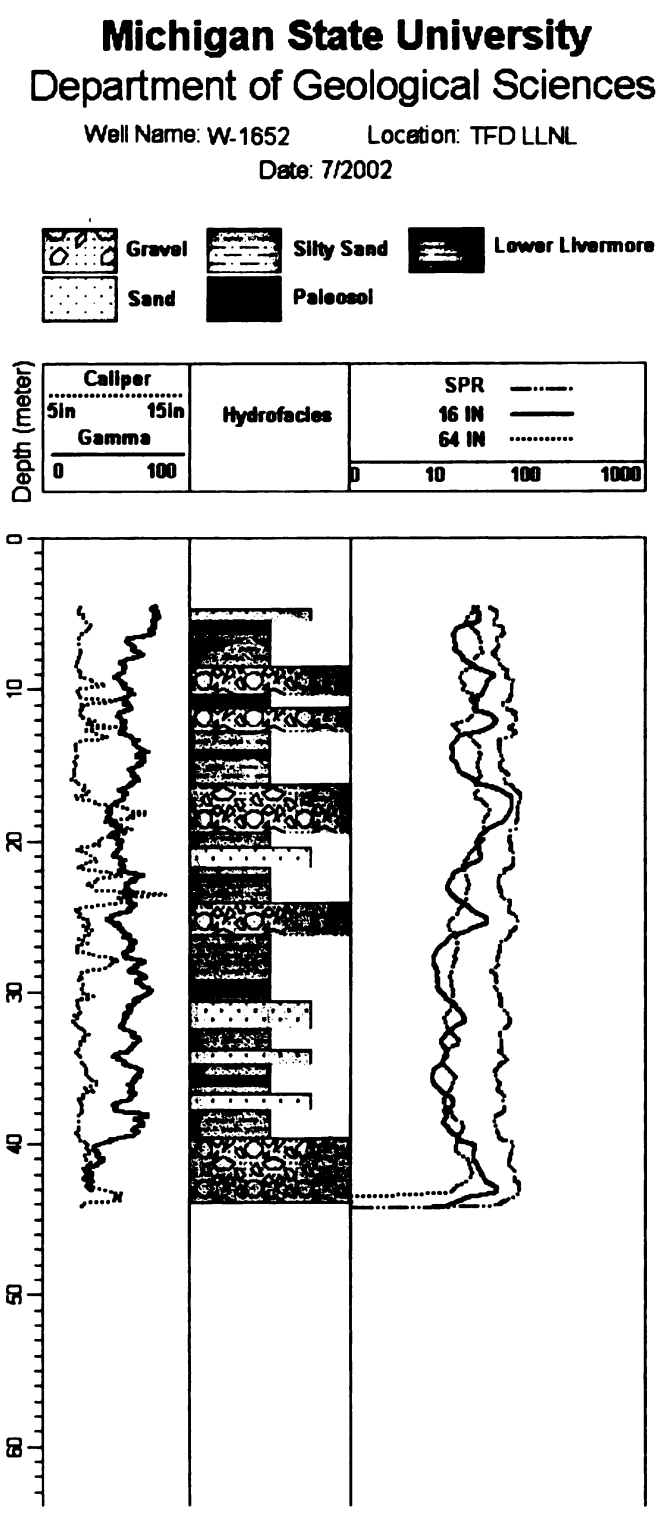

Figure B.26: Geophysical well logs and core descriptions for well 1652.

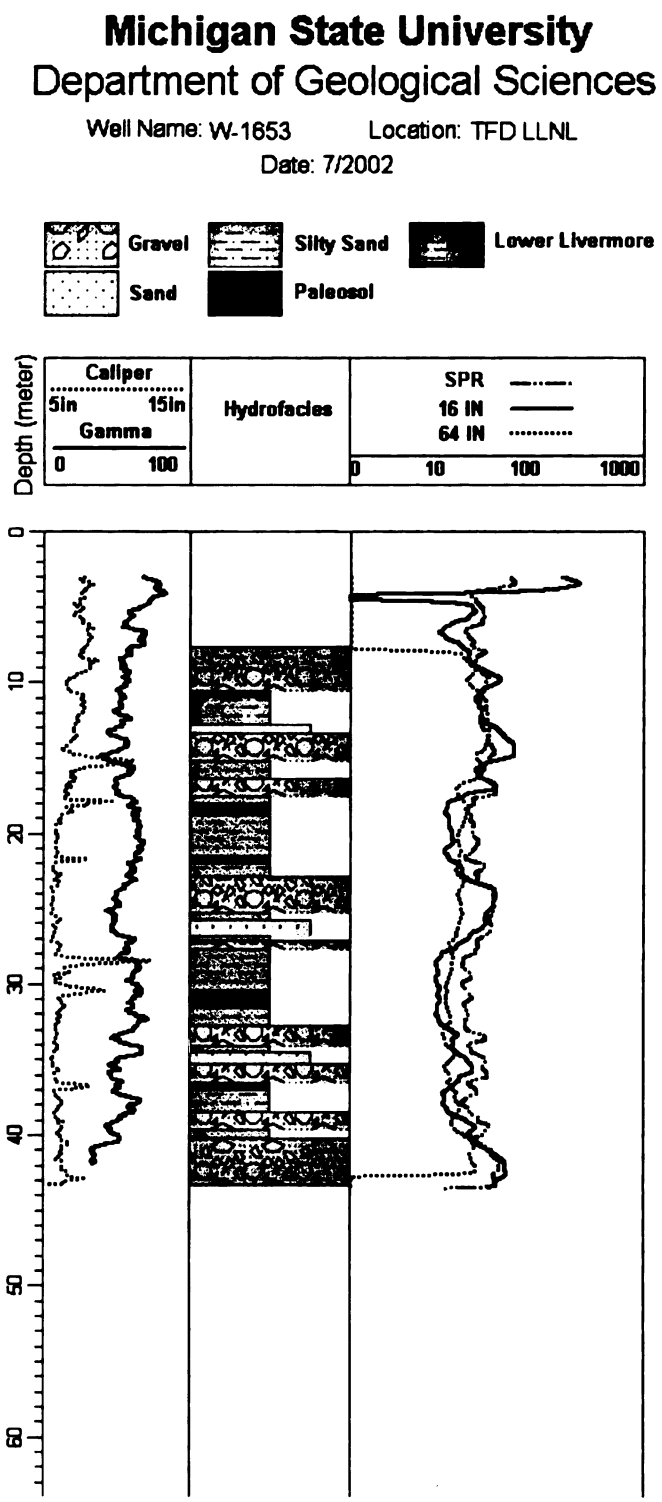

Figure B.27: Geophysical well logs and core descriptions for well 1653.

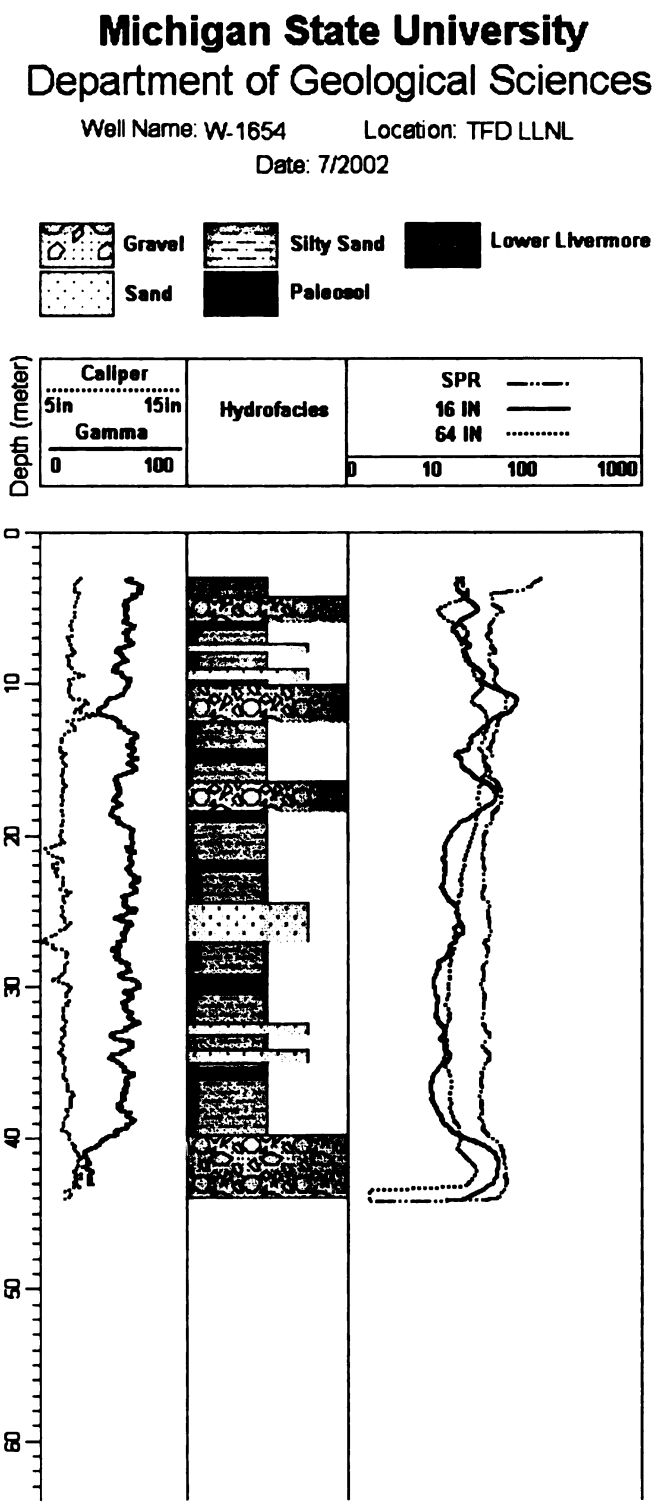

Figure B.28: Geophysical well logs and core descriptions for well 1654.

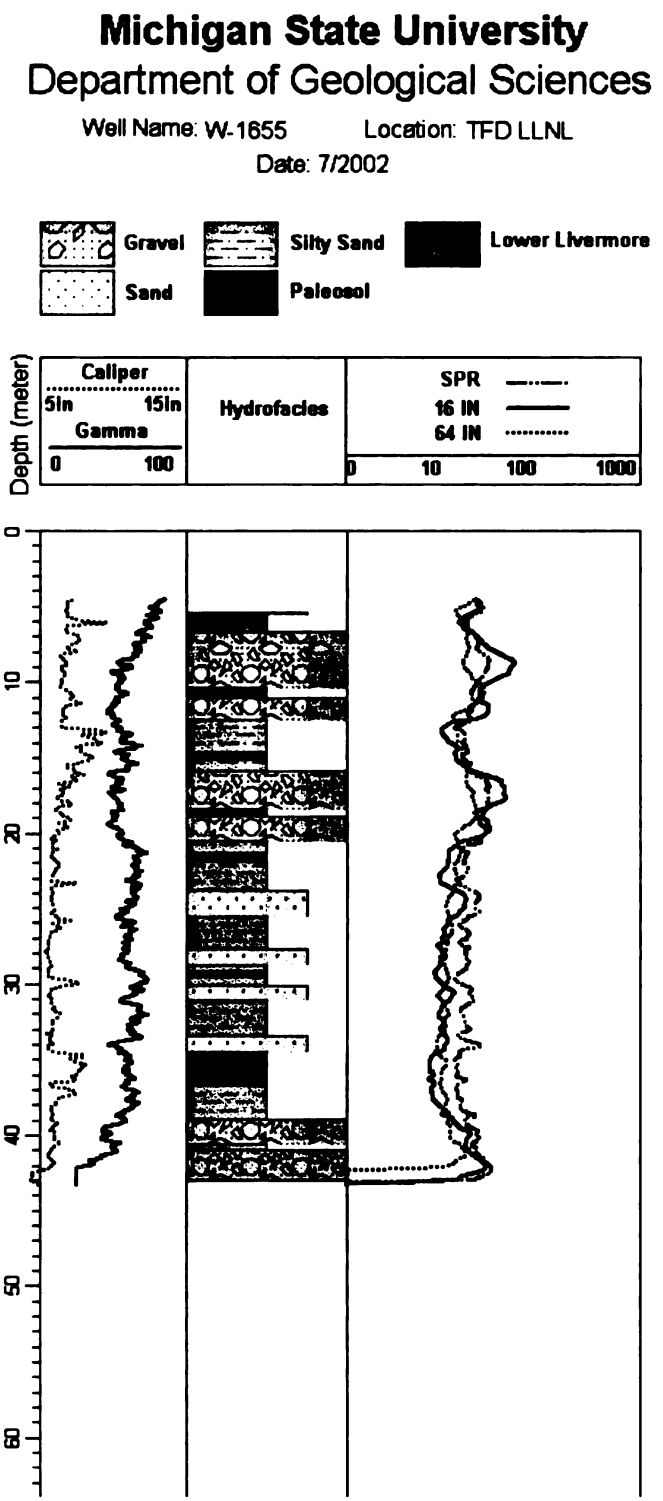

Figure B.29: Geophysical well logs and core descriptions for well 1655.

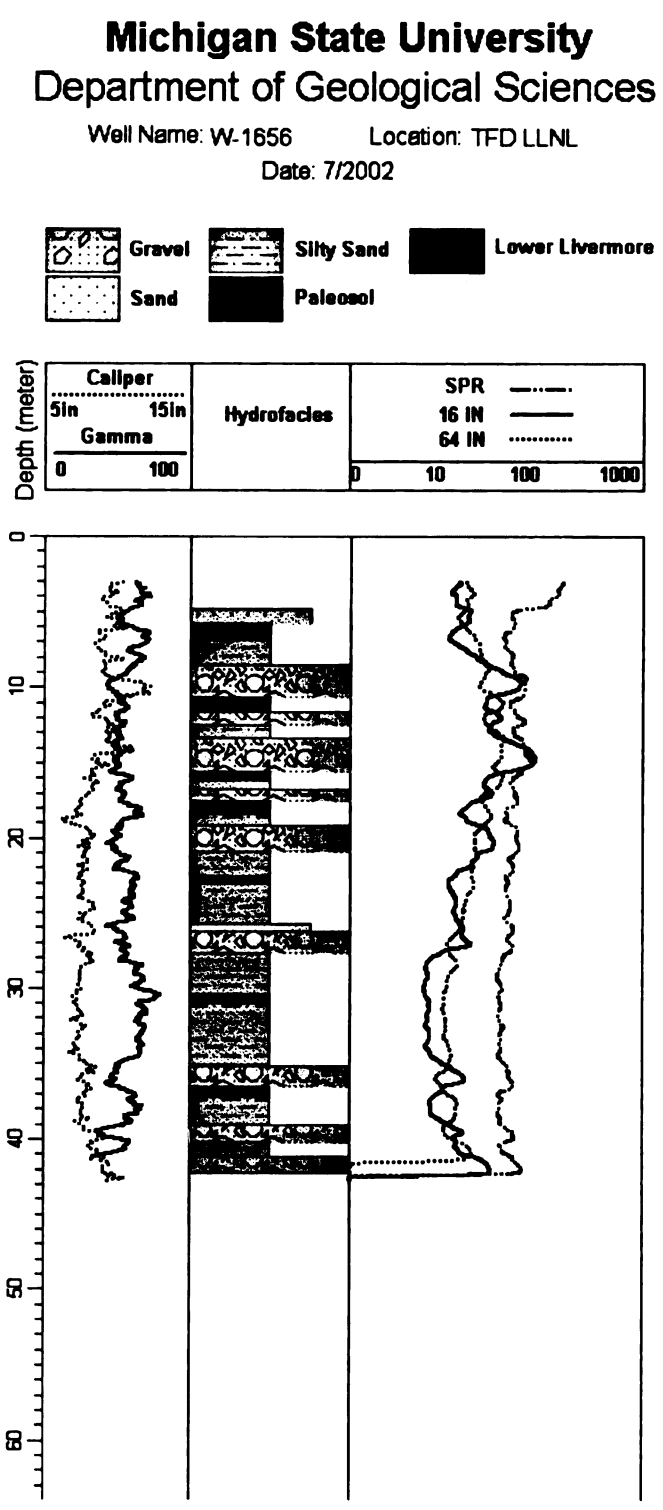

Figure B.30: Geophysical well logs and core descriptions for well 1656.

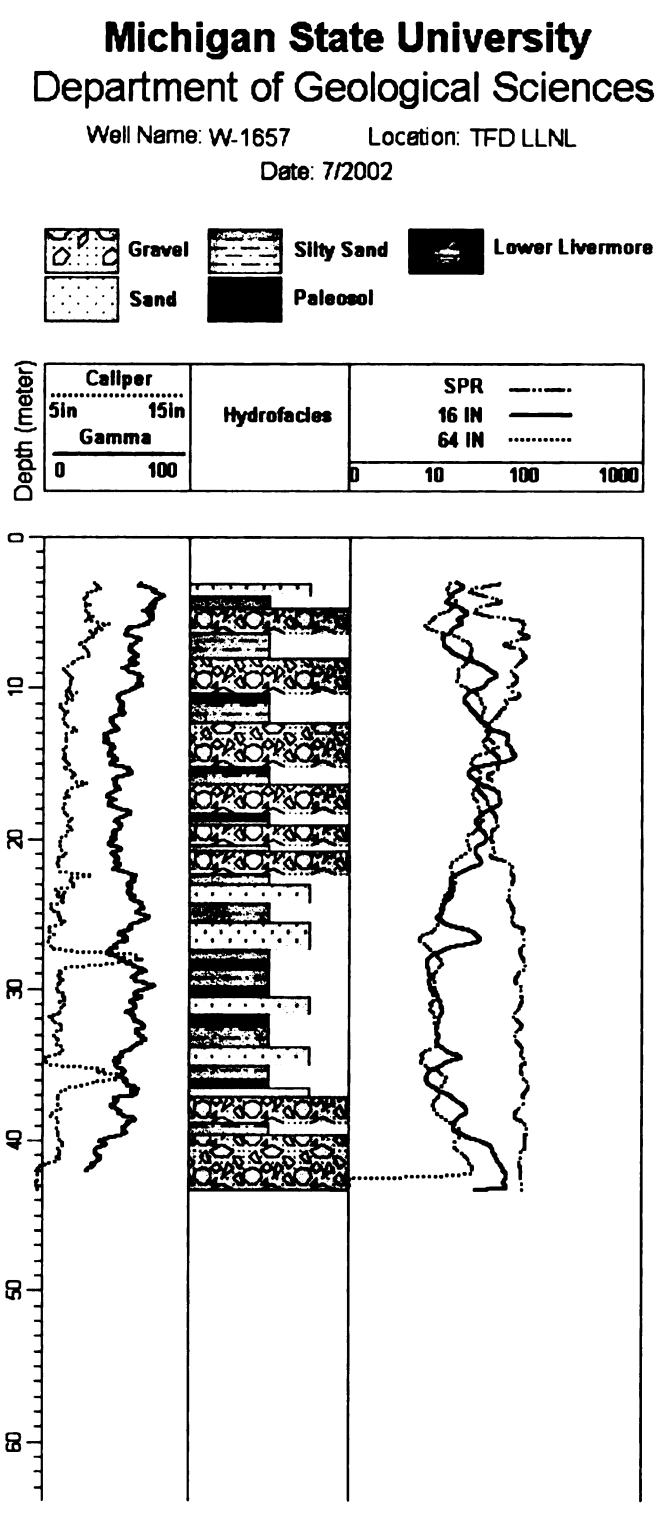

Figure B.31: Geophysical well logs and core descriptions for well 1657.

Appendix C

Cross Sections

This appendix contains fourteen cross-sections through the Helipad Site study area, LLNL California. Well locations through which cross sections are generated are shown in Figure C.1 and C.8. The stratigraphy shown in these cross sections (C.2 through C.7, and C.9 through C.16) was used to define sequence boundaries used in the geostatistical characterization described in Chapter 3 and Appendix F. Paleosol surfaces are informally named Aa through F following Weissmann (2001).

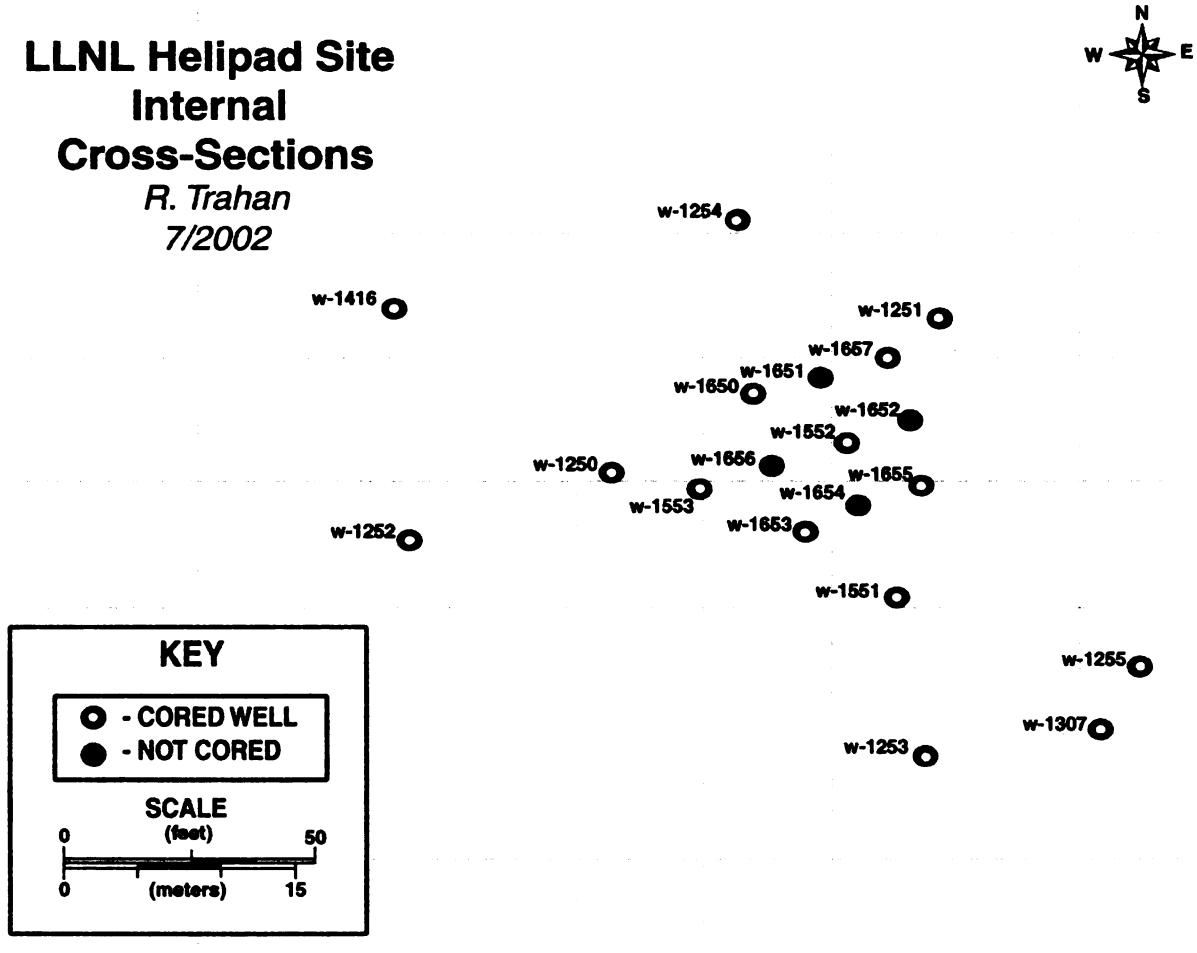

Figure C.1: Location of wells at the Helipad Site where wells with or without core are indicated.

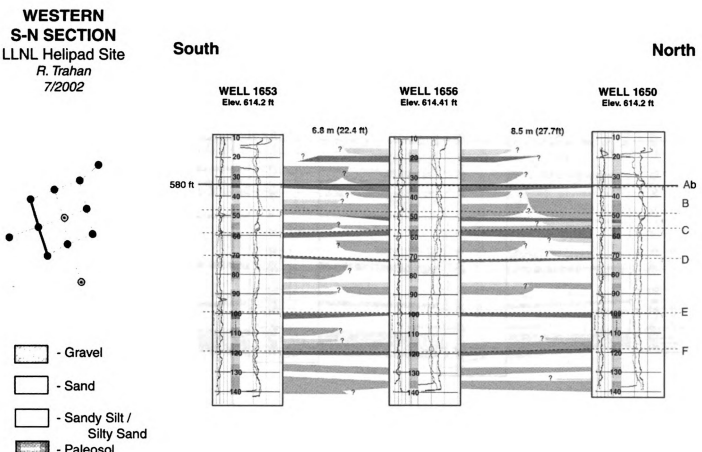

Figure C.2: South to north trending cross-section through the western central helipad area.

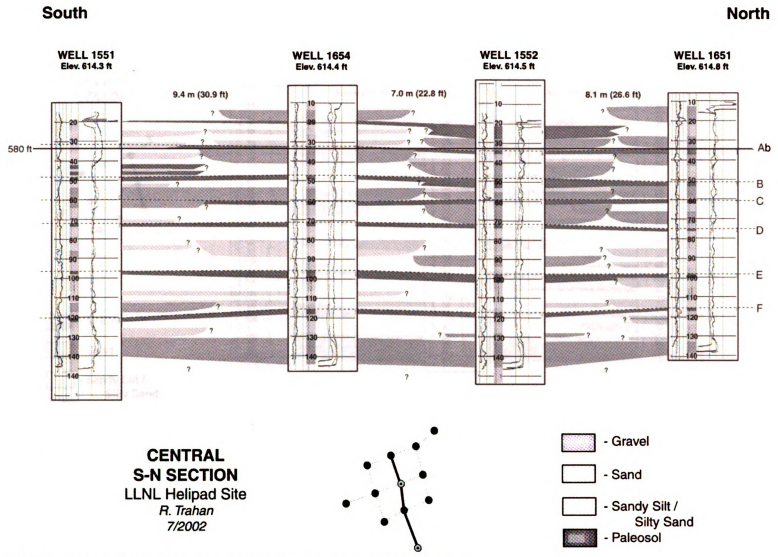

Figure C.3: South to north trending cross-section through the central helipad area.

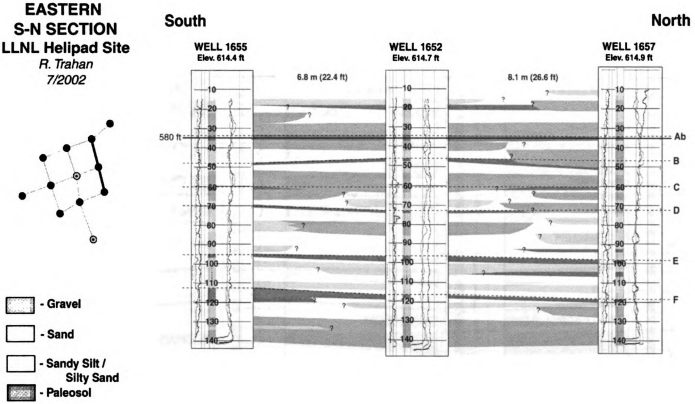

Figure C.4: South to north trending cross-section through the eastern central helipad area.

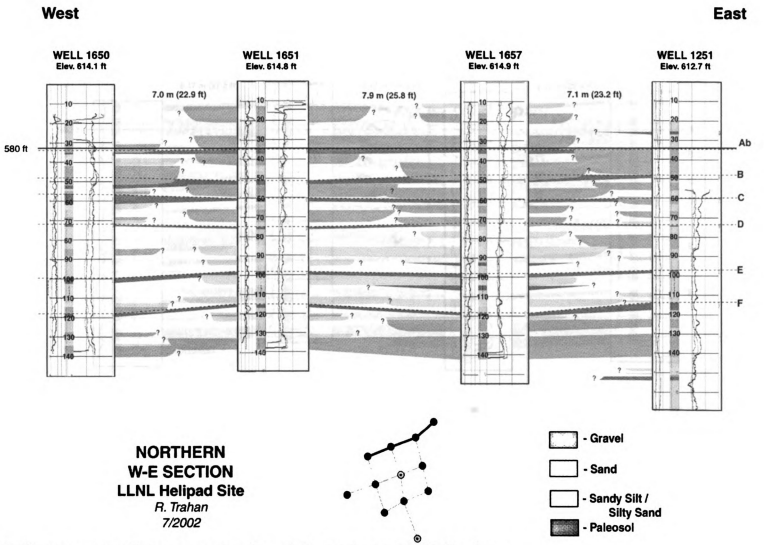

Figure C.5: West to east trending cross-section through the northern central helipad area.

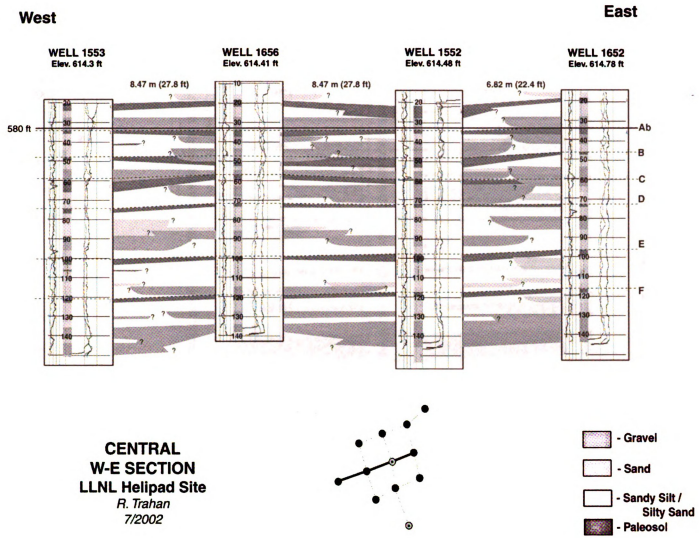

Figure C.6: West to east trending cross-section through the central helipad area.

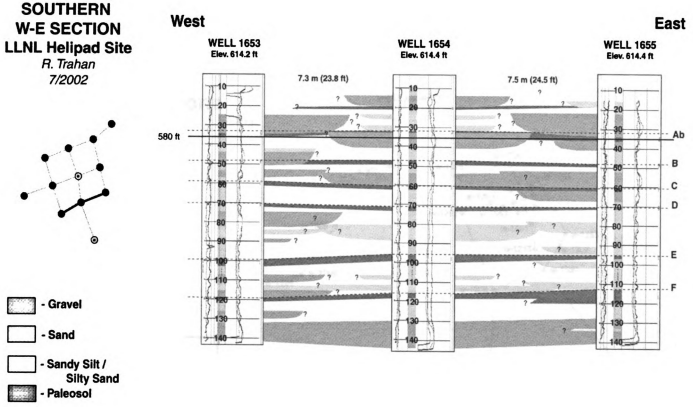

Figure C.7: West to east trending cross-section through the southern central helipad area.

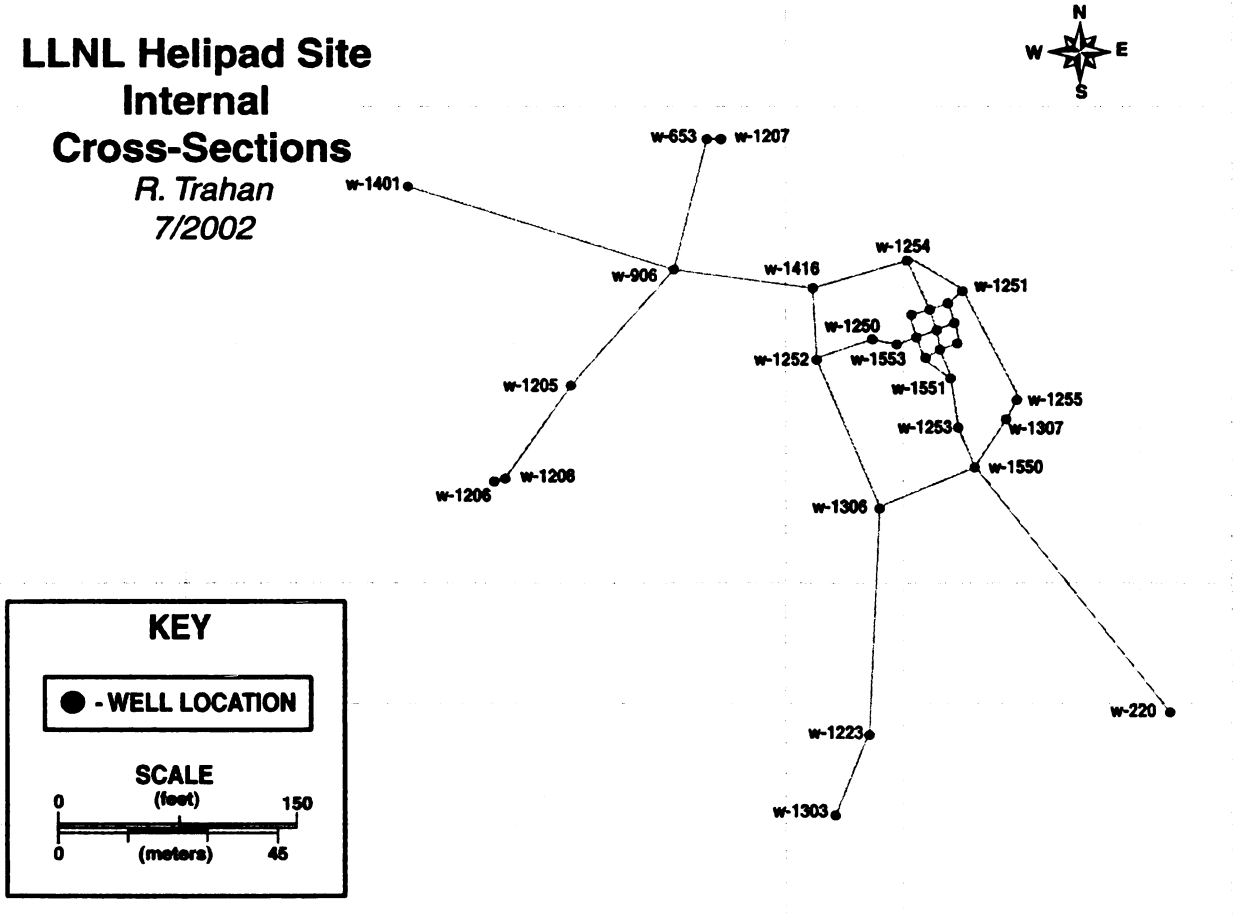

Figure C.8: Location of all wells within the Helipad Site study area used for site characterization.

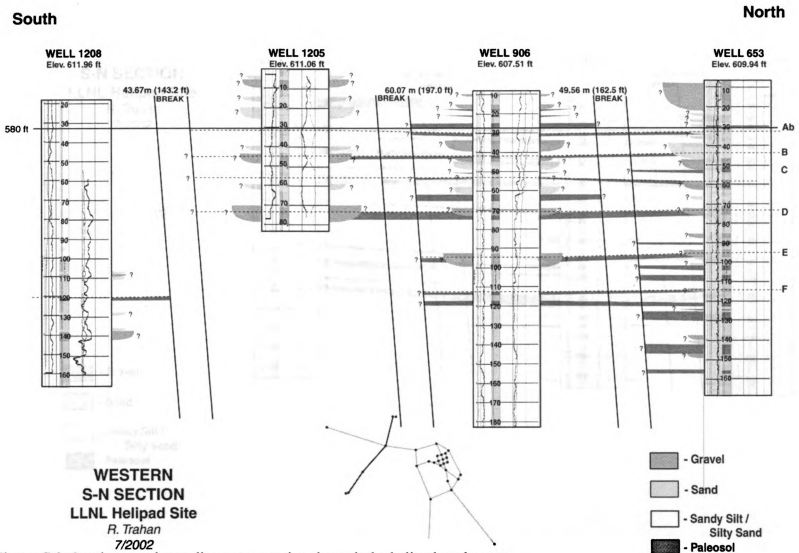

Figure C.9: South to north trending cross-section through the helipad study area.

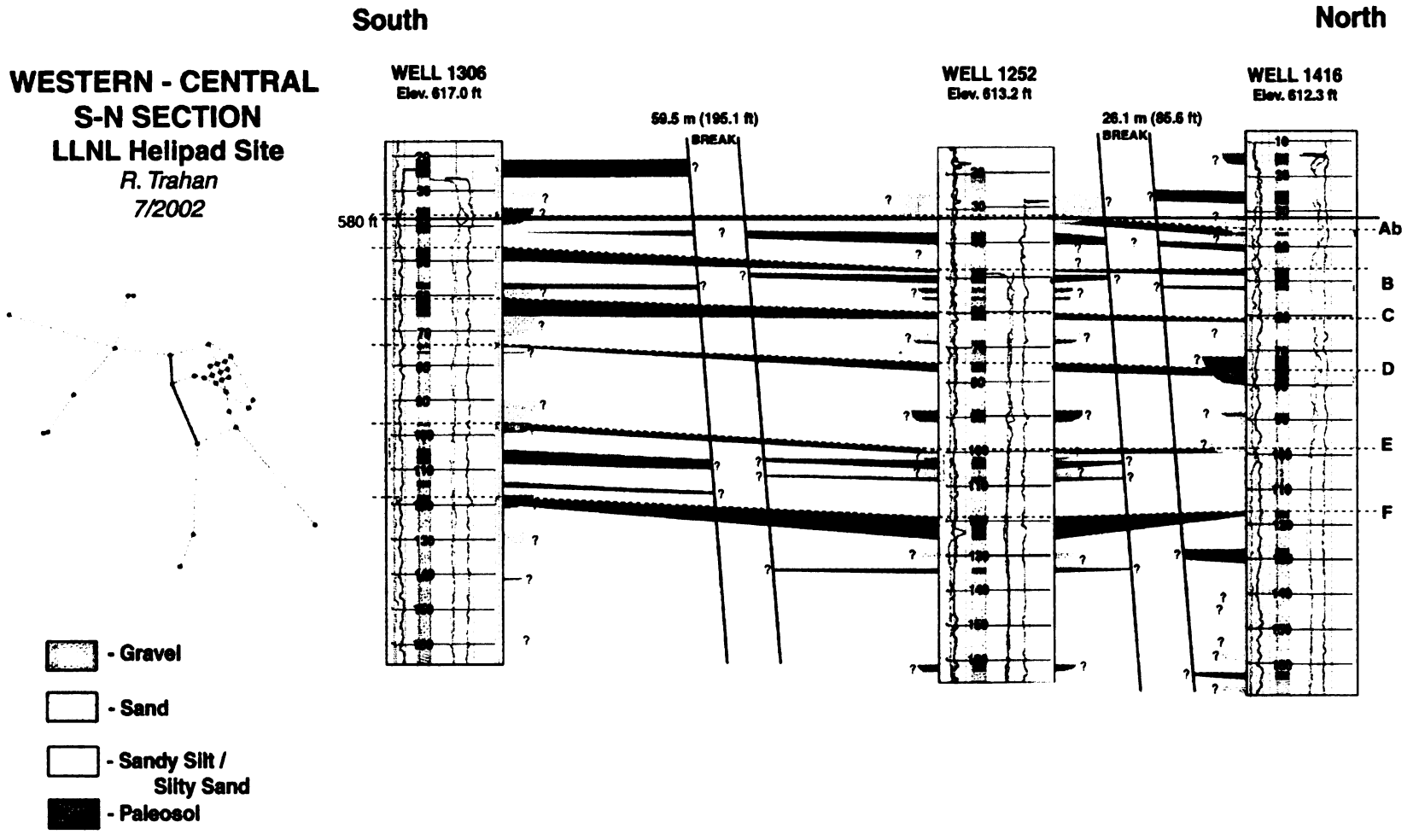

Figure C.10: South to north trending cross-section through the helipad study area.

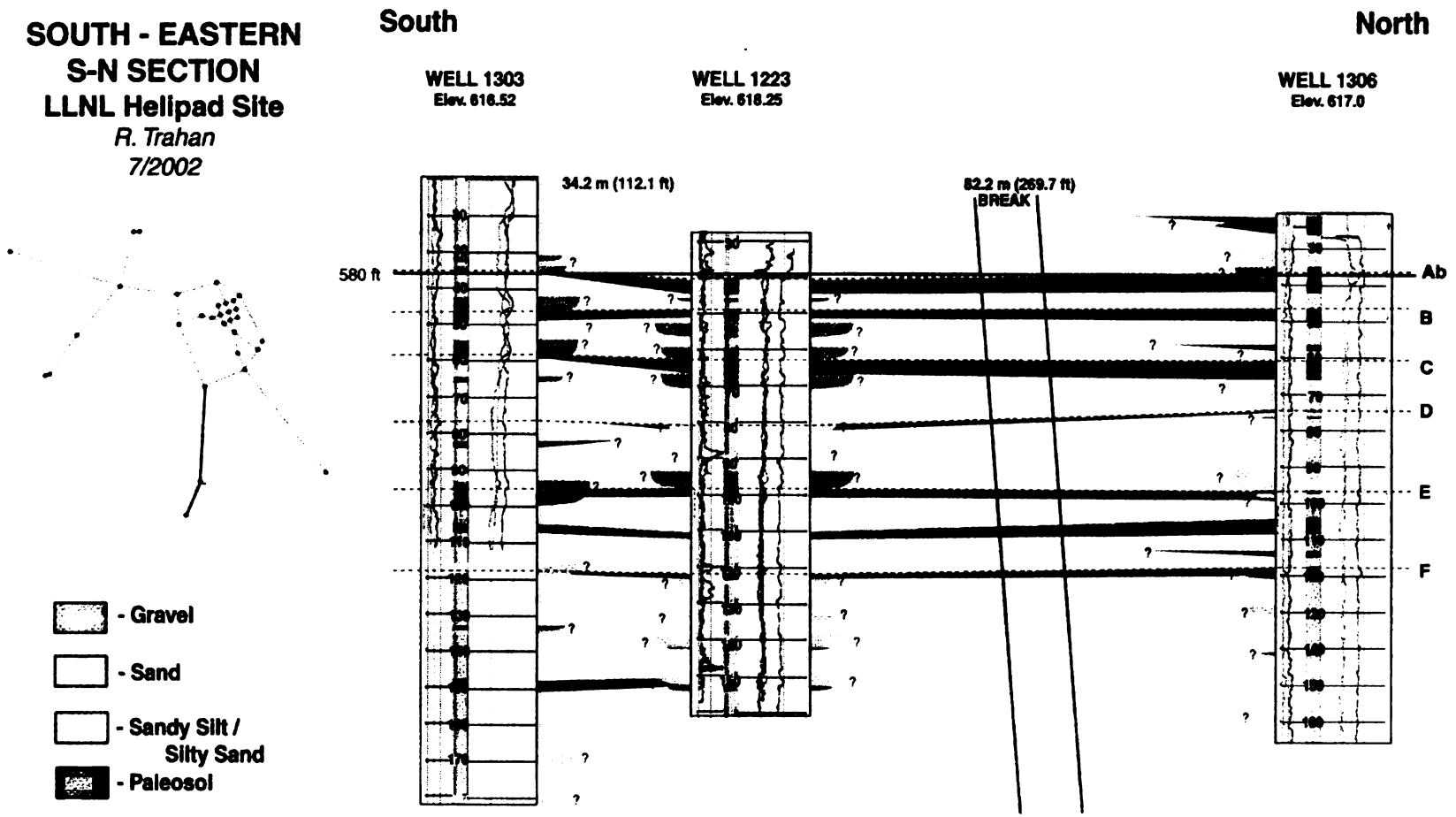

Figure C.11: South to north trending cross-section through the helipad study area.

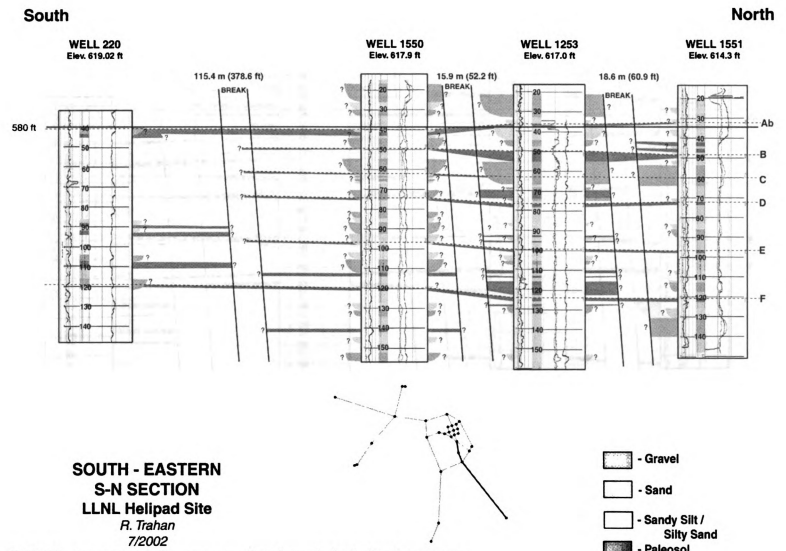

Figure C.12: West to east trending cross-section through the helipad study area.

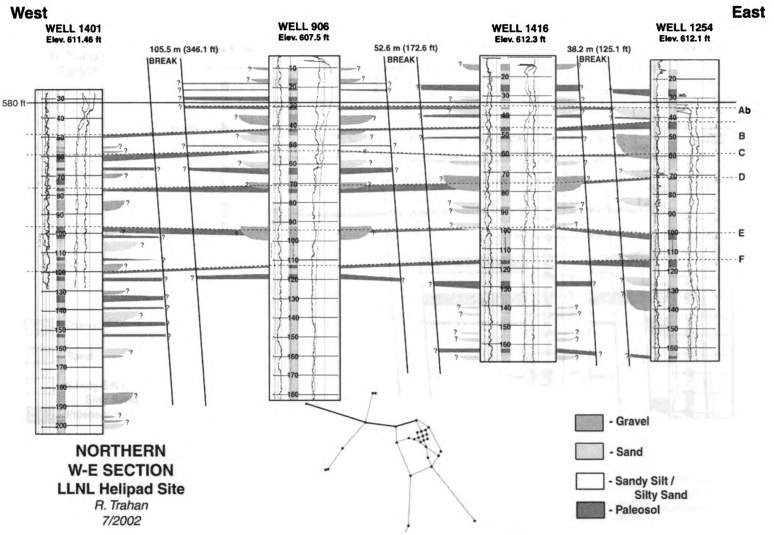

Figure C.13: West to east trending cross-section through the helipad study area.

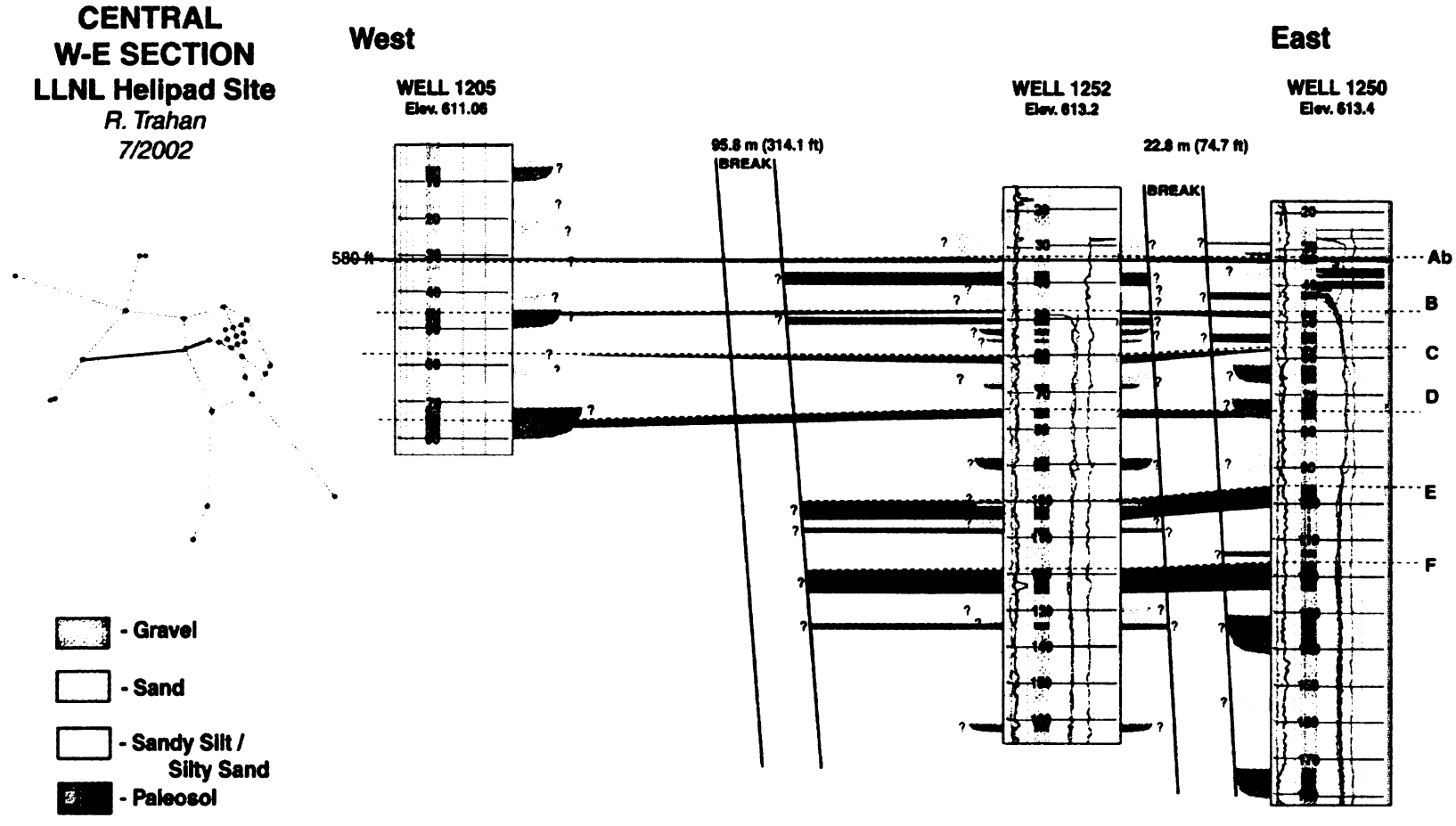

Figure C.14: West to east trending cross-section through the helipad study area.

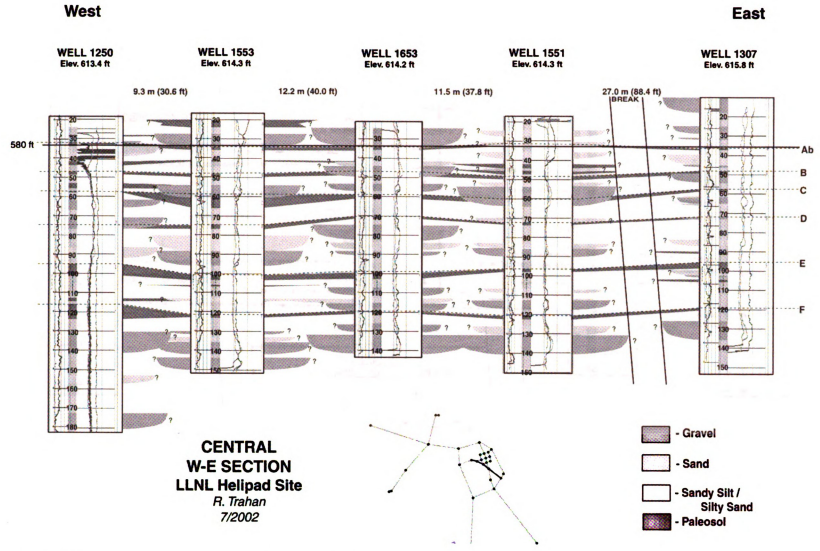

Figure C .15: West to east trending cross-section through the helipad study area.

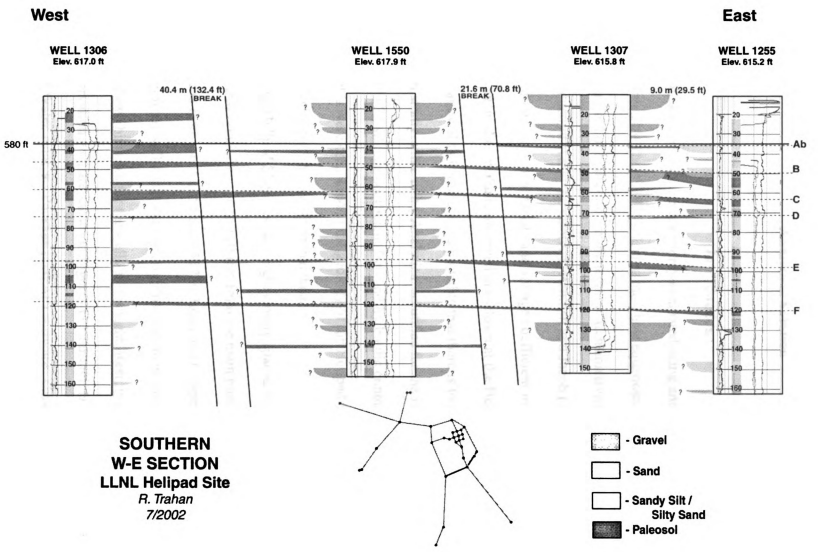

Figure C.16: West to east trending cross-section through the helipad study area.

Appendix D

Analytical Solution

Introduction

Pumping test results are commonly evaluated using analytical solutions following those first derived by Theis (1935). Using the Theis equations and following a set of assumptions, a field of hydraulic parameters (i.e. transmissivity, storage coefficient, and hydraulic conductivity) may be resolved. Hantush and Jacob (1955) first developed an analytical solution for transmissivity and storage coefficient in a leaky aquifer. This type of solution was used to evaluate observed drawdown at the Helipad Site. Within the context of an alluvial fan aquifer, it is probable that there is to a degree, vertical fluid flow between stratigraphic units. Analytical solutions for the Helipad Site include transmissivity (T), storage coefficient (Ss) and hydraulic conductivity (K). Solutions of T, Ss, and K fields were compared to the geology of the Helipad Site. The type curve with a 0.01 leakage factor had the best fit to that data.

For the Helipad Site, there are eight closely spaced observation wells (1650 series wells) that range from 30 to 110 feet from the main pumping well (1551). Pumping from this site is from wells 1551 and 1552 at 3gpm and 0.5gpm, respectfully, however only pumping from well 1552 was used for this analytical solution. Listed in table D.1 is a set of drawdown histories for the wells at this sight. Results of the analytical solutions for each observation well are shown in Figures D.1 through D.8. Analytical solutions used Ground Water Analysis Package (GWAP) software. These results are then plotted in

a map view of the central Helipad Site and contoured for geologic assessment (Figures D.10 through D.12).

Assumptions for Analytical Solutions

There are several assumptions that must be made in calculation of analytical solutions. For calculation of solutions at the Helipad Site, a confined leaky aquifer was assumed. The following is a list of assumptions that must be made for analytical solutions to be valid (Batu, 1998):

- Confined leaky aquifer assumptions –
    - Aquifer properties –
        - Homogeneous and isotropic.
        - Horizontal and has a constant thickness overlain by a confining layer having a constant vertical hydraulic conductivity and thickness. This confining layer is assumed to have a constant head plain.
        - Infinite and laterally extensive.
        - Compressible and completely elastic.
    - Well properties –
        - Has an infinitely small diameter.
        - Fully penetrating.
        - Discharges at a constant rate.
        - Head loss through the screen is negligible.

        - Discharge to well is derived exclusively from storage in the aquifer.
    - Other properties–
        - Water is immediately released from storage in the aquifer.
        - Storage in the aquifer is proportional to head.
        - Water has uniform density and viscosity.
        - Darcy's equation describes fluid flow.
        - Flow is horizontal and is directed toward the pumping well.

Methods

In order to determine T, Ss, and K for each observation well, type curve matching was constructed using the Ground Water Analysis Package (GWAP) software. An analytical solution for each observation well required:

- An aquifer thickness –
    - For the aquifer thickness, the maximum thickness for any sand or gravel channel visible across the well screen interval was assumed to be the main aquifer. This thickness of these channels was recorded as the aquifer thickness for calculation of the analytical solution.
- Pumping well discharge –
    - Pumping within the alluvial fan aquifer over the observation period was from wells 1551 and 1552. Well 1551 had a pumping rate of 3gpm while well 1552 only had a pumping rate of 0.5gpm. For calculation of a solution, it was assumed that pumping from well 1552 was negligible and

a pumping rate of 3gpm from well 1551 was assumed to be the primary source of pumping.

- Radius of pumping well –
    - Wells drilled at LLNL use a standard six inch radius well tubing. A well radius of 0.5 feet was used for the analysis.
- Distance from observation well to pumping well –
    - Distances from pumping well to observation wells were calculated using the Pythagoras thorium. Given the northing and easting coordinates for each of these wells, distances between pumping (1551) and observation wells (1650 series) was calculated.
- Time and drawdown –
    - A table of time and drawdown was inserted into GWAP. Time is measured in minutes and drawdown is measured in feet. An abbreviated drawdown set is listed in table D.1 for 1650 series wells used.
- Curve matching –
    - A type curve for a confined leaky aquifer with a leakage factor of 0.01 was used to match drawdown data for each observation well. Early time drawdown was matched with the type curve. Results of these solutions are listed in figures D.1 through D.8.

Results

The following are a series of type curve matches for wells 1650, 1651, 1652, 1653, 1654, 1655, 1656, and 1657 (Figures D.1 through D.8). Listed within each figure

is a solution for transmissivity (T), storativity (Ss), and hydraulic conductivity (K). Also listed within each figure are aquifer thickness (b), type curve (r/B), and the leakage factor (B). A summary of this information is listed in Table D.2.

Using observed drawdown histories (Appendix H) located at the Helipad Site (Figure D.9), values listed in Table D.2 are mapped. Figures D.10 through D.12 illustrate the distribution of hydraulic properties (T, S, and K) across the central Helipad study area. The distributions of hydraulic properties show a centrally located north – south trending zone of increased T, S and K. This zone may translate to a channel sand or gravel unit passing through this area. To the east and west of this zone are smaller values of T, S, and K. These zones may translate to overbank deposits lateral to a main channel deposit.

However, results of the analytical solution are contrary to the observed geology for the Helipad Site. The geology of this site (Appendix C) shows a higher conducting gravel channel passing through wells 1650, 1656, and 1653 which also is in correlation to a higher observed drawdown. This gravel channel transitions to a lower conductive sand channel that thins to the east of wells 1650, 1656, and 1653 corresponding to a moderate to low observed drawdown.

Conclusions

Evaluation of pumping test results for determination of the distributions of hydraulic properties for the Helipad Site may be solved using an analytical solution. However, there are several assumptions that must be made for this type of solution to be valid. If these assumptions are made, then distributions of transmissivity, storativity, and hydraulic conductivity may be mapped. This distribution of hydraulic properties is related

to the heterogeneity at this site. Heterogeneity is illustrated through a north-south trending zone of increased hydraulic properties which may relate to a channel deposit passing through this site. From previous geologic investigations (Chapter 2), the Arroyo Seco shows signs of a northern migration across the LLNL site. The distributions of hydraulic propertied (Figures D.10 – D.12) may be evidence of this channel.

However, the distributions of T and K fields are contrary to the geology of this site. Assumptions for a confined leaky aquifer were made in the analytical solution. In a heterogeneous alluvial aquifer, many of these assumptions are broken. This may account for the discrepancy between results and the observed geology at the Helipad Site. In an analytical solution, T is inversely proportional to drawdown such that high drawdown is associated with low T. However, geologically high drawdown is related to location within the channel and not necessarily a low T.

DRAWDOWN **Start date - 4-27-00 at 14:20**

Time (min)	w1650	w1651	w1652	w1653	w1654	w1655	w1656	w1657
0	0.00	0.00	0.00	0.00	0.00	0.00	0.00	0.00
50	0.45	0.05	0.16	0.66	0.60	0.19	0.54	0.07
100	0.73	0.11	0.33	0.97	0.97	0.33	0.81	0.17
150	0.90	0.18	0.47	1.16	1.19	0.43	0.97	0.25
200	1.03	0.23	0.58	1.28	1.33	0.51	1.10	0.33
250	1.13	0.28	0.67	1.38	1.44	0.57	1.20	0.39
300	1.21	0.32	0.75	1.46	1.53	0.62	1.28	0.45
350	1.28	0.37	0.81	1.52	1.60	0.67	1.34	0.49
400	1.35	0.40	0.87	1.58	1.67	0.71	1.41	0.54
450	1.41	0.43	0.93	1.63	1.73	0.74	1.46	0.58
500	1.46	0.46	0.98	1.67	1.78	0.77	1.51	0.62
550	1.50	0.49	1.02	1.71	1.82	0.80	1.55	0.66
600	1.54	0.52	1.06	1.74	1.86	0.83	1.58	0.69
650	1.57	0.54	1.09	1.77	1.89	0.84	1.61	0.72
700	1.60	0.56	1.12	1.78	1.91	0.85	1.64	0.74
750	1.62	0.57	1.15	1.80	1.93	0.87	1.66	0.77
800	1.64	0.59	1.17	1.82	1.95	0.88	1.68	0.79
850	1.67	0.61	1.19	1.83	1.97	0.89	1.70	0.80
900	1.69	0.63	1.21	1.85	1.99	0.91	1.72	0.82
950	1.71	0.65	1.23	1.86	2.01	0.92	1.74	0.84
1000	1.73	0.67	1.25	1.87	2.03	0.93	1.75	0.86
1050	1.74	0.69	1.26	1.89	2.04	0.94	1.77	0.88
1100	1.76	0.70	1.28	1.89	2.05	0.95	1.78	0.89
1150	1.77	0.71	1.29	1.90	2.06	0.96	1.78	0.90
1200	1.77	0.71	1.29	1.89	2.06	0.96	1.78	0.91
1250	1.77	0.73	1.30	1.89	2.05	0.96	1.78	0.92
1300	1.77	0.73	1.30	1.88	2.05	0.96	1.78	0.93
1350	1.77	0.74	1.30	1.88	2.05	0.96	1.78	0.93
1400	1.78	0.75	1.30	1.87	2.05	0.96	1.78	0.93
1440	1.78	0.75	1.30	1.87	2.05	0.96	1.78	0.93

Table D.1: Listed above are accumulative drawdown readings at a specified time after pumping commencement. Drawdown histories for wells 1650, 1651, 1652, 1653, 1654, 1655, 1656, and 1657 are recorded.

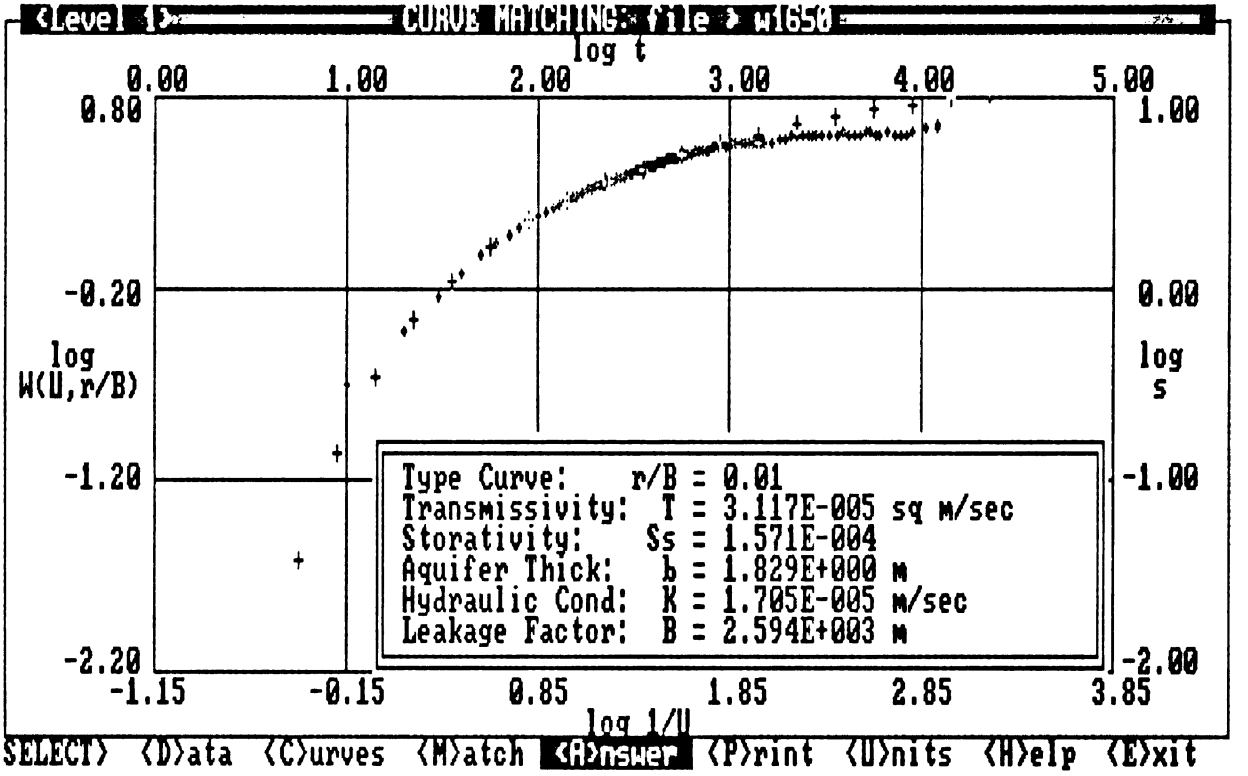

Figure D.1: Curve match and analytical solution for well 1650.

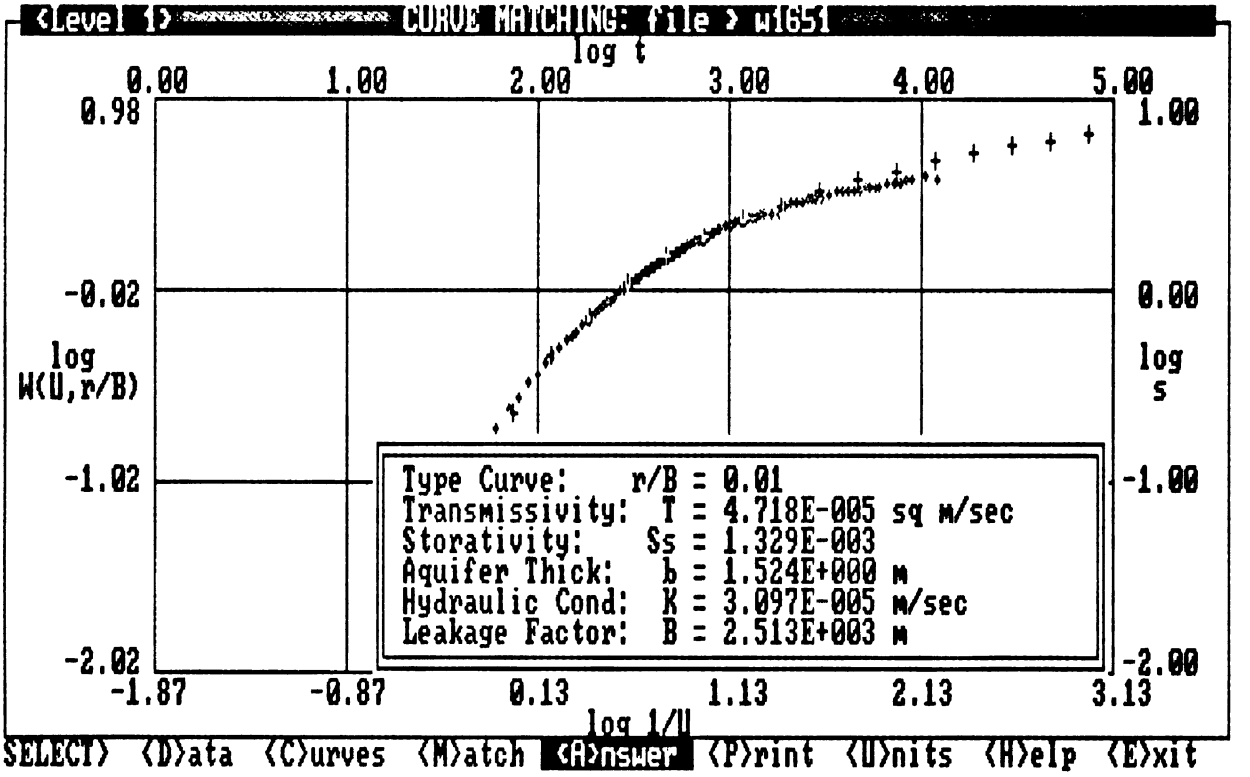

Figure D.2: Curve match and analytical solution for well 1651.

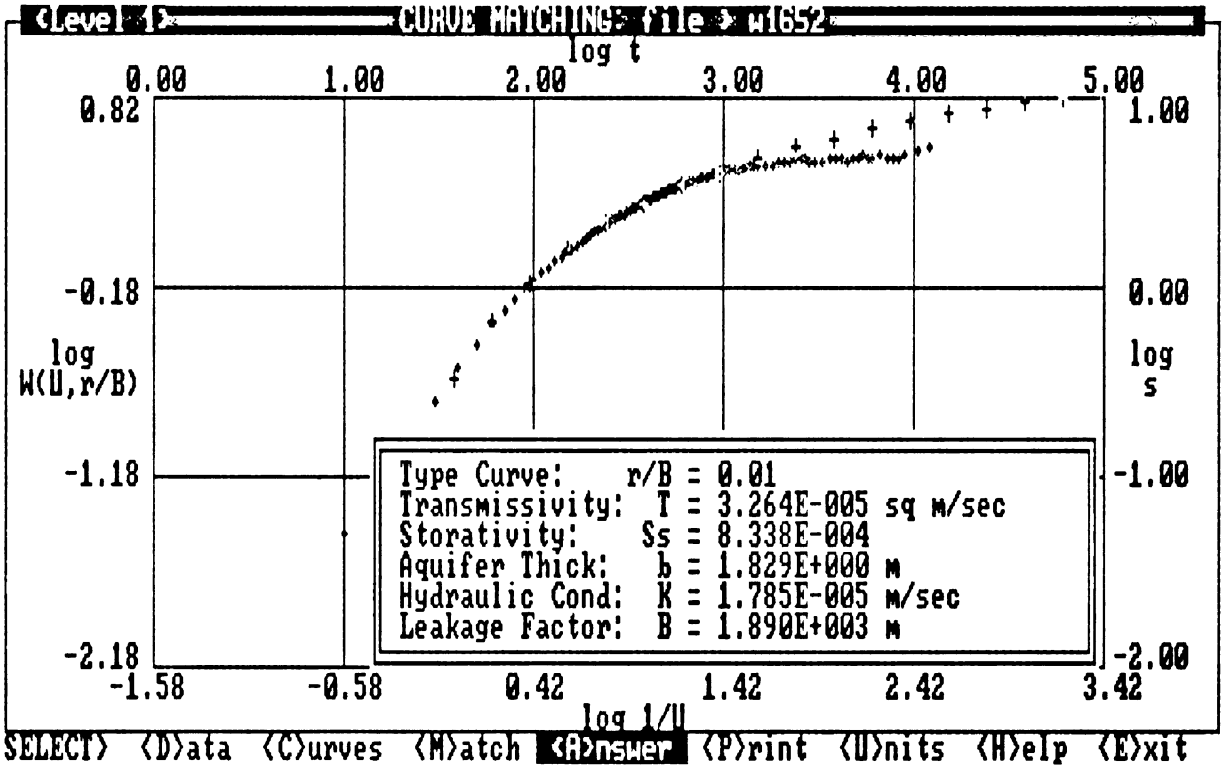

Figure D.3: Curve match and analytical solution for well 1652.

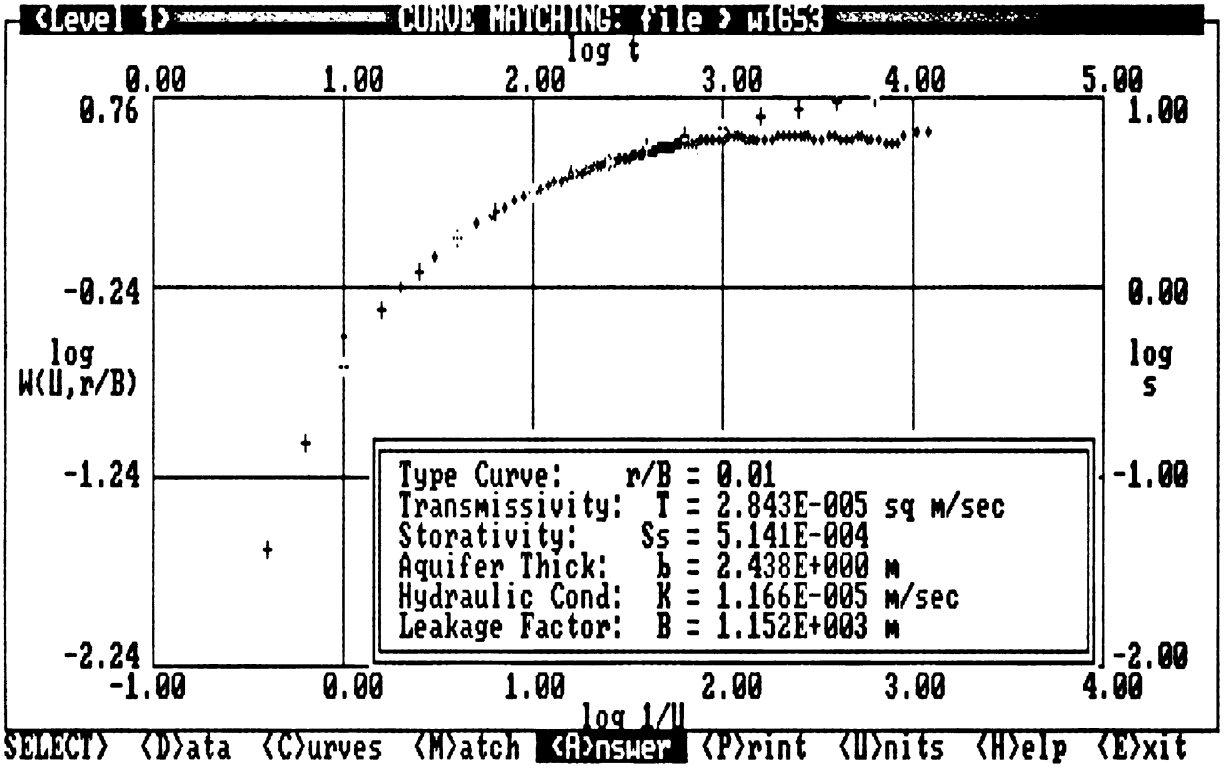

Figure D.4: Curve match and analytical solution for well 1653.

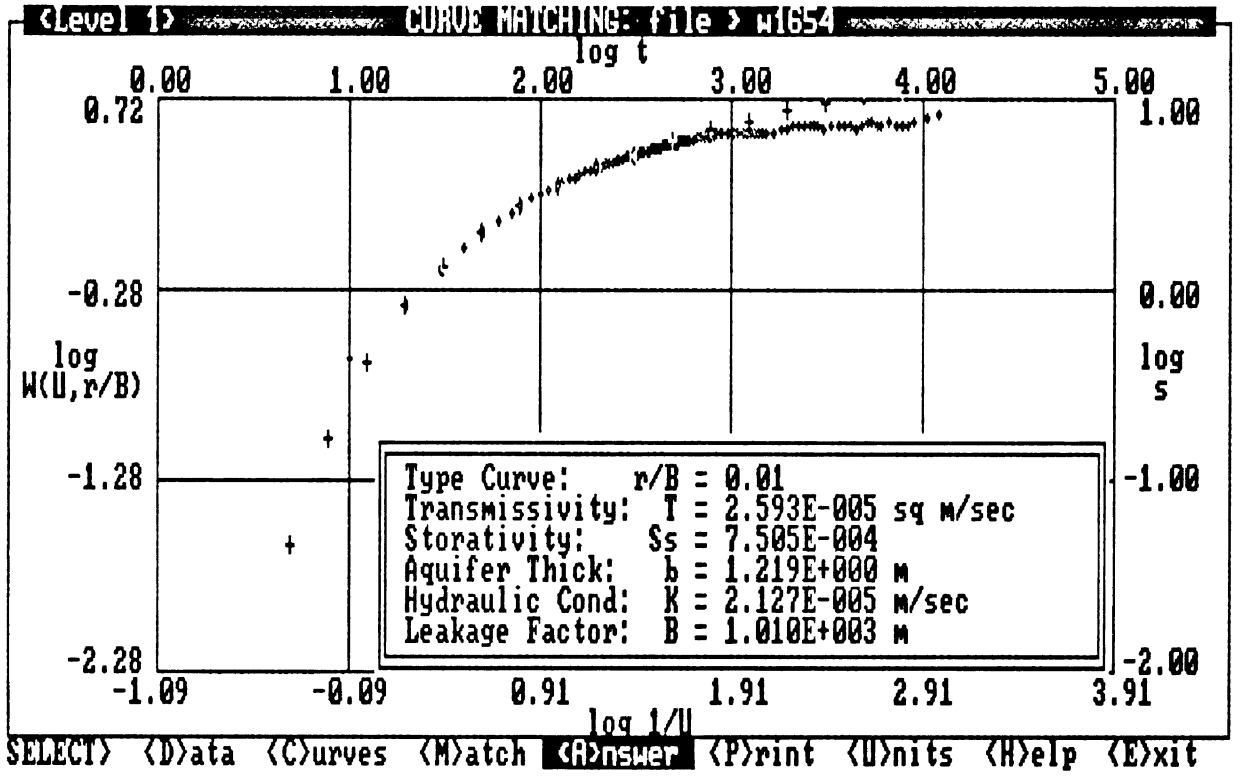

Figure D.5: Curve match and analytical solution for well 1654.

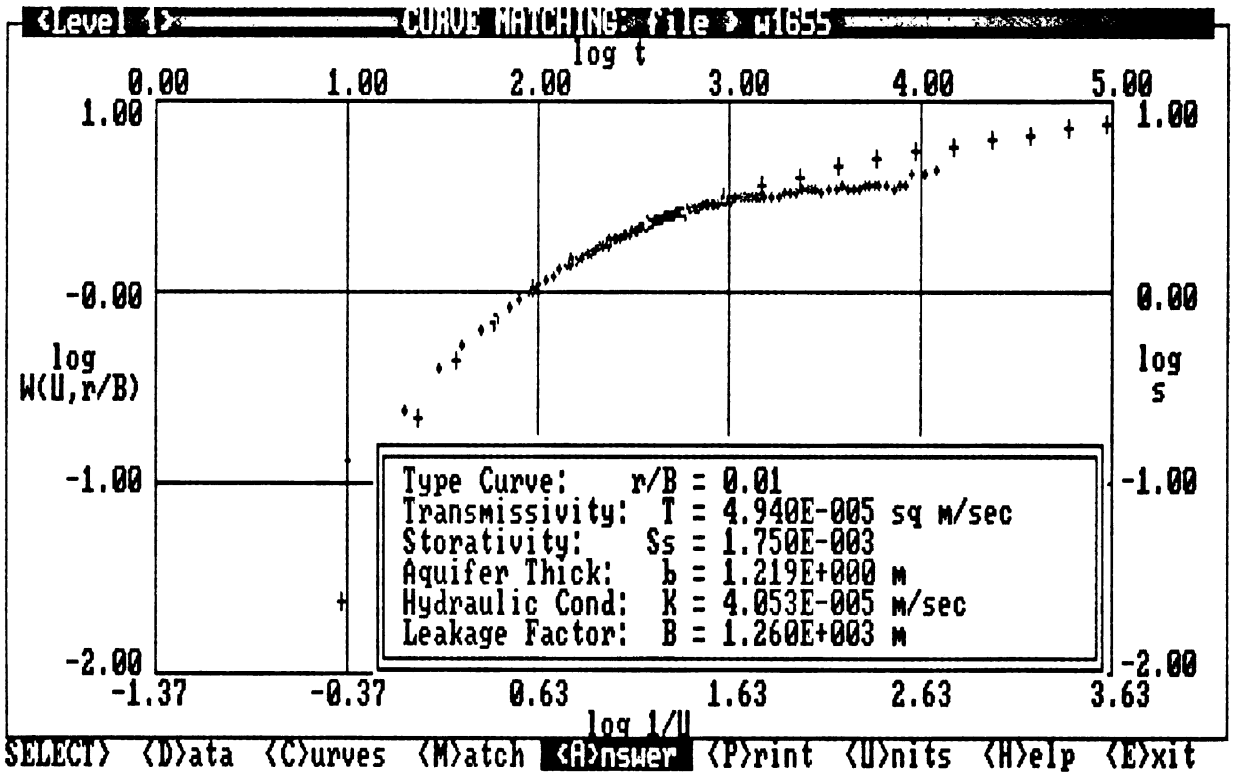

Figure D.6: Curve match and analytical solution for well 1655.

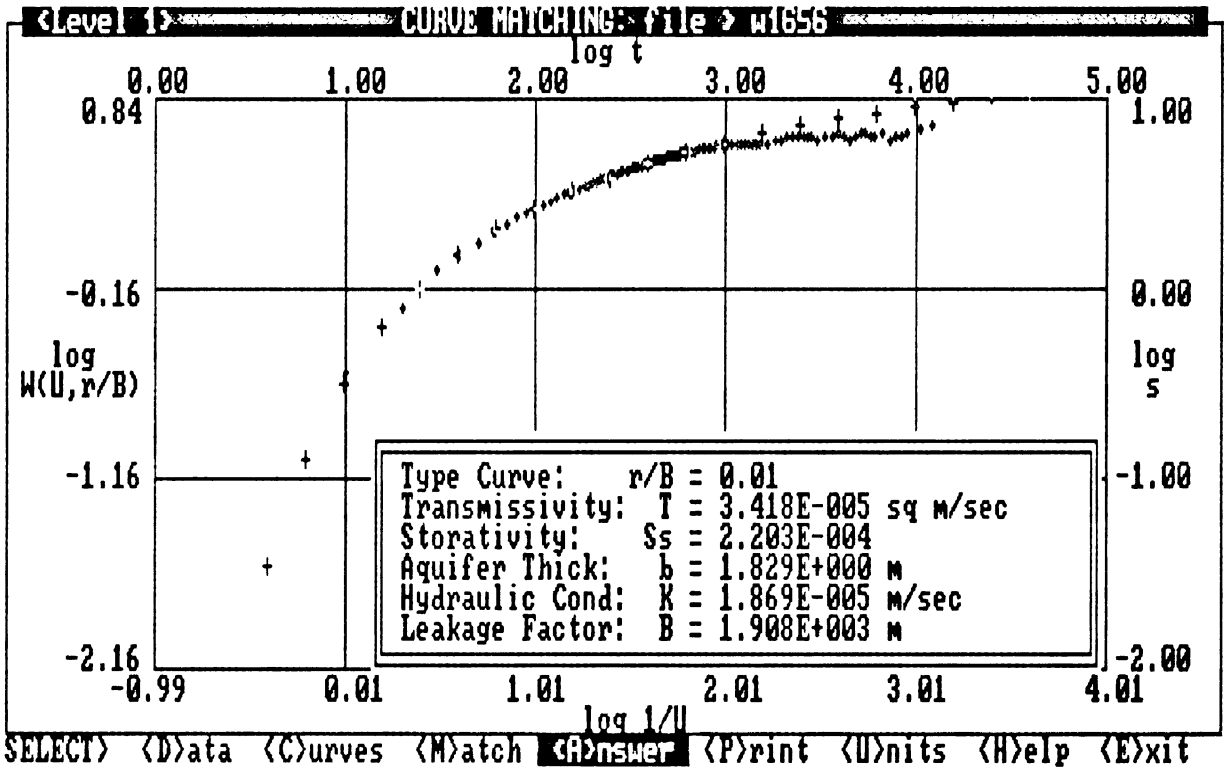

Figure D.7: Curve match and analytical solution for well 1656.

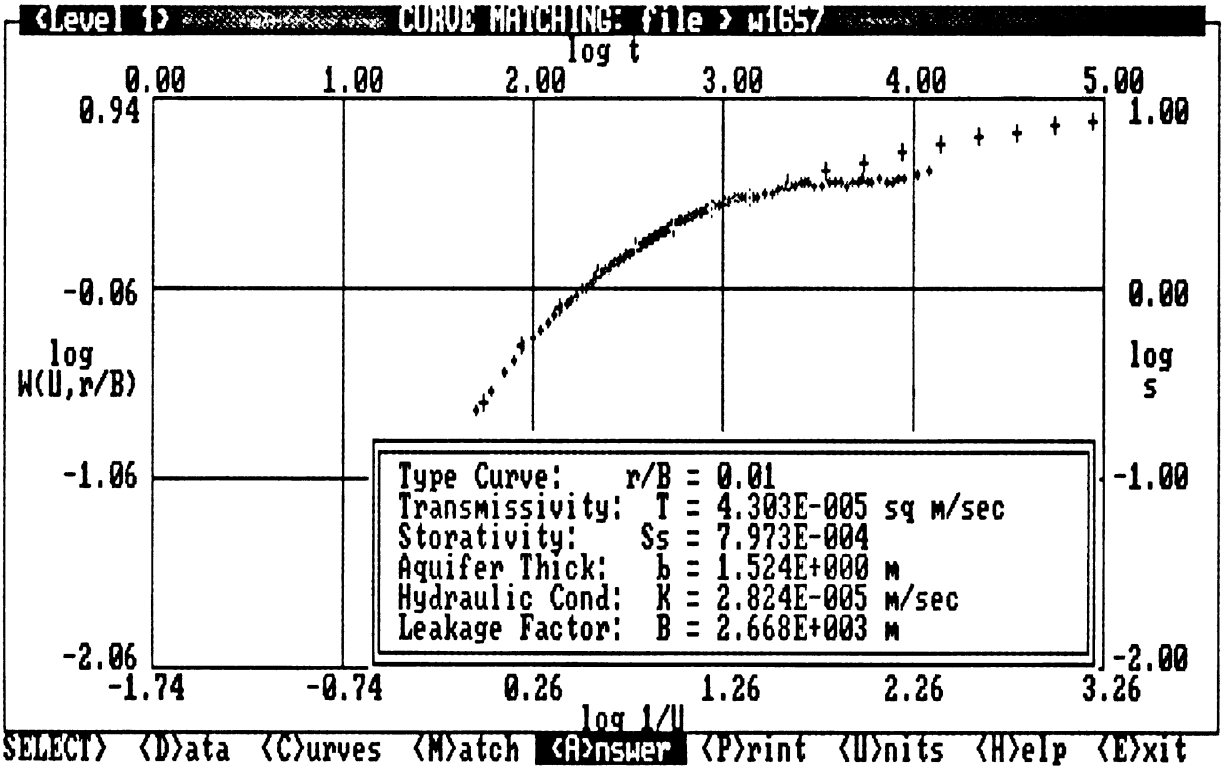

Figure D.8: Curve match and analytical solution for well 1657.

Well	Type Curve	Transmissivity (m^2/day)	Storativity	Aquifer thickness (meter)	Hydraulic conductivity (m/day)	Leaky Factor (meter)
1650	0.01	2.693	1.571e-4	1.829	1.473	2.594e3
1651	0.01	4.076	1.329e-3	1.524	2.675	2.513e3
1652	0.01	2.820	8.338e-4	1.829	1.542	1.890e3
1653	0.01	2.456	5.141e-4	2.438	1.007	1.152e3
1654	0.01	2.240	7.505e-4	1.219	3.502	1.260e3
1655	0.01	4.268	1.750e-3	1.219	1.837	1.010e3
1656	0.01	2.9531	2.203e-4	1.829	1.615	1.908e3
1657	0.01	3.717	7.973e-4	1.524	2.433	2.668e3

Table D.2: Summary table of hydraulic parameters from analytic solutions, result are recorded in meter and day units.

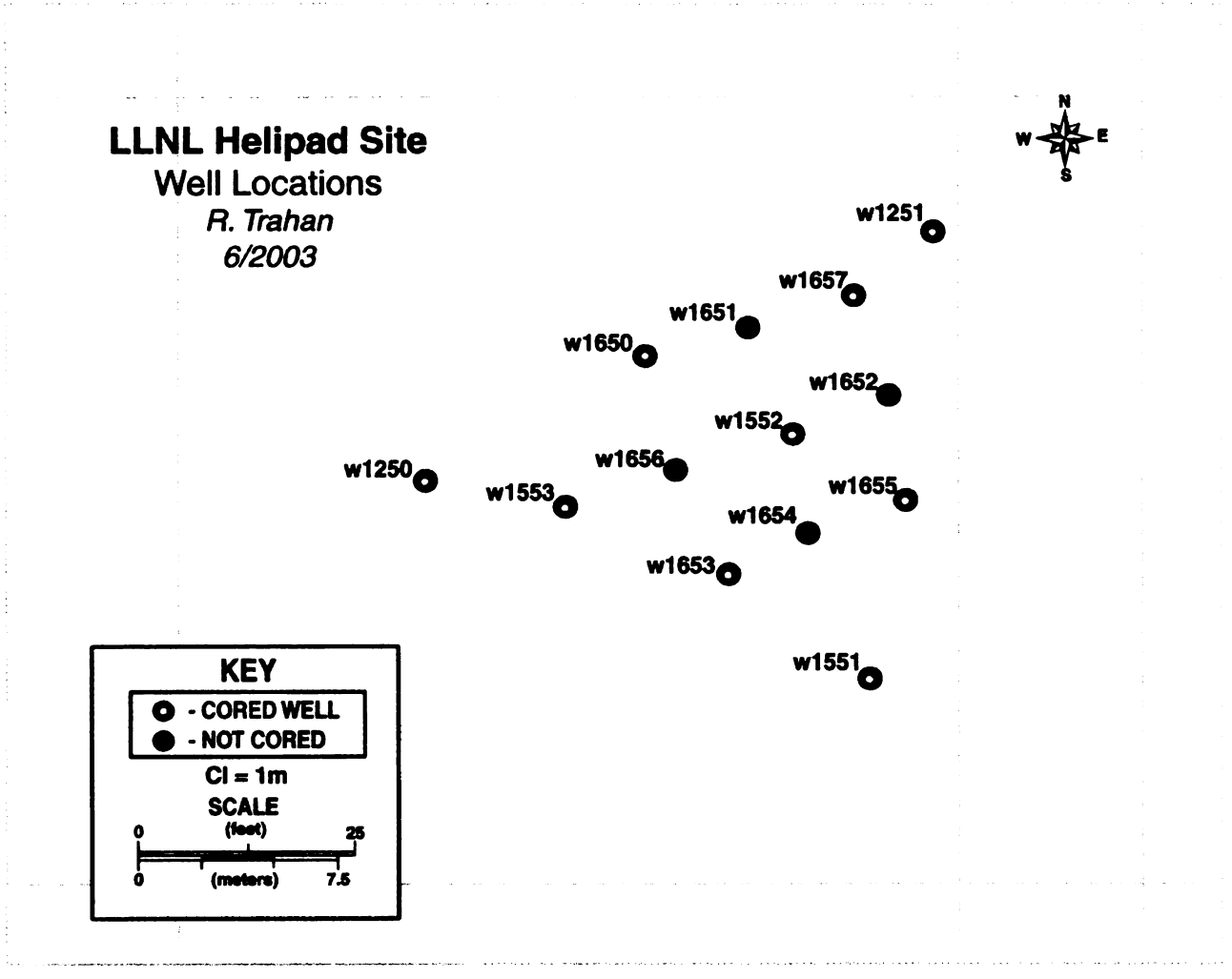

Figure D.9: Location of observation wells at the central helipad study area. Drawdown histories at wells 1650, 1651, 1652, 1653, 1654, 1655, 1656, and 1657 are used for an analytical evaluation of pumping test results.

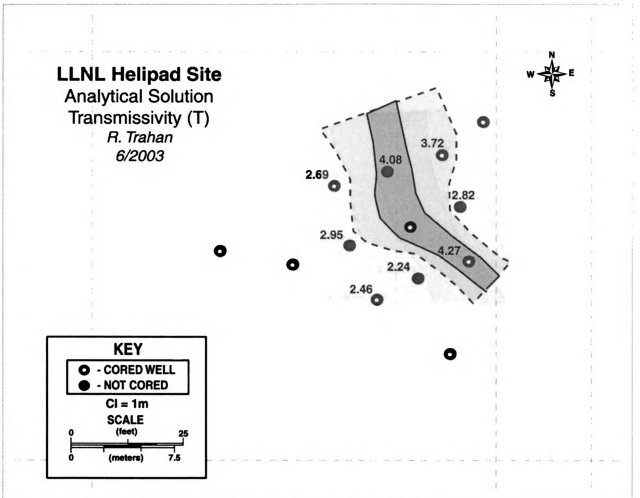

Figure D.10: Contour map of transmissivities. The distribution of transmissivities shows a channel passing through wells 1651 and 1654.

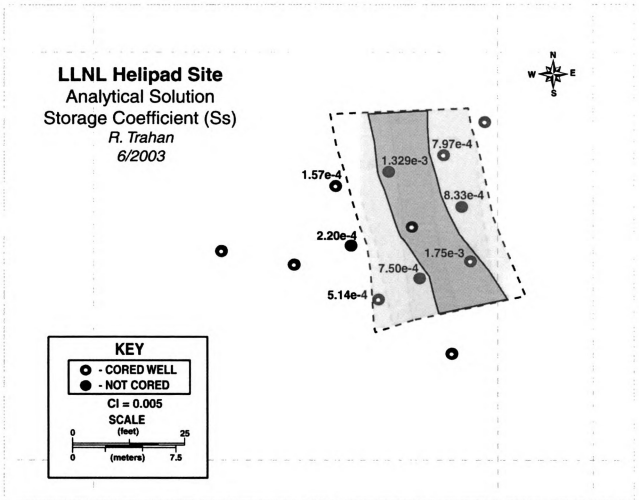

Figure D.11: Contour map of storage coefficient values. The distribution of storage coefficients shows a channel passing through wells 1651 and 1654.

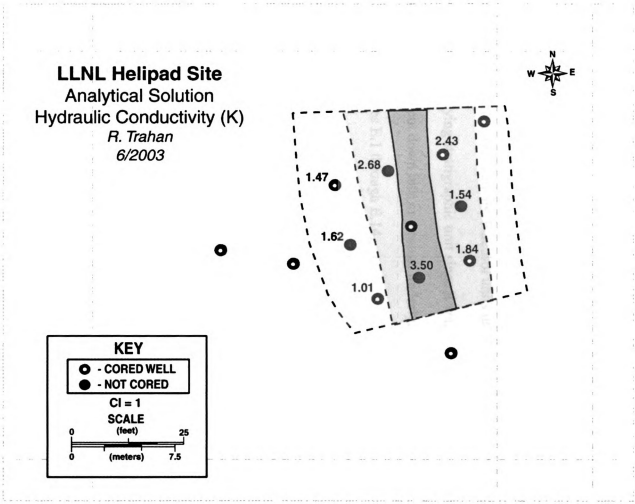

Figure D.12: Contour map of hydraulic conductivity values. The distribution of hydraulic conductivity shows a channel trending north and passing through well 1654.

Appendix E

Isopach Maps

Isopach maps were developed within the central model region to estimate mean channel lengths, widths, and channel orientation for each stratigraphic unit. These parameters were used in the Markov chain model development and geostatistical simulations (Appendix F). Each stratigraphic unit (Aa through F) may contain multiple channels; therefore, an average orientation and width from each stratigraphic unit was used for geostatistical realizations. Paleosol units used average channel orientations and widths from overlying stratigraphic unit since it was assumed that channels formed in these units would cut down into or through underlying paleosol layers. Isopach maps are illustrated in figures E.1 through E.14.

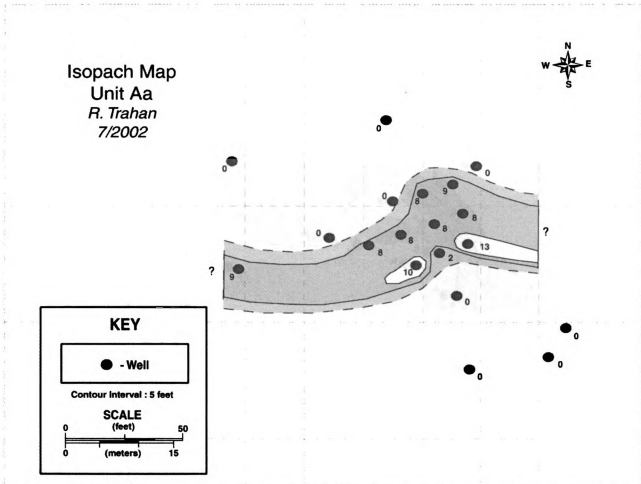

Figure E.1: Contour isopach map of channel deposits (i.e. sand and gravel) for the Aa unit.

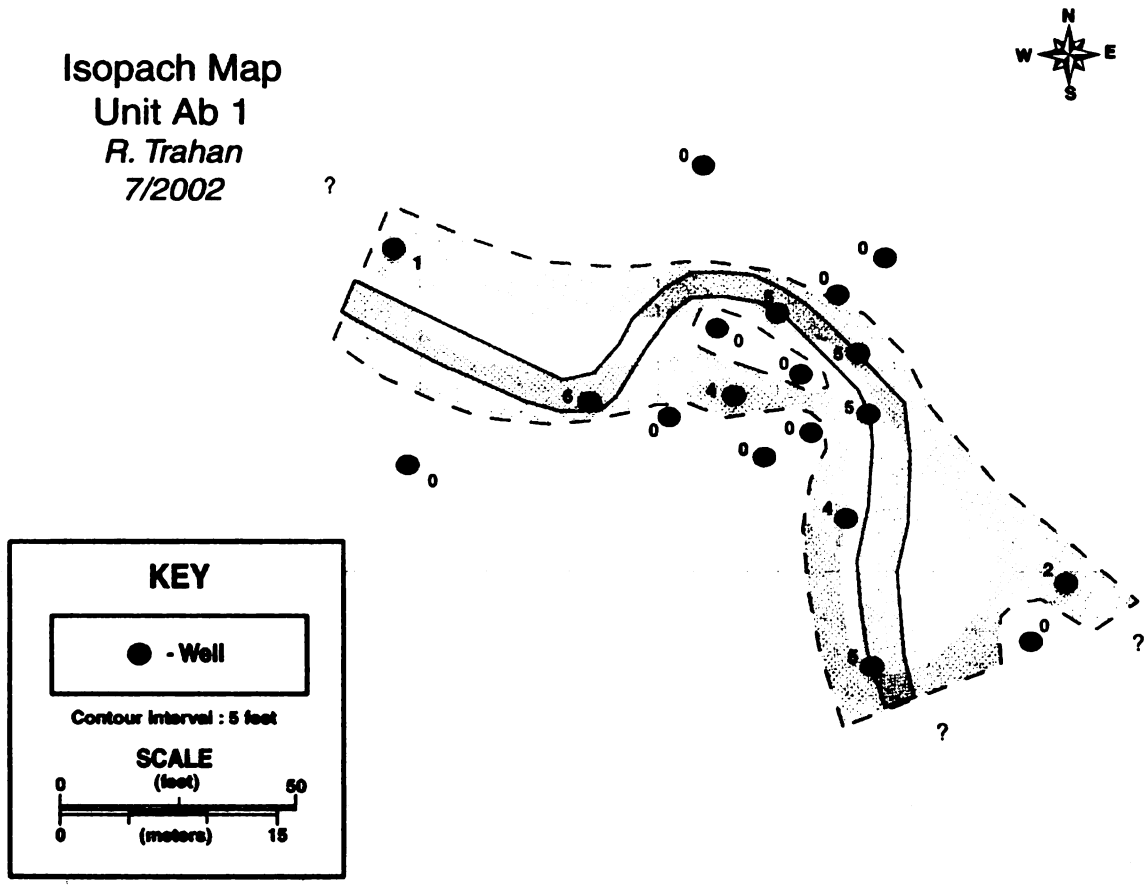

Figure E.2: Contour isopach map of channel deposits (i.e. sand and gravel) within the upper portion of the Ab unit.

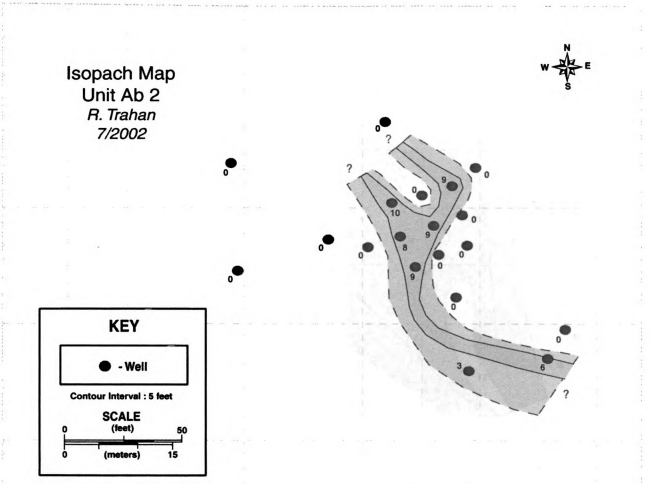

Figure E.3: Contour isopach map of channel deposits (i.e. sand and gravel) within the lower portion of the Ab unit.

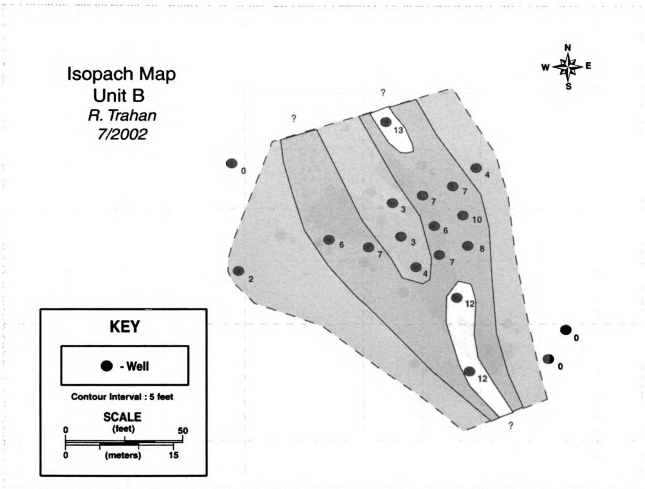

Figure E.4: Contour isopach map of channel deposits (i.e. sand and gravel) within the B unit.

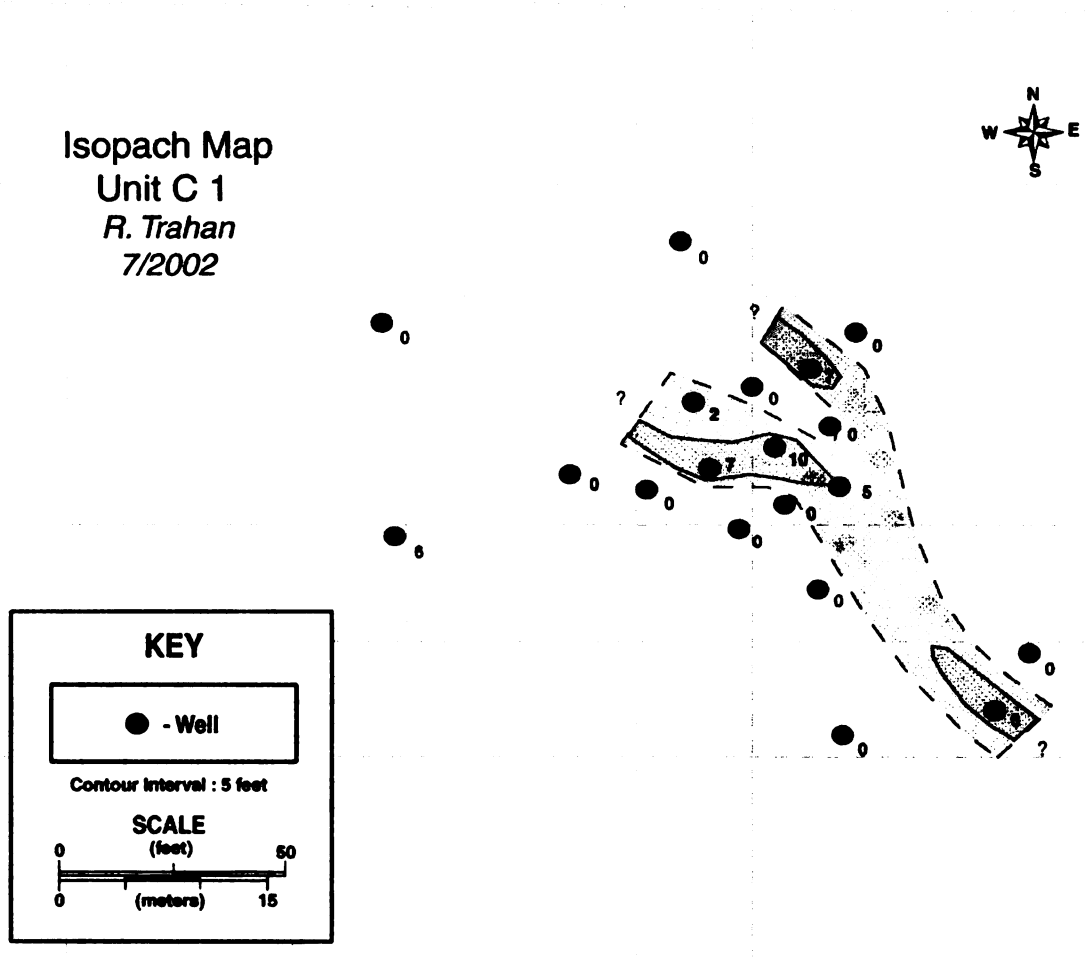

Figure E.5: Contour isopach map of channel deposits (i.e. sand and gravel) within the upper portion of the C unit.

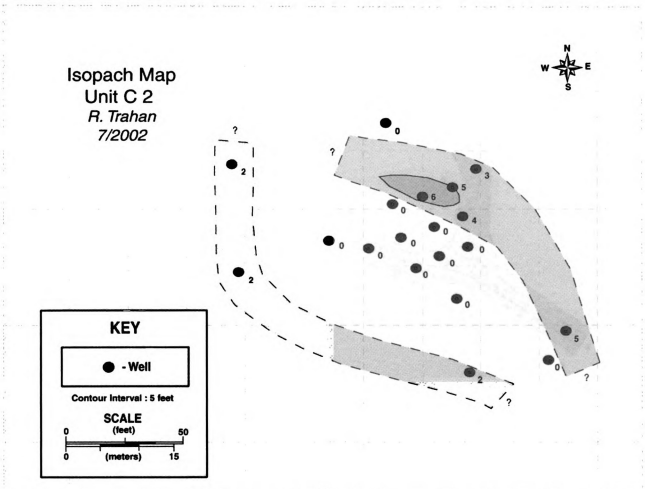

Figure E.6: Contour isopach map of channel deposits (i.e. sand and gravel) within the lower portion of the C unit.

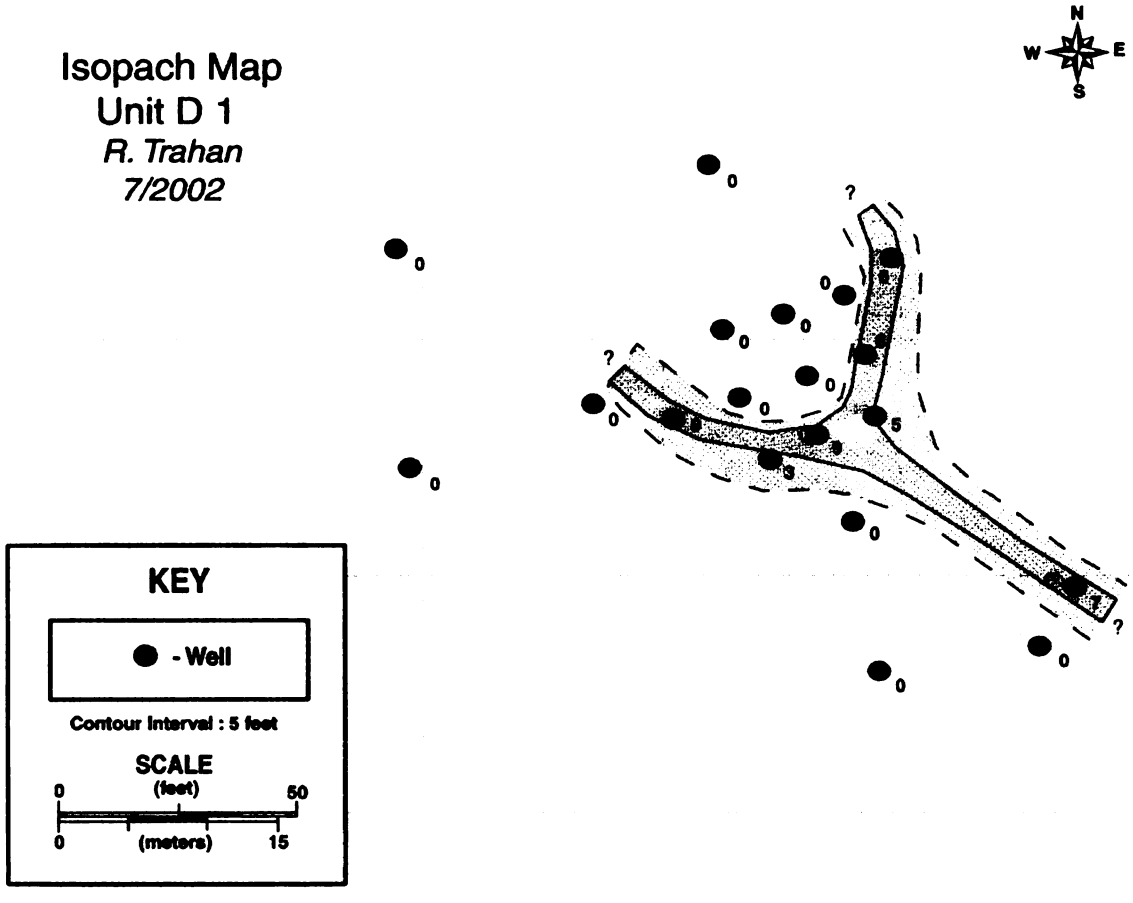

Figure E.7: Contour isopach map of channel deposits (i.e. sand and gravel) within the upper portion of the D unit.

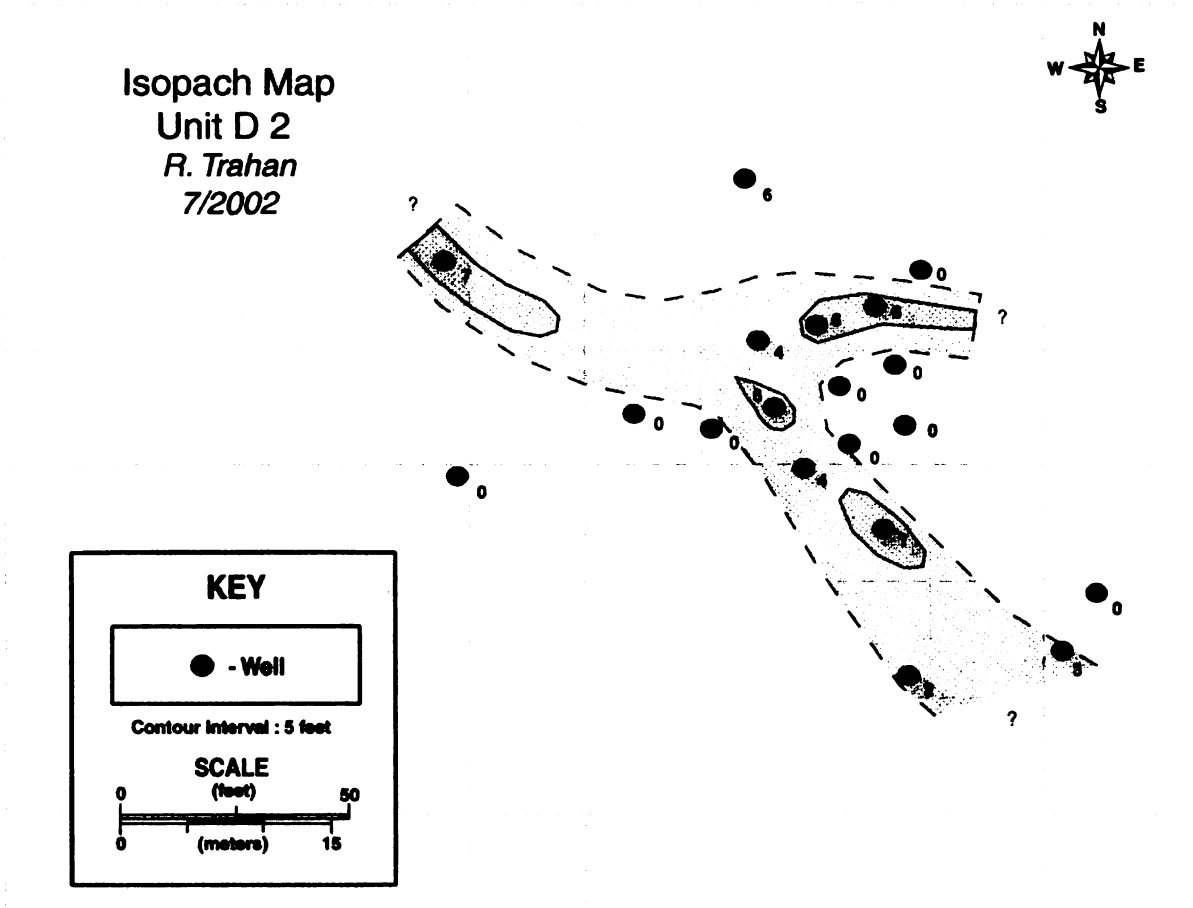

Figure E.8: Contour isopach map of channel deposits (i.e. sand and gravel) within the middle portion of the D unit.

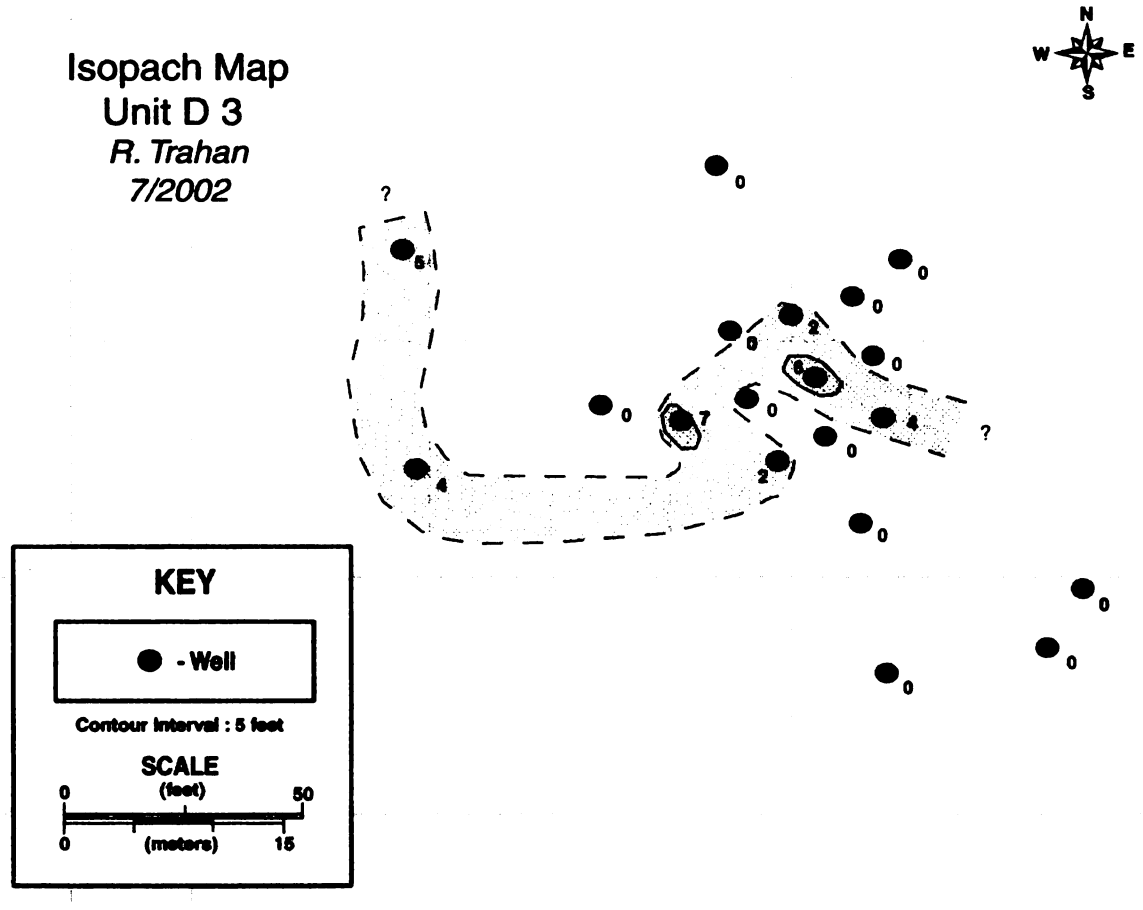

Figure E.9: Contour isopach map of channel deposits (i.e. sand and gravel) within the lower portion of the D unit.

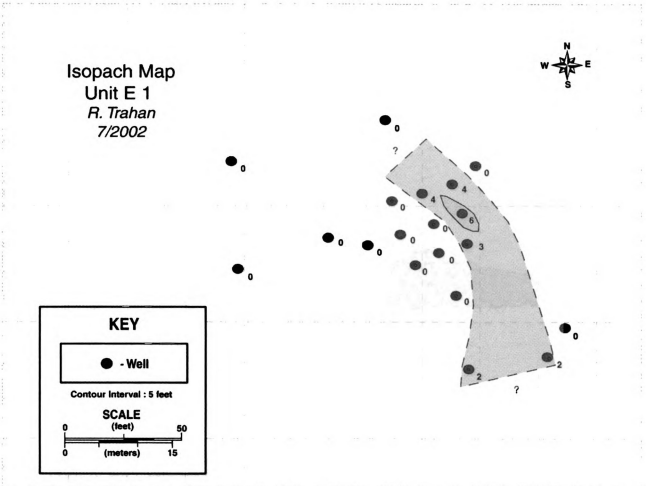

Figure E.10: Contour isopach map of channel deposits (i.e. sand and gravel) within the upper portion of the E unit.

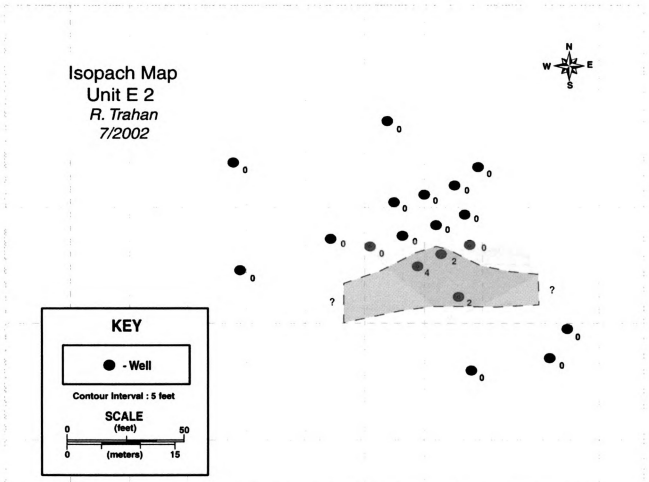

Figure E.11: Contour isopach map of channel deposits (i.e. sand and gravel) within the middle portion of the E unit.

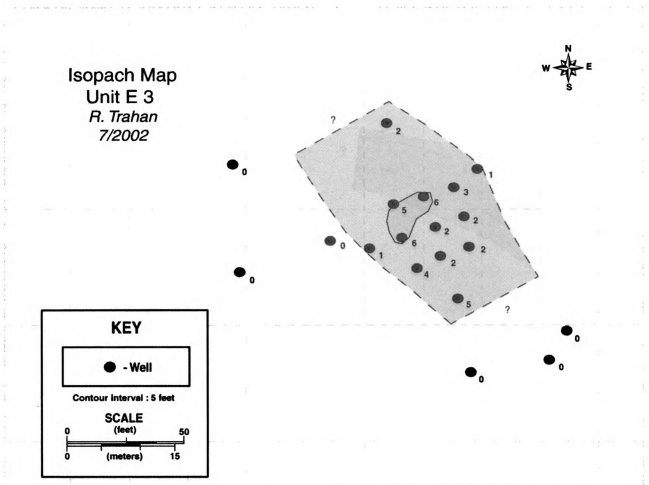

Figure E.12: Contour isopach map of channel deposits (i.e. sand and gravel) within the lower portion of the E unit.

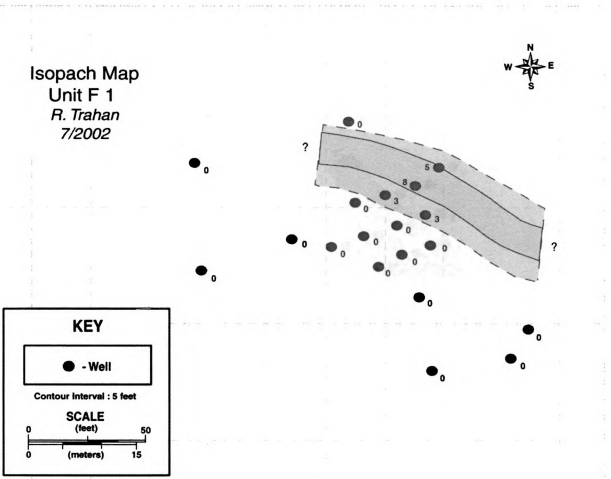

Figure E.13: Contour isopach map of channel deposits (i.e. sand and gravel) within the upper portion of the F unit.

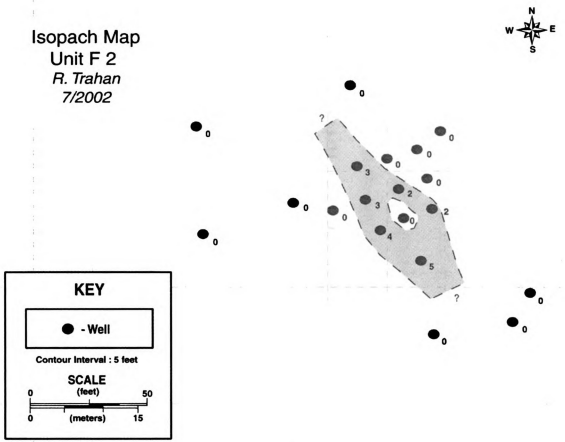

Figure E.14: Contour isopach map of channel deposits (i.e. sand and gravel) within the lower portion of the F unit.

Appendix F

Transition Probability Geostatistics

Introduction

Transition probability geostatistics is an indicator geostatistical method. This method can be used to estimate the spatial distribution of user defined categories which are based on geologic information (i.e. well core and geophysical logs). At the Helipad Site transition probability geostatistical models were generated for two conceptual model types – a full transition probability geostatistical model and a stratigraphic transition probability geostatistical model. Outlined in the following sections are steps taken in developing each of these model types. This includes, Markov chain model development, defining stratigraphic units, incorporating geologic information in the form of channel widths, lengths, and orientations, and combining individually modeled stratigraphic units to produce a stratigraphic transition probability geostatistical realization. This outline is divided into two sections based on conceptual model type.

Transition Probability Model Development

Listed below are the procedures that were taken in developing both transition probability geostatistical simulations. It is important to note that there is a T-PROGS interface within GMS 4.0 that allows you to develop transition probability geostatistical models. However, during the initial development of these model types, GMS 4.0 was not available. Also, development of transition probability models outside of GMS allows the user to have more flexibility in generating realizations in terms of matching Markov

chain models to measured data, generating larger realizations, and was necessary for development of our stratigraphic simulations. In model development GAMEAS, GRAFXX, MCMOD, TPSIM, and CHUNK programs were used. Listed below is an outline for procedures in model development. Carle (1999) fully describes this software and data formats required.

Procedures for transition probability geostatistical simulation –

- Hydrofacies categories from core / geophysical well log data were initially discretized to 0.5 meter spacing. From these measurements, the vertical (z-direction) transition probabilities between hydrofacies and proportions of individual hydrofacies were calculated using GAMEAS.
- The results of this calculation showed that the silty sand hydrofacies had the highest overall proportion (Table F.1). In the conceptual model development, the silty sand hydrofacies was interpreted to fill in around all other categories (cross-section interpretations, Appendix C). Based on this, the silty sand hydrofacies was designated as the background category.
- Using GRAFXX, the 1-D transition probabilities were plotted as a matrix of graphs. This was done to asses the data quality and interpret juxtaposition relationships between hydrofacies.
- MCMOD was used to develop a vertical Markov chain model fit to measured transition probabilities. GRAFXX was then used again to plot both the Markov chain model and the measured data. This Markov chain model was then adjusted to best fit the measured data through manipulation of the

embedded transition probabilities (Figure F1). The resulting vertical embedded transition probabilities are listed in Table F.2.

- The horizontal (x and y-directions) Markov chain models were developed using geologic reasoning and the application of Walther's law, in that the lateral juxtaposition tendencies are assumed to have the same statistics as the vertical upward juxtaposition tendencies. Lateral facies distributions were also assumed to be symmetrical. Horizontal juxtaposition values were then adjusted so that embedded transition probabilities were no longer negative.
- At this point, mean channel lengths and widths were incorporated. Lengths and widths of channel hydrofacies were measured from isopach maps for the E stratigraphic unit (Appendix E) and were incorporated into the horizontal embedded transition probabilities at an azimuth of 340 degrees (Table F.2).
- Within the TPSIM parameter file, the model dimensions as well as the grid dimensions were assigned to match the grid dimensions developed for the groundwater numerical model (described in Appendix G). TPSIM was run to generate multiple realizations for the spatial distribution of hydrofacies. There were 26 realizations generated, one transition probability geostatistical simulation and 25 stratigraphic transition probability geostatistical simulations.
- Cell dimensions used to produce this realization were 2 x 2 x 0.5 meter (north-south, east-west, and vertical directions respectively) in dimension. Full simulation dimensions are 362 meters east to west, 310 meters north to south, and 39 meters vertically. In total each realization contains 2,188,290 cells.

Procedures for the stratigraphic transition probability geostatistical simulation –

- Using laterally-extensive paleosol markers, the aquifer at the Helipad Site was subdivided into several stratigraphic units or zones (described in chapters 2 and 3, Figure 3.2). Top and bottom surfaces were generated from these correlations and were modeled across the study area using an inverse distance linear algorithm. As a result, thirteen zones were identified. These included six paleosol zones (Ab through F) and seven stratigraphic zones (Aa through F). However, only those zones that were below the water table were modeled (C through F).
- For this modeling approach, individual stratigraphic and paleosol zones were modeled using different Markov chain models.
- Hydrofacies categories from core / geophysical well log data were discretized to 0.5 meter spacing. However, the vertical (z-direction) transition probabilities were calculated over a discrete interval for each zone. These intervals were defined by top and bottom elevations from modeled paleosol surfaces. Transition probabilities and proportions for each zone were calculated with GAMEAS.
- The results of these calculations showed that within each stratigraphic zone the silty sand hydrofacies consistently had the highest proportions (Table F.1). For stratigraphic zones (C, D, E and F), the silty sand hydrofacies was assigned as the background category. In paleosol zones, the paleosol hydrofacies consistently had the highest proportions (Table F.1) and was set as the background category for each of these zones (D, E, and F).

- GRAFXX was used to plot the 1-D transition probabilities as a matrix of graphs for each zone. Again, this was done to asses the data quality and interpret juxtaposition relationships between hydrofacies.
- MCMOD was used to develop vertical Markov chain models for each individual zone. GRAFXX was then used again to superimpose these Markov chain models over the measured data for corresponding stratigraphic and paleosol zones. Markov chain models were then adjusted for each zone to best fit the measured data through manipulation of embedded transition probabilities (GRAFFXX plots for each zone resemble Figure F.1). The resulting vertical embedded transition probabilities are listed in Tables F.3 through F.9.
- Using the same reasoning as stated above, off-diagonal vertical upward embedded transition probabilities were assigned to horizontal embedded transition probabilities for each zone. For these models, symmetry was assumed. These values were then adjusted to so that embedded transition probabilities were no longer negative.
- Mean channel lengths and widths were incorporated into each zone (paleosol zones used mean channel lengths and widths from overlying stratigraphic zones). Lengths and widths of channel hydrofacies were measured from isopach maps for multiple channels within each zone (Appendix E). These were incorporated into corresponding horizontal embedded transition probabilities (Tables F.3 through F.9).

- For this modeling approach, each zone was simulated over the entire simulation block volume (even though conditioning data only existed over a limited portion of this block). TPSIM was used to generate these simulations.
- Following methods of Weissmann and Fogg (1999), simulations generated for each of the individual zones (C through F) were merged to create a final whole aquifer realization of the Helipad Site (Figure F.2).
- Out of each simulated zone, only those specific cells bounded between corresponding paleosol top and bottom surfaces were used. This was accomplished using a FORTRAN Code (Appendix I).
- Following this methodology, 25 total realizations were generated to resolve the spatial distribution of hydrofacies for the Helipad Site. Each of these realizations is illustrated in Figures F.3 through F.8.

Conclusions

Each of the resulting realizations (Figures F.2 through F.8) reflects aspects of the physical heterogeneity that exist in an alluvial fan system. These geostatistical realizations reflect juxtaposition tendencies, proportions and channel length, width, and orientations of the real system. Also, this modeling approach tends to preserve a fining upward character observed in well logs. Gravel hydrofacies are observed to be located beneath sand hydrofacies, similarly, sand hydrofacies are observed to be below silty sand hydrofacies.

Using a stratigraphic transition probability geostatistical approach, channel orientations associated with different stratigraphic zones are better preserved. Also, by

simulating each stratigraphic zone separately, unconformities are preserved where hydrofacies are discontinuous across stratigraphic boundaries preserving the larger scale heterogeneity of the system. In total, one transition probability geostatistical realization and twenty-five stratigraphic transition probability geostatistical realizations were developed. Distributions of hydrofacies for each of these realizations were used in numerical groundwater models (described in Appendix G).

Global Proportions:

	Gravel Hydrofacies	Sand Hydrofacies	Silty Sand Hydrofacies	Paleosol Hydrofacies
TPG Simulation	0.24	0.12	0.52	0.13
C zone	0.26	0.12	0.59	0.04
D paleosol	0.40	0.03	0.08	0.50
D zone	0.15	0.19	0.62	0.036
E paleosol	0.22	0.04	-	0.74
E zone	0.08	0.19	0.64	0.10
F paleosol	0.11	0.04	-	0.85
F zone	0.22	0.08	0.65	0.05

Table F.1: Proportions of hydrofacies for the TPG simulation and for each stratigraphic zone of the layered simulation. E and F paleosol zones lack the *silty sand* hydrofacies and are modeled excluding this category.

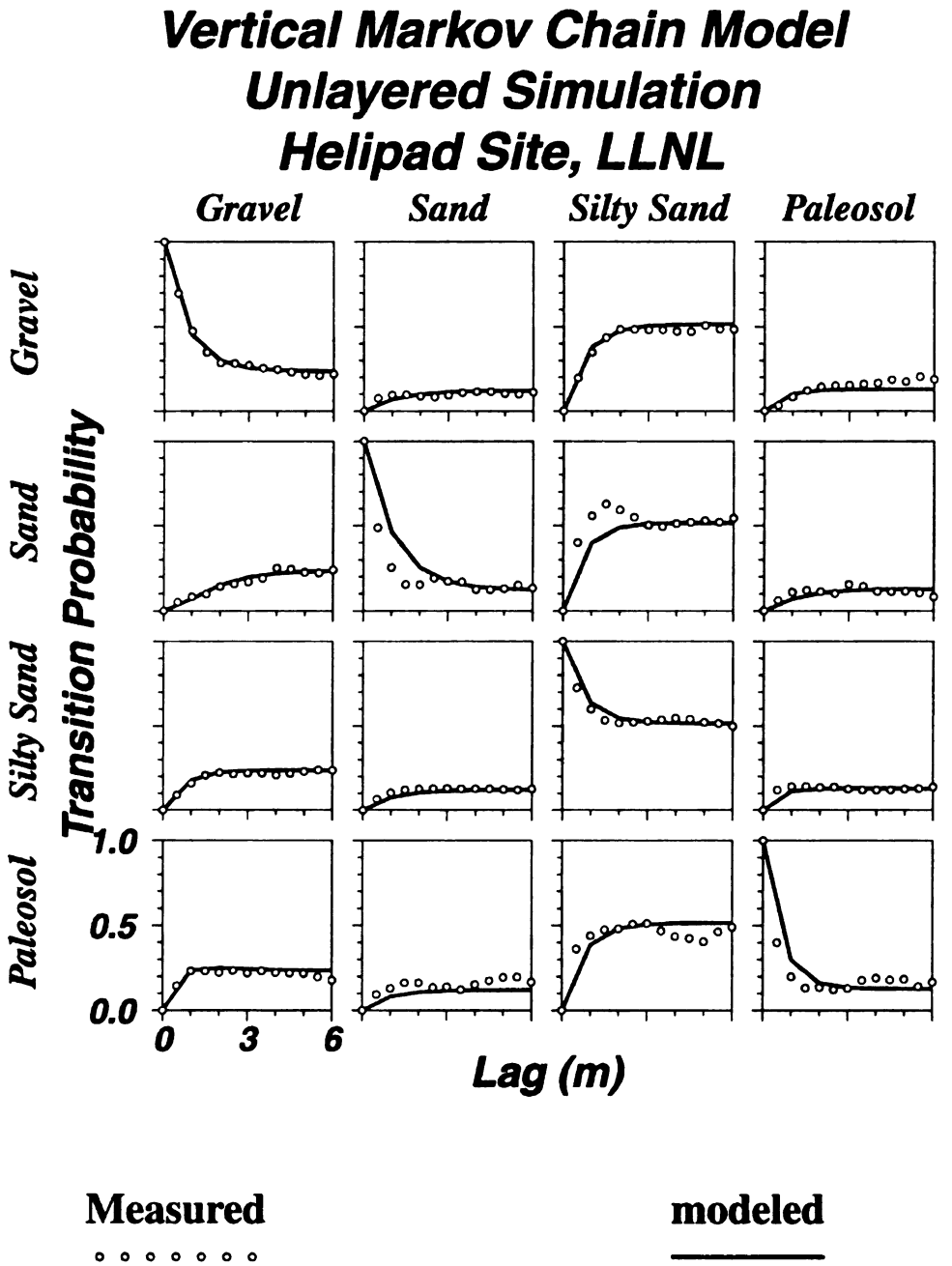

Figure F.1: Vertical Markov chain model fit to measured facies data for the transition probability geostatistical simulation modeling approach.

Vertical (z-direction) embedded transition probabilities

	Gravel	*Sand*	*Silty Sand*	*Paleosol*
Gravel	L=1.013	0.1000	**0.7000**	0.2000
Sand	0.0010	L=1.200	**0.8660**	0.1000
Silty Sand	**0.4632**	**0.1716**	**L=1.490**	**0.3651**
Paleosol	0.4000	0.1000	**0.5000**	L=0.700

Horizontal (x-direction) embedded transition probabilities

	Gravel	*Sand*	*Silty Sand*	*Paleosol*
Gravel	L=5.000	0.0974	**0.8747**	0.0278
Sand	0.1900	L=5.000	**0.7958**	0.0142
Silty Sand	**0.6601**	**0.3079**	**L=8.223**	**0.0319**
Paleosol	0.3600	0.0940	**0.5460**	L=35.000

Horizontal (y-direction) embedded transition probabilities

	Gravel	*Sand*	*Silty Sand*	*Paleosol*
Gravel	L=50.000	0.0974	**0.7074**	0.1950
Sand	0.1900	L=50.000	**0.7106**	0.0993
Silty Sand	**0.5172**	**0.2663**	**L=79.660**	**0.2163**
Paleosol	0.3600	0.0940	**0.5460**	L=50.000

Table F.2: Embedded transition probability matrices for the transition probability geostatistical simulation. These matrices are read as transition probabilities from the row hydrofacies to the column hydrofacies. (Labels: L, mean length. Bold numbers indicate background category with computed values listed in the table.)

Vertical (z-direction) embedded transition probabilities

	Gravel	*Sand*	*Silty Sand*	*Paleosol*
Gravel	L=.600	0.0620	**0.8970**	0.0410
Sand	0.0001	L=0.620	**0.9998**	0.0001
Silty Sand	**0.6507**	**0.2402**	**L=0.987**	**0.1089**
Paleosol	0.5100	0.2600	**0.2300**	L=0.500

Horizontal (x-direction) embedded transition probabilities

	Gravel	*Sand*	*Silty Sand*	*Paleosol*
Gravel	L=7.000	0.0597	**0.9379**	0.0022
Sand	0.1300	L=7.000	**0.8651**	0.0048
Silty Sand	**0.6816**	**0.2890**	**L=11.598**	**0.0293**
Paleosol	0.0500	0.0500	**0.9000**	L=25.000

Horizontal (y-direction) embedded transition probabilities

	Gravel	*Sand*	*Silty Sand*	*Paleosol*
Gravel	L=60.000	0.0597	**0.9338**	0.0064
Sand	0.1300	L=60.000	**0.8560**	0.0139
Silty Sand	**0.6472**	**0.2728**	**L=94.824**	**0.0798**
Paleosol	0.0500	0.0500	**0.9000**	L=75.000

Table F.3: Embedded transition probability matrices for the C zone. These matrices are read as transition probabilities from the row hydrofacies to the column hydrofacies. (Labels: L, mean length. Bold numbers indicate background category with computed values listed in the table.)

Vertical (z-direction) embedded transition probabilities

	Gravel	*Sand*	*Silty Sand*	*Paleosol*
Gravel	L=3.000	0.0500	0.0500	**0.9000**
Sand	0.8000	L=3.000	0.0500	**0.1500**
Silty Sand	0.2666	0.0166	L=3.000	**0.3651**
Paleosol	**0.8623**	**0.0898**	**0.5000**	**L=3.593**

Horizontal (x-direction) embedded transition probabilities

	Gravel	*Sand*	*Silty Sand*	*Paleosol*
Gravel	L=7.000	0.0500	0.0262	**0.9237**
Sand	0.8000	L=7.000	0.0210	**0.1790**
Silty Sand	0.0400	0.0020	L=2.000	**0.9580**
Paleosol	**0.5907**	**0.0072**	**0.4020**	**L=35.596**

Horizontal (y-direction) embedded transition probabilities

	Gravel	*Sand*	*Silty Sand*	*Paleosol*
Gravel	L=50.000	0.0350	0.0375	**0.9275**
Sand	0.2800	L=25.000	0.04875	**0.67125**
Silty Sand	0.0800	0.0130	L=20.000	**0.9070**
Paleosol	**0.6456**	**0.0584**	**0.2959**	**L=43.506**

Table F.4: Embedded transition probability matrices for the D paleosol. These matrices are read as transition probabilities from the row hydrofacies to the column hydrofacies. (Labels: L, mean length. Bold numbers indicate background category with computed values listed in the table.)

Vertical (z-direction) embedded transition probabilities

	Gravel	*Sand*	*Silty Sand*	*Paleosol*
Gravel	L=0.950	0.2100	**0.7899**	0.000001
Sand	0.0510	L=0.800	**0.9489**	0.000001
Silty Sand	**0.3397**	**0.4304**	**L=1.505**	**0.1527**
Paleosol	0.0570	0.2630	**0.6800**	L=0.380

Horizontal (x-direction) embedded transition probabilities

	Gravel	*Sand*	*Silty Sand*	*Paleosol*
Gravel	L=5.000	0.2141	**0.7859**	0.000001
Sand	0.1700	L=5.000	**0.8300**	0.00000
Silty Sand	**0.4199**	**0.5585**	**L=11.086**	**0.0214**
Paleosol	0.000002	0.000001	**0.9999**	L=30.000

Horizontal (y-direction) embedded transition probabilities

	Gravel	*Sand*	*Silty Sand*	*Paleosol*
Gravel	L=50.000	0.2141	**0.7859**	0.000001
0Sand	0.1700	L=50.000	**0.8299**	0.000001
Silty Sand	**0.3793**	**0.5047**	**L=100.124**	**0.1162**
Paleosol	0.000005	0.000007	**0.9999**	L=50.000

Table F.5: Embedded transition probability matrices for the D zone. These matrices are read as transition probabilities from the row hydrofacies to the column hydrofacies. (Labels: L, mean length. Bold numbers indicate background category with computed values listed in the table.)

Vertical (z-direction) embedded transition probabilities

	Gravel	*Sand*	*Paleosol*
Gravel	L=3.000	0.0500	**0.9500**
Sand	0.2750	L=3.000	**0.7250**
Paleosol	**0.8781**	**0.1218**	**L=9.327**

Vertical (x-direction) embedded transition probabilities

	Gravel	*Sand*	*Paleosol*
Gravel	L=5.000	0.0491	**0.9509**
Sand	0.2700	L=5.000	**0.7300**
Paleosol	**0.8775**	**0.1225**	**L=15.520**

Vertical (y-direction) embedded transition probabilities

	Gravel	*Sand*	*Paleosol*
Gravel	L=50.000	0.1000	**0.9600**
Sand	0.1100	L=25.000	**0.8900**
Paleosol	**0.7478**	**0.2521**	**L=131.019**

Table F.6: Embedded transition probability matrices for the E paleosol. These matrices are read as transition probabilities from the row hydrofacies to the column hydrofacies. (Labels: L, mean length. Bold numbers indicate background category with computed values listed in the table.)

Vertical (z-direction) embedded transition probabilities

	Gravel	*Sand*	*Silty Sand*	*Paleosol*
Gravel	L=0.530	0.9000	**0.0200**	0.0800
Sand	0.0070	L=0.550	**0.9430**	0.0500
Silty Sand	**0.2739**	**0.3848**	**L=1.721**	**0.3412**
Paleosol	0.2800	0.4000	**0.3200**	L=0.650

Horizontal (x-direction) embedded transition probabilities

	Gravel	*Sand*	*Silty Sand*	*Paleosol*
Gravel	L=8.000	0.8789	**0.0229**	0.0981
Sand	0.3700	L=8.000	**0.5680**	0.06196
Silty Sand	**0.0165**	**0.9741**	**L=47.168**	**0.0093**
Paleosol	0.3800	0.5700	**0.0500**	L=40.000

Horizontal (y-direction) embedded transition probabilities

	Gravel	*Sand*	*Silty Sand*	*Paleosol*
Gravel	L=50.000	0.7126	**0.2335**	0.0538
Sand	0.3000	L=50.000	**0.6637**	0.0362
Silty Sand	**0.0850**	**0.5741**	**L=148.694**	**0.3408**
Paleosol	0.0500	0.0800	**0.8700**	L=60.000

Table F.7: Embedded transition probability matrices for the E zone. These matrices are read as transition probabilities from the row hydrofacies to the column hydrofacies. (Labels: L, mean length. Bold numbers indicate background category with computed values listed in the table.)

Vertical (z-direction) embedded transition probabilities

	Gravel	*Sand*	*Paleosol*
Gravel	L=3.000	0.0500	**0.9500**
Sand	0.1501	L=3.000	**0.8498**
Paleosol	**0.7704**	**0.2295**	**L=18.269**

Vertical (x-direction) embedded transition probabilities

	Gravel	*Sand*	*Paleosol*
Gravel	L=8.000	0.0599	**0.9400**
Sand	0.1800	L=8.000	**0.8200**
Paleosol	**0.7748**	**0.2251**	**L=49.516**

Vertical (y-direction) embedded transition probabilities

	Gravel	*Sand*	*Paleosol*
Gravel	L=50.000	0.0466	**0.9533**
Sand	0.0700	L=25.000	**0.9300**
Paleosol	**0.6061**	**0.3938**	**L=238.705**

Table F.8: Embedded transition probability matrices for the F paleosol. These matrices are read as transition probabilities from the row hydrofacies to the column hydrofacies. (Labels: L, mean length. Bold numbers indicate background category with computed values listed in the table.)

Vertical (z-direction) embedded transition probabilities

	Gravel	*Sand*	*Silty Sand*	*Paleosol*
Gravel	L=1.35	0.1300	**0.8600**	0.0100
Sand	0.0010	L=0.520	**0.8990**	0.1000
Silty Sand	**0.4550**	**0.3434**	**L=1.770**	**0.2015**
Paleosol	0.0010	0.0690	**0.9300**	L=0.560

Horizontal (x-direction) embedded transition probabilities

	Gravel	*Sand*	*Silty Sand*	*Paleosol*
Gravel	L=7.000	0.1277	**0.8622**	0.0100
Sand	0.3600	L=7.000	**0.5405**	0.0995
Silty Sand	**0.8123**	**0.1807**	**L=18.976**	**0.0069**
Paleosol	0.1900	0.6700	**0.1400**	L=30.000

Horizontal (y-direction) embedded transition probabilities

	Gravel	*Sand*	*Silty Sand*	*Paleosol*
Gravel	L=50.000	0.0931	**0.8955**	0.0113
Sand	0.2100	L=40.000	**0.6423**	0.1476
Silty Sand	**0.6736**	**0.2143**	**L=108.212**	**0.1121**
Paleosol	0.0500	0.2900	**0.6600**	L=50.000

Table F.9: Embedded transition probability matrices for the F zone. These matrices are read as transition probabilities from the row hydrofacies to the column hydrofacies. (Labels: L, mean length. Bold numbers indicate background category with computed values listed in the table.)

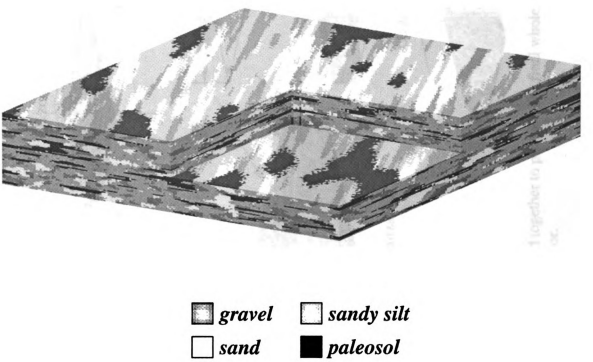

Figure F.2: Full realization following methods for an TPG simulation approach. Four categories are used (gravel, sand, silty sand, and paleosol) to characterize the geology at the Helipad Study Site, LLNL.

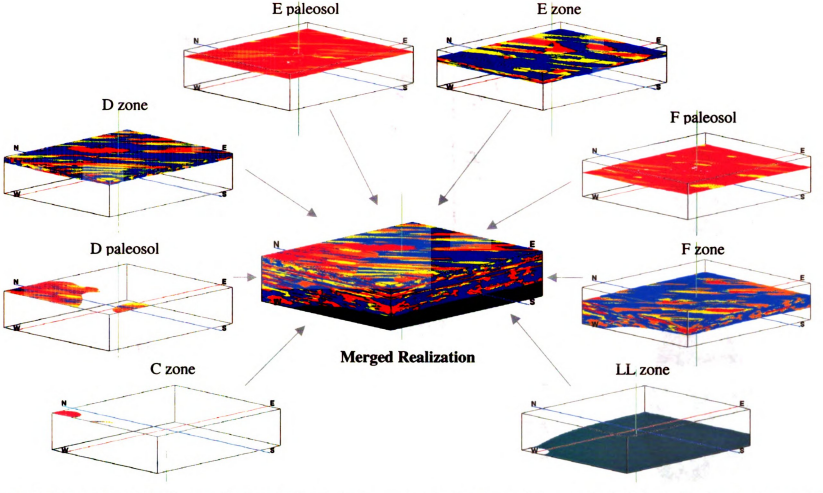

Figure F.3: Separately modeled zones (C through F zones) are merged together to produce one final whole realization for the spatial distribution of hydrofacies at the Helipad Site. Image presented in color.

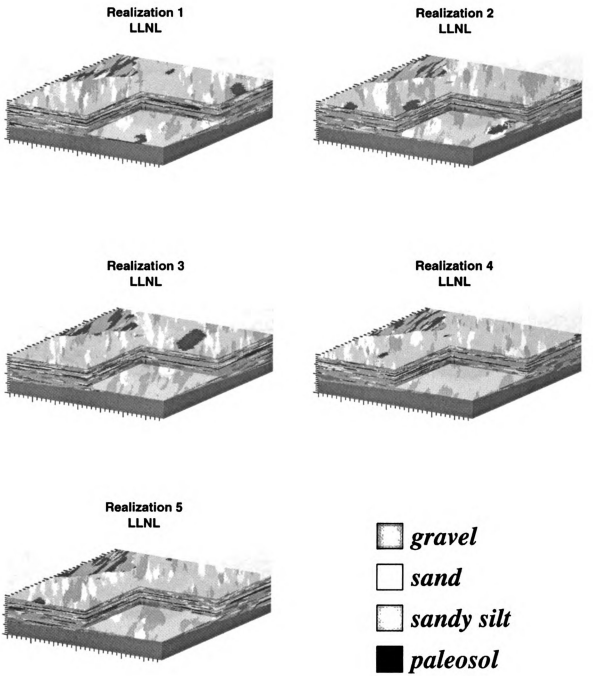

Figure F.4: Full realization (1 through 5) following methods for a zoned simulation approach. Four categories are used (gravel, sand, silty sand, and paleosol) to characterize the geology at the Helipad Study Site, LLNL.

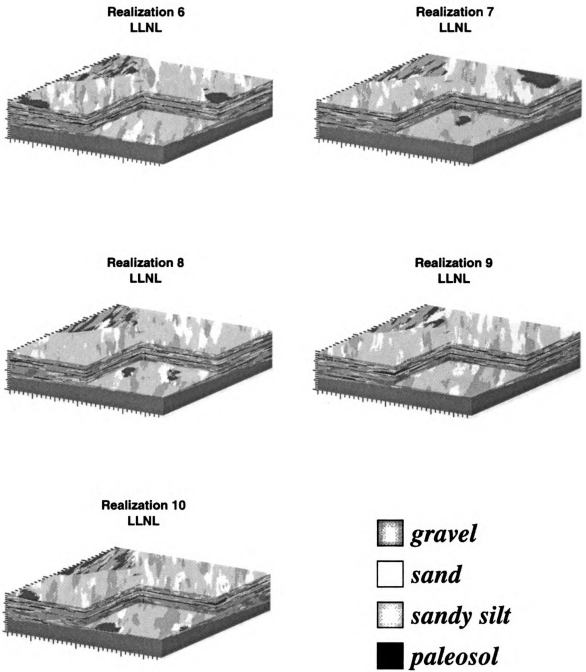

Figure F.5: Full realization (6 through 10) following methods for a zoned simulation approach. Four categories are used (gravel, sand, silty sand, and paleosol) to characterize the geology at the Helipad Study Site, LLNL.

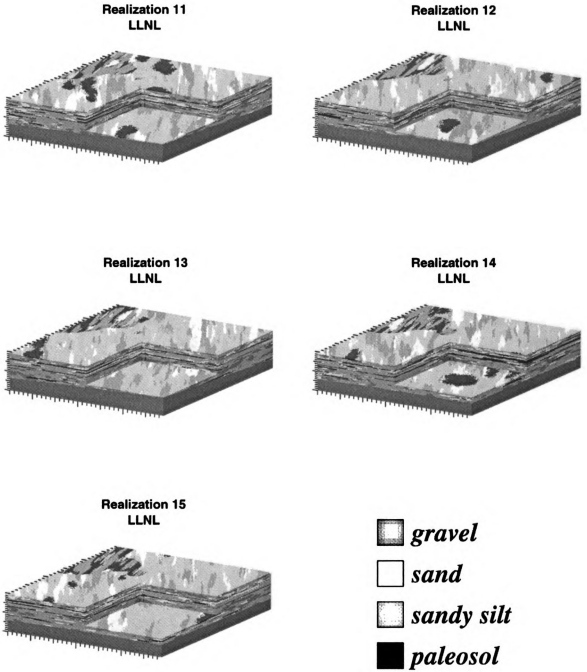

Figure F.6: Full realization (11 through 15) following methods for a zoned simulation approach. Four categories are used (gravel, sand, silty sand, and paleosol) to characterize the geology at the Helipad Study Site, LLNL.

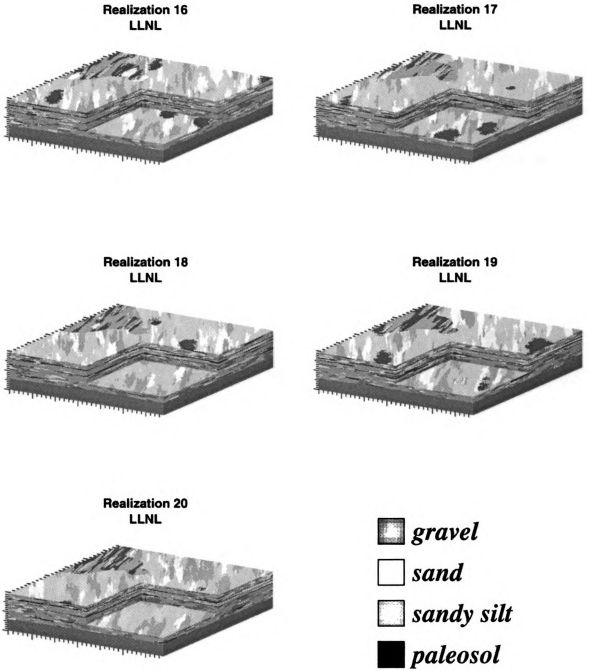

Figure F.7: Full realization (16 through 20) following methods for a zoned simulation approach. Four categories are used (gravel, sand, silty sand, and paleosol) to characterize the geology at the Helipad Study Site, LLNL.

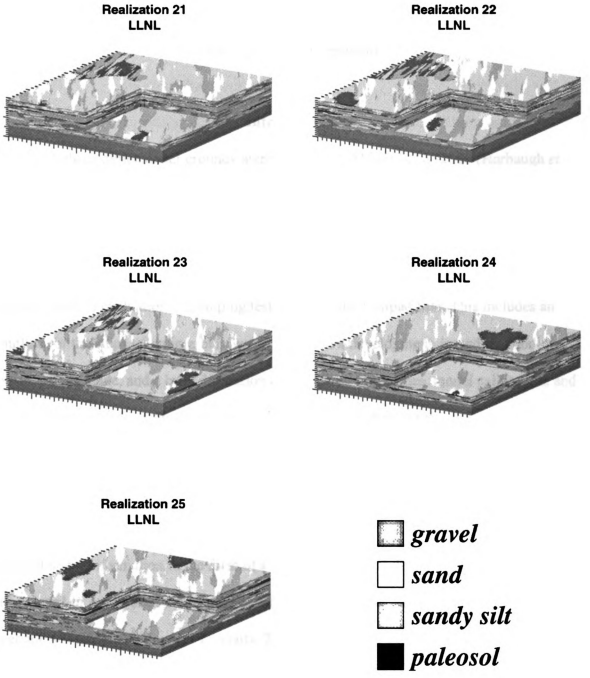

Figure F.8: Full realization (21 through 25) following methods for a zoned simulation approach. Four categories are used (gravel, sand, silty sand, and paleosol) to characterize the geology at the Helipad Study Site, LLNL.

Appendix G

GMS Model Development

Introduction

A three-dimensional groundwater flow model, MODFLOW-2000 (Harbaugh *et al.*, 2000), was applied for computation of steady state and transient heads for the Helipad study area, Lawrence Livermore National Laboratory (LLNL). The following sections are a discussion of groundwater flow model development for each of the four numerical models used in evaluation of pumping test results at the Helipad Site. This includes an outline for the steps taken in groundwater flow model development, boundary condition assumptions made, and a brief discussion of optimization routines, model calibration, and hydraulic properties incorporated for solutions to head distributions.

Model development

Listed below are procedures used for grid development and incorporation of geostatistical information in the form of a three-dimensional distribution of hydrofacies (discussed in Appendix F). In model development, Groundwater Modeling Software version 4.0 (Brigham Young University, 2000) was used to write files needed by MODFLOW-2000 for computation. Due to the large size of these models, and the inability of GMS to calculate heads at observation wells, computation of head distributions was run from a command prompt outside of GMS 4.0. Modifications were made to some of these files as needed to acquirer head solutions.

Procedures for groundwater flow model development –

- Grid –
    - Grid and cell dimensions were set equal to transition probability geostatistical simulations.
    - Cell dimensions have a maximum size of 2 x 2 x 0.5 meters across an area of 362 meters (east-west) by 310 meters (north-south) by 39 meters (vertical direction).
    - The origin for the model area was set at 4239.5 (x), 2083.5 (y), and 124.5 (z). This origin placed well 1654 at the center of the grid.
- Wells locations –
    - Prior to inputting well locations, well coordinates within the study area wells were rotated around an origin. Well locations were rotated 20 degrees clockwise around the origin. This was done to align the groundwater flow model with the principle groundwater flow direction observed at this location (Figure 2.8).
- Grid refinement –
    - The grid cell size was refined around pumping wells to a minimum cell size of 0.15 meters with a bias of 1.2 to better resolve head distributions near pumping wells. This was also done to minimize numerical error that is generally associated with pumping wells.
    - In this refined grid, hydrofacies were assigned to each cell based on the location of cell center. If the coordinate of a cell center fell within the boundary of a hydrofacies, that hydrofacies would be assigned to that cell.

- Geologic information (Homogeneous-Layered and Homogeneous-Layered with paleosol) –
    - Top and bottom paleosol surfaces were generated with Rockware 2002 software (RockWorks Inc., 2002) as a result of paleosol correlations made across the study area (appendix C).
    - A tabular 2-D scatter set was exported from Rockworks 2002 for each paleosol top and bottom surface. These scatter sets were then imported into GMS and interpolated using an inverse distance method algorithm.
        - For the Homogeneous-Layered model, top paleosol surfaces were incorporated to segregate homogeneous layers.
        - For the Homogeneous-Layered model with paleosol layers, both top and bottom paleosol surfaces scatter point sets were interpolated to separate model layers.
- Geologic information (transition probability geostatistics) –
    - Using GMS to generate a generic .mfs file for the Helipad Site grid domain, material ID's (hydrofacies categories) were inserted under the DMAT heading in place of the 1 (this heading must also be changed to MAT). Material ID's are inserted as one continuous column of numbers (output from FORTRAN code). Note, output file from FORTAN code assigned a negative value to material ID's that were used as conditioning points for transition probability geostatistical simulations. This file is then saved and GMS reopened (for this

procedure to work properly, the .mst file must be deleted, this will not affect the overall model).

- Using a FORTRAN code (Appendix I), simulation .bgr files were converted to a list of material ID's (accounting for sequential order).

- Pumping –
  - Pumping from wells 1551 and 1552 was set over a screened interval between appropriate top and bottom elevations.
  - Wells 1551 and 1552 had a pumping rate of 16.33m^3/d and 2.27m^3/d, respectfully. These pumping rates were held constant throughout the duration of the pumping test at the Helipad Site.
  - For solutions to head distributions, a two stress period simulation was run. The first stress period was manually set to steady state within the .dis file. The second stress period was set to transient with a 1.2 multiplier over 25 time increments
- Observation wells –
  - Due to the large size of these models, an observation well file was developed following GMS observation-process documentation (Hill *et al.*, 2000) for each of the 1200, 1500, and 1600 series observation wells. This file was set to record head at observation locations for each time step of each stress period.
  - Observation points were placed within the highest conductive material with the screened interval (the greatest amount of drawdown was observed within these units).

- Model Boundaries
    - Eastern and western boundaries were assigned as constant head boundaries with northern and southern boundaries assigned as no-flow boundaries. This created a west trending flow gradient similar to that observed at the study area.
- Modifications to generic model –
    - As a result of scaling material ID's to fit the refined grid, the location of conditioned points used in generation of geostatistical realizations were slightly shifted (a few cells in to the right-left or up-down). Observation point locations were adjusted to account for this discrepancy.
    - At the constant head boundaries, cells became dry while Modflow calculated heads. This resulted in the simulation failing to converge. To correct for this problem, constant head cells were manually assigned to a material 3 ID (silty sand hydrofacies). This prevented cells from drying out during calculation of heads.

Assumptions

In development of any groundwater model, there are certain assumptions about the system that must be made for simplification of the problem. The following is a list of assumptions that were made in development of groundwater models used for evaluation of pumping test conducted at the Helipad Site:

- Boundaries conditions –

- The climate associated with this region is arid; the annual precipitation recorded at this location is 34 cm/year (U.S. Department of Energy, 1998). The pumping test was conducted from late Aril to early May. Given a relatively low recorded average precipitation and the pumping test was conducted during the middle to late spring months, precipitation as a recharge into the groundwater model is set to zero for the steady state simulation and over course of the observed pumping test period.
- The two streams located in the vicinity of the LLNL facility are the Arroyo Seco and Arroyo Las Positas. The Arroyo Seco is located well to the south west of the LLNL property (approximately 1 mile from the Helipad Site). The Arroyo Las Positas has been redirected following the eastern and northern portion of the LLNL property approximately 0.5 miles from the study site. Both of these streams are intermittent and are assumed to have no major influence to the ten day pumping test conducted at the Helipad Site. Drainage streams across the LLNL property are cement lined and assumed to be disconnected from the aquifer system. There is a large retention pond in close proximity to the Helipad Site. However, this retention pond is lined and assumed to be disconnected from the aquifer system.
- The LLNL site is currently undergoing remediation, primary remedial efforts at this site involve pump and treat methods. Across the LLNL property there are a series of pumping wells extraction water out of

multiple stratigraphic horizons at relatively low rates. For the purpose of pumping test evaluation at the Helipad Site, drawdown histories were analyzed. It was assumed that pumping from wells other then 1551 and 1552 would not affect these results.

- Drawdown histories for observation wells at the study site show an oscillation. This oscillation is attributed to night and day power consumption. More power is available during night hours allowing pumping rates to be slightly elevated. Drawdown histories were therefore evaluated during the first 24 hours of operation, after this it was assumed that the system came to equilibrium where drawdown oscillated around a mean value.
- Cell dimensions used in modeling efforts were assumed to be small enough to capture finer scale heterogeneities associated with alluvial fan architecture.

Optimization

Two parameter estimation routines were evaluated in optimizing our groundwater models. These included the MODFLOW-2000 PES (Hill *et al.*, 2000) and the PEST Doherty *et al.* (2000) routines. Both of these methods rely on the observation process which calculates head values for comparison with measured or observed head values. To quantify this comparison, a variety of statistics are calculated including weighted least-squares objective function. A series of output files are written for graphical analysis of these statistics. While running the observation process, sensitivities are simultaneously

calculated using a sensitivity-equation. This process diagnoses inadequate data, identifies parameters that may not be optimized, and evaluates the utility of proposed new data (Hill *et al.*, 2000). Finally, the parameter estimation process used a modified Gauss-Newton method to adjust variable values defined by the user.

Executables for both the PES and PEST routines require a set of input files which are described in detail in the User Guide to the Observation, Sensitivity, and Parameter-Estimation Processes documentation (Hill *et al.*, 2000). As a result of running these programs, user defined variable parameters, such as hydraulic conductivity and storage coefficients are adjusted following a set of statistics to minimize the weighted sum of squares. For our numerical groundwater models, both routines were evaluated for optimization of material properties of geostatistical realizations.

Hydraulic conductivity and storativity values for channel gravel and sand, and floodplain silty sands were set for the optimization routines. However, there were problems with using the PES and PEST routines. Due to the large size of the model, the optimization process required between a few days to weeks to run. Between every iteration, user defined variable parameters are updated. The model is rerun for a solution to the weighted sum of squares. Between iterations, the pumping well file was not updated for new values used for material ID's. Since the well file is calculated for material properties within each cell, failing to update this well file resulted in false weighted sum of square values rendering the optimization routines invalid. This error was observed for both PES and PEST routines. Because of this error, PES and PEST could not be used. Therefore groundwater models were manually calibrated to match observed drawdown values.

Calibration

Initial values (hydraulic conductivity and storativity) used for gravel, sand, silty sand, and paleosol materials were obtained from calibrated model results from a nearby study site. Carle *et al.* (1998) used similar material types (channel, debris, overbank deposits) in a transition probability geostatistical model from a nearby study site at LLNL, these values are listed in Table G.1. Using the spatial distribution of hydrofacies from realization one, hydraulic conductivity and storativity values for channel, sand, and silty sand materials were then calibrated to match drawdown histories observed in the 1650 series wells. Final calibrated values from this simulation were then used in the transition probability geostatistical simulation.

Homogeneous-Layered models were calibrated individually by assigning reasonable generic hydraulic properties to each model layer. Anisotropic values as well as hydraulic properties were adjusted to best fit drawdown histories for the Homogeneous -Layered model. Only hydraulic properties were adjusted for the Homogeneous-Layered model with paleosol layers, paleosol layers are assigned a relatively low conductivity value which negates the need to assign anisotropy to prevent vertical fluid flow across stratigraphic zones. Table G.2 lists final calibrated K and S values used in each modeling approach.

Conclusions

A three-dimensional groundwater flow model was applied for computation of steady state and transient heads for the Helipad study area, Lawrence Livermore National Laboratory (LLNL). Each modeling approach used the same methods for groundwater

model development. Following a set of assumptions, solutions for head distributions for each modeling approach was returned. To better match drawdown histories observed at the study site, both parameter-optimization and calibration techniques were used. However, optimization routines (PES and PEST) failed to update pumping well files which greatly impacted end results. Therefore, this method was only used as an evaluation tool for calibration of these models. Those materials that are most sensitive were adjusted. The results of calibration produced drawdown histories that are a relatively close match to observed values (see appendix H and discussion in chapter 3). Due to time limitations, optimization routines could not be further explored.

Homogeneous-Layered Model:				
Layers	Hydraulic Conductivity (m/d)	Horizontal Anisotropy	Vertical Anisotropy	Specific Storage (1/m)
C zone	1	1	0.1	0.00018
D zone	1	1	0.1	0.00021
E zone	1	1	0.1	0.00026
F zone	1	1	0.1	0.0002
Lower Livermore	1	1	0.1	0.0003

Homogeneous-Layered Model with Paleosol Layers				
Layers	Hydraulic Conductivity (m/d)	Horizontal Anisotropy	Vertical Anisotropy	Specific Storage (1/m)
Paleosol layers	0.00004628	1	1	0.0007
C zone	1	1.8	1	0.00018
D zone	1	1.8	1	0.00021
E zone	1	1.8	1	0.00026
F zone	1	1.8	1	0.002
Lower Livermore	1	1.8	1	0.0003

Transition Probability Geostatistical Simulation:				
Hydofacies	Hydraulic Conductivity (m/d)	Horizontal Anisotropy	Vertical Anisotropy	Specific Storage (1/m)
Gravel	5.18	1	1	0.0001
Sand	2	1	1	0.0002
Silty Sand	0.01728	1	1	0.0003
Paleosol	0.00004628	1	1	0.0007
Lower Livermore	0.01728	1	1	0.0003

Table G.1: Listed above are initial hydraulic properties assigned to either layers or material (hydrofacies) used in each of the four modeling approaches. Values listed are initial values incorporated into each modeling approach.

Homogeneous-Layered Model:				
Layers	Hydraulic Conductivity (m/d)	Horizontal Anisotropy	Vertical Anisotropy	Specific Storage (1/m)
C zone	1	1	0.1	0.00018
D zone	1	1	0.1	0.00021
E zone	**0.25614**	**4.47**	**0.2546**	**0.0007523**
F zone	1	1	0.1	0.0002
Lower Livermore	1	1	0.1	0.0003

Homogeneous-Layered Model with Paleosol Layers				
Layers	Hydraulic Conductivity (m/d)	Horizontal Anisotropy	Vertical Anisotropy	Specific Storage (1/m)
Paleosol layers	0.00004628	1	1	0.0007
C zone	1	1.8	1	0.00018
D zone	1	1.8	1	0.00021
E zone	**0.5**	1.8	1	**0.00005**
F zone	1	1.8	1	0.002
Lower Livermore	1	1.8	1	0.0003

Transtion Probability Geostatistical Simulation:				
Hydofacies	Hydraulic Conductivity (m/d)	Horizontal Anisotropy	Vertical Anisotropy	Specific Storage (1/m)
Gravel	**30**	1	1	**0.00005**
Sand	2	1	1	0.0002
Silty Sand	**0.009**	1	1	0.0003
Paleosol	0.00004628	1	1	0.0007
Lower Livermore	0.01728	1	1	0.0003

Table G.2: Listed above are hydraulic properties assigned to either layers or material (hydrofacies) used in each of the four modeling approaches. Values listed have been calibrated for to best match drawdown histories observed (for comparison purpose, geostatistical models all used the same values calibrated from realization one).

Appendix H

Drawdown Results

This appendix contains drawdown histories for the observed pumping test (Figure H.1) as well as pumping test results from each of the four conceptual models (drawdown at initial time of pumping are normalized to zero) – the Homogeneous-Layered conceptual model, the Homogeneous-Layered conceptual model that incorporated low hydraulically conductive paleosol layers, the transition probability geostatistical conceptual model, and the stratigraphic transition probability geostatistical conceptual model. These conceptual models were evaluated within GMS 4.0 (Brigham Young University, 2000) and used Moflow-2000 (Harbaugh et al., 2000) to solve for head distributions at observation wells.

Calculations of head distributions for the models were solved in a two step manor. The first step solved for a steady state head distribution across the model area without pumping. The second step calculated head distributions for 25 time steps using a 1.2 multiplier for a steady pumping rate (described in Appendix G). The difference between steady state heads and head values during the transient Modflow simulation resulted in drawdown histories at each observation point. Figures H.2 through H.30 are drawdown histories simulated with Modflow-2000 (Harbaugh et al., 2000). Also, map views are presented for comparison of drawdown result for each conceptual model type.

Overall, realizations XX and XX preformed the best; realizations xx xx did not perform as well. For those realizations that preformed well, it was characteristics of discrete gravel bodies (~8m by 20m) within elongate sand channels (~15m by 40m) were

observed. Channel bodies that were over elongate resulted in lower drawdown, those realizations that show very discrete channel bodies resulted in high drawdown.

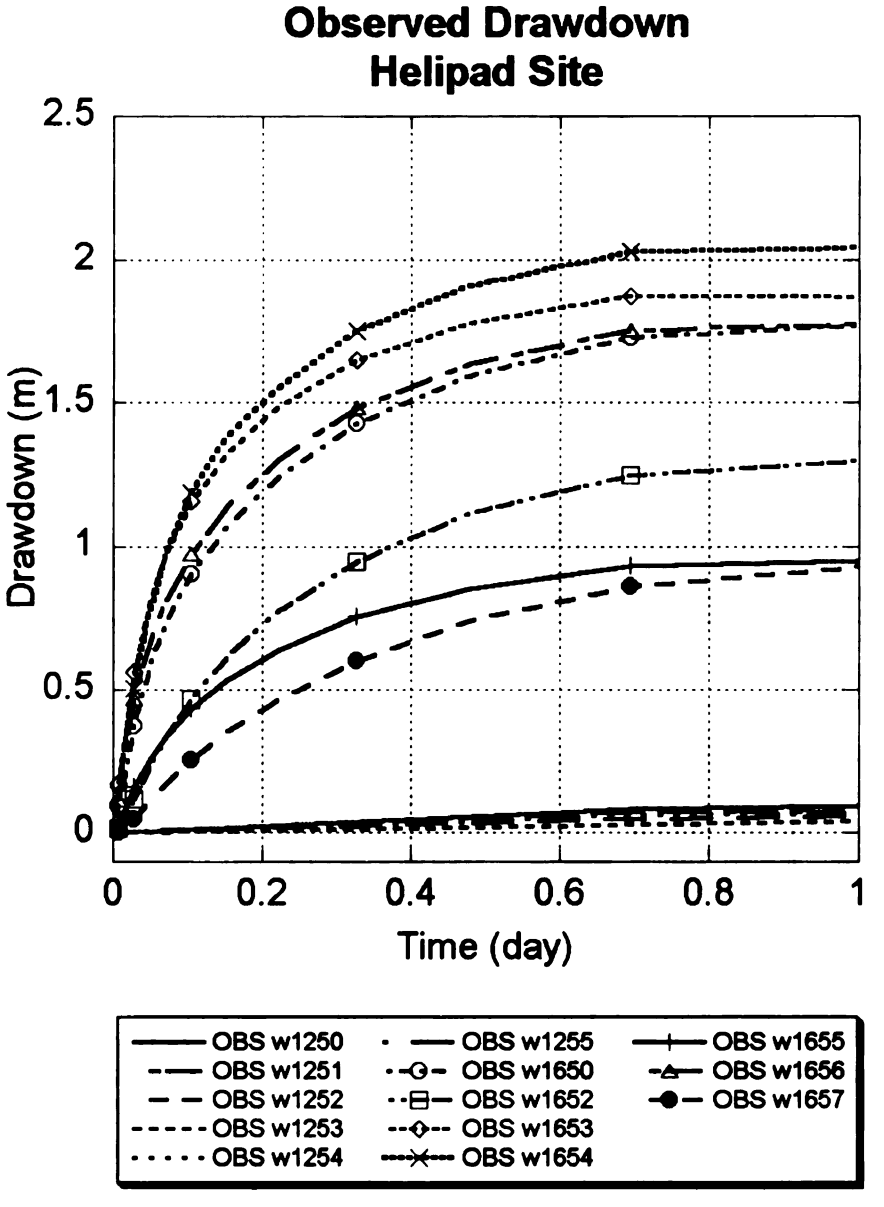

Figure H.1: Observed drawdown histories for 1650 series wells and 1250 series wells are depicted for the Helipad Site (1650 series wells are screened within HSU 3, 1250 wells are Screen across HSU 4). As a result of pumping (1650 series wells) there is little to no observed drawdown in1250 series wells.

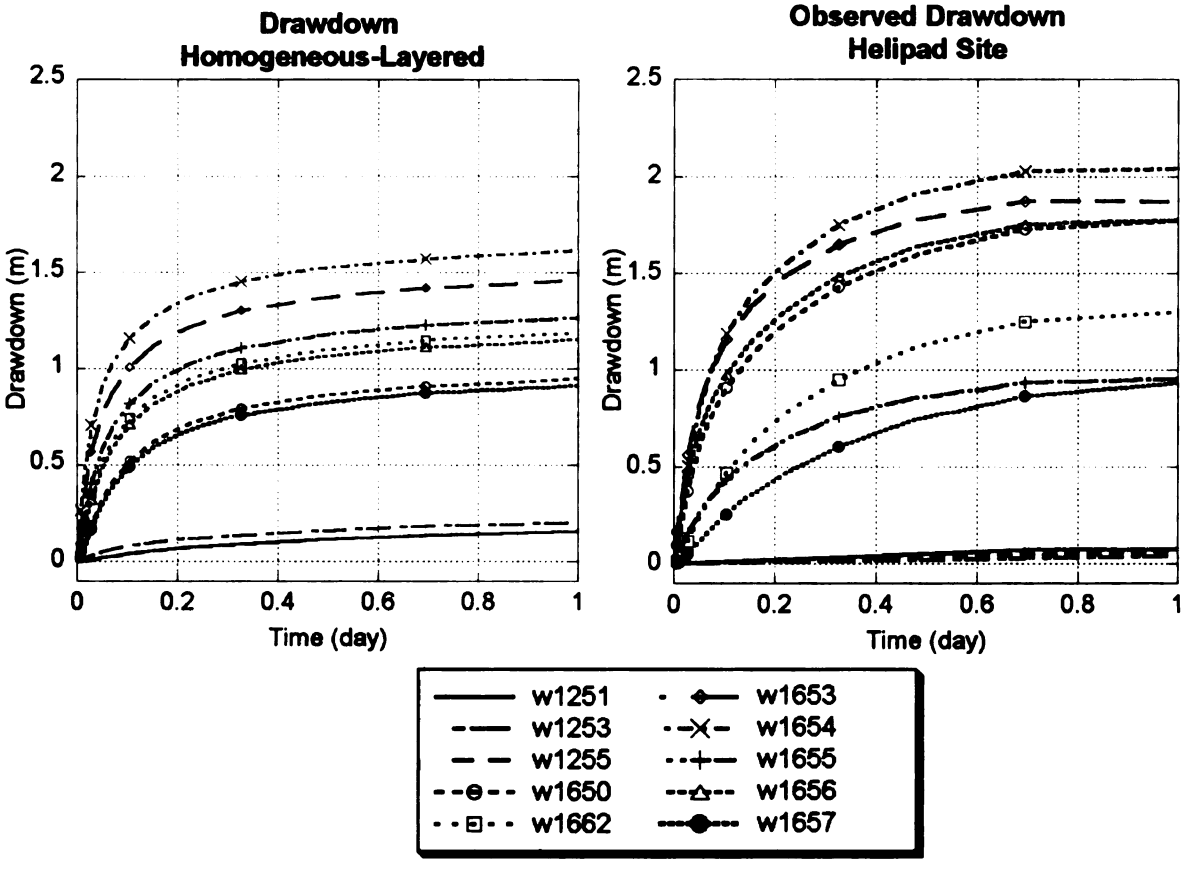

Figure H.2: Simulated drawdown histories for 1650 series and 1250 series wells within the Homogeneous-Layered conceptual model. Simulated results show minor drawdown in1250 series wells.

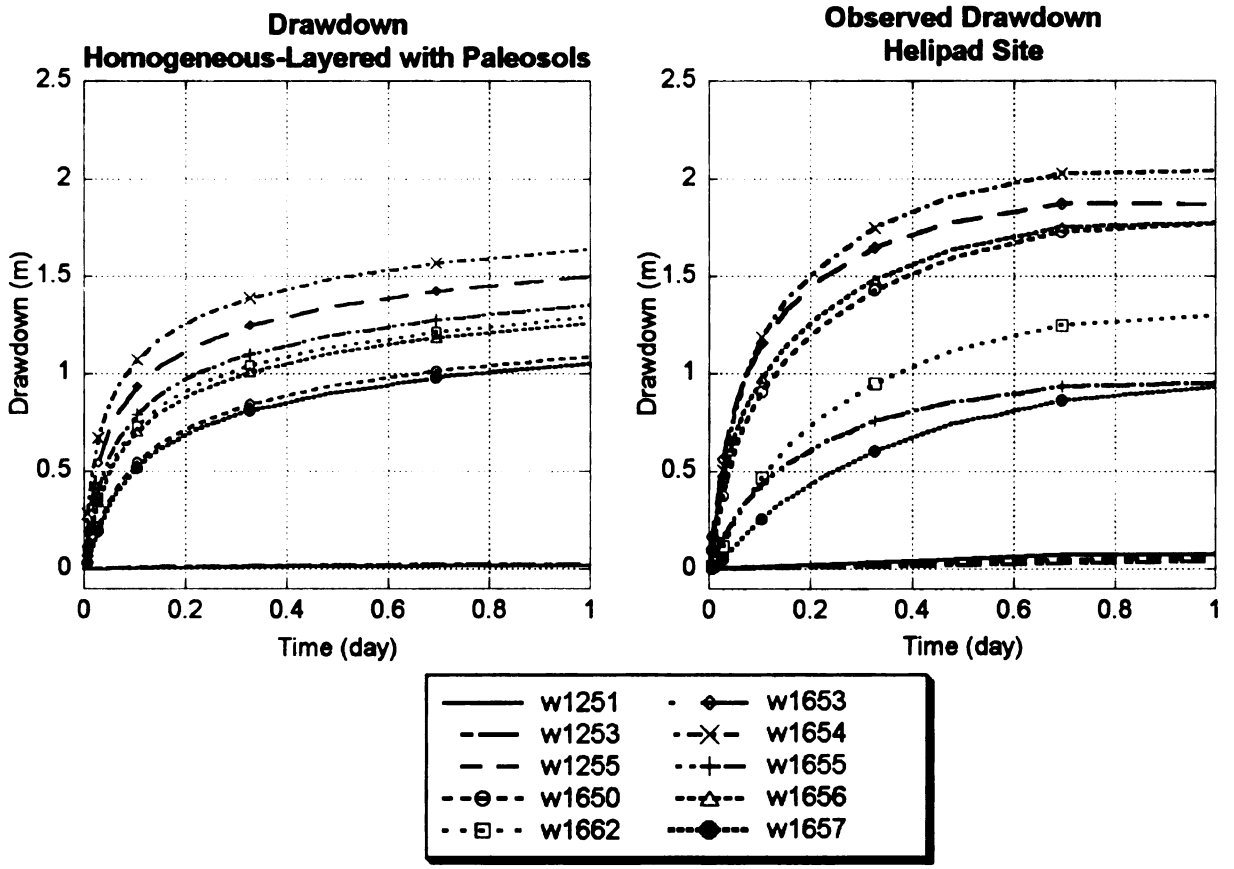

Figure H.3: Simulated drawdown histories for 1650 series and 1250 series wells within the Homogeneous-Layered conceptual model with paleosol layers. Simulated results show minor drawdown in1250 series wells.

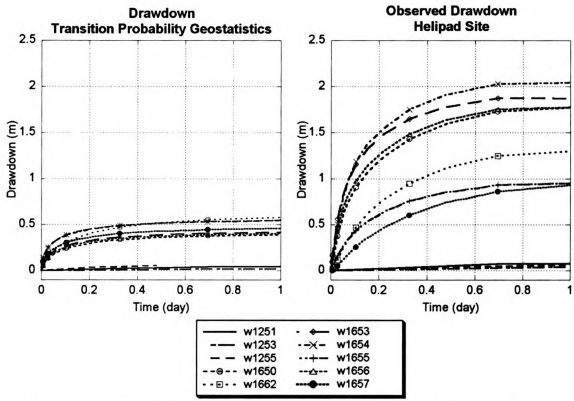

Figure H.4a: Simulated drawdown histories for 1650 series and 1250 series wells within the transition probability geostatistical conceptual model. Simulated results show minor drawdown in1250 series wells.

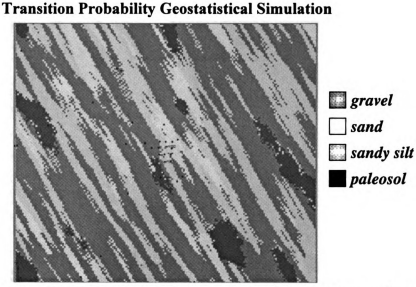

Figure H.4b: Map view of the spatial distribution of hydrofacies for the transition probability geostatistical conceptual model. Map view is from the 24th model layer (lower portion of the sand and gravel channel for the E stratigraphic unit).

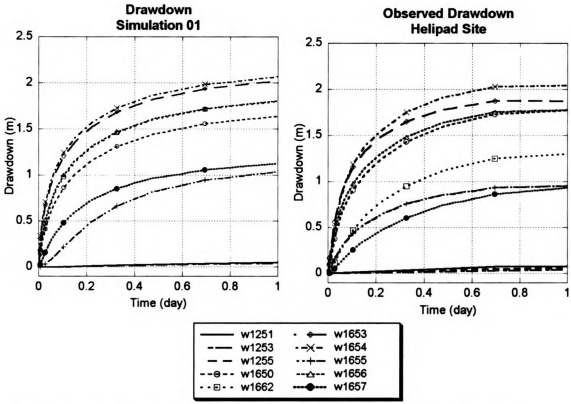

Figure H.5a: Simulated drawdown histories for 1650 series and 1250 series wells within the stratigraphic transition probability geostatistical conceptual model. Simulated results show minor drawdown in1250 series wells.

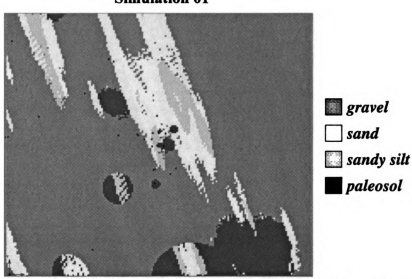

Figure H.5b: Map view of the spatial distribution of hydrofacies for the stratigraphic transition probability geostatistical conceptual model. Map view is from the 24th model layer (lower portion of the sand and gravel channel for the E stratigraphic unit).

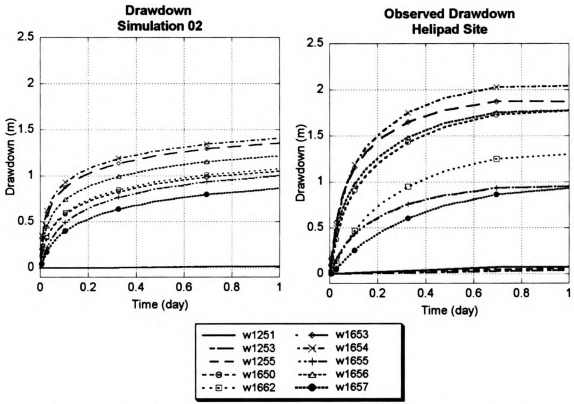

Figure H.6a: Simulated drawdown histories for 1650 series and 1250 series wells within the stratigraphic transition probability geostatistical conceptual model. Simulated results show minor drawdown in1250 series wells.

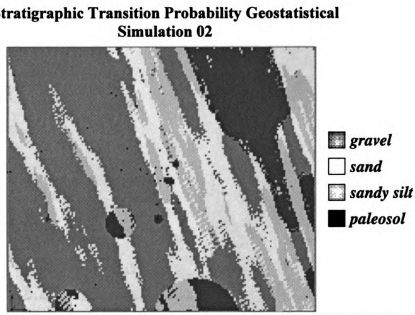

Figure H.6b: Map view of the spatial distribution of hydrofacies for the stratigraphic transition probability geostatistical conceptual model. Map view is from the 24th model layer (lower portion of the sand and gravel channel for the E stratigraphic unit).

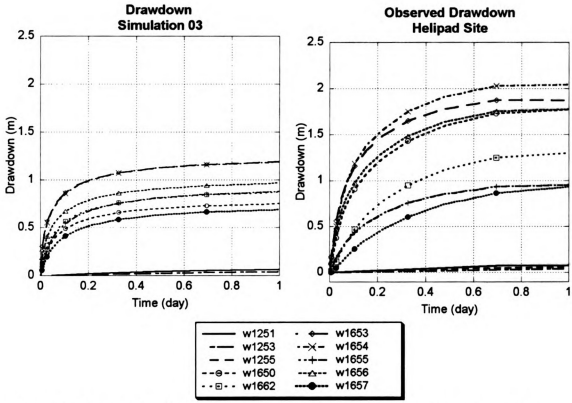

Figure H.7a: Simulated drawdown histories for 1650 series and 1250 series wells within the stratigraphic transition probability geostatistical conceptual model. Simulated results show minor drawdown in1250 series wells.

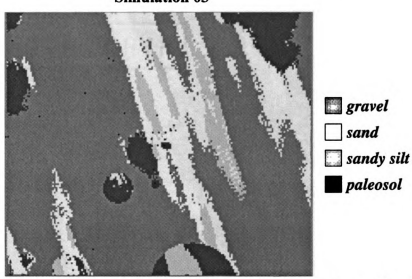

Figure H.7b: Map view of the spatial distribution of hydrofacies for the stratigraphic transition probability geostatistical conceptual model. Map view is from the 24th model layer (lower portion of the sand and gravel channel for the E stratigraphic unit).

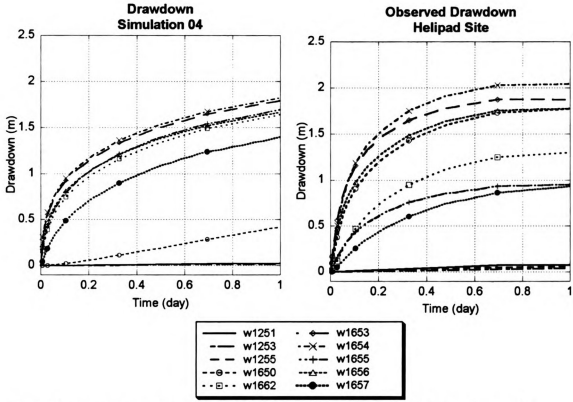

Figure H.8a: Simulated drawdown histories for 1650 series and 1250 series wells within the stratigraphic transition probability geostatistical conceptual model. Simulated results show minor drawdown in1250 series wells.

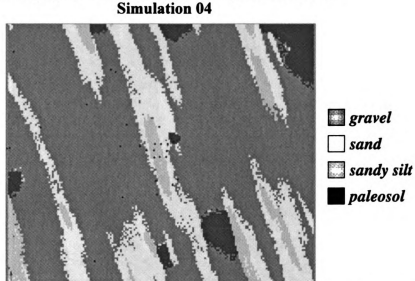

Figure H.8b: Map view of the spatial distribution of hydrofacies for the stratigraphic transition probability geostatistical conceptual model. Map view is from the 24th model layer (lower portion of the sand and gravel channel for the E stratigraphic unit).

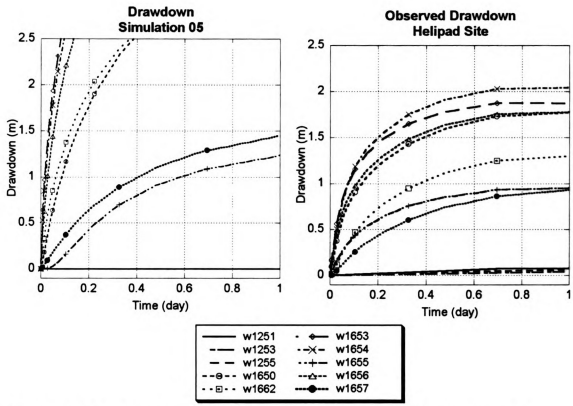

Figure H.9a: Simulated drawdown histories for 1650 series and 1250 series wells within the stratigraphic transition probability geostatistical conceptual model. Simulated results show minor drawdown in1250 series wells.

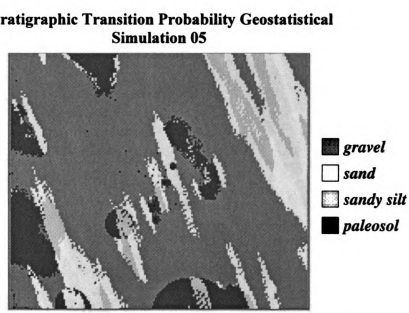

Figure H.9b: Map view of the spatial distribution of hydrofacies for the stratigraphic transition probability geostatistical conceptual model. Map view is from the 24th model layer (lower portion of the sand and gravel channel for the E stratigraphic unit).

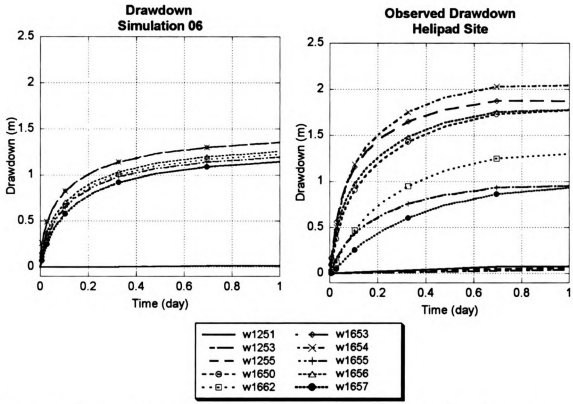

Figure H.10a: Simulated drawdown histories for 1650 series and 1250 series wells within the stratigraphic transition probability geostatistical conceptual model. Simulated results show minor drawdown in1250 series wells.

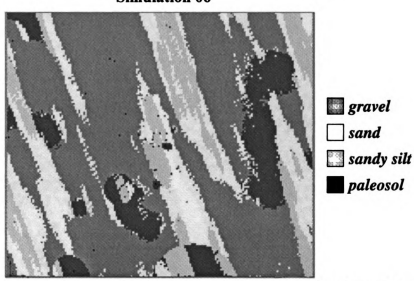

Figure H.10b: Map view of the spatial distribution of hydrofacies for the stratigraphic transition probability geostatistical conceptual model. Map view is from the 24th model layer (lower portion of the sand and gravel channel for the E stratigraphic unit).

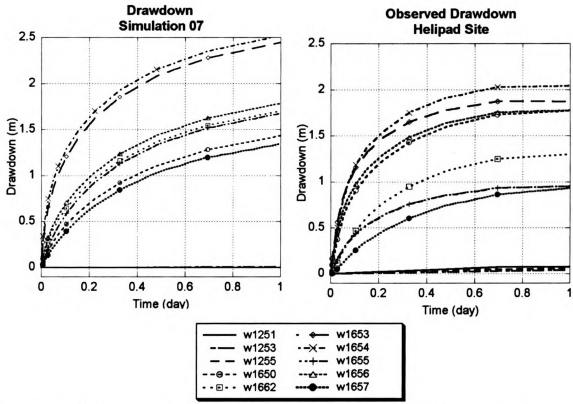

Figure H.11a: Simulated drawdown histories for 1650 series and 1250 series wells within the stratigraphic transition probability geostatistical conceptual model. Simulated results show minor drawdown in1250 series wells.

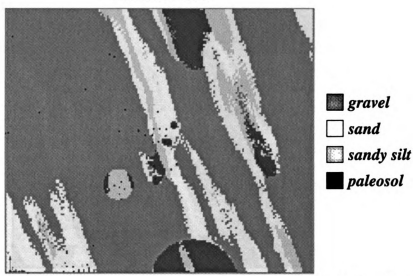

Figure H.11b: Map view of the spatial distribution of hydrofacies for the stratigraphic transition probability geostatistical conceptual model. Map view is from the 24th model layer (lower portion of the sand and gravel channel for the E stratigraphic unit).

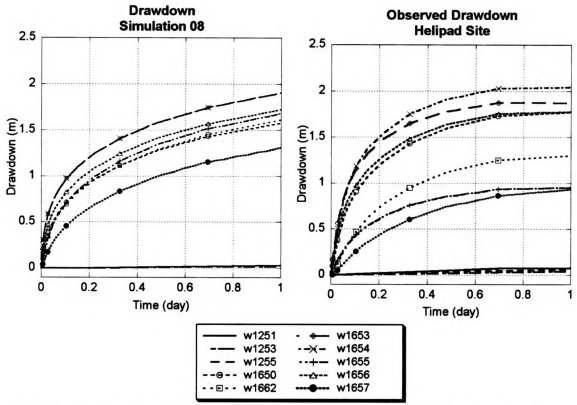

Figure H.12a: Simulated drawdown histories for 1650 series and 1250 series wells within the stratigraphic transition probability geostatistical conceptual model. Simulated results show minor drawdown in1250 series wells.

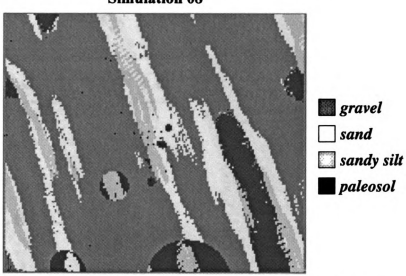

Figure H.12b: Map view of the spatial distribution of hydrofacies for the stratigraphic transition probability geostatistical conceptual model. Map view is from the 24th model layer (lower portion of the sand and gravel channel for the E stratigraphic unit).

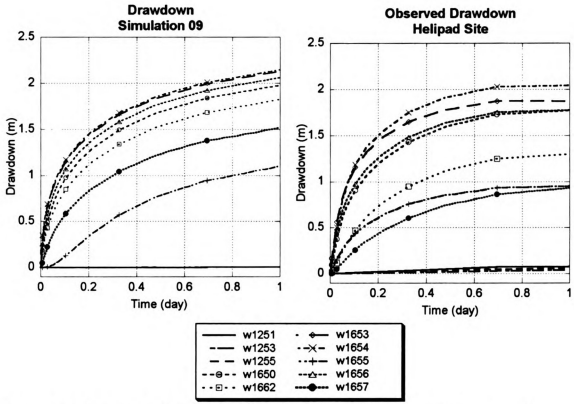

Figure H.13a: Simulated drawdown histories for 1650 series and 1250 series wells within the stratigraphic transition probability geostatistical conceptual model. Simulated results show minor drawdown in1250 series wells.

Stratigraphic Transition Probability Geostatistical Simulation 09

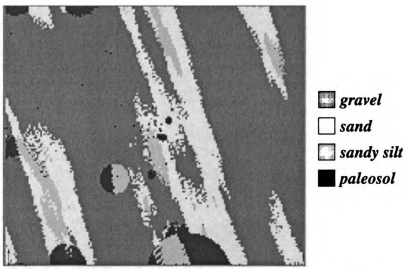

Figure H.13b: Map view of the spatial distribution of hydrofacies for the stratigraphic transition probability geostatistical conceptual model. Map view is from the 24th model layer (lower portion of the sand and gravel channel for the E stratigraphic unit).

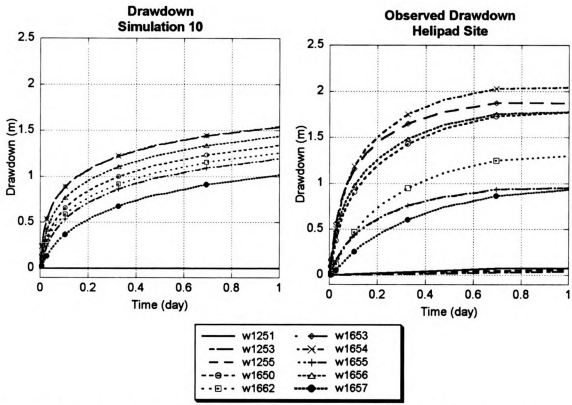

Figure H.14a: Simulated drawdown histories for 1650 series and 1250 series wells within the stratigraphic transition probability geostatistical conceptual model. Simulated results show minor drawdown in1250 series wells.

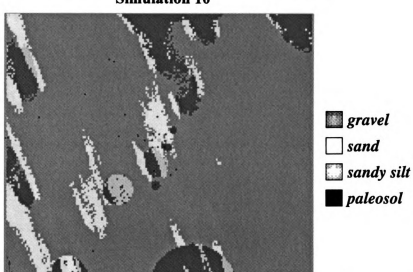

Figure H.14b: Map view of the spatial distribution of hydrofacies for the stratigraphic transition probability geostatistical conceptual model. Map view is from the 24th model layer (lower portion of the sand and gravel channel for the E stratigraphic unit).

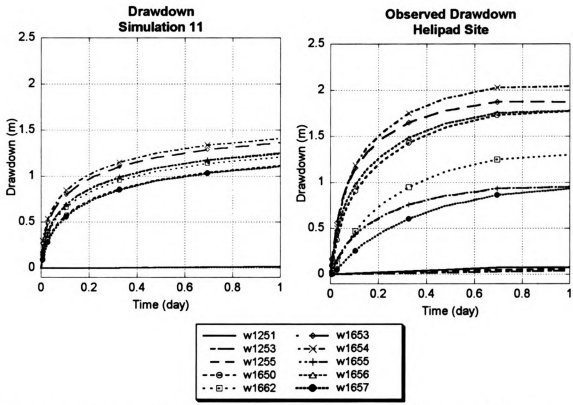

Figure H.15a: Simulated drawdown histories for 1650 series and 1250 series wells within the stratigraphic transition probability geostatistical conceptual model. Simulated results show minor drawdown in1250 series wells.

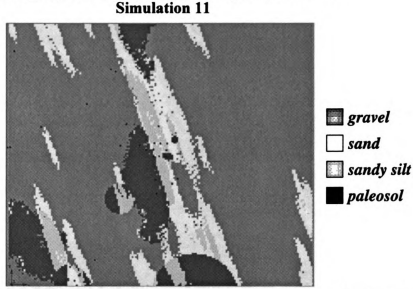

Figure H.15b: Map view of the spatial distribution of hydrofacies for the stratigraphic transition probability geostatistical conceptual model. Map view is from the 24th model layer (lower portion of the sand and gravel channel for the E stratigraphic unit).

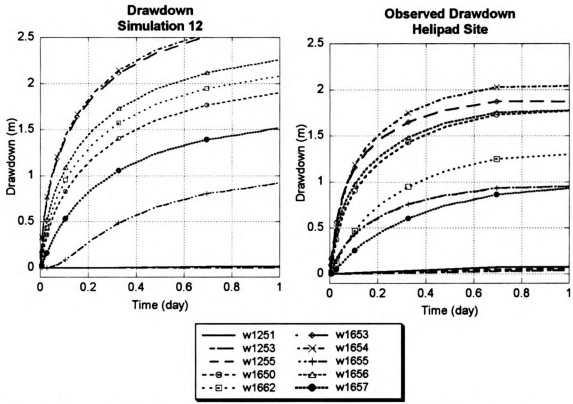

Figure H.16a: Simulated drawdown histories for 1650 series and 1250 series wells within the stratigraphic transition probability geostatistical conceptual model. Simulated results show minor drawdown in1250 series wells.

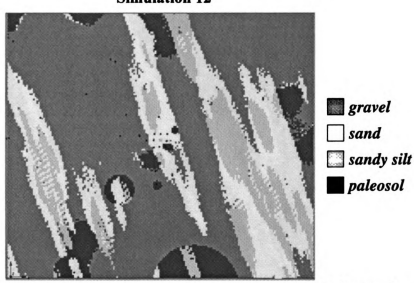

Figure H.16b: Map view of the spatial distribution of hydrofacies for the stratigraphic transition probability geostatistical conceptual model. Map view is from the 24th model layer (lower portion of the sand and gravel channel for the E stratigraphic unit).

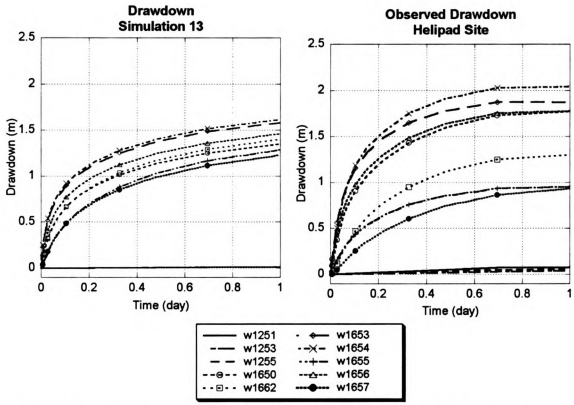

Figure H.17a: Simulated drawdown histories for 1650 series and 1250 series wells within the stratigraphic transition probability geostatistical conceptual model. Simulated results show minor drawdown in1250 series wells.

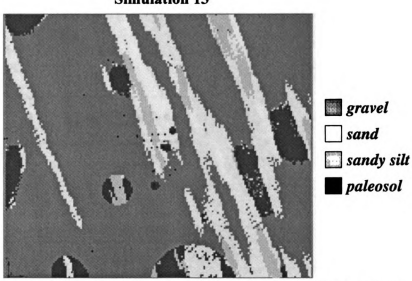

Figure H.17b: Map view of the spatial distribution of hydrofacies for the stratigraphic transition probability geostatistical conceptual model. Map view is from the 24th model layer (lower portion of the sand and gravel channel for the E stratigraphic unit).

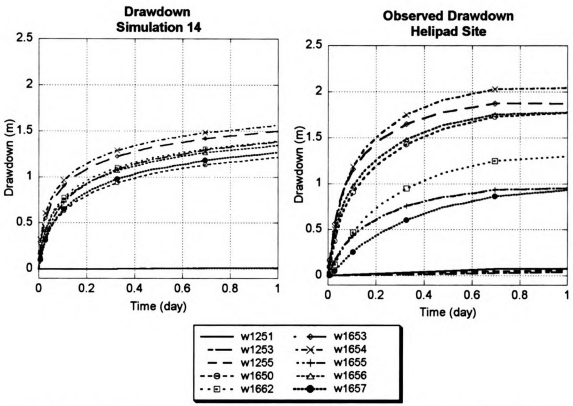

Figure H.18a: Simulated drawdown histories for 1650 series and 1250 series wells within the stratigraphic transition probability geostatistical conceptual model. Simulated results show minor drawdown in1250 series wells.

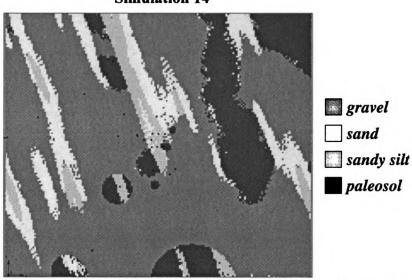

Figure H.18b: Map view of the spatial distribution of hydrofacies for the stratigraphic transition probability geostatistical conceptual model. Map view is from the 24th model layer (lower portion of the sand and gravel channel for the E stratigraphic unit).

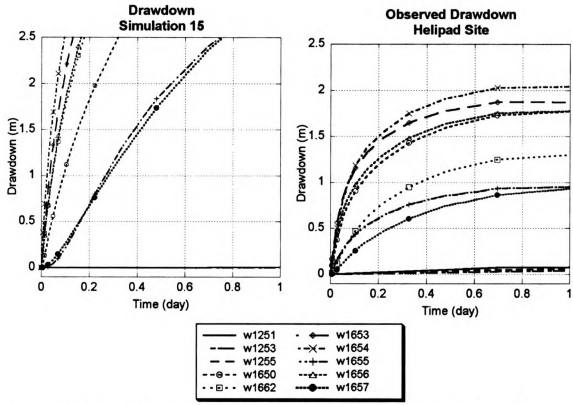

Figure H.19a: Simulated drawdown histories for 1650 series and 1250 series wells within the stratigraphic transition probability geostatistical conceptual model. Simulated results show minor drawdown in1250 series wells.

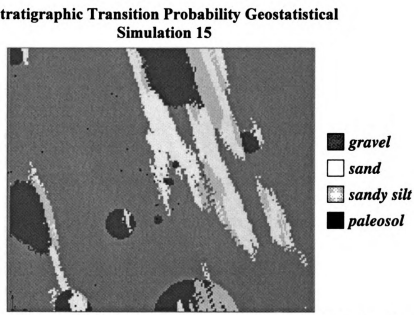

Figure H.19b: Map view of the spatial distribution of hydrofacies for the stratigraphic transition probability geostatistical conceptual model. Map view is from the 24th model layer (lower portion of the sand and gravel channel for the E stratigraphic unit).

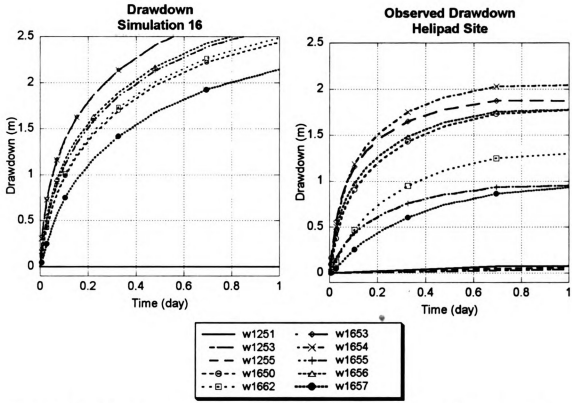

Figure H.20a: Simulated drawdown histories for 1650 series and 1250 series wells within the stratigraphic transition probability geostatistical conceptual model. Simulated results show minor drawdown in1250 series wells.

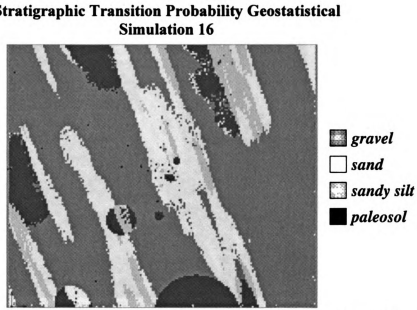

Figure H.20b: Map view of the spatial distribution of hydrofacies for the stratigraphic transition probability geostatistical conceptual model. Map view is from the 24th model layer (lower portion of the sand and gravel channel for the E stratigraphic unit).

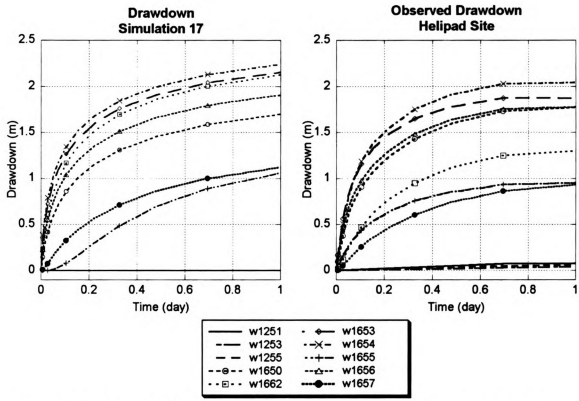

Figure H.21a: Simulated drawdown histories for 1650 series and 1250 series wells within the stratigraphic transition probability geostatistical conceptual model. Simulated results show minor drawdown in1250 series wells.

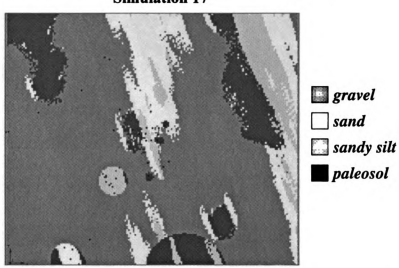

Figure H.21b: Map view of the spatial distribution of hydrofacies for the stratigraphic transition probability geostatistical conceptual model. Map view is from the 24th model layer (lower portion of the sand and gravel channel for the E stratigraphic unit).

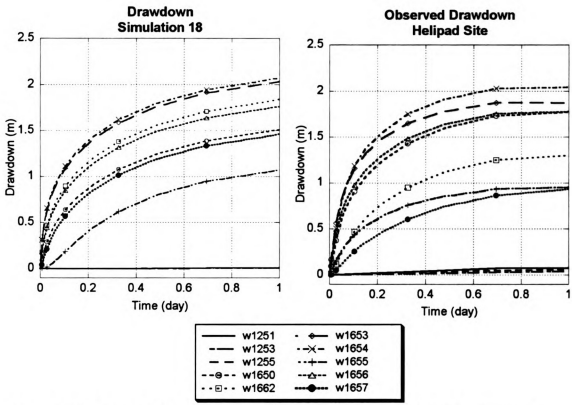

Figure H.22a: Simulated drawdown histories for 1650 series and 1250 series wells within the stratigraphic transition probability geostatistical conceptual model. Simulated results show minor drawdown in1250 series wells.

Stratigraphic Transition Probability Geostatistical Simulation 18

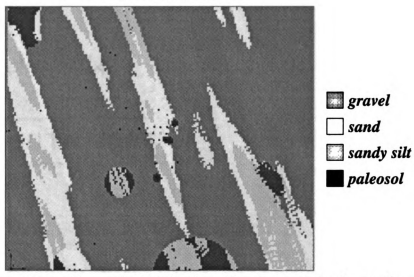

Figure H.22b: Map view of the spatial distribution of hydrofacies for the stratigraphic transition probability geostatistical conceptual model. Map view is from the 24th model layer (lower portion of the sand and gravel channel for the E stratigraphic unit).

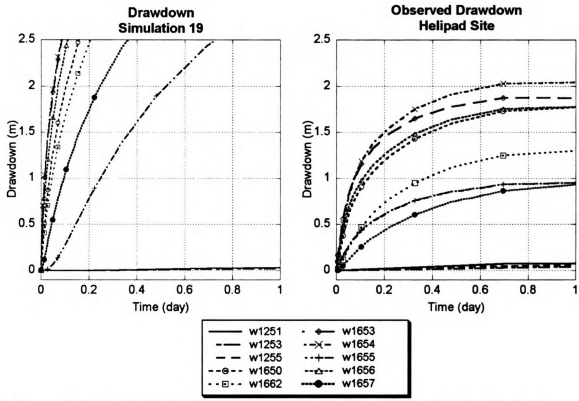

Figure H.23a: Simulated drawdown histories for 1650 series and 1250 series wells within the stratigraphic transition probability geostatistical conceptual model. Simulated results show minor drawdown in1250 series wells.

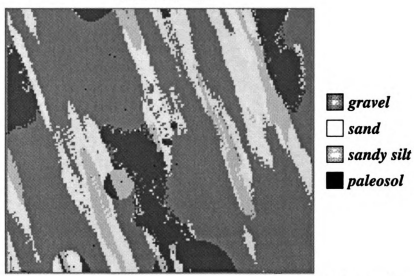

Figure H.23b: Map view of the spatial distribution of hydrofacies for the stratigraphic transition probability geostatistical conceptual model. Map view is from the 24th model layer (lower portion of the sand and gravel channel for the E stratigraphic unit).

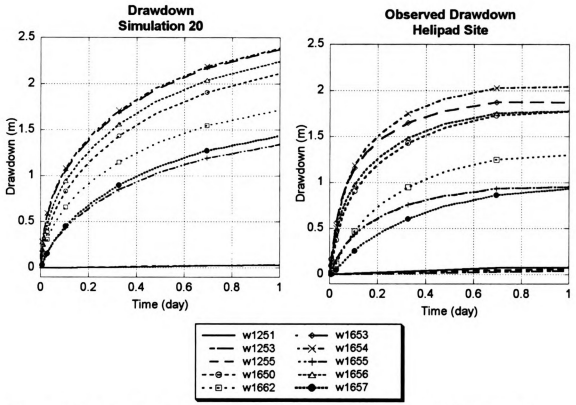

Figure H.24a: Simulated drawdown histories for 1650 series and 1250 series wells within the stratigraphic transition probability geostatistical conceptual model. Simulated results show minor drawdown in1250 series wells.

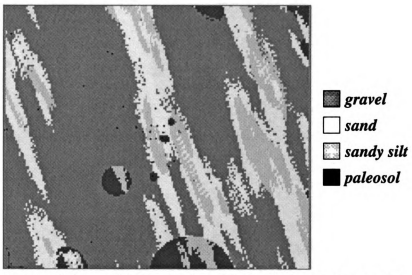

Figure H.24b: Map view of the spatial distribution of hydrofacies for the stratigraphic transition probability geostatistical conceptual model. Map view is from the 24th model layer (lower portion of the sand and gravel channel for the E stratigraphic unit).

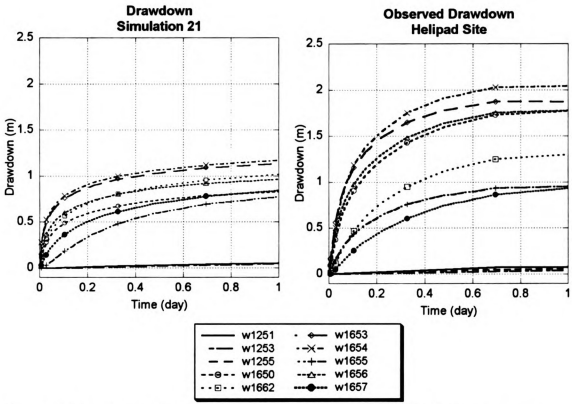

Figure H.25a: Simulated drawdown histories for 1650 series and 1250 series wells within the stratigraphic transition probability geostatistical conceptual model. Simulated results show minor drawdown in1250 series wells.

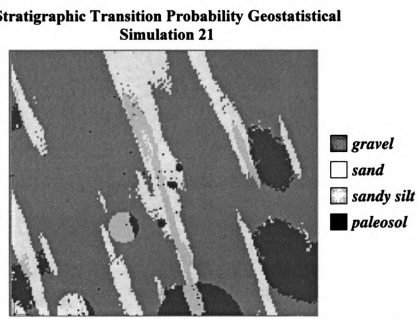

Figure H.25b: Map view of the spatial distribution of hydrofacies for the stratigraphic transition probability geostatistical conceptual model. Map view is from the 24th model layer (lower portion of the sand and gravel channel for the E stratigraphic unit).

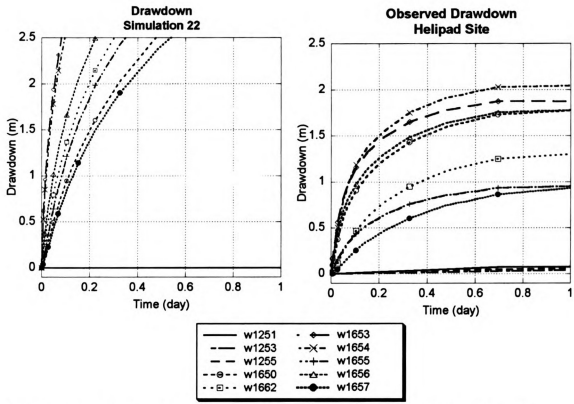

Figure H.26a: Simulated drawdown histories for 1650 series and 1250 series wells within the stratigraphic transition probability geostatistical conceptual model. Simulated results show minor drawdown in1250 series wells.

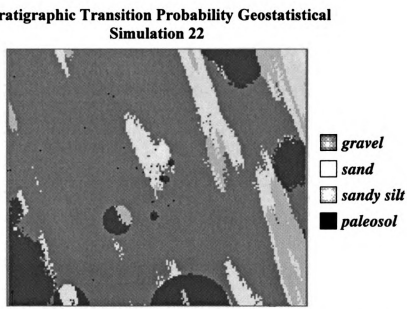

Figure H.26b: Map view of the spatial distribution of hydrofacies for the stratigraphic transition probability geostatistical conceptual model. Map view is from the 24th model layer (lower portion of the sand and gravel channel for the E stratigraphic unit).

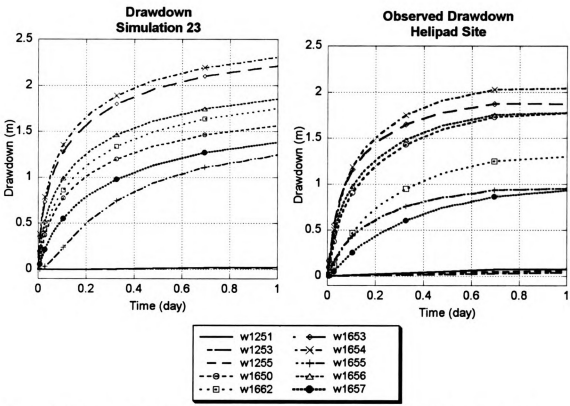

Figure H.27a: Simulated drawdown histories for 1650 series and 1250 series wells within the stratigraphic transition probability geostatistical conceptual model. Simulated results show minor drawdown in1250 series wells.

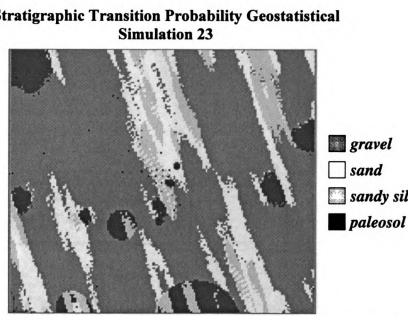

Figure H.27b: Map view of the spatial distribution of hydrofacies for the stratigraphic transition probability geostatistical conceptual model. Map view is from the 24th model layer (lower portion of the sand and gravel channel for the E stratigraphic unit).

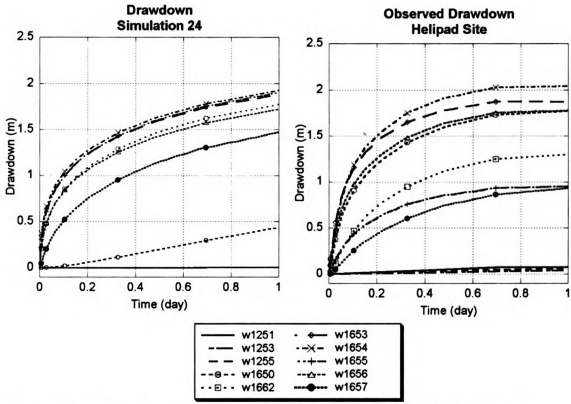

Figure H.28a: Simulated drawdown histories for 1650 series and 1250 series wells within the stratigraphic transition probability geostatistical conceptual model. Simulated results show minor drawdown in1250 series wells.

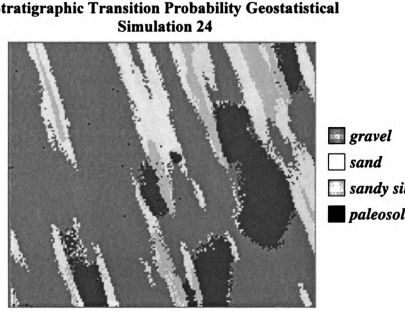

Figure H.28 Map view of the spatial distribution of hydrofacies for the stratigraphic transition probability geostatistical conceptual model. Map view is from the 24th model layer (lower portion of the sand and gravel channel for the E stratigraphic unit).

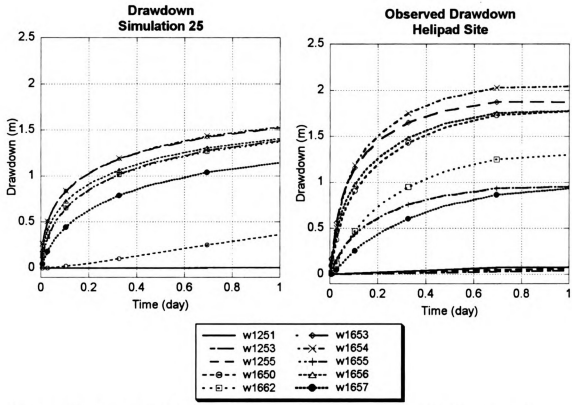

Figure H.29a: Simulated drawdown histories for 1650 series and 1250 series wells within the stratigraphic transition probability geostatistical conceptual model. Simulated results show minor drawdown in1250 series wells.

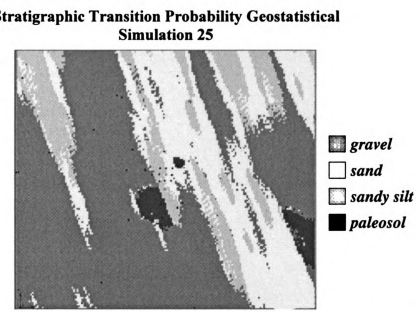

Figure H.29 Map view of the spatial distribution of hydrofacies for the stratigraphic transition probability geostatistical conceptual model. Map view is from the 24th model layer (lower portion of the sand and gravel channel for the E stratigraphic unit).

Appendix I

FORTRAN Code

There were two FORTRAN codes developed to reformat output binary grid files (bgr) generated with T-PROGS (Carle 1999) to formats that could be read into GMS 4.0 (Brigham Young University, 2002) and Rockworks 2002 (Rockware Inc., 2002). The stratigraphic TPSIM code was developed to read each of the full block simulations (C through F) and top and bottom paleosol surfaces. This code outputs a category file (corresponding to materials read by GMS) and Rockworks files (for visualization of realizations, Appendix F). The transition probability geostatistical TPSIM code was developed to read in realizations generated by TPSIM and output files for GMS and Rockworks in the same manor as the previous code. These codes are listed below.

```
      program sequences
c Program to create an output file to be used in a 3D
realization
c of the LLNL study area - lists sequence number for C, D,
E, and F.
c Created for 9/02 simulations.
c DO NOT USE WITHOUT ADJUSTMENT FOR SPECIFICS...NOTE:  SOME
PALEOSOL
C ZONES ONLY HAVE 3 CATEGORIES, 1-GRAVEL, 2-SAND, 3-
PALEOSOL.  THESE
C ARE ADJUSTED IN THIS PROGRAM TO GIVE PALEOSOL AS CAT = 4.
c revisions 11/8/02:  read in telescoping grid from GMS and
output heterogeneity
c Declaration of variables
      parameter nx=181, ny=155, nz=79, base=124.25
      parameter ix=206, iy=194

      logical*1 iseq(nx*ny*nz),icat(nx*ny*nz)
      logical*1 ccat(nx*ny*nz),dpcat(nx*ny*nz)
      logical*1 dcat(nx*ny*nz),epcat(nx*ny*nz)
      logical*1 ecat(nx*ny*nz),fpcat(nx*ny*nz)
      logical*1 fcat(nx*ny*nz)
      real sc(nx*ny),sd(nx*ny),se(nx*ny),sf(nx*ny)
      real sbc(nx*ny),sbd(nx*ny),sbe(nx*ny),sbf(nx*ny)
      real sc1(nx,ny),sd1(nx,ny), se1(nx,ny),sf1(nx,ny)
      real sbc1(nx,ny),sbd1(nx,ny),sbe1(nx,ny),sbf1(nx,ny)
      real sll(nx*ny),sll1(nx,ny)
      real elev
      real cond(nx*ny*nz)
      real xg(ix),yg(iy)
      integer idim(3)
      character*40 parfl
      character*40 cbfil
      character*40 dtfil
      character*40 dbfil
      character*40 etfil
      character*40 ebfil
      character*40 ftfil
      character*40 fbfil
      character*40 llfil
      character*40 seqfil
      character*40 catfil
      character*40 cbgr
      character*40 dpbgr
      character*40 dbgr
```

```
      character*40 epbgr
      character*40 ebgr
      character*40 fpbgr
      character*40 fbgr
      character*40 gmsfil
      character*40 rckfil1
      character*40 rckfil2
      character*40 rckfil3
      character*40 rckfil4
      character*40 rckfil
      character*40 gmsin
      character*40 gmsref
      nxy=nx*ny
      nxya=(nx-1)*(ny-1)
      nxyz=nx*ny*nz
      dx=2.
      dy=2.
      dz=0.5
c  Where are the data???????
      print*,'input par file name?:'
c  Open input and output files
      read(5,'(a40)') parfl
      print*,'input file name:', parfl
      open(1,file=parfl,status='old')
      read(1,'(a)') cbfil
      read(1,'(a)') dtfil
      read(1,'(a)') dbfil
      read(1,'(a)') etfil
      read(1,'(a)') ebfil
      read(1,'(a)') ftfil
      read(1,'(a)') fbfil
      read(1,'(a)') llfil
      read(1,'(a)') cbgr
      read(1,'(a)') dpbgr
      read(1,'(a)') dbgr
      read(1,'(a)') epbgr
      read(1,'(a)') ebgr
      read(1,'(a)') fpbgr
      read(1,'(a)') fbgr
      read(1,'(a)') seqfil
      read(1,'(a)') catfil
      read(1,'(a)') gmsfil
      read(1,'(a)') rckfil1
      read(1,'(a)') rckfil2
      read(1,'(a)') rckfil3
      read(1,'(a)') rckfil4
      read(1,'(a)') rckfil
```

```
      read(1,*)sx,sy,sz
      read(1,*)cond0,cond1,cond2,cond3,cond4,cond5
      read(1,'(a)') gmsin
      read(1,'(a)') gmsref
      close(1)
      open(2,file=seqfil,status='unknown',form='unformatted'
)
      open(3,file=catfil,status='unknown',form='unformatted'
)
      open(4,file='dbg.txt',status='unknown')
      irank=3
      write(2) irank
      write(2) nx,ny,nz
      write(3) irank
      write(3) nx,ny,nz
c  Read data from ASCII file to fill arrays. Sequence
boundaries!
      print*,'reading Rockware grids'
      open(1,file=cbfil,status='old')
      do i=1,nx
        do j=1,ny
          read(1,*) sbc1(i,j)
        enddo
      enddo
      close(1)
      open(1,file=dtfil,status='old')
      do i=1,nx
        do j=1,ny
          read(1,*) sd1(i,j)
        enddo
      enddo
      close(1)
      open(1,file=dbfil,status='old')
      do i=1,nx
        do j=1,ny
          read(1,*) sbd1(i,j)
        enddo
      enddo
      close(1)
      open(1,file=etfil,status='old')
      do i=1,nx
        do j=1,ny
          read(1,*) se1(i,j)
        enddo
      enddo
      close(1)
      open(1,file=ebfil,status='old')
```

```
      do i=1,nx
        do j=1,ny
          read(1,*) sbe1(i,j)
        enddo
      enddo
      close(1)
      open(1,file=ftfil,status='old')
      do i=1,nx
        do j=1,ny
          read(1,*) sf1(i,j)
        enddo
      enddo
      close(1)
      open(1,file=fbfil,status='old')
      do i=1,nx
        do j=1,ny
          read(1,*) sbf1(i,j)
        enddo
      enddo
      close(1)
      open(1,file=llfil,status='old')
      do i=1,nx
        do j=1,ny
          read(1,*) sll1(i,j)
        enddo
      enddo
      close(1)
c read data from bgr files for each sequence
      print*,'reading bgr files'
       open(8,file=cbgr,status='old',form='unformatted')
       read(8) irank
       print*,'irank=',irank
       read(8) (idim(i),i=1,3)
       nxyz=idim(1)*idim(2)*idim(3)
         read(8) (ccat(i),i=1,nxyz)
       close(8)
       open(8,file=dpbgr,status='old',form='unformatted')
       read(8) irank
       print*,'irank=',irank
       read(8) (idim(i),i=1,3)
       nxyz=idim(1)*idim(2)*idim(3)
         read(8) (dpcat(i),i=1,nxyz)
       close(8)
       open(8,file=dbgr,status='old',form='unformatted')
       read(8) irank
       print*,'irank=',irank
       read(8) (idim(i),i=1,3)
```

```
      nxyz=idim(1)*idim(2)*idim(3)
        read(8) (dcat(i),i=1,nxyz)
      close(8)
      open(8,file=epbgr,status='old',form='unformatted')
      read(8) irank
      print*,'irank=',irank
      read(8) (idim(i),i=1,3)
      nxyz=idim(1)*idim(2)*idim(3)
        read(8) (epcat(i),i=1,nxyz)
      close(8)
      open(8,file=ebgr,status='old',form='unformatted')
      read(8) irank
      print*,'irank=',irank
      read(8) (idim(i),i=1,3)
      nxyz=idim(1)*idim(2)*idim(3)
        read(8) (ecat(i),i=1,nxyz)
      close(8)
      open(8,file=fpbgr,status='old',form='unformatted')
      read(8) irank
      print*,'irank=',irank
      read(8) (idim(i),i=1,3)
      nxyz=idim(1)*idim(2)*idim(3)
        read(8) (fpcat(i),i=1,nxyz)
      close(8)
      open(8,file=fbgr,status='old',form='unformatted')
      read(8) irank
      print*,'irank=',irank
      read(8) (idim(i),i=1,3)
      nxyz=idim(1)*idim(2)*idim(3)
        read(8) (fcat(i),i=1,nxyz)
      close(8)
c     print*,'now converting 3 cat to 4 cat models'
c change 3 category zones to 4 category models
c     do k=1,nz
c          do j=1,ny
c               do i=1,nx
c                    ijk=i+((j-1)*nx)+((k-1)*nx*ny)
c                    if(cpcat(ijk).eq.3)cpcat(ijk)=4
c                    if(cpcat(ijk).eq.-3)cpcat(ijk)=-4
c                    if(epcat(ijk).eq.3)epcat(ijk)=4
c                    if(epcat(ijk).eq.-3)epcat(ijk)=-4
c                    if(fpcat(ijk).eq.3)fpcat(ijk)=4
c                    if(fpcat(ijk).eq.-3)fpcat(ijk)=-4
c               enddo
c          enddo
c     enddo
c     print*,'finished doing that...'
```

```
c fill in surface arrays
      write(4,'(a40)') 'warnings to report'
      print*,'filling it all in...bored yet?'
      do j=1,ny
           do i=1,nx
                ixy=i+((j-1)*nx)
                sc(ixy)=sc1(i,j)
                sbc(ixy)=sbc1(i,j)
                sd(ixy)=sd1(i,j)
                sbd(ixy)=sbd1(i,j)
                se(ixy)=se1(i,j)
                sbe(ixy)=sbe1(i,j)
                sf(ixy)=sf1(i,j)
                sbf(ixy)=sbf1(i,j)
                sll(ixy)=sll1(i,j)
                if(sbc(ixy).le.sd(ixy)) write(4,'(a40)')
      *              'WARNING: sbc>sd:  ',i,j
                if(sd(ixy).le.sbd(ixy)) write(4,'(a40)')
      *              'WARNING: sd>sbd:  ',i,j
                if(sbd(ixy).le.se(ixy)) write(4,'(a40)')
      *              'WARNING: sbd>se:  ',i,j
                if(se(ixy).le.sbe(ixy)) write(4,'(a40)')
      *              'WARNING: se>sbe  ',i,j
                if(sbe(ixy).le.sf(ixy)) write(4,'(a40)')
      *              'WARNING: sbe>sf  ',i,j
                if(sf(ixy).le.sbf(ixy)) write(4,'(a40)')
      *              'WARNING: sf>sbf  ',i,j
                if(sbf(ixy).le.sll(ixy)) write(4,'(a40)')
      *              'WARNING: sll>sbf:  ',i,j
c check for thin paleosols...increase to keep it present.
                if(sd(ixy)-
sbd(ixy).le.0.5)sd(ixy)=sbd(ixy)+0.6
                if(se(ixy)-
sbe(ixy).le.0.5)se(ixy)=sbe(ixy)+0.6
                if(sf(ixy)-
sbf(ixy).le.0.5)sf(ixy)=sbf(ixy)+0.6
           enddo
      enddo
c fill in bgr final grid array with proper code
      do k=1,nz
        elev=(k*dz)+base-(0.5*dz)
        do j=1,ny
           do i=1,nx
                ij=i+((j-1)*nx)
                ijk=((k-1)*nx*ny)+i+((j-1)*nx)
                if(elev.gt.sbc(ij)) then
                     icat(ijk)=5
```

```
                    iseq(ijk)=5
                endif
                if(elev.gt.sd(ij).and.elev.le.sbc(ij)) then
                    icat(ijk)=ccat(ijk)
                    v=ccat(ijk)
                    if(ccat(ijk).lt.0) v=ccat(ijk)*(-1)
                    iseq(ijk)=v+20
                endif
                if(elev.gt.sbd(ij).and.elev.le.sd(ij)) then
                    icat(ijk)=dpcat(ijk)
                    v=dpcat(ijk)
                    if(dpcat(ijk).lt.0) v=dpcat(ijk)*(-1)
                    iseq(ijk)=v+30
                endif
                if(elev.gt.se(ij).and.elev.le.sbd(ij)) then
                    icat(ijk)=dcat(ijk)
                    v=dcat(ijk)
                    if(dcat(ijk).lt.0) v=dcat(ijk)*(-1)
                    iseq(ijk)=v+40
                endif
                if(elev.gt.sbe(ij).and.elev.le.se(ij)) then
                    icat(ijk)=epcat(ijk)
                    if(icat(ijk).eq.3) icat(ijk)=4
                    if(icat(ijk).eq.-3) icat(ijk)=-4
                    v=epcat(ijk)
                    if(epcat(ijk).lt.0) v=epcat(ijk)*(-1)
                    if(v.eq.3) v=4
                    iseq(ijk)=v+50
                endif
                if(elev.gt.sf(ij) .and. elev.le.sbe(ij))
then
                    icat(ijk)=ecat(ijk)
                    v=ecat(ijk)
                    if(ecat(ijk).lt.0) v=ecat(ijk)*(-1)
                    iseq(ijk)=v+60
                endif
                if(elev.gt.sbf(ij).and.elev.le.sf(ij)) then
                    icat(ijk)=fpcat(ijk)
                    if(icat(ijk).eq.3) icat(ijk)=4
                    if(icat(ijk).eq.-3) icat(ijk)=-4
                    v=fpcat(ijk)
                    if(fpcat(ijk).lt.0) v=fpcat(ijk)*(-1)
                    if(v.eq.3) v=4
                    iseq(ijk)=v+70
                endif
                if(elev.gt.sll(ij).and.elev.le.sbf(ij)) then
                    icat(ijk)=fcat(ijk)
```

```
                    v=fcat(ijk)
                    if(fcat(ijk).lt.0) v=fcat(ijk)*(-1)
                    iseq(ijk)=v+80
                endif
                if(elev.le.sll(ij)) then
                    icat(ijk)=6
                    iseq(ijk)=90
                endif
            enddo
          enddo
        enddo
        write(2) (iseq(k),k=1,nxyz)
        write(3) (icat(k),k=1,nxyz)
        close(2)
        close(3)
c Prepare the gms and rockware input files
        print*, 'printing gms and rockware files'
        open(1,file=rckfil1,status='unknown')
        open(2,file=rckfil2,status='unknown')
        open(3,file=rckfil3,status='unknown')
        open(4,file=rckfil4,status='unknown')
        open(5,file=rckfil,status='unknown')
        open(6,file=gmsfil,status='unknown')
        open(7,file=gmsin,status='old')
        open(8,file=gmsref,status='unknown')
c writing Rockware files
        do k=1,nz
            do j=1,ny
                do i=1,nx
                    ijk=i+((j-1)*nx)+((k-1)*nx*ny)
                    x=sx+(2.*(i-1))
                    y=sy+(2.*(j-1))
                    z=sz+(0.5*(k-1))
                    if (icat(ijk).eq.1) then
                        cond(ijk)=cond1
                        write(1,14) x,y,z,icat(ijk)
                        write(5,14) x,y,z,iseq(ijk)
                    endif
                    if (icat(ijk).eq.2) then
                        cond(ijk)=cond2
                        write(2,14) x,y,z,icat(ijk)
                        write(5,14) x,y,z,iseq(ijk)
                    endif
                    if (icat(ijk).eq.3) then
                        cond(ijk)=cond3
                        write(3,14) x,y,z,icat(ijk)
                        write(5,14) x,y,z,iseq(ijk)
```

```
                    endif
                    if (icat(ijk).eq.4) then
                         cond(ijk)=cond4
                         write(4,14) x,y,z,icat(ijk)
                         write(5,14) x,y,z,iseq(ijk)
                    endif
                    if (icat(ijk).eq.0) then
                         cond(ijk)=cond0
                         write(5,14) x,y,z,iseq(ijk)
                    endif
                    if (icat(ijk).eq.5) then
                         cond(ijk)=cond5
                         write(5,14) x,y,z,iseq(ijk)
                    endif
     if(k.eq.20) print*,'youre now on layer 20...hang in
there'
     if(k.eq.50) print*,'youre now on layer 50...hang in
there'
     if(k.eq.70) print*,'youre now on layer 70...hang in
there'
     if(k.eq.90) print*,'youre now on layer 90...hang in
there'
   14 format(3(f7.1),1x,i4)
   15      format(i8,1x,3(f7.1),1x,e10.3)
                enddo
           enddo
     enddo
c writing GMS full grid file

     do k=nz,1,-1
          do j=ny,1,-1
               do i=1,nx
                    ijk=i+((j-1)*nx)+((k-1)*nx*ny)
                    write(6,'(i2)') icat(ijk)
               enddo
          enddo
     enddo
c writing GMS telescoping grid file
c     read refined grid x,y locations
     read(7,*) sx,sy
     print*,'filling in refined grid'
     print*,ix,nx,iy,ny
     do i=1,ix
          read(7,*) xg(i)
     enddo
     do j=1,iy
          read(7,*) yg(j)
```

```
      enddo
      do k=nz,1,-1
           do j=iy,1,-1
                yga=(yg(j)-sy)/dy
                nycell=(int(yga))+1
                do i=1,ix
                     xga=(xg(i)-sx)/dx
                     nxcell=(int(xga))+1
                     ijk=nxcell+((nycell-1)*nx)+((k-
1)*nx*ny)
                     write(8,'(i2)') icat(ijk)
                enddo
           enddo
      enddo
      print*,'gms and rockware files completed'
      print*,'Goodbye!'
       close(1)
       close(2)
       close(3)
       close(4)
       close(5)
       close(6)
       print*,'****************************'
       print*,'GMS and RockWare files written.'
       print*,'****************************'
       print*,'(:'
       stop
       end
```

Transition Probability Geostatistical TPSIM Code

```
      program Transition Probability Geostatistical TPSIM
c Program to create an output file to be used in a 3D
realization
c of the LLNL study area - lists sequence number for C, D,
E, and F.
c Created for 9/02 simulations.
c DO NOT USE WITHOUT ADJUSTMENT FOR SPECIFICS...NOTE:  SOME
PALEOSOL
C ZONES ONLY HAVE 3 CATEGORIES, 1-GRAVEL, 2-SAND, 3-
PALEOSOL.  THESE
C ARE ADJUSTED IN THIS PROGRAM TO GIVE PALEOSOL AS CAT = 4.
c revisions 11/8/02:  read in telescoping grid from GMS and
output heterogeneity
c                     file.
c Declaration of variables
      parameter nx=181, ny=155, nz=79, base=124.25
      parameter ix=206, iy=194
      logical*1 iseq(nx*ny*nz),icat(nx*ny*nz)
      real sim1(nx,ny)
      real cond(nx*ny*nz)
      real xg(ix),yg(iy)
      integer idim(3)
      character*40 parfl
      character*40 simbgr
      character*40 gmsfil
      character*40 rckfil1
      character*40 rckfil2
      character*40 rckfil3
      character*40 rckfil4
      character*40 rckfil
      character*40 gmsin
      character*40 gmsref
      nxy=nx*ny
      nxya=(nx-1)*(ny-1)
      nxyz=nx*ny*nz
      dx=2.
      dy=2.
      dz=0.5
c  Where are the data???????
```

```
      print*,'input par file name?:'   !  Open input and
output files
      read(5,'(a40)') parfl
      print*,'input file name:', parfl
      open(1,file=parfl,status='old')
      read(1,'(a)') simbgr
      read(1,'(a)') gmsfil
      read(1,'(a)') rckfil1
      read(1,'(a)') rckfil2
      read(1,'(a)') rckfil3
      read(1,'(a)') rckfil4
      read(1,'(a)') rckfil
      read(1,*)sx,sy,sz
      read(1,*)cond0,cond1,cond2,cond3,cond4,cond5
      read(1,'(a)') gmsin
      read(1,'(a)') gmsref
      close(1)
c  Read data from ASCII file to fill arrays. Sequence
boundaries!
      print*,'red in par file'
c read data from bgr files for each sequence
      print*,'reading bgr files'
       open(8,file=simbgr,status='old',form='unformatted')
       read(8) irank
      print*,'irank = ',irank
       print*,'irank=',irank
       read(8) (idim(i),i=1,3)
       nxyz=idim(1)*idim(2)*idim(3)
         read(8) (icat(i),i=1,nxyz)
       close(8)
      print*,'red in simbgr'
c Prepare the gms and rockware input files
      print*, 'printing gms and rockware files'
      open(1,file=rckfil1,status='unknown')
      open(2,file=rckfil2,status='unknown')
      open(3,file=rckfil3,status='unknown')
      open(4,file=rckfil4,status='unknown')
      open(5,file=rckfil,status='unknown')
      open(6,file=gmsfil,status='unknown')
      open(7,file=gmsin,status='old')
      open(8,file=gmsref,status='unknown')
c writing Rockware files
      do k=1,nz
           do j=1,ny
                do i=1,nx
                     ijk=i+((j-1)*nx)+((k-1)*nx*ny)
                     x=sx+(2.*(i-1))
```

```
                    y=sy+(2.*(j-1))
                    z=sz+(0.5*(k-1))
                    if (icat(ijk).eq.1) then
                         cond(ijk)=cond1
                         write(1,14) x,y,z,icat(ijk)
                         write(5,14) x,y,z,icat(ijk)
                    endif
                    if (icat(ijk).eq.2) then
                         cond(ijk)=cond2
                         write(2,14) x,y,z,icat(ijk)
                         write(5,14) x,y,z,icat(ijk)
                    endif
                    if (icat(ijk).eq.3) then
                         cond(ijk)=cond3
                         write(3,14) x,y,z,icat(ijk)
                         write(5,14) x,y,z,icat(ijk)
                    endif
                    if (icat(ijk).eq.4) then
                         cond(ijk)=cond4
                         write(4,14) x,y,z,icat(ijk)
                         write(5,14) x,y,z,icat(ijk)
                    endif
                    if (icat(ijk).eq.0) then
                         cond(ijk)=cond0
                         write(5,14) x,y,z,icat(ijk)
                    endif
                    if (icat(ijk).eq.5) then
                         cond(ijk)=cond5
                         write(5,14) x,y,z,icat(ijk)
                    endif
     if(k.eq.50) print*,'youre now on layer 50...hang in
there'
   14 format(3(f7.1),1x,i4)
   15     format(i8,1x,3(f7.1),1x,e10.3)
               enddo
          enddo
     enddo
c writing GMS full grid file
     do k=nz,1,-1
          do j=ny,1,-1
               do i=1,nx
                    ijk=i+((j-1)*nx)+((k-1)*nx*ny)
                    write(6,'(i2)') icat(ijk)
               enddo
          enddo
     enddo
c writing GMS telescoping grid file
```

```
c     read refined grid x,y locations
      read(7,*) sx,sy
      print*,'filling in refined grid'
      print*,ix,nx,iy,ny
      do i=1,ix
           read(7,*) xg(i)
      enddo
      do j=1,iy
           read(7,*) yg(j)
      enddo
      do k=nz,1,-1
           do j=iy,1,-1
                yga=(yg(j)-sy)/dy
                nycell=(int(yga))+1
                do i=1,ix
                     xga=(xg(i)-sx)/dx
                     nxcell=(int(xga))+1
                     ijk=nxcell+((nycell-1)*nx)+((k-
1)*nx*ny)
                     write(8,'(i2)') icat(ijk)
                enddo
           enddo
      enddo
      print*,'gms and rockware files completed'
      print*,'Goodbye!'
       close(1)
       close(2)
       close(3)
       close(4)
       close(5)
       close(6)
       close(7)
       close(8)
       print*,'*****************************'
       print*,'GMS and RockWare files written.'
       print*,'*****************************'
       print*,'(:'
       stop
       end
```

Bibliography

Batu, V., 1998, Aquifer Hydraulics : A Comprehensive Guide to Hydraulic Data Analysis: New York / Chichester / Weinheim / Brisbane / Singapore / Toronto, John Wiley & Sons, Inc., 727 p.

Bennett, G., and Weissman, G.S., 2001, Geostatistical and deterministic modeling of alluvial fan hydrostratigraphy at the Lawrence Livermore National Laboratory: North Central GSA Meeting, p. 1.

Biteman, S., Hyndman, D.W., Phanikumar, M.S., and Weissmann, G.S., in press, Integration of sedimentologic and hydrologic properties for improved transport simulations: detailed characterization of a glacial outwash aquifer at the Schoolcraft Bioremediation Site, Michigan: Submitted for an SEPM special publication on Hydrogeophysics and Hydrostratigraphy (edited by John Bridge and David Hyndman).

Blake, R. G., 1997, Hydrostratigraphic analysis-ground water cleanup at Lawrence Livermore National Laboratory, Lawrence Livermore National Laboratory, p. 1.

Blake, R. G., Noyes, C.M., and Maley, M.P., 1995, Hydrostratigraphic analysis - the key to cost-effective ground water cleanup at Larwence Livermore National Laboratory, Larwence Livermore National Laboratory, p. 12.

Boutt, D. F., Hyndman, D.W., Pijanowski, B.C., and Long, D.T, 2001, Identifying Potential Land Use-derived Solute Sources to Stream Baseflow Using Ground Water Models and GIS: Ground Water, v. 36, p. 224-34.

Carle, S. F., 1996a, A trransition probability-based approach to geostatistical charaterization of hydrostratigraphic architecture: Dissertation thesis, University of California, Davis, 233 p.

Carle, S. F., 1999, T-PROGS: Transition Proability Geostatistical Software Version 2.1, Davis, CA, University of California, Davis, p. 84.

Carle, S. F., and Fogg, G. E., 1996b, Transition probability-based indicator geostatistics: Mathmatical Geology, v. 28.

Carle, S. F., LaBolle, E. M., Weissman, G. S., VanBrocklin, D., Fogg, G. E., 1998, Conditioned simulation of hydrofacies architecture; a transition probability/Markov approach,, *in* G. S. a. D. Fraser, J. M., ed., Hydrogeology Models of Sedimentary Aquifers, v. 1, p. 147-170.

Carpender, D. W., Puchlik, K.P., ramirez, A.L., Wagoner, J.L., Knuass, K.G., and Kasmeyer, P.W., 1980, Status Report on the Geology of Larwence Livermore National Laboratory Site and Adjacent Areas, Larwence Livermore National Laboratory.

Carpender, D. W., Sweeney, J. J., Kasameyer, P. W., Burkhard, N. R., Knauss, K. G., and Shlemon, R. J., 1984, Geology of the Lawrence Livermore National Laboratory Site and Adjacent Areas, Livermore California, Lawrence Livermore National Laboratory, University of California, p. 150.

CDWR, 1966, Evaluation of Ground Water Resources: Livermore and Sunol Valleys, Geology, Bulletin 118-2, Sacramento, CA, State of Califonia, Department of Water Resources.

CDWR, 1974, Evoluation of Ground Water Resources: Livermore and Sunol Valleys, Bulletin 118-2, Geology, State of California, Department of Water Resources, Sacramento CA.

Copty, N. K., and Findikakis, A.N., 2002, Stocastic Analysis of Pumping Test Drawdown Data in Heterogeneous Geologic Formations: Briding the gap between measurement and modeling in heterogeneous media.

Dibblee, T. W., 1980, Preliminary geologic map of the Altamont Quadrangle, Alameda County, California, US Geological Survey.

Dibblee, T. W., and Darrow, R.L., 1981, Geology of the Northern Diablo Range and Livermore Valley Area, *in* F. E.V., ed., Geology of Central and Northern Diablo Range, California, Pacific Section of SEPM, Los Angeles, p. 77-112.

Dickinson, W. R., 1965, Folded Thrust Contact Between Franciscan Rocks adn Panoche Group in the Diablo Range of Centeral California: Geological Society of America, Golden, CO, Special Paper 82, p. 248-249.

Doherty, J., Brebber, L., and Whyte, P., 2000, PEST: Model-Independent Parameter Estimation, Watermark Numerical Computing, p. 249.

Dominic, D. F., Ritzi, R.W., Jr.,, 1996, Geostatistical analysis of facies distributions in a buried-valley aquifer: American Association of Petroleum Geologists 1996 annual convention, p. 36.

Energy, U. S. D. o., 1998, Environmental restoration at Larwence Livermore National Laboroatory, U.S. Department of Energy, p. 24.

Ernst, W. G., 1970, Tectonic Contact Between the Franciscan Melange and the Great Valley Sequence - Crustal Expression of a Late Mesozoic Benioff Zone: Journel of Geophysical Research, v. 75, p. 886-901.

Eschard R., E. a., 1998, Combining Sequence Stratigtraphy, Geostatical Simulations and Production Data for Modeling a Fluvial Reservoir in the Chaunoy Field (Triassic, France): AAPG Bulitin, v. 82, p. 545-586.

Fogg, G. E., Carle, S.F., and Green, C., 1998, Connected-network paradigm for the alluvial aquifer system, *in* D. Zhang, Winter, L.C., ed., Theory, modeling, and field investigation in hydrogeology; a special volume in honor of Shlomo P. Neuman's 60th birthday, Special Paper - Geological Society of America: Meeting: Shlomo P. Neuman; recent advances after 30 years of exceptional contributions to well hydraulics, numerical modeling, and field investigations, Tucson, AZ, United States, Oct. 17, 1998., p. 25-42.

Freeze, R. A., Cherry, J. A., 1979, Groundwater: Englewood Cliffs, Prentice Hall, 604 p.

Freyberg, D. L., 1986, A natural gradient experiment on solute transport in a sand aquifer; 2, Spatial moments and the advection and dispersion of nonreactive tracers: Water Resources Research, v. 22, p. 2031-2046.

Froukh, L. J., 2002, Groundwater modeling in aquifers with highly karstic and heterogeneous characteristics (KHC) in Palistine: Bridging the gap between measurement and modeling heterogeneous media.

Gaud, M. N., Smith, Gary A., 2001, Evaluating the transition of lithofacies to hydrofacies using outcrop data: Geological Society of America, v. 33, p. 16.

Gloaguen, E., Chouteau, M., Marcotte, D., and Chapuis, R., 2001, Estimation of hydraulic conductivity of an unconfined aquifer using cokriging of GPR and hydrostratigraphic data: Journel of Applied Geophysics, v. 47, p. 135-152.

Hamilton, W., 1969, Mesozoic California and the Underflow of the Pacific Mantle: Geologic Society of America Bulletin, v. 80, p. 2409-2430.

Hantush, M. S., and Jacob, C. E., 1955, Nonsteady radial flow in an infinite leaky aquifer: Trans. American Geophysical Union, v. 36, p. 95-100.

Harbaugh, A. W., Banta, E.R., Hill, M.C., and Mcdonald, M.G, 2000, Modflow-2000, The U.S. Geological Survey Modular Ground-Water Model--User Guid to Modularization conceptsand the Ground-Water Flow Process, Reson, Virginia, U.S. Geological Survey, p. 121.

Harrach, R. J., Gallegos, G.M., Failor, R.A., Christofferson, E., Tate, P.J., Brandstetter, E.R., Larson, J.M., McIntyre, J.R., Fields, B.C., Brown, R.A., Garcia, L.M., and Grayson, A.R., 1995, Environmental report 1994, Livermore, CA, Lawrence Livermore National Laboratory, p. 357.

Hill, M. C., Banta, E.R., Harbaugh, A.W., and Anderman, E.R., 2000, Modflow-2000, The U.S. Geological Survey Modualr Ground-Water Model--Userguid to the Observation, Sensitivity, and Parameter-Estimation Process and Three Post-Processing Programs, Denver, Colorado, U.S. Geological Survey, p. 209.

Howard, A. D., 1979, Geologic History of Middle California: California Natural History Guides, University of California Press, 113 p.

Hsu, K. J., 1971, Franciscan Melanges as a Model for Eugeosynclinal Sedimantation and Underthrusting Tectonics: Journeal of Geophysical Research, v. 76, p. 1162-1170.

Huey, A. S., 1948, Geology of the Telsa Quadrangle, California: California Division of Mines, Bulletin, v. 140, p. 52.

Inc., R., 2002, Rockworks2002, Golden, Colorado, RockWare Incorparated, p. 328.

Klingbeil, R., Kleineidam, S., Asprion, U., Aigner, T., Teutsch, G., 1999, Relating Lithofaces to hydrofacies; outcrop-based hydrogeologic charaterization of Quaternary gravel deposits: Sedimentary Geology, v. 129, p. 253-264.

Koltermann, C. E. a. G., S.M, 1996, Heterogeneity in sedimentary deposits; a review of structure-imitating, process-imitating, and descriptive approaches,: Water Resources Research, v. 32, p. 2617-2658.

Kruseman, G. P., and de Ridder, N. A., 1990, Analysis and evaluation of pumping test data: Wageningen, ILRI Publication 47.

Newman, S. P., and Witherspoon, Paul A., 1972, Fiels Determination of the Hydraulic Properties of Leaky Multiple Aquifer Systems: Water Resources Research, v. 8, p. 1284-1298.

Noyes, C. M., Maley, M.P., and Blake, R., 1997, Hydrostratigraphic analisis-implimenting cost-effective superfund ground water cleanup, Larwence Livermore National Laboratory, p. 7.

Noyes, C. M., Maley, M.P., and Blake, R., 2000, Defining Hydrostratigraphic Units within the Heterogeneous Alluvial Sediments at Lawrence Livermore National Laboratory, Lawrence Livermore National Laboratory, p. 33.

Passinos, P. V., 2001, Well test to characterize idealized lateral heterogeneities: Maters thesis, Clemson Univerity, Clemson, SC, United States, 159 p.

Ritzi, R. W., Jr., Dominic, D.F., Brown, N.R., Kausch, K.W., McAlenney, P.J., and Basial, M.J., 1995, Hydrofacies distribution and correlation in the Miami Valley aquifer system: Water Resources Research, v. 31, p. 3271-3281.

Ritzi, R. W., JR., Jayne, D.F., Zahradnik, A.J., Field, A.A., and Fogg, G.E., 1994, Geostatistical modeling of heterogeneity in glaciofluvial, buried-valley aquifers: Ground Water, v. 32, p. 666-674.

(RWQCB), S. F. B. R. W. Q. C. B., 1982, Water Quality Control Plan, Oakland, CA, San Francisco Bay Basin, State of California.

Schad, H., and Teutsch, G., 1994a, Effects of the investigation scale on pumping test results in heterogeneous porous aquifers, *in* H. S. Wheater, Raats, P.A.C., and Armstrong, A.C., ed., Field, laboratory and modelling studies of flow and transport processes: Meeting: 17th general assembly of the European Geophysical Society symposium on Field, laboratory and modelling studies of flow and transport processes, Edinburgh, United Kingdom, Journal of Hydrology.

Schad, H., and Teutsch, G., 1994b, Effects of the investigation scale on pumping test results in heterogeneous porus aquifers: Journal of hydrology, v. 159, p. 61-77.

Sudicky, E. A., 1986, A natural gradient experiment on solute transport in a sand aquifer; spatial variability of hydraulic conductivity and its role in the dispersion process: Water Resources Research, v. 22, p. 2069-2083.

Sweeney, J. J., and Springer, J.E., 1981, Geology of Southeastern Livermore Valley, Alameda County, California, Livermore,CA, Larwence Livermore National Laboratory.

Teles, V., Perrier, E., Delay, F., and Marsily, Gh. de, 2002, Generation of alluvial aquifers with a new gentic/stochastic sedimentation model: comparison with geostatistical approaches by means of groundwater flow simulations: Bridging the gap between measurement and modeling heterogeneous media.

Theis, C. V., 1935, The relation between the lowering of piezometric surface and the rate and duration of the discharge of a well using groundwater storage: Trans American Geophysical Union, v. 16, p. 519-524.

Thorpe, R. K., Isherwood, W.F., Dresen, M.D., and Webster-Scholten, C.P., 1990, CERCLA Remedial Investigation Report for the LLNL Livermore Site, Livermore, CA, Lawrence Livermore National Laboratory.

University, B. Y., 2002, Department of Defence Groundwater Modeling System (GMS), Version 4.0, Salt Lake City, UT.

Webb, E. K., and Davis, J.m.,, 1998, Simulation of the spatial heterogeneity of geological properties: an overview, *in* G. S. a. D. Fraser, J. M., ed., Hydrogeologic Models of Sedimentary Aquifers, SEPM Concepts in Hydrogeology and Enviromental Geology No. 1, p. 1-24.

Weissmann, G. S., 1999a, Toward new models of subsurface heterogeneity: An alluvial fan sequence framewqork with transition probability geostatistics: Dissertation thesis, University of California, Davis, 279 p.

Weissmann, G. S., 2001, Geologic Characterization of the Helipad Site (TFD), Lawrence Livermore National Laboratory, California, East Lansing Michigan, Michigan State University, p. 62.

Weissmann, G. S., in press, Influence of incised valley fill deposits on hydrogeology of a glacially-influenced, stream-dominated alluvial fan, *in* J. B. a. D. Hyndman, ed., SEPM special publication on Hydrogeophysics and Hydrostratigraphy.

Weissmann, G. S., and Fogg, G. E., 1999b, Multi-scale Alluvial Fan Hetrogeneity modeled with transition probability geostatistics in a sequence stratigraphic framework: Journel of Hydrology, v. 226, p. 48-65.

Weissmann, G. S., Carle, S.A., and Fogg, G.E., 1999c, Three-dimensional hydrofacies modeling based on soil survey analysis and transition probability geostatistics: Water Resources Research, v. 35, p. 1761-1770.

Weissmann, G. S., Mount, J.F., and Fogg, G.E., 2002a, Glacially-driven cycles in accumulation space and sequence stratigraphy of a stream-dominated alluvial fan, San Joaquin Valley, Califonia, U.S.A: Journeal of Sedimentary Research, v. 72, p. 240-251.

Weissmann, G. S., Yong, Z., LaBolle, E.M., and Fogg, G.E., 2002b, Modeling environmental tracer-based groundwater ages in heterogeneous aquifers: Water Resources Research.

Yang, Y. s., Cronin, A.A., Elliot, T., and Kalin, R.M., 2002, Characterizing heterogeneous hydrogeological systems through inverse groundwater flow and geochemical modeling: Bridging the gap between measurement and modeling heterogeneous media.

Zhan, H., Wang, L.V., and Park, E., 2001, On the horizontal-well pumping test in anisotropic confined aquifers: Journal of hydrology, v. 252, p. 37-50.

Zhang, Y., Weissmann, G.S., Fogg, G.E., Williamson, R.J., and Labolle, E.M., 2000, Effect of multi-scale heterogeneity on predictive uncertainty and groundwater age dates: AGU 2000 fall meeting, p. 434.

MICHIGAN STATE UNIVERSITY LIBRARIES
3 1293 02461 8872